

**High Order Finite Difference Methods for Interface Problems
with Singularities**

by

Qiwei Feng

A thesis submitted in partial fulfillment of the requirements for the degree of

Doctor of Philosophy

in

Applied Mathematics

Department of Mathematical and Statistical Sciences
University of Alberta

© Qiwei Feng, 2022

Abstract

Interface problems arise in many applications such as modeling of underground waste disposal, oil reservoirs, composite materials, and many others. The coefficient a , the source term f , the solution u and the flux $a\nabla u \cdot \vec{n}$ are possibly discontinuous across the interface curve Γ in such problems. In realistic problems, the coefficient a may have large jumps across the interface curve, or it can be highly oscillatory across the whole domain. This leads to accuracy deterioration and huge condition numbers of resulting linear systems. In order to obtain reasonable numerical solutions, higher order numerical schemes are desirable.

In Chapter [2](#) we propose a sixth order compact 9-point finite difference method (FDM) on uniform Cartesian grids, for Poisson interface problems with singular sources in a rectangular domain. The matrix A in the resulting linear system $Ax = b$, following from the proposed compact 9-point scheme, is independent of any source terms f , jump conditions, and interface curves Γ . We prove the sixth order convergence rate for the proposed compact 9-point scheme using the discrete maximum principle. Our numerical experiments confirm the sixth order of accuracy of the proposed compact 9-point scheme. This chapter has been published in *Computers and Mathematics with Applications* in 2021.

In Chapter [3](#), elliptic interface problems with discontinuous and high-contrast piecewise smooth coefficients in a rectangle are considered. We propose a high order compact 9-point FDM and a high order local calculation for approximation of the solution u and the gradient ∇u respectively. The scheme is developed on uniform Cartesian grids, avoiding the transformation into local coordinates. We also numerically verify the sign conditions of our proposed compact 9-point scheme and prove the fourth order convergence rate by the discrete maximum principle. Our numerical experiments confirm the fourth order accuracy for the numerically approximated solution u in both l_2 and l_∞ norms, and the fourth/third order accuracy for the numerically approximated gradient $((u_h)_x, (u_h)_y)$ in the l_2/l_∞ norm. This chapter has been published in *Applied Mathematics and Computation* in 2022.

In Chapter [4](#), we propose an efficient and flexible way to achieve the implementation of a hybrid FDM in uniform Cartesian meshes for elliptic interface problems with discontinuous and high-contrast piecewise smooth coefficients in a rectangular domain. The scheme utilizes a 9-point compact stencil with a sixth order accuracy for interior regular points and 13-point stencil with a fifth order accuracy for interior irregular points. Near the boundary, the stencil is reduced to six points and near the domain corners - to four points, and the corresponding discretization has a sixth order of accuracy on uniform Cartesian meshes, for various boundary conditions (Dirichlet, Neumann and Robin). Our numerical experiments confirm the flexibility and the accuracy order in l_2 and l_∞ norms.

In Chapter [5](#), we present a sixth order compact FDM on uniform Cartesian meshes for the Helmholtz equation with singular sources, and any possible combination of boundary conditions (Dirichlet, Neumann, and impedance) in a rectangular domain. To reduce the pollution effect, we propose a new pollution minimization strategy that is based on the average truncation error of plane waves. Our numerical experiments demonstrate the superiority of the proposed compact finite difference scheme with reduced pollution effect, as compared to several state-of-the-art finite difference schemes in the literature, particularly in the critical pre-asymptotic region where kh is near 1 with k being the wavenumber and h the mesh size. This chapter has been submitted in *SIAM Journal on Scientific Computing*.

In Chapter [6](#), we propose a sixth order compact 9-point FDM on uniform Cartesian meshes for elliptic interface problems with particular intersecting interfaces and four discontinuous constant coefficients in a square domain, where the solution is smooth enough, and interface curves are horizontal and vertical straight lines. The formulas of proposed sixth order compact 9-point finite difference scheme are constructed explicitly for all grid points (regular points, interface points, and the intersection point). We prove the order 6 convergence of our proposed compact 9-point scheme by the discrete maximum principle. Our numerical experiments confirm the flexibility and the sixth order accuracy in l_2 and l_∞ norms of our proposed compact 9-point scheme.

Preface

The results in Chapters 2 to 4 and 6 are joint work with Bin Han and Peter Mineev. The results in Chapter 5 are joint work with Bin Han and Michelle Michelle.

Acknowledgements

First of all, I want to express my sincere thanks to my supervisor Dr. Peter Minev and co-supervisor Bin Han. They always help me to get a deep understanding of my research and come up with new ideas. They encourage, support and help me with their patience and enthusiasm, when I have been stuck in the research stalemate. I could not finish my PhD research without their efforts. Besides my supervisors, I deeply appreciate for the considerations, suggestions, time, and patience from Dr. Rong-Qing Jia, Dr. Zhilin Li, and Dr. Xinwei Yu in my thesis committee.

I am also very grateful for the resources and financial support from Dr. Peter Minev, Dr. Bin Han, Natural Sciences and Engineering Research Council of Canada (NSERC), Department of Mathematical and Statistical Sciences, Faculty of Graduate Studies and Research (FGSR) at the University of Alberta, Westgrid, and Compute Canada.

Moreover, many thanks to all the professors who have taught me courses during my PhD study at University of Alberta. Last but not least, I really appreciate the encouragement and support from my parents and friends.

Table of Contents

1 Introduction	1
1.1 Background	1
1.2 Preliminaries	7
1.2.1 Basic definitions	7
1.2.2 Error measures in numerical experiments	11
1.3 Thesis structure	12
1.4 Contributions	14
2 Sixth Order Compact 9-Point Finite Difference Schemes for Poisson Interface Problems with Singular Sources	17
2.1 Introduction and problem formulation	17
2.2 Sixth order compact 9-point finite difference schemes using uniform Cartesian grids	21
2.2.1 Stencils for regular points	23
2.2.2 Stencils for irregular points	26
2.2.3 Convergence analysis	30
2.3 Numerical experiments	33
2.3.1 Numerical examples with known u , smooth Γ and $\Gamma \cap \partial\Omega = \emptyset$	33
2.3.2 Numerical examples with known u , smooth Γ and $\Gamma \cap \partial\Omega \neq \emptyset$	34
2.3.3 One numerical example with known u , sharp-edged Γ and $\Gamma \cap \partial\Omega = \emptyset$	36
2.3.4 Numerical examples with unknown u , smooth Γ and $\Gamma \cap \partial\Omega = \emptyset$	38
2.3.5 Numerical examples with unknown u , smooth Γ and $\Gamma \cap \partial\Omega \neq \emptyset$	41
2.3.6 One numerical example with unknown u , sharp-edged Γ and $\Gamma \cap \partial\Omega = \emptyset$	44
2.4 Conclusion	44
2.5 Proof of Theorem 2.4	46
3 A High Order Compact 9-Point Finite Difference Scheme for Elliptic Interface Problems with Discontinuous and High-Contrast Coefficients	53

3.1	Introduction and problem formulation	53
3.2	Preliminary	55
3.3	A high order compact 9-point finite difference scheme for computing u using uniform Cartesian grids	59
3.3.1	Stencils for regular points	59
3.3.2	Stencils for irregular points	61
3.3.3	Convergence analysis	65
3.4	A high order local approximation for computing ∇u using uniform Cartesian grids	71
3.4.1	Compute ∇u at regular points	71
3.4.2	Compute ∇u at irregular points	73
3.5	Numerical experiments	75
3.5.1	Numerical examples with u known	75
3.5.2	Numerical examples with u unknown	78
3.6	Conclusion	81
3.7	Proof of Theorem 3.3	83
4	Hybrid Finite Difference Schemes for Elliptic Interface Problems with Discontinuous and High-Contrast Variable Coefficients	87
4.1	Introduction and problem formulation	87
4.2	Hybrid finite difference methods using uniform Cartesian grids	91
4.2.1	Stencils for regular points (interior)	92
4.2.2	Stencils for boundary and corner points	93
4.2.3	Stencils for irregular points	99
4.3	Numerical experiments	103
4.3.1	Numerical examples with known u	103
4.3.2	Numerical examples with unknown u	109
4.4	Conclusion	112
4.5	Proofs of Theorems 4.1 to 4.8	114
5	Sixth Order Compact Finite Difference Methods for 2D Helmholtz Equations with Singular Sources and Reduced Pollution Effect	117
5.1	Introduction and problem formulation	117
5.2	Sixth order compact finite difference schemes with reduced pollution effect using uniform cartesian grids	119
5.2.1	Stencils for regular points (interior)	123
5.2.2	Stencils for boundary and corner points	124

5.2.3	Stencils for irregular points	129
5.3	Numerical experiments	131
5.3.1	Numerical examples with no interfaces	131
5.3.2	Numerical examples with interfaces	133
5.4	Conclusion	135
5.5	Proofs of Theorems 5.2 to 5.5	136
6	Sixth Order Compact 9-Point Finite Difference Schemes for Elliptic Inter-	
	face Problems with Particular Intersecting Interfaces	144
6.1	Introduction and problem formulation	144
6.2	Sixth order compact 9-point finite difference schemes using uniform Cartesian	
	grids	146
6.2.1	Stencils for regular points	148
6.2.2	Stencils for interface points	148
6.2.3	Stencils for the intersection point	152
6.2.4	Convergence analysis	153
6.3	Numerical experiments	154
6.4	Conclusion	157
6.5	Proofs of Theorems 6.2 to 6.6	157
7	Future Work	171
	Bibliography	173

List of Tables

2.1	Performance in Example 2.1 of the proposed sixth order compact 9-point finite difference scheme in Theorems 2.3 and 2.5 on uniform Cartesian meshes with $h = 2^{-J} \times 2\pi$. κ is the condition number of the coefficient matrix.	33
2.2	Performance in Example 2.2 of the proposed sixth order compact 9-point finite difference scheme in Theorems 2.3 and 2.5 on uniform Cartesian meshes with $h = 2^{-J} \times 1$	34
2.3	Performance in Example 2.3 of the proposed sixth order compact 9-point finite difference scheme in Theorems 2.3 and 2.5 on uniform Cartesian meshes with $h = 2^{-J} \times 3\pi$	35
2.4	Performance in Example 2.4 of the proposed sixth order compact 9-point finite difference scheme in Theorems 2.3 and 2.5 on uniform Cartesian meshes with $h = 2^{-J} \times 1$	36
2.5	Performance in Example 2.5 of the proposed sixth order compact 9-point finite difference scheme in Theorems 2.3 and 2.5 on uniform Cartesian meshes with $h = 2^{-J} \times 3\pi$	37
2.6	Performance in Examples 2.6 and 2.7 of the proposed sixth order compact 9-point finite difference scheme in Theorems 2.3 and 2.5 on uniform Cartesian meshes with the same mesh size $h = 2^{-J} \times 2\pi$	38
2.7	Performance in Examples 2.8 and 2.9 of the proposed sixth order compact 9-point finite difference scheme in Theorems 2.3 and 2.5 on uniform Cartesian meshes with the same mesh size $h = 2^{-J} \times 2\pi$	40
2.8	Performance in Example 2.10 of the proposed sixth order compact 9-point finite difference scheme in Theorems 2.3 and 2.5 on uniform Cartesian meshes with $h = 2^{-J} \times 1$	41
2.9	Performance in Examples 2.11 and 2.12 of the proposed sixth order compact 9-point finite difference scheme in Theorems 2.3 and 2.5 on uniform Cartesian meshes with $h = 2^{-J} \times 2\pi$ and $h = 2^{-J} \times 3.5$ respectively.	43

2.10 Performance in Examples 2.13 and 2.14 of the proposed sixth order compact 9-point finite difference scheme in Theorems 2.3 and 2.5 on uniform Cartesian meshes with $h = 2^{-J} \times 2\pi$ and $h = 2^{-J} \times 3\pi$ respectively.	44
3.1 Case 1 of Example 3.1 with $b = 10$, $C = 0.1$, $\Omega = (-1, 1)^2$ and $h = 2/N_1$. The ratio r_1 is equal to $\ u_h - u\ _\infty$ of [69, 2nd-IIM] divided by $\ u_h - u\ _\infty$ of our proposed method and the ratio r_2 is equal to $\ u_h - u\ _\infty$ of [110, 2nd-EJIIM] divided by $\ u_h - u\ _\infty$ of our proposed method. In other words, for the same grid size h with $h = 2/N_1$, the errors of [69, 2nd-IIM] and [110, 2nd-EJIIM] are r_1 and r_2 times larger than those of our proposed method, respectively.	76
3.2 Case 1 of Example 3.1 with $C = 0.1$, $\Omega = (-1, 1)^2$ and $h = 2/N_1$. The ratio r_1 is equal to $\ u_h - u\ _\infty/ u(1, 1) $ of [117, 2nd-IIM] divided by $\ u_h - u\ _\infty/ u(1, 1) $ of our proposed method and the ratio r_2 is equal to $\ u_h - u\ _\infty/ u(1, 1) $ of [117, 4th-IIM] divided by $\ u_h - u\ _\infty/ u(1, 1) $ of our proposed method. In other words, for the same grid size h with $h = 2/N_1$, the errors of [117, 2nd-IIM] and [117, 4th-IIM] are r_1 and r_2 times larger than those of our proposed method, respectively.	76
3.3 Case 2 of Example 3.1 with $b = 10$, $\Omega = (-1, 1)^2$ and $h = 2/N_1$. The ratio r_1 is equal to $\ u_h - u\ _\infty$ of [119, 2nd-MIB] divided by $\ u_h - u\ _\infty$ of our proposed method and the ratio r_2 is equal to $\ u_h - u\ _\infty$ of [69, 2nd-IIM] divided by $\ u_h - u\ _\infty$ of our proposed method. In other words, for the same grid size h with $h = 2/N_1$, the errors of [119, 2nd-MIB] and [69, 2nd-IIM] are r_1 and r_2 times larger than those of our proposed method, respectively.	77
3.4 Case 3 and Case 4 of Example 3.1. The ratio r_1 is equal to $\ u_h - u\ _\infty$ of [17, 2nd-IIM] divided by $\ u_h - u\ _\infty$ of our proposed method and the ratio r_2 is equal to $\ u_h - u\ _\infty$ of [39, 2nd-AMIB] divided by $\ u_h - u\ _\infty$ of our proposed method. In other words, for the same grid size h , the errors of [17, 2nd-IIM] and [39, 2nd-AMIB] are r_1 and r_2 times larger than those of our proposed method, respectively.	77
3.5 Performance in Example 3.2 of our proposed method on uniform Cartesian meshes with $h = 2^{-J} \times 2\pi$	77
3.6 Performance in Example 3.3 of our proposed method on uniform Cartesian meshes with $h = 2^{-J} \times 7$	78
3.7 Performance in Example 3.4 of our proposed method on uniform Cartesian meshes with $h = 2^{-J} \times 4\pi/3$	79

3.8	Performance in Example 3.5 of our proposed method on uniform Cartesian meshes with $h = 2^{-J} \times 5$.	80
3.9	Performance in Example 3.6 of our proposed method on uniform Cartesian meshes with $h = 2^{-J} \times 3$.	81
4.1	Performance in Example 4.1 of our proposed hybrid finite difference scheme and compact 9-point scheme on uniform Cartesian meshes with $h = 2^{-J} \times 3$. κ is the condition number of the coefficient matrix.	105
4.2	Performance in Example 4.2 of our proposed hybrid finite difference scheme and compact 9-point scheme on uniform Cartesian meshes with $h = 2^{-J} \times 9$. κ is the condition number of the coefficient matrix.	106
4.3	Performance in Example 4.3 of our proposed hybrid finite difference scheme on uniform Cartesian meshes with $h = 2^{-J} \times 5$.	106
4.4	Performance in Example 4.4 of our proposed hybrid finite difference scheme on uniform Cartesian meshes with $h = 2^{-J} \times 4$.	107
4.5	Performance in Example 4.5 of our proposed hybrid finite difference scheme on uniform Cartesian meshes with $h = 2^{-J} \times 5$.	108
4.6	Performance in Example 4.6 of our proposed hybrid finite difference scheme on uniform Cartesian meshes with $h = 2^{-J} \times 5$.	109
4.7	Performance in Example 4.7 of our proposed hybrid finite difference scheme on uniform Cartesian meshes with $h = 2^{-J} \times 2\pi$.	110
4.8	Performance in Example 4.8 of our proposed hybrid finite difference scheme on uniform Cartesian meshes with $h = 2^{-J} \times \pi$.	111
4.9	Performance in Example 4.9 of our proposed hybrid finite difference scheme on uniform Cartesian meshes with $h = 2^{-J} \times 5$.	112
4.10	Performance in Example 4.10 of our proposed hybrid finite difference scheme on uniform Cartesian meshes with $h = 2^{-J} \times 2\pi$.	113
5.1	Numerical results for Example 5.1 with $h = 1/2^J$. The ratio r is equal to $\frac{\ u_h - u\ _{2,w}}{\ u\ _{2,w}}$ of [20] divided by $\frac{\ u_h - u\ _{2,w}}{\ u\ _{2,w}}$ of our proposed method. In other words, for the same mesh size h with $h = 2^{-J}$, the error of [20] is r times larger than that of our proposed method.	132
5.2	Numerical results of Example 5.2 with $h = 1/2^J$ and $k = 300$. The ratio r_1 is equal to $\frac{\ u_h - u\ _2}{\ u\ _2}$ of [104] divided by $\frac{\ u_h - u\ _2}{\ u\ _2}$ of our proposed method and the ratio r_2 is equal to $\frac{\ u_h - u\ _2}{\ u\ _2}$ of [111] divided by $\frac{\ u_h - u\ _2}{\ u\ _2}$ of our proposed method. In other words, for the same grid size h with $h = 2^{-J}$, the errors of [104] and [111] are r_1 and r_2 times larger than those of our proposed method, respectively.	132

5.3	Numerical results of Example 5.3 with $h = 1/2^J$ using our proposed method.	133
5.4	Numerical results of Example 5.4 with $h = 1/2^J$ using our proposed method.	133
5.5	Numerical results of Examples 5.5 to 5.7 with $h = (l_2 - l_1)/2^J$ using our proposed method.	135
6.1	Performance in Example 6.1 of our proposed sixth order compact 9-point finite difference scheme on uniform Cartesian meshes with $h = 2^{-J} \times 1$	154
6.2	Performance in Example 6.2 of our proposed sixth order compact 9-point finite difference scheme on uniform Cartesian meshes with $h = 2^{-J} \times 1$	155
6.3	Performance in Example 6.3 of our proposed sixth order compact 9-point finite difference scheme on uniform Cartesian meshes with $h = 2^{-J} \times 1$	156

List of Figures

1.1	The problem region $\Omega = (-\pi, \pi)^2$ and the two subregions $\Omega_+ = \{(x, y) \in \Omega : \psi(x, y) > 0\}$ and $\Omega_- = \{(x, y) \in \Omega : \psi(x, y) < 0\}$ partitioned by the interface curve $\Gamma = \{(x, y) \in \Omega : \psi(x, y) = 0\}$ with the functions $\psi(x, y) = x^2 + y^2 - 2$ (left) and $\psi(x, y) = y - \cos(x)$ (right). Note that $\Omega \setminus \Gamma = \Omega_+ \cup \Omega_-$	8
1.2	An example of regular points. The curve in red color is the interface curve Γ .	9
1.3	Examples for irregular points. The curve in red color is the interface curve Γ .	10
1.4	Examples for irregular points. The curve in red color is the interface curve Γ .	10
1.5	Examples for irregular points. The curve in red color is the interface curve Γ .	11
1.6	A compact 9-point scheme in the interior point (left), compact 6-point schemes in boundary side points (middle) and compact 4-point schemes in corner points (right). Red points are the centered points.	11
2.1	The problem region $\Omega = (-\pi, \pi)^2$ and the two subregions $\Omega_+ = \{(x, y) \in \Omega : \psi(x, y) > 0\}$ and $\Omega_- = \{(x, y) \in \Omega : \psi(x, y) < 0\}$ partitioned by the interface curve $\Gamma = \{(x, y) \in \Omega : \psi(x, y) = 0\}$ with the functions $\psi(x, y) = x^2 + y^2 - 2$ (left) and $\psi(x, y) = y - \cos(x)$ (right). Note that $\Omega \setminus \Gamma = \Omega_+ \cup \Omega_-$	18
2.2	Red trapezoid: $\{u^{(m,n)} : (m, n) \in \Lambda_{M+1}^1\}$ with $M = 6$. Blue trapezoid: $\{u^{(m,n)} : (m, n) \in \Lambda_{M+1}^2\}$ with $M = 6$. Note that $\Lambda_{M+1} = \Lambda_{M+1}^1 \cup \Lambda_{M+1}^2$	22
2.3	Top row for Example 2.1: the interface curve Γ (left), the numerical solution u_h (middle) and the error $u - u_h$ (right) with $h = 2^{-7} \times 2\pi$. Bottom row for Example 2.2 with $K = 500$: the interface curve Γ (left), the numerical solution u_h (middle) and the error $u - u_h$ (right) with $h = 2^{-12} \times 1$	35
2.4	Top row for Example 2.3: the interface curve Γ (left), the numerical solution u_h (middle) and the error $u - u_h$ (right) with $h = 2^{-7} \times 3\pi$. Bottom row for Example 2.4 with $K = 500$: the interface curve Γ (left), the numerical solution u_h (middle) and the error $u - u_h$ (right) with $h = 2^{-12} \times 1$	37
2.5	Example 2.5: the interface curve Γ (left), the numerical solution u_h (middle) and the error $u - u_h$ (right) with $h = 2^{-7} \times 3\pi$	37

2.6	Top row for Example 2.6: the interface curve Γ (left) and the numerical solution u_h (right) with $h = 2^{-7} \times 2\pi$. Bottom row for Example 2.7: the interface curve Γ (left) and the numerical solution u_h (right) with $h = 2^{-7} \times 2\pi$.	39
2.7	Top row for Example 2.8: the interface curve Γ (left) and the numerical solution u_h (right) with $h = 2^{-7} \times 2\pi$. Bottom row for Example 2.9: the interface curve Γ (left) and the numerical solution u_h (right) with $h = 2^{-7} \times 2\pi$.	40
2.8	Top row for Example 2.10: the interface curve Γ (left), the numerical solution u_h with $K = 5$, $h = 2^{-7} \times 1$ (middle) and the numerical solution u_h with $K = 50$, $h = 2^{-8} \times 1$ (right). Bottom row for Example 2.10 with $K = 500$ and $h = 2^{-11} \times 1$: the numerical solution u_h in $(0, 1)^2$ (left), the numerical solution u_h in $(0.32, 0.4) \times (0.34, 0.4)$ (middle) and the numerical solution u_h in $(0.25, 0.3) \times (0.4, 0.5)$ (right).	42
2.9	Top row for Example 2.11: the interface curve Γ (left) and the numerical solution u_h (right) with $h = 2^{-7} \times 2\pi$. Bottom row for Example 2.12: the interface curve Γ (left) and the numerical solution u_h (right) with $h = 2^{-7} \times 3.5$.	43
2.10	Top row for Example 2.13: the interface curve Γ (left) and the numerical solution u_h (right) with $h = 2^{-7} \times 2\pi$. Bottom row for Example 2.14: the interface curve Γ (left) and the numerical solution u_h (right) with $h = 2^{-7} \times 3\pi$.	45
3.1	The problem region $\Omega = (-\pi, \pi)^2$ and the two subregions $\Omega_+ = \{(x, y) \in \Omega : \psi(x, y) > 0\}$ and $\Omega_- = \{(x, y) \in \Omega : \psi(x, y) < 0\}$ partitioned by the interface curve $\Gamma = \{(x, y) \in \Omega : \psi(x, y) = 0\}$ with the function $\psi(x, y) = x^2 + y^2 - 2$.	54
3.2	Red trapezoid: $\{u^{(m,n)} : (m, n) \in \Lambda_{M+1}^1\}$ with $M = 4$. Blue trapezoid: $\{u^{(m,n)} : (m, n) \in \Lambda_{M+1}^2\}$ with $M = 4$. Note that $\Lambda_{M+1} = \Lambda_{M+1}^1 \cup \Lambda_{M+1}^2$.	57
3.3	Red trapezoid: $\{a^{(m,n)} : (m, n) \in \Lambda_M\}$ with $M = 4$. Blue trapezoid: $\{f^{(m,n)} : (m, n) \in \Lambda_{M-1}\}$ with $M = 4$.	58
3.4	One simple example for irregular points. The curve in red color is the interface curve $\Gamma = \{(x, y) \in \Omega : 2x - y = 0\}$, the left of Γ is Ω_- and the right of Γ is Ω_+ .	64
3.5	Five cases of irregular points when h is sufficiently small. The curve in red color is the interface curve Γ . The center point is the irregular point (x_i, y_j) .	67
3.6	Top row for Example 3.2: the interface curve Γ (left), the coefficient $a(x, y)$ (middle) and the numerical solution u_h (right) with $h = 2^{-8} \times 2\pi$. Bottom row for Example 3.2: the error $ u_h - u $ (left), the numerical $(u_h)_x$ (middle) and the error $ (u_h)_x - u_x $ (right) with $h = 2^{-8} \times 2\pi$.	78

3.7	Top row for Example 3.3: the interface curve Γ (left), the coefficient $a(x, y)$ (middle) and the numerical solution u_h (right) with $h = 2^{-8} \times 7$. Bottom row for Example 3.3: the error $ u_h - u $ (left), the numerical $(u_h)_x$ (middle) and the error $ (u_h)_x - u_x $ (right) with $h = 2^{-8} \times 7$	79
3.8	Example 3.4: the interface curve Γ (first panel), the coefficient $a(x, y)$ (second panel), the numerical solution u_h (third panel), and the numerical $(u_h)_x$ (fourth panel) with $h = 2^{-8} \times 4\pi/3$	80
3.9	Example 3.5: the interface curve Γ (first panel), the coefficient $a(x, y)$ (second panel), the numerical solution u_h (third panel), and the numerical $(u_h)_x$ (fourth panel) with $h = 2^{-8} \times 5$	80
3.10	Example 3.6: the interface curve Γ (first panel), the coefficient $a(x, y)$ (second panel), the numerical solution u_h (third panel), and the numerical $(u_h)_x$ (fourth panel) with $h = 2^{-8} \times 3$	81
4.1	For irregular points, the 9-point scheme (left) and the 13-point scheme (right). The curve in red color is the interface curve Γ	88
4.2	An example for the boundary configuration in (4.1), where α and β are two smooth 1D functions in y and x directions respectively.	89
4.3	Example 4.1: the interface curve Γ (first panel), the coefficient $a(x, y)$ (second panel), the numerical solution u_h (third panel), and the error $ u_h - u $ (fourth panel) with $h = 2^{-8} \times 3$, where u_h is computed by our proposed hybrid finite difference scheme.	105
4.4	Example 4.2: the interface curve Γ (first panel), the coefficient $a(x, y)$ (second panel), the numerical solution u_h (third panel), and the error $ u_h - u $ (fourth panel) with $h = 2^{-7} \times 9$, where u_h is computed by our proposed hybrid finite difference scheme.	106
4.5	Example 4.3: the interface curve Γ (first panel), the coefficient $a(x, y)$ (second panel), the numerical solution u_h (third panel), and the error $u - u_h$ (fourth panel) with $h = 2^{-8} \times 5$, where u_h is computed by our proposed hybrid finite difference scheme.	107
4.6	Example 4.4: the interface curve Γ (first panel), the coefficient $a(x, y)$ (second panel), the numerical solution u_h (third panel), and the error $ u_h - u $ (fourth panel) with $h = 2^{-8} \times 4$, where u_h is computed by our proposed hybrid finite difference scheme.	108

4.7	Example 4.5: the interface curve Γ (first panel), the coefficient $a(x, y)$ (second panel), the numerical solution u_h (third panel), and the error $ u_h - u $ (fourth panel) with $h = 2^{-8} \times 5$, where u_h is computed by our proposed hybrid finite difference scheme.	108
4.8	Example 4.6: the interface curve Γ (left), the coefficient $a(x, y)$ (middle) and the numerical solution u_h (right) with $h = 2^{-8} \times 5$, where u_h is computed by our proposed hybrid finite difference scheme. In order to show the graph of $a(x, y)$ clearly, we rotate the graph of $a(x, y)$ by $\pi/2$ in this figure.	110
4.9	Example 4.7: the interface curve Γ (left), the coefficient $a(x, y)$ (middle) and the numerical solution u_h (right) with $h = 2^{-8} \times 2\pi$, where u_h is computed by our proposed hybrid finite difference scheme. In order to show the graph of $a(x, y)$ clearly, we rotate the graph of $a(x, y)$ by $\pi/2$ in this figure.	110
4.10	Example 4.8: the interface curve Γ (left), the coefficient $a(x, y)$ (middle) and the numerical solution u_h (right) with $h = 2^{-8} \times \pi$, where u_h is computed by our proposed hybrid finite difference scheme.	111
4.11	Example 4.9: the interface curve Γ (left), the coefficient $a(x, y)$ (middle) and the numerical solution u_h (right) with $h = 2^{-8} \times 5$. In order to show the graph of u_h clearly, we rotate the graph of u_h by $\pi/2$ in this figure.	112
4.12	Example 4.10: the interface curve Γ (left), the coefficient $a(x, y)$ (middle) and the numerical solution u_h (right) with $h = 2^{-8} \times 2\pi$, where u_h is computed by our proposed hybrid finite difference scheme.	113
5.1	Red trapezoid: $\{u^{(m,n)} : (m, n) \in \Lambda_{M+1}^{V,1}\}$ with $M = 6$. Blue trapezoid: $\{u^{(m,n)} : (m, n) \in \Lambda_{M+1}^{V,2}\}$ with $M = 6$. Note that $\Lambda_{M+1} = \Lambda_{M+1}^{V,1} \cup \Lambda_{M+1}^{V,2}$	120
5.2	Red rectangle: $\{u^{(m,n)} : (m, n) \in \Lambda_{M+1}^{H,1}\}$ with $M = 6$. Blue triangle: $\{u^{(m,n)} : (m, n) \in \Lambda_{M+1}^{H,2}\}$ with $M = 6$. Note that $\Lambda_{M+1} = \Lambda_{M+1}^{H,1} \cup \Lambda_{M+1}^{H,2}$	121
5.3	An illustration for the boundary configuration in (5.18), where $\psi(x, y) = x^2 + y^2 - 2$	127
5.4	First row: the real part of u_h in Example 5.4, where $k = 200$ and $h = 1/2^9$ (left), $k = 400$ and $h = 1/2^{10}$ (middle), $k = 800$ and $h = 1/2^{11}$ (right). Second row: the imaginary part of u_h in Example 5.4, where $k = 200$ and $h = 1/2^9$ (left), $k = 400$ and $h = 1/2^{10}$ (middle), $k = 800$ and $h = 1/2^{11}$ (right).	134
5.5	$y^2/2 + x^2/(1+x^2) = 1/2$ (left), $x^4 + 2y^4 = 1/2$ (middle), and $y^2 - 2x^2 + x^4 = 1/2$ (right).	134
6.1	An illustration for (6.1)	145

6.2	Red trapezoid: $\{u_p^{(m,n)} : (m,n) \in \Lambda_M^{V,1}\}$ with $M = 7$ and $p = 1, 2, 3, 4$. Blue trapezoid: $\{u_p^{(m,n)} : (m,n) \in \Lambda_M^{V,2}\}$ with $M = 7$ and $p = 1, 2, 3, 4$. Note that $\Lambda_M = \Lambda_M^{V,1} \cup \Lambda_M^{V,2}$.	147
6.3	Red rectangle: $\{u_p^{(m,n)} : (m,n) \in \Lambda_M^{H,1}\}$ with $M = 7$ and $p = 1, 2, 3, 4$. Blue triangle: $\{u_p^{(m,n)} : (m,n) \in \Lambda_M^{H,2}\}$ with $M = 7$ and $p = 1, 2, 3, 4$. Note that $\Lambda_M = \Lambda_M^{H,1} \cup \Lambda_M^{H,2}$.	148
6.4	Compact 9-point schemes for irregular points of (6.1) (the center red point is not the intersection point)	149
6.5	An illustration for the compact 9-point scheme for the intersection point of (6.1)	152
6.6	Example 6.1: the coefficient $a(x,y)$ (left), the numerical solution u_h (middle) and the error $ u_h - u $ (right) with $h = 2^{-7} \times 1$, where u_h is computed by our proposed sixth order compact 9-point finite difference scheme.	155
6.7	Example 6.2: the coefficient $a(x,y)$ (left), the numerical solution u_h (middle) and the error $ u_h - u $ (right) with $h = 2^{-6} \times 1$, where u_h is computed by our proposed sixth order compact 9-point finite difference scheme.	156
6.8	Example 6.3: the coefficient $a(x,y)$ (left), the numerical solution u_h (middle) and the error $ u_h - u $ (right) with $h = 2^{-7} \times 1$, where u_h is computed by our proposed sixth order compact 9-point finite difference scheme.	156

Chapter 1

Introduction

1.1 Background

Interface problems are common in many practical problems such as modeling of composite materials, oil reservoir simulations, nuclear waste disposal, and other flows in porous media [56]. For example, in groundwater or oil reservoir modelling the permeability of the porous medium can change drastically across the interface between various geological layers and this can significantly affect the transport process [94]. The coefficient of the heterogeneous and anisotropic diffusion problem may also be highly oscillatory, and may contain a wide range of various spatial scales, so very fine meshes are required in any standard finite difference/element discretization in order to capture small scale features. Thus, speed and storage are two important criteria in choosing suitable algorithms for solving such problems.

Physical backgrounds for interface problems

By Darcy's law [105], we have

$$\vec{v} = -\frac{k}{\mu}\nabla u,$$

where \vec{v} represents the velocity of the fluid flow through a porous medium, k is the permeability, μ is the viscosity of the fluid and u is the pressure. Let ρ denote the density and ϕ denote the porosity of the medium. Then we have

$$\frac{\partial(\phi\rho)}{\partial t} + \nabla \cdot (\rho\vec{v}) = f,$$

by the conservation law. To simplify the problem, we consider the elliptic case as follows:

$$\nabla \cdot (\rho\vec{v}) = \nabla \cdot \left(-\rho\frac{k}{\mu}\nabla u\right) = -\nabla \cdot (a\nabla u) = f, \quad (1.1)$$

where $a = \rho \frac{k}{\mu}$. When μ is also a constant, a only depends on the permeability k . Because of the porous medium, k can be discontinuous, i.e., a is discontinuous across the corresponding interface.

Realistic applications that lead to interface problems

- (1) Groundwater or oil reservoir transport; the interface results from various geological layers which significantly affects the speed and quantity of the oil pumping.
- (2) Water purification with porous materials like foam metals.
- (3) In catalytic reactions the catalyst is usually distributed in a very thin layer over an interface, thus leading to problems with abrupt changes in material properties.
- (4) Problems with the discontinuous solution and/or discontinuous flux also appear in multicomponent incompressible flows with or without the interfacial tension.

Motivations for higher order compact finite difference schemes

- (1) Due to the porous medium, the solution is highly oscillatory.
- (2) The coefficient $a = \rho \frac{k}{\mu}$ in (1.1) may have abrupt jumps across the interface, leads to the pollution effect in the error.
- (3) To obtain a reasonable solution, a very fine mesh size is required for lower order schemes.
- (4) The grid size requirement for high order schemes is less stringent than low order ones.
- (5) Compared with finite element or volume methods, in finite difference methods we do not need to integrate high-frequency functions.
- (6) Since compact 9-point schemes only have nine non-zero bands in corresponding matrices, it is efficient to assemble and solve such linear systems.

Difficulties with higher order compact schemes

- (1) The discontinuities of the coefficient a , the source term f , the solution u and the flux $a \nabla u \cdot \vec{n}$ require the derivation of complicated transmission equations in order to construct high order compact schemes.
- (2) Compared with the piecewise constant coefficient, the piecewise smooth coefficient would significantly increase the complexity of the implementation.

- (3) Higher order compact schemes need to use higher order derivatives of the interface curve, so the computation of system matrices A is complicated.
- (4) If two jump conditions are both inhomogeneous (i.e., the solution and the flux are both discontinuous), the derivation of correction terms in b for higher order schemes is also challenging.
- (5) For high-frequency solutions, we need to solve systems $Ax = b$, where the size of A is very large.
- (6) There are 72 different configurations in 2D (see Figs. [1.3](#) to [1.5](#)), depending on the way the interface curve partitions the stencil.
- (7) Compact schemes near corners of the domain are difficult to be derived (see Fig. [1.6](#)), if the domain is rectangular and non-Dirichlet boundary conditions are imposed (see Figs. [4.2](#) and [5.3](#)).
- (8) For elliptic interface problems with intersecting interfaces and four discontinuous coefficients (see Figs. [6.1](#) and [6.5](#)), many transmission conditions are used to derive compact schemes with sixth order of accuracy.

The literature review

1. Poisson interface problems (the only singularity is from the source term)

One source of singularity in the solution of elliptic problems is the presence of singularities in the source term. One possible regularization of Dirac delta functions is analyzed in [\[102\]](#). The finite difference discretization of Poisson interface problems are considered by [\[103\]](#). In [\[60\]](#), the authors combine the idea of the immersed interface methods with a continuous finite element discretization to derive a high order finite element method for Poisson equations with jumps in the solution and its flux across smooth interfaces. Elliptic problems with point-located Dirac delta source terms are considered in [\[26\]](#). A second order approximation to the singular source is combined with a second order finite difference approximation of the operator on Cartesian grids with hanging nodes, that allow for local refinements around the singular points. In [\[89\]](#), the third order compact finite difference scheme was constructed for Poisson interface problems. Another finite difference version of the immersed interface method is used to solve the heat diffusion with singular sources in [\[63\]](#).

2. Elliptic interface problems

One possible approach to the resolution of the elliptic interface problem was provided by the immersed interface methods (IIM) proposed by LeVeque and Li (see [\[69, 71, 72, 74, 75, 89\]](#) and the references therein). The main idea behind this approach is to adjust the finite

difference approximation of the differential operators in the vicinity of the interface using Taylor expansions, so that the approximation order remains similar to the order of the approximation in the regions where no singularities are present, thus avoiding the need of a local grid refinement. It has been combined with finite difference, finite volume, and finite element spatial discretizations (e.g., the second order immersed finite volume element methods [30], the second order immersed finite element methods [42, 53]), with various degree of accuracy. The second order explicit-jump immersed interface method (EJIIM), introduced in [110], was based on the same idea, however, instead of modification of the discrete operators, it modified explicitly the right hand side of the problem, and derived a second order finite difference scheme for problems with discontinuous, piecewise constant coefficients. In fact this approach is quite similar to the famous immersed boundary method (IBM) of Peskin [90]. [23] considered anisotropic elliptic interface problems whose coefficient matrix is symmetric semi-positive definite and derived a hybrid discretization involving finite elements away of the interfaces, and an immersed interface finite difference approximation near or at the interfaces. The error in the maximum norm is order $O(h^2 \log \frac{1}{h})$. [117] derived a new fourth order IIM for elliptic interface problems with piecewise smooth coefficients. The second order fast iterative immersed interface method (FIIIM) for the piecewise constant case was proposed in [72].

Since the goal of Chapters 2, 3, 5 and 6 is to develop a compact high-order finite difference scheme, we provide our literature review on the works employing such discretizations as following. Exploiting the idea of the IIM, in [35] the authors constructed a fourth order compact finite difference method for the Helmholtz equation with discontinuous coefficients across straight vertical line interfaces. [17] derived a compact finite difference method for elliptic interface problems with piecewise smooth coefficients, so that the solution and its gradient can both achieve a second order of accuracy. By adding intermediate unknown variables and using the Schur complement, [89] derived the third order compact FD method for elliptic interface problems with piecewise constant but discontinuous coefficients. [75, Section 7.2.7] proposed a fourth order compact finite difference scheme for elliptic interface problems with piecewise constant coefficients. The fourth order compact finite difference scheme for elliptic interface problems with intersecting interfaces was discussed in [4]. Moreover, the fourth order compact finite difference schemes for the elliptic equations on irregular domains were derived in [59, 75]. For elliptic interface problems with discontinuous coefficients in one-dimensional spaces, the section 3 of [51] proved the existence of the compact 3-point finite difference scheme with arbitrarily high accuracy orders.

Furthermore, for the elliptic interface problems with discontinuous coefficients and singular sources, a high-order method was constructed by combining a Discontinuous Galerkin

(DG) spatial discretization and IBM in [10], and the matched interface and boundary (MIB) methods were proposed in [39, 112, 113, 118, 119]. The related papers of MIB for the elliptic interface problems can be summarized as: second order MIB [113], fourth order MIB [118], fourth order MIB with the FFT acceleration [39], sixth order MIB [112, 119].

High jumps in the coefficient functions can cause severe singularities in the exact solutions of the equations [8, 14, 40, 64, 65, 66, 67, 68, 87, 88, 92, 93]. In general, the solutions of such problems have limited smoothness and the error analysis of their approximations by finite elements, [27], and finite differences, [96], for problems with weak solutions could be used. However, such error estimates show convergence rates that are lower than the observed in the computational practice for interface problems. Thus, an accurate tailored approximation and an error analysis which takes into account the specificity of such problem is an important and challenging task. Singular solutions, induced by discontinuous coefficients of singular sources can be approximated using a continuous finite element approximation, by enriching the basis with singular functions located in the proper spatial locations, as considered in [6, 14, 40, 47, 66, 67, 68]. Alternatively, a posteriori error estimates can be used to devise grid refinement algorithms, as demonstrated for example in [93], where such estimates were provided in case of interface problems with discontinuous coefficients. Several other numerical techniques for elliptic interface problems are based on (continuous and discontinuous) finite element and finite volume methods (e.g., see [5, 9, 29, 30, 42, 47, 52, 53, 77]).

In addition to the treatment of interface problems, Taylor expansions can be used to derive high order compact finite difference schemes for regular elliptic problems. A family of fourth and sixth order compact finite difference methods for the three-dimensional Poisson equation were derived in [114]. [98] concluded that the highest order for a compact finite difference method for the two-dimensional Poisson's equation on uniform grids is sixth. There also exist some sixth order compact finite difference schemes for the parabolic equation [73], the Helmholtz equation ([86, 104, 111]) and the Burgers' equation [97].

3. Helmholtz equations

The authors in [83] considered the interior impedance problem and discovered that the quasi-optimality in the hp -finite element method setting can be achieved by choosing a polynomial degree p and a mesh size h such that $p \geq C \log(k)$ (for some positive C independent of k , h , p) and kh/p is small enough. The authors in [24] found that for sufficiently small $k^{2p+1}h^{2p}$, the leading pollution term in an upper bound of the standard Sobolev H^1 -norm is $k^{2p+1}h^{2p}$. This coincides with the numerical dispersion studied in [3, 58]. For order 2 finite difference methods, [16, 18] found that $k^3h^2 \leq C$ (for some positive C independent of k , h) is required to obtain a reasonable solution. Meanwhile, for order 4 finite difference method, [21] found that $k^5h^4 \leq C$ (for some positive C independent of k , h) is required to obtain a

reasonable solution.

When a large wavenumber k is present, the mesh size used in the discretization of the Helmholtz equation has to be very small to obtain a reasonable solution. That is, the size of the coefficient matrix becomes very large. Additionally, the matrix arising from standard discretization of the Helmholtz equation is sign-indefinite. In numerical computations, we observe these coefficient matrices are ill-conditioned especially in the region where kh is small (i.e., the region where the approximated solution is reasonable). Thus, a lot of research effort has been invested in developing ways to cope with these enormous ill-conditioned linear systems. Various preconditioners and domain decomposition methods have been developed over the years (see [41] and references therein). Many variants of finite element/Galerkin/variational methods have been explored. For example, [36, 37] relaxed the inter-element continuity condition and imposed penalty terms on jumps across the element edges. A class of Trefftz methods, where the trial and test functions consist of local solutions to the underlying (homogeneous) Helmholtz equation, were considered in [55] and references therein. In recent years, multiscale finite element method has also become an appealing alternative to deal with the pollution effect [91]. By minimizing the ratio between the true and numerical wavenumbers, [16, 18, 21, 101, 111] derived the schemes with minimum dispersion. The resulting stencils have accuracy orders 2 in [16, 18], 4 in [21], and 6 in [111]. The number of points used in the proposed stencil varies from 9 in [16, 111], 13 in [22], and both 17 and 25 in [21]. Other studies on finite difference methods that do not explicitly consider the numerical dispersion are [11] (a 4th order compact FDM on polar coordinates), [12] (a 4th order compact FDM), [104] (a 6th order compact FDM), and [116] (a 6th order FDM with non-compact stencils for corners and boundaries). The authors in [89] proposed a 3rd order compact immersed interface method for Helmholtz interface problems. A characterization of the pollution effect in terms of eigenvalues was done in [25]. The authors in [20] showed that the order of the numerical dispersion matches the order of the finite difference scheme for all plane wave solutions. It is widely accepted that the pollution effect in standard discretizations arising from finite element and finite difference methods cannot be eliminated for 2D and higher dimensions [7]. However, in 1D, the pollution free finite difference methods were derived in [51, 107], which are used to solve special 2D Helmholtz equations [51, 108].

4. Boundary Treatments

A comprehensive literature review of the finite difference approximation of mixed boundary conditions in rectangular domains can be found in [76]. In addition, one should also mention the following literature concerned with the discretization of the boundary conditions for elliptic/Helmholtz problems: the sixth order 6-point finite difference scheme for

1-side Neumann and 3-side Dirichlet boundary conditions of Helmholtz equations with constant wave numbers [86], the sixth order 5-point or 6-point finite difference schemes for 1-side Neumann/Robin and 3-side Dirichlet boundary conditions of Helmholtz equations with variable wave numbers [104], the fourth order MIB for 4-side Robin boundary conditions of elliptic interface problems [39], up to 8th order MIB for mixed boundary conditions of Dirichlet, Neumann and Robin with all constant coefficients of Poisson/Helmholtz equations [38].

Finite difference methods have also been successfully applied to various boundary conditions in non-rectangular domains. In [95] a fourth order MIB for Dirichlet, Neumann, and Robin boundary conditions has been proposed. [110] developed a second order explicit-jump immersed interface method for problems with Dirichlet and Neumann boundary conditions, and [59, 75] proposed fourth order finite difference schemes for various combinations of boundary conditions. The method of difference potentials was studied in ([13] fourth order accuracy, [82] fourth and sixth order accuracy) to handle a domain with a smooth nonconforming boundary and mixed boundary conditions.

1.2 Preliminaries

1.2.1 Basic definitions

Let $\Omega = (l_1, l_2) \times (l_3, l_4)$ be a two-dimensional rectangular region. We define a smooth curve

$$\Gamma := \{(x, y) \in \Omega : \psi(x, y) = 0\},$$

which partitions Ω into two subregions: $\Omega_+ := \{(x, y) \in \Omega : \psi(x, y) > 0\}$ and $\Omega_- := \{(x, y) \in \Omega : \psi(x, y) < 0\}$, where $\psi(x, y)$ is a smooth function in 2D. We also define $a_{\pm} := a\chi_{\Omega_{\pm}}$, $f_{\pm} := f\chi_{\Omega_{\pm}}$ and $u_{\pm} := u\chi_{\Omega_{\pm}}$. Because we shall use uniform Cartesian meshes, we require that the longer side of Ω should be a multiple of the shorter side of Ω . Without loss of generality, we can assume $l_4 - l_3 = N_0(l_2 - l_1)$ for some positive integer N_0 . For any positive integer $N_1 \in \mathcal{N}$, we define $N_2 := N_0N_1$ and then the grid size is $h := (l_2 - l_1)/N_1 = (l_4 - l_3)/N_2$.

Let $x_i = l_1 + ih$ and $y_j = l_3 + jh$ for $i = 1, \dots, N_1 - 1$ and $j = 1, \dots, N_2 - 1$. Because in most chapters we are only interested in compact 9-point finite difference schemes on uniform Cartesian grids, for a compact 9-point stencil centered at the center point (x_i, y_j) , the compact 9-point stencil involves nine points $(x_i + kh, y_j + lh)$ for $k, l \in \{-1, 0, 1\}$. Now the interface curve Γ splits these nine points into two groups depending on whether these points

lie inside Ω_+ or Ω_- . The particular examples for $\psi(x, y) = x^2 + y^2 - 2$ and $\psi(x, y) = y - \cos(x)$ are illustrated in Fig. [1.1](#).

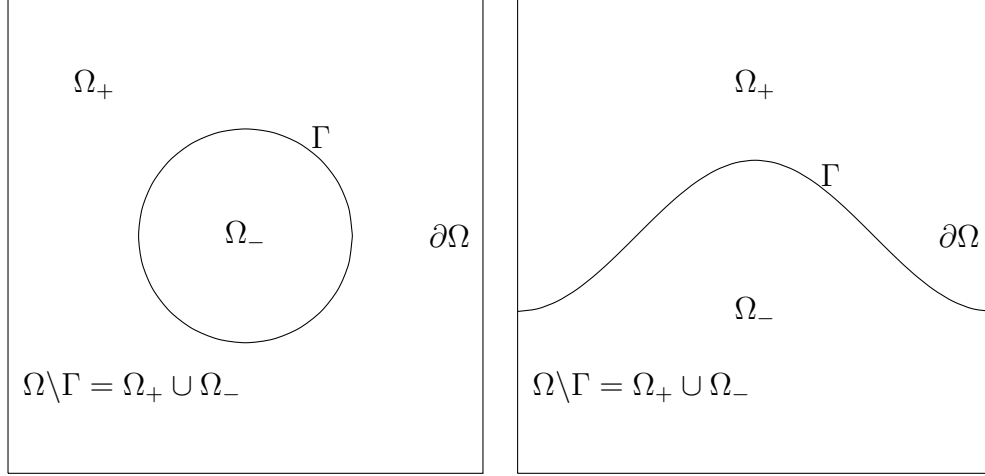


Figure 1.1: The problem region $\Omega = (-\pi, \pi)^2$ and the two subregions $\Omega_+ = \{(x, y) \in \Omega : \psi(x, y) > 0\}$ and $\Omega_- = \{(x, y) \in \Omega : \psi(x, y) < 0\}$ partitioned by the interface curve $\Gamma = \{(x, y) \in \Omega : \psi(x, y) = 0\}$ with the functions $\psi(x, y) = x^2 + y^2 - 2$ (left) and $\psi(x, y) = y - \cos(x)$ (right). Note that $\Omega \setminus \Gamma = \Omega_+ \cup \Omega_-$.

If a grid point lies on the curve Γ , then the grid point lies on the boundaries of both Ω_+ and Ω_- . For simplicity we may assume that the grid point belongs to Ω_- and we can use the interface conditions to handle such a grid point. Therefore, we naturally define

$$d_{i,j}^+ := \{(k, \ell) : k, \ell \in \{-1, 0, 1\}, \psi(x_i + kh, y_j + \ell h) > 0\} \quad (1.2)$$

and

$$d_{i,j}^- := \{(k, \ell) : k, \ell \in \{-1, 0, 1\}, \psi(x_i + kh, y_j + \ell h) \leq 0\}. \quad (1.3)$$

That is, the interface curve Γ splits the nine points in a compact 9-point stencil into two disjoint sets $\{(x_{i+k}, y_{j+\ell}) : (k, \ell) \in d_{i,j}^+\} \subseteq \Omega_+$ and $\{(x_{i+k}, y_{j+\ell}) : (k, \ell) \in d_{i,j}^-\} \subseteq \Omega_- \cup \Gamma$. We say that a grid/center point (x_i, y_j) is a *regular point* if $d_{i,j}^+ = \emptyset$ or $d_{i,j}^- = \emptyset$. That is, the center point (x_i, y_j) of a stencil is regular if all its nine points are completely inside Ω_+ (hence $d_{i,j}^- = \emptyset$) or inside $\Omega_- \cup \Gamma$ (i.e., $d_{i,j}^+ = \emptyset$). See Fig. [1.2](#) for an example of regular points. Otherwise, the center point (x_i, y_j) of a stencil is called an *irregular point* if $d_{i,j}^+ \neq \emptyset$ and $d_{i,j}^- \neq \emptyset$. That is, the interface curve Γ splits the nine points into two disjoint nonempty sets. As explained before, up to symmetry and a rigid motion, all the compact 9-point stencils at an irregular point can be classified into nine typical cases, see Figs. [1.3](#) to [1.5](#) for these nine typical cases.

Because some indices (k, ℓ) may come from $d_{i,j}^+$ while others from $d_{i,j}^-$, we need to link information on Ω_+ and Ω_- at the base point $(x_i^*, y_j^*) \in \Gamma$. To do so, instead of using the

level set function ψ to describe the interface curve Γ , we shall now assume that we have a parametric equation for Γ near the base point (x_i^*, y_j^*) . We can easily obtain such a parametric equation by locally solving $\psi(x, y) = 0$ near the base point (x_i^*, y_j^*) for either x or y . That is, it suffices to consider one of the following two relatively simple parametric representations of Γ :

$$x = t + x_i^*, \quad y = r(t) + y_j^* \quad \text{or} \quad x = r(t) + x_i^*, \quad y = t + y_j^*, \quad \text{for } t \in (-\epsilon, \epsilon) \quad \text{with } \epsilon > 0, \quad (1.4)$$

for a smooth function r , since Γ is assumed to be smooth. Note that the parameter corresponding to the base point (x_i^*, y_j^*) is $t = 0$ with $r(0) = 0$. It is important to notice that we do not need to actually solve $\psi(x, y) = 0$ to get the function r , because we only need the derivatives of $r(t)$ at $t = 0$, which can be easily obtained from $\psi(x, y) = 0$ through the Implicit Function Theorem. To cover the above two cases of parametric equations in (1.4) for Γ together, we discuss the following general parametric equation for Γ :

$$x = r(t) + x_i^*, \quad y = s(t) + y_j^*, \quad (r'(t))^2 + (s'(t))^2 > 0 \quad \text{for } t \in (-\epsilon, \epsilon) \quad \text{with } \epsilon > 0. \quad (1.5)$$

Note that the parameter t for the base point (x_i^*, y_j^*) is $t = 0$ and it is important to notice that $r(0) = s(0) = 0$.

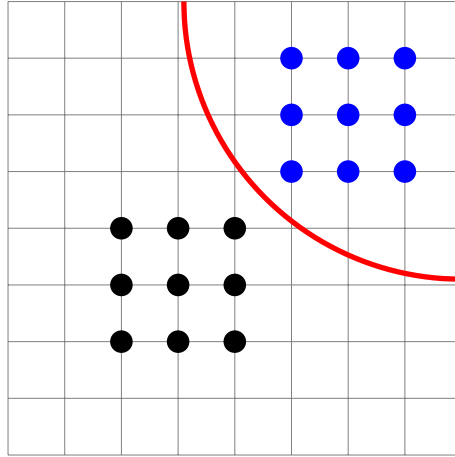


Figure 1.2: An example of regular points. The curve in red color is the interface curve Γ .

Before we discuss the schemes at a regular or an irregular point (x_i, y_j) , let us introduce some notations. We first pick up and fix a base point (x_i^*, y_j^*) inside the open square $(x_i - h, x_i + h) \times (y_j - h, y_j + h)$, i.e., we can say

$$x_i^* = x_i - v_0 h \quad \text{and} \quad y_j^* = y_j - w_0 h \quad \text{with} \quad -1 < v_0, w_0 < 1. \quad (1.6)$$

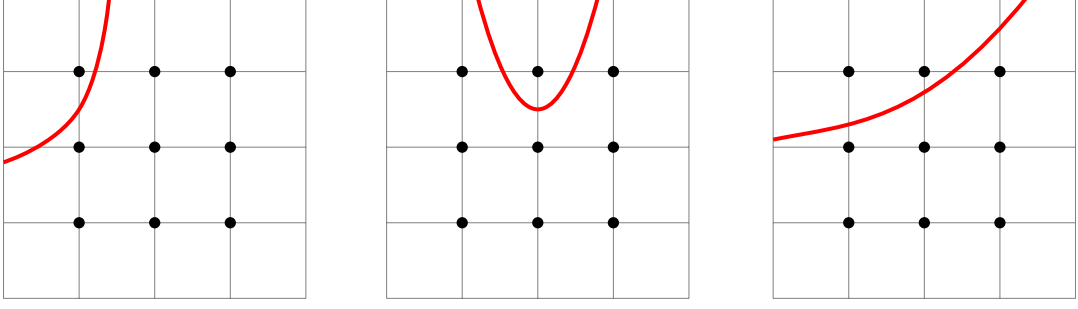


Figure 1.3: Examples for irregular points. The curve in red color is the interface curve Γ .

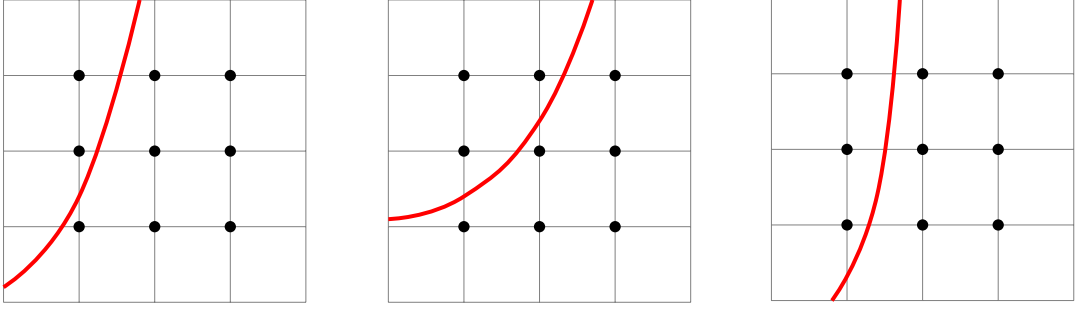


Figure 1.4: Examples for irregular points. The curve in red color is the interface curve Γ .

For simplicity, we shall use the following notions:

$$a^{(m,n)} := \frac{\partial^{m+n} a}{\partial^m x \partial^n y}(x_i^*, y_j^*), \quad u^{(m,n)} := \frac{\partial^{m+n} u}{\partial^m x \partial^n y}(x_i^*, y_j^*) \quad \text{and} \quad f^{(m,n)} := \frac{\partial^{m+n} f}{\partial^m x \partial^n y}(x_i^*, y_j^*), \quad (1.7)$$

which are just their (m, n) th partial derivatives at the base point (x_i^*, y_j^*) . Define $\mathbb{N}_0 := \mathbb{N} \cup \{0\}$, the set of all nonnegative integers. For a nonnegative integer $K \in \mathbb{N}_0$, we define

$$\Lambda_K := \{(m, n - m) : n = 0, \dots, K \text{ and } m = 0, \dots, n\}, \quad K \in \mathbb{N}_0. \quad (1.8)$$

For a smooth function u , its value $u(x + x_i^*, y + y_j^*)$ for small x, y can be well approximated through its Taylor polynomial below:

$$u(x + x_i^*, y + y_j^*) = \sum_{(m,n) \in \Lambda_{M+1}} \frac{u^{(m,n)}}{m!n!} x^m y^n + \mathcal{O}(h^{M+2}), \quad x, y \in (-2h, 2h). \quad (1.9)$$

In other words, in a neighborhood of the base point (x_i^*, y_j^*) , the function u is well approximated and completely determined by the partial derivatives of u of total degree less than $M + 2$ at the base point (x_i^*, y_j^*) , i.e., by the unknown quantities $u^{(m,n)}$, $(m, n) \in \Lambda_{M+1}$. In the same way, $a(x + x_i^*, y + y_j^*)$ and $f(x + x_i^*, y + y_j^*)$ can be approximated similarly for small x, y . For $x \in \mathbb{R}$, the floor function $\lfloor x \rfloor$ is defined to be the largest integer less than or equal

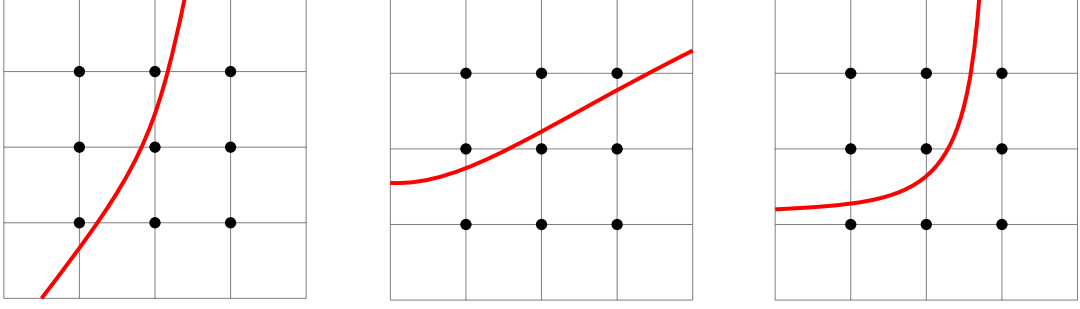


Figure 1.5: Examples for irregular points. The curve in red color is the interface curve Γ .

to x . For an integer m , we define

$$\text{odd}(m) := \begin{cases} 0, & \text{if } m \text{ is even,} \\ 1, & \text{if } m \text{ is odd.} \end{cases}$$

That is, $\text{odd}(m) = m - 2\lfloor m/2 \rfloor$ and $\lfloor m/2 \rfloor = \frac{m - \text{odd}(m)}{2}$.

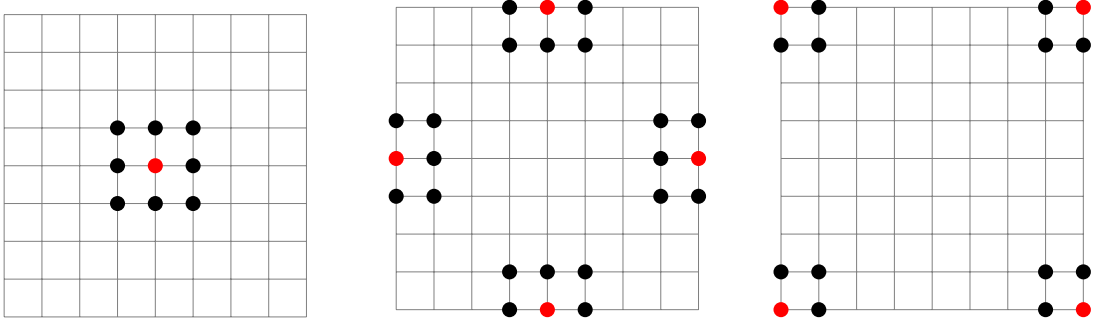


Figure 1.6: A compact 9-point scheme in the interior point (left), compact 6-point schemes in boundary side points (middle) and compact 4-point schemes in corner points (right). Red points are the centered points.

1.2.2 Error measures in numerical experiments

Let $\Omega = (l_1, l_2) \times (l_3, l_4)$ with $l_4 - l_3 = N_0(l_2 - l_1)$ for some positive integer N_0 . For a given $J \in \mathbb{N}_0$, we define $h := (l_2 - l_1)/N_1$ and let $x_i = l_1 + ih$ and $y_j = l_3 + jh$ for $i = 0, 1, \dots, N_1$ and $j = 0, 1, \dots, N_2$ with $N_2 := N_0N_1$. Let $u(x, y)$ be the exact solution and $(u_h)_{i,j}$ be the numerical solution at (x_i, y_j) using the mesh size h . If the exact solution is available, the accuracy of the scheme is verified by the errors $\frac{\|u_h - u\|_2}{\|u\|_2}$ and $\|u_h - u\|_\infty$, where

$$\|u_h - u\|_2^2 := h^2 \sum_{i=0}^{N_1} \sum_{j=0}^{N_2} ((u_h)_{i,j} - u(x_i, y_j))^2, \quad \|u\|_2^2 := h^2 \sum_{i=0}^{N_1} \sum_{j=0}^{N_2} (u(x_i, y_j))^2,$$

$$\|u_h - u\|_\infty := \max_{0 \leq i \leq N_1, 0 \leq j \leq N_2} |(u_h)_{i,j} - u(x_i, y_j)|.$$

Otherwise, we quantify the errors by

$$\begin{aligned} \|u_h - u_{h/2}\|_2^2 &:= h^2 \sum_{i=0}^{N_1} \sum_{j=0}^{N_2} \left((u_h)_{i,j} - (u_{h/2})_{2i,2j} \right)^2, \\ \|u_h - u_{h/2}\|_\infty &:= \max_{0 \leq i \leq N_1, 0 \leq j \leq N_2} \left| (u_h)_{i,j} - (u_{h/2})_{2i,2j} \right|. \end{aligned}$$

Let $(u_x(x, y), u_y(x, y))$ be the exact gradient of the exact solution and $((u_h)_x)_{i,j}, ((u_h)_y)_{i,j}$ be its numerical approximation at (x_i, y_j) using the mesh size h . If the exact solution u is available, the convergence rate of the numerical approximation of the gradient is verified by the errors $\frac{\|\nabla u_h - \nabla u\|_2}{\|\nabla u\|_2}$ and $\|\nabla u_h - \nabla u\|_\infty$, where

$$\begin{aligned} \|\nabla u_h - \nabla u\|_2^2 &:= h^2 \sum_{i=1}^{N_1-1} \sum_{j=1}^{N_2-1} \left(((u_h)_x)_{i,j} - u_x(x_i, y_j) \right)^2 + \left(((u_h)_y)_{i,j} - u_y(x_i, y_j) \right)^2, \\ \|\nabla u\|_2^2 &:= h^2 \sum_{i=1}^{N_1-1} \sum_{j=1}^{N_2-1} \left(u_x(x_i, y_j) \right)^2 + \left(u_y(x_i, y_j) \right)^2, \\ \|\nabla u_h - \nabla u\|_\infty &:= \max_{1 \leq i \leq N_1-1, 1 \leq j \leq N_2-1} \left| ((u_h)_x)_{i,j} - u_x(x_i, y_j) \right| + \left| ((u_h)_y)_{i,j} - u_y(x_i, y_j) \right|. \end{aligned}$$

If it is not, we quantify the errors by $\|\nabla u_h - \nabla u_{h/2}\|_2$ and $\|\nabla u_h - \nabla u_{h/2}\|_\infty$, where

$$\begin{aligned} \|\nabla u_h - \nabla u_{h/2}\|_2^2 &:= h^2 \sum_{i=1}^{N_1-1} \sum_{j=1}^{N_2-1} \left(((u_h)_x)_{i,j} - ((u_{h/2})_x)_{2i,2j} \right)^2 + \left(((u_h)_y)_{i,j} - ((u_{h/2})_y)_{2i,2j} \right)^2, \\ \|\nabla u_h - \nabla u_{h/2}\|_\infty &:= \max_{1 \leq i \leq N_1-1, 1 \leq j \leq N_2-1} \left| ((u_h)_x)_{i,j} - ((u_{h/2})_x)_{2i,2j} \right| + \left| ((u_h)_y)_{i,j} - ((u_{h/2})_y)_{2i,2j} \right|. \end{aligned}$$

1.3 Thesis structure

In Chapter [2](#), we derive the sixth and seventh order compact 9-point finite difference schemes at regular and irregular points for Poisson interface problems with two non-homogeneous jump functions g_0^Γ, g_1^Γ respectively (i.e., $-\nabla^2 u = f$ in $\Omega \setminus \Gamma$, $[u] = g_0^\Gamma$ and $[\nabla u \cdot \vec{n}] = g_1^\Gamma$ on Γ). We provide an expression for the jump of certain derivatives of the solution, due to the interface conditions. Using the discrete maximum principle, we prove the convergence rate of order 6 for the proposed scheme. We provide numerical experiments to check the convergence rate measured in l_2 and l_∞ norms.

In Chapter [3](#), we solve the elliptic interface problems with discontinuous, piecewise smooth and high-contrast coefficients a , and two non-homogeneous jump functions g_0^Γ, g_1^Γ (i.e., $-\nabla \cdot (a\nabla u) = f$ in $\Omega \setminus \Gamma$, $[u] = g_0^\Gamma$ and $[a\nabla u \cdot \vec{n}] = g_1^\Gamma$ on Γ). For the regular points, we construct the explicit formulas of the fourth order compact 9-point finite difference scheme for the numerical solution. For the irregular points, we derive the third order compact 9-point finite difference scheme for the numerical solution. We numerically verify the sign conditions of our proposed compact 9-point finite difference scheme and prove the fourth order convergence rate by the discrete maximum principle. On the other hand, the formulas for the local calculation of the gradient approximation at regular and irregular points are also proposed. We provide numerical results to verify the convergence rate measured in the l_2 and l_∞ norms for the numerical solution u_h , and the gradient approximation ∇u_h .

In Chapter [4](#), we also focus on the elliptic interface problems with discontinuous, piecewise smooth and high-contrast coefficients on a rectangular domain. We derive the compact 9-point finite difference scheme with sixth order accuracy for regular points. We propose the 6-point schemes with sixth order accuracy for the side points of the boundary conditions (see Fig. [4.2](#) for an illustration) $\frac{\partial u}{\partial \vec{n}} + \alpha u = g_1$ in $\partial\Omega|_1$, $\frac{\partial u}{\partial \vec{n}} = g_3$ in $\partial\Omega|_3$ and $\frac{\partial u}{\partial \vec{n}} + \beta u = g_4$ in $\partial\Omega|_4$ with two smooth functions α and β . We also construct the 4-point schemes with sixth order accuracy for the corner points of the boundary conditions (see Fig. [4.2](#) for an illustration) $\frac{\partial u}{\partial \vec{n}} + \alpha u = g_1$ in $\partial\Omega|_1$, $\frac{\partial u}{\partial \vec{n}} = g_3$ in $\partial\Omega|_3$ and $\frac{\partial u}{\partial \vec{n}} + \beta u = g_4$ in $\partial\Omega|_4$ with two smooth functions α and β . The 13-point finite difference scheme with fifth order accuracy for irregular points is constructed too. In order to achieve the implementation effectively for the 13-point scheme, we derive the details of efficient implementation. We present numerical examples with contrast ratios $\sup(a_+)/\inf(a_-) = 10^{-3}, 10^{-6}, 10^6, 10^7$ in l_2 and l_∞ norms of our proposed hybrid scheme.

In Chapter [5](#), we derive a sixth order compact 9-point finite difference scheme with reduced pollution effect to solve Helmholtz interface problems with two non-homogeneous jump functions g_0^Γ, g_1^Γ (i.e., $\Delta u + k^2 u = f$ in $\Omega \setminus \Gamma$, $[u] = g_0^\Gamma$ and $[\nabla u \cdot \vec{n}] = g_1^\Gamma$ on Γ). We start our discussion by constructing the interior finite difference stencil with reduced pollution. Second, we construct the sixth order boundary (6-point) and corner (4-point) finite difference stencils with reduced pollution. Third, we construct the compact 9-point interface finite difference stencil. When constructing a discretization stencil, we start with a general expression that allows us to recover all possible sixth order finite difference schemes. Then, we determine the remaining free parameters in the stencil by using our new pollution minimization strategy that is based on the average truncation error of plane waves. We present several numerical experiments to demonstrate the performance of our proposed compact scheme.

In Chapter [6](#), we propose a sixth order compact 9-point finite difference scheme for elliptic interface problems with particular intersecting interfaces and four discontinuous constant coefficients (see Fig. [6.1](#) for an illustration). Note that the solution is smooth enough, the intersection point is the cross point of one horizontal straight line and one vertical straight line. The uniform Cartesian mesh size h is chosen such that the centered points of all the irregular points lie on the closure of the interface curve (see Figs. [6.4](#) and [6.5](#) for illustrations). First, we construct the explicit formula of the sixth order compact 9-point finite difference scheme for regular points. Second, we derive the explicit formula of the seventh order compact 9-point finite difference scheme for interface points (see Fig. [6.4](#) for an illustration). Third, we derive the explicit formula of the seventh order compact 9-point finite difference scheme for the intersection point (see Fig. [6.5](#) for an illustration). We prove the sixth order convergence rate of our proposed compact 9-point finite difference scheme by the discrete maximum principle. We provide numerical results to verify the convergence rate measured in the l_2 and l_∞ norms for our proposed compact 9-point scheme.

In Chapter [7](#), we shall discuss some future work.

1.4 Contributions

Our contributions of Chapter [2](#) are as follows: To our best knowledge, so far there were no compact 9-point finite difference schemes available in the literature, that can achieve fifth or sixth order for Poisson interface problems with singular source terms. We construct the sixth order compact 9-point finite difference schemes on uniform meshes for Poisson interface problems with two non-homogeneous jump conditions and provide explicit formulas for the coefficients of the linear equations. The explicit formulas are independent on how the interface curve partitions the nine points in a stencil, so one can handle the 72 different cases configurations of the nine-point stencil with respect to the interface. The matrix A of the linear equations $Ax = b$, appearing after the discretization, is fixed for any source terms, two jump conditions and interface curves, and this allows for an easy design of preconditioners if iterative methods are used for the solution of the linear system associated with interface problems. The independence of A also allows us to directly use the zero extension and the FFT acceleration in [\[39\]](#) to solve $Ax = b$ without adding new unknown variables to obtain the augmented system and using the Schur complement to solve it. This is particularly useful in case of moving boundary problems. Furthermore, we prove the order 6 convergence for the proposed scheme using the discrete maximum principle. Our numerical experiments confirm the flexibility and the sixth order accuracy in l_2 and l_∞ norms of the proposed schemes.

Our contributions of Chapter [3](#) are as follows: To our best knowledge, so far there were

no compact 9-point finite difference schemes available in the literature, that can achieve third or fourth order for the elliptic interface problems with piecewise smooth coefficients on uniform meshes. We construct a high order compact 9-point finite difference scheme for the numerical solution on uniform meshes for elliptic interface problems with discontinuous, piecewise smooth and high-contrast coefficients (the ratio $\sup(a_+)/\inf(a_-) \approx 10^{-3}$ and 10^6), discontinuous source terms and two non-homogeneous jump conditions. We also numerically verify the sign conditions of our proposed compact 9-point scheme and prove the fourth order convergence rate by the discrete maximum principle. We compare our proposed compact 9-point finite difference scheme with the second order IIM, EJIIM, MIB and AMIB. Since the accuracy order in irregular points of our proposed scheme is three, the numerical results show that our proposed compact 9-point scheme produces smaller errors than the second order IIM, EJIIM, MIB and AMIB. We also compare our proposed compact 9-point finite difference scheme with the fourth order IIM, the numerical results show that our proposed compact 9-point scheme also produces smaller errors than the fourth order IIM. Since our proposed scheme does not require to change coordinates into the local coordinates and solve an optimization problem which are two basic steps for IIM, it is simpler for readers to derive our schemes, and perform the corresponding implementations. MIB methods do not use the high order jump conditions, so our method could derive a higher order scheme than MIB methods in the same number of points of the stencils. Conversely, for the same accuracy order, our method could form a sparser matrix of the global corresponding linear system than the MIB methods. Our numerical experiments confirm the flexibility and the fourth order accuracy for the numerically approximated solutions u_h in both l_2 and l_∞ norms, and the fourth/third order accuracy for the numerically approximated gradients $((u_h)_x, (u_h)_y)$ in the l_2/l_∞ norm.

Our contributions of Chapter 4 are as follows: To our best knowledge, so far there were no 13-point finite difference schemes for irregular points available in the literature, that can achieve fifth or sixth order for elliptic interface problems with discontinuous coefficients. We propose a hybrid (13-point for irregular points and compact 9-point for interior regular points) finite difference scheme, which demonstrates six order accuracy in the l_2 and l_∞ norms in all our numerical experiments, for elliptic interface problems with discontinuous, variable and high-contrast coefficients, discontinuous source terms and two non-homogeneous jump conditions. The proposed hybrid scheme demonstrates a robust sixth-order convergence for the challenging cases of high-contrast ratios of the coefficients a_\pm : $\sup(a_+)/\inf(a_-) = 10^{-3}, 10^{-6}, 10^6, 10^7$. From the numerical results, we find that if we only replace the 13-point scheme for irregular points by the 9-point scheme in Chapter 3, then the numerical errors increase significantly, while the condition number only slightly decreases. Thus, the proposed

hybrid scheme could significantly improve the numerical performance with a slight increase in the complexity of the corresponding linear system.

Our contributions of Chapter 5 are as follows: Our proposed compact (9-point, 6-point, 4-point) finite difference scheme attains at least sixth accuracy order everywhere on the domain. Our method differs from existing dispersion minimization methods in the literature in several ways. First, our method does not require us to compute the numerical wavenumber. Second, we use our pollution minimization procedure in the construction of all interior, boundary, and corner stencils. Our proposed compact finite difference scheme with reduced pollution effect outperforms several state-of-the-art finite difference schemes in the literature, particularly in the pre-asymptotic critical region where kh is near 1. When a large wavenumber k is present, this means that our proposed finite difference scheme is more accurate than others at a computationally feasible grid size. For each corner, we explicitly provide a 4-point stencil with at least sixth order accuracy and reduced pollution effect. For each side, we explicitly give a 6-point stencil with at least sixth order accuracy and reduced pollution effect. To the best of our knowledge, our present work is the first paper to comprehensively study the construction of corner and boundary finite difference stencils for all possible combinations of boundary conditions (Dirichlet, Neumann, and impedance boundary conditions) on a rectangular domain. For the irregular points, we derive a seventh order compact 9-point finite difference scheme to handle nonzero jump functions at the interface. Similar as Chapter 2, for a fixed wavenumber k and for any given interface and boundary data, the coefficient matrix of our linear system does not change; only the vector on the right-hand side of the linear system changes. In the numerical experiments, we compare our proposed scheme with the latest compact schemes. The numerical results show that our proposed scheme could produce smaller errors even the coefficients of our scheme are simpler.

Our contributions of Chapter 6 are as follows: To our best knowledge, so far there were no compact 9-point finite difference schemes available in the literature, that can achieve fifth or sixth order for elliptic interface problems with intersecting interfaces. We construct the sixth order compact 9-point finite difference scheme on uniform meshes with intersecting interfaces and 4 discontinuous constant coefficients. The formulas of proposed sixth order compact 9-point finite difference scheme are constructed explicitly for all grid points (regular points, interface points, and the intersection point). We prove the sixth order convergence rate of our proposed compact 9-point finite difference scheme by the discrete maximum principle. Our numerical experiments confirm the flexibility and the sixth order accuracy in l_2 and l_∞ norms of our proposed compact 9-point scheme.

Chapter 2

Sixth Order Compact 9-Point Finite Difference Schemes for Poisson Interface Problems with Singular Sources

2.1 Introduction and problem formulation

The Poisson interface problem with singular sources arise in many applications. In chemical reaction-diffusion processes, the solution u represents the chemical concentration [63, 15]. In case of catalytic reactions the catalyst is usually distributed in a very thin layer over an interface Γ , and therefore the reaction can be considered as occurring on a $d - 1$ -dimensional manifold in a d -dimensional space. Such reactions result in a continuous chemical concentration u , but a discontinuous gradient ∇u across the interface Γ , i.e., $g_0^\Gamma = 0$ and $g_1^\Gamma \neq 0$ on Γ in (2.1). Problems with discontinuous solutions and/or discontinuous fluxes appear also in multicomponent incompressible flows with or without interfacial tension. As discussed by [70], if surface tension is present at the interface the incompressibility constraint, applied to the momentum equation yields a pressure Poisson equation with a dipole source (the gradient of the delta function representing the interfacial tension alongside the fluid-fluid interface). Since such a source function is difficult to approximate, its effect can be modeled via interface jump conditions for the pressure and its gradient. The solution for the velocity is always continuous across the interface, however, If the viscosities of the fluids on both sides of the interface differ, its flux has a jump there. So, both the velocity and the pressure can be subject to elliptic problems with jumps of the solution or its flux across fluid-fluid or

fluid-elastic-structure interfaces.

Let $\Omega = (l_1, l_2) \times (l_3, l_4)$ be a two-dimensional rectangular region. Let also ψ be a smooth two-dimensional function and consider a smooth curve $\Gamma := \{(x, y) \in \Omega : \psi(x, y) = 0\}$, which partitions Ω into two subregions: $\Omega_+ := \{(x, y) \in \Omega : \psi(x, y) > 0\}$ and $\Omega_- := \{(x, y) \in \Omega : \psi(x, y) < 0\}$. We define $f_{\pm} := f\chi_{\Omega_{\pm}}$ and $u_{\pm} := u\chi_{\Omega_{\pm}}$. The particular examples for $\psi(x, y) = x^2 + y^2 - 2$ and $\psi(x, y) = y - \cos(x)$ are illustrated in Fig. 2.1. We now state the

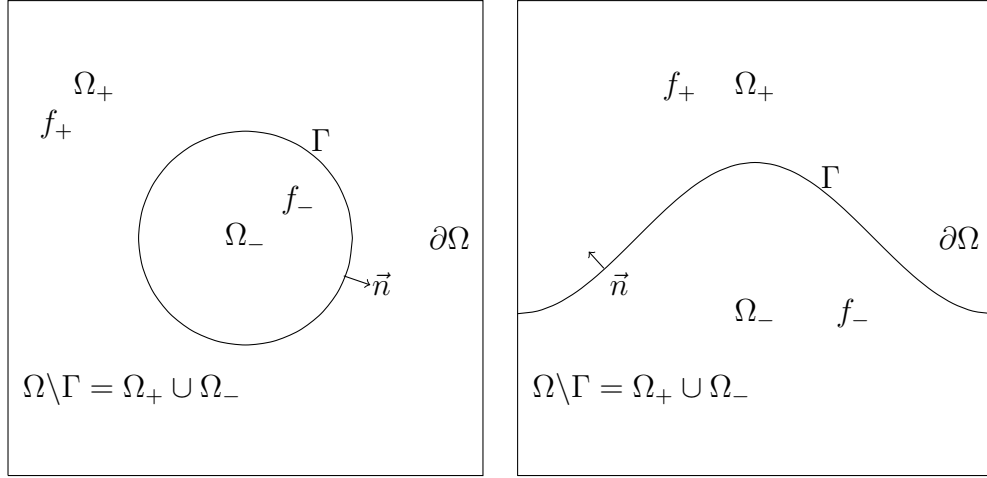


Figure 2.1: The problem region $\Omega = (-\pi, \pi)^2$ and the two subregions $\Omega_+ = \{(x, y) \in \Omega : \psi(x, y) > 0\}$ and $\Omega_- = \{(x, y) \in \Omega : \psi(x, y) < 0\}$ partitioned by the interface curve $\Gamma = \{(x, y) \in \Omega : \psi(x, y) = 0\}$ with the functions $\psi(x, y) = x^2 + y^2 - 2$ (left) and $\psi(x, y) = y - \cos(x)$ (right). Note that $\Omega \setminus \Gamma = \Omega_+ \cup \Omega_-$.

Poisson interface problem with singular sources as follows:

$$\begin{cases} -\nabla^2 u = f & \text{in } \Omega \setminus \Gamma, \\ [u] = g_0^\Gamma & \text{on } \Gamma, \\ [\nabla u \cdot \vec{n}] = g_1^\Gamma & \text{on } \Gamma, \\ u = g & \text{on } \partial\Omega, \end{cases} \quad (2.1)$$

which, if $g_0^\Gamma = 0$, can be equivalently rewritten as

$$\begin{cases} -\nabla^2 u = f - g_1^\Gamma \delta_\Gamma & \text{in } \Omega, \\ u = g & \text{on } \partial\Omega. \end{cases}$$

Here \vec{n} is the unit normal vector of Γ pointing towards Ω_+ , and for a point $(x_0, y_0) \in \Gamma$,

$$[u](x_0, y_0) := \lim_{(x,y) \in \Omega_+, (x,y) \rightarrow (x_0,y_0)} u(x, y) - \lim_{(x,y) \in \Omega_-, (x,y) \rightarrow (x_0,y_0)} u(x, y), \quad (2.2)$$

$$[\nabla u \cdot \vec{n}](x_0, y_0) := \lim_{(x,y) \in \Omega_+, (x,y) \rightarrow (x_0, y_0)} \nabla u(x, y) \cdot \vec{n} - \lim_{(x,y) \in \Omega_-, (x,y) \rightarrow (x_0, y_0)} \nabla u(x, y) \cdot \vec{n}. \quad (2.3)$$

The conditions in (2.2) and (2.3) are called jump conditions for interface problems. Note that $g_0^\Gamma, g_1^\Gamma : \Gamma \rightarrow \mathbb{R}$ are essentially one-dimensional functions only defined on the interface curve Γ . To obtain our sixth order compact 9-point finite difference scheme in Section 2.2 near a given point $(x_i^*, y_j^*) \in \Gamma$, we only need to employ one-dimensional functions $g_0^\Gamma \circ \gamma$ and $g_1^\Gamma \circ \gamma$ on $(-\theta, \theta)$ by using a local parametric equation $\gamma : (-\epsilon, \epsilon) \rightarrow \Gamma$ with $\epsilon > 0$, $\gamma(0) = (x_i^*, y_j^*)$, and $\|\gamma'(0)\|_2 \neq 0$ (see the proof of Theorem 2.4 in Section 2.5 for details). But for simplicity of presentation, we often state both g_0^Γ and g_1^Γ as functions of x and y in our numerical examples.

In this chapter we consider the Poisson interface problem in (2.1) under the following assumptions (Note that the main results in this chapter have been written in [32]):

- (A1) The solution u and the source term f should be both smooth in each of the subregions Ω_+ and Ω_- . Precisely, u and f should have uniformly continuous partial derivatives of (total) orders up to seven and five, respectively in each subregion.
- (A2) The interface curve Γ is smooth in the sense that for each $(x^*, y^*) \in \Gamma$, there exists a local parametric equation: $\gamma : (-\epsilon, \epsilon) \rightarrow \Gamma$ with $\epsilon > 0$ such that $\gamma(0) = (x^*, y^*)$ and $\|\gamma'(0)\|_2 \neq 0$. Furthermore, $x(t)$ and $y(t)$ in (1.5) should both have uniformly continuous derivatives of (total) order up to seven for the variable $t = 0$.
- (A3) g_0^Γ and g_1^Γ are smooth on Γ in the sense that for each $(x^*, y^*) \in \Gamma$, the one-dimensional functions $g_0^\Gamma \circ \gamma$ and $g_1^\Gamma \circ \gamma$ have uniformly continuous derivatives of orders up to six and seven, respectively, where γ is given in (A2).

The remainder of this chapter is organized as follows.

In Section 2.2, we derive the sixth order compact 9-point finite difference scheme at regular and irregular points, and discuss their consistency in Theorem 2.3 and Theorem 2.5 correspondingly. Here the center of a stencil is called a regular point if it, together with all other eight points in the stencil are completely inside Ω_+ or are completely outside Ω_+ . Otherwise, it is called an irregular point. We also give a simple proof for the maximum order of compact 9-point schemes which are based on Taylor expansion and our sort of technique at regular points. In Theorem 2.4 we provide an expression for the jump of certain derivatives of the solution, due to the interface conditions. In 2D there are 72 different configurations for the stencil, depending on how the interface curve partitions the nine points in it. Up to a symmetry and rigid motion, all configurations at an irregular point can be classified into nine typical cases, see Figs. 1.3 to 1.5 for a graphical representation of these configurations. Using

the discrete maximum principle, we prove the convergence rate of order 6 for the proposed scheme in Theorem 2.7

In Section 2.3, we provide numerical experiments to check the convergence rate measured in l_2 and l_∞ norms. We test the numerical examples in the following six cases:

- u is known, Γ is smooth and Γ does not intersect $\partial\Omega$ (includes a high frequency example);
- u is known, Γ is smooth and Γ intersects $\partial\Omega$ (includes a high frequency example);
- u is known, Γ is sharp-edged and Γ does not intersect $\partial\Omega$;
- u is unknown, Γ is smooth and Γ does not intersect $\partial\Omega$ (includes a high frequency example);
- u is unknown, Γ is smooth and Γ intersects $\partial\Omega$;
- u is unknown, Γ is sharp-edged and Γ does not intersect $\partial\Omega$.

In Section 2.4, we summarize the main contributions of this chapter. Finally, in Section 2.5 we shall provide the detailed proof for Theorem 2.4, which plays a key role in our development of the compact stencils at irregular points in Section 2.2.

Remark 2.1. The general elliptic interface problem is given by replacing the partial differential equation and the second jump condition in (2.1) by $-\nabla \cdot (a\nabla u) = f$ and $[a\nabla u \cdot \vec{n}] = g_1^\Gamma$, respectively, where the coefficient a is discontinuous across the interface curve Γ . In addition to the finite element, the finite volume and DG methods, several methods such as IIM ([69, 75, 89]), MIB ([113, 119]), and EJIIM ([110]) are proposed for the general elliptic interface problem. The Poisson interface problem considered in this chapter is a special case of the general elliptic interface problem with $a = 1$ and we obtain a sixth order compact 9-point finite difference scheme for such Poisson interface problem. The main ideas in this chapter for the simpler Poisson interface problem can be generalized to the general elliptic interface problem which has been addressed in Chapter 3. However, as discussed in Chapter 3 for the general elliptic interface problem, a compact 9-point finite difference scheme near the interface curve can only achieve no more than third order accuracy. See Chapter 3 for details on the general elliptic interface problem.

2.2 Sixth order compact 9-point finite difference schemes using uniform Cartesian grids

Because the function u is a solution to the partial differential equation in (2.1), we shall see that all the quantities $u^{(m,n)}$, $(m, n) \in \Lambda_{M+1}$ are not independent of each other. In fact, we have:

Lemma 2.2. *Let u be a function satisfying $-\nabla^2 u = f$ in $\Omega \setminus \Gamma$. If a point $(x_i^*, y_j^*) \in \Omega \setminus \Gamma$, then*

$$u^{(m,n)} = (-1)^{\lfloor \frac{m}{2} \rfloor} u^{(\text{odd}(m), n+m-\text{odd}(m))} + \sum_{\ell=1}^{\lfloor m/2 \rfloor} (-1)^\ell f^{(m-2\ell, n+2\ell-2)}, \quad \forall (m, n) \in \Lambda_{M+1}^2, \quad (2.4)$$

where the subsets Λ_{M+1}^1 and Λ_{M+1}^2 of Λ_{M+1} are defined by

$$\Lambda_{M+1}^2 := \Lambda_{M+1} \setminus \Lambda_{M+1}^1 \quad \text{with} \quad \Lambda_{M+1}^1 := \{(\ell, k - \ell) : k = \ell, \dots, M + 1 - \ell \text{ and } \ell = 0, 1\}. \quad (2.5)$$

Proof. By our assumption, we have $u_{xx} + u_{yy} = -f$ in $\Omega \setminus \Gamma$. Therefore, we obtain

$$u^{(m+2,n)} + u^{(m,n+2)} = -f^{(m,n)}, \quad \forall m, n \in \mathbb{N}_0. \quad (2.6)$$

Hence, for $(m, n) \in \Lambda_{M+1}^2$, we have $m \geq 2$ and

$$u^{(m,n)} = -f^{(m-2,n)} - u^{(m-2,n+2)}, \quad (m, n) \in \Lambda_{M+1}^2.$$

Then we can recursively apply the above identity $\frac{m-\text{odd}(m)}{2} - 1$ times to get (2.4). \square

For the convenience of the reader, see Fig. 2.2 for an illustration of the quantities $u^{(m,n)}$, $(m, n) \in \Lambda_{M+1}^1$ and $(m, n) \in \Lambda_{M+1}^2$ in Lemma 2.2 with $M = 6$.

For $M = 6$, the identities in (2.4) of Lemma 2.2 for $u^{(m,n)}$, $(m, n) \in \Lambda_7^2$ can be explicitly given by

$$\begin{aligned} u^{(2,1)} &= -f^{(0,1)} - u^{(0,3)}, & u^{(2,2)} &= -f^{(0,2)} - u^{(0,4)}, & u^{(2,3)} &= -f^{(0,3)} - u^{(0,5)}, & u^{(2,4)} &= -f^{(0,4)} - u^{(0,6)}, \\ u^{(2,5)} &= -f^{(0,5)} - u^{(0,7)}, & u^{(3,0)} &= -f^{(1,0)} - u^{(1,2)}, & u^{(3,1)} &= -f^{(1,1)} - u^{(1,3)}, & u^{(3,2)} &= -f^{(1,2)} - u^{(1,4)}, \\ u^{(3,3)} &= -f^{(1,3)} - u^{(1,5)}, & u^{(3,4)} &= -f^{(1,4)} - u^{(1,6)}, & u^{(4,0)} &= -f^{(2,0)} + f^{(0,2)} + u^{(0,4)}, \\ u^{(4,1)} &= -f^{(2,1)} + f^{(0,3)} + u^{(0,5)}, & u^{(4,2)} &= -f^{(2,2)} + f^{(0,4)} + u^{(0,6)}, & u^{(4,3)} &= -f^{(2,3)} + f^{(0,5)} + u^{(0,7)}, \\ u^{(5,0)} &= -f^{(3,0)} + f^{(1,2)} + u^{(1,4)}, & u^{(5,1)} &= -f^{(3,1)} + f^{(1,3)} + u^{(1,5)}, & u^{(5,2)} &= -f^{(3,2)} + f^{(1,4)} + u^{(1,6)}, \\ u^{(6,0)} &= -f^{(4,0)} + f^{(2,2)} - f^{(0,4)} - u^{(0,6)}, & u^{(6,1)} &= -f^{(4,1)} + f^{(2,3)} - f^{(0,5)} - u^{(0,7)}, \\ u^{(7,0)} &= -f^{(5,0)} + f^{(3,2)} - f^{(1,4)} - u^{(1,6)}. \end{aligned}$$

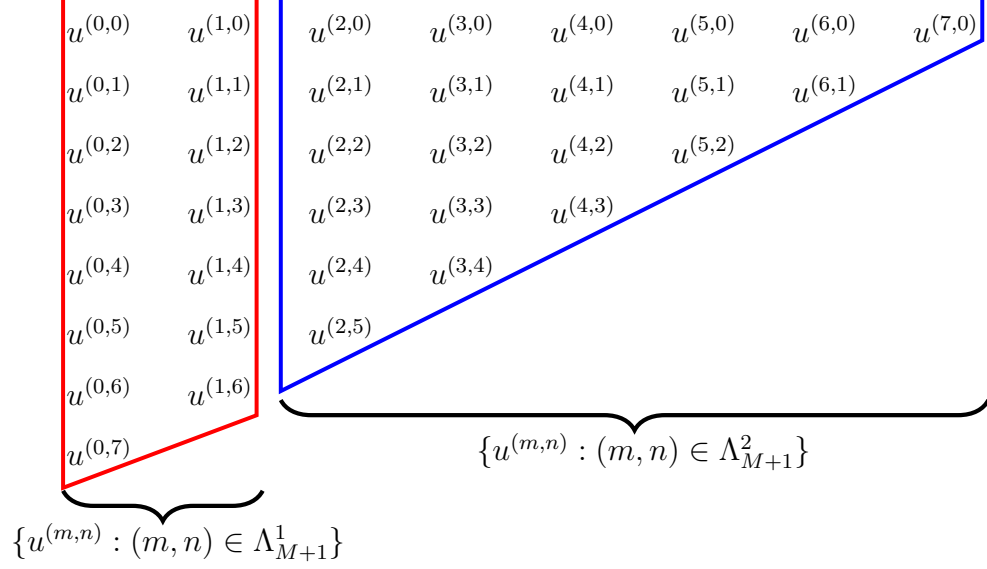


Figure 2.2: Red trapezoid: $\{u^{(m,n)} : (m, n) \in \Lambda_{M+1}^1\}$ with $M = 6$. Blue trapezoid: $\{u^{(m,n)} : (m, n) \in \Lambda_{M+1}^2\}$ with $M = 6$. Note that $\Lambda_{M+1} = \Lambda_{M+1}^1 \cup \Lambda_{M+1}^2$.

Note that the cardinality of Λ_{M+1} equals the sum of the cardinalities of Λ_{M+1}^1 and Λ_{M-1} . The identities in (2.4) of Lemma 2.2 show that every $u^{(m,n)}$, $(m, n) \in \Lambda_{M+1}$ can be written as a linear combination of the quantities $u^{(m,n)}$, $(m, n) \in \Lambda_{M+1}^1$ and $f^{(m,n)}$, $(m, n) \in \Lambda_{M-1}$. Conversely, by (2.6), every $f^{(m,n)}$, $(m, n) \in \Lambda_{M-1}$ and every $u^{(m,n)}$, $(m, n) \in \Lambda_{M+1}^1$ can be trivially written as linear combinations of $u^{(m,n)} \in \Lambda_{M+1}$. Because the source term f is known, this can reduce the number of constraints on $u^{(m,n)}$, $(m, n) \in \Lambda_{M+1}$ for the function u satisfying (2.1). Now using (2.4), we can rewrite the approximation of $u(x + x_i^*, y + y_j^*)$ in (1.9) as follows:

$$\begin{aligned}
\sum_{(m,n) \in \Lambda_{M+1}} \frac{u^{(m,n)}}{m!n!} x^m y^n &= \sum_{(m,n) \in \Lambda_{M+1}^1} \frac{u^{(m,n)}}{m!n!} x^m y^n + \sum_{(m,n) \in \Lambda_{M+1}^2} \frac{u^{(m,n)}}{m!n!} x^m y^n \\
&= \sum_{(m,n) \in \Lambda_{M+1}^1} u^{(m,n)} G_{M+1,m,n}(x, y) + \sum_{(m,n) \in \Lambda_{M-1}} f^{(m,n)} Q_{M+1,m,n}(x, y),
\end{aligned}$$

where $G_{M+1,m,n}$ and $Q_{M+1,m,n}$ are polynomials uniquely determined by the identities in (2.4). Explicitly,

$$G_{M+1,m,n}(x, y) := \sum_{\ell=0}^{\lfloor \frac{n}{2} \rfloor} (-1)^\ell \frac{x^{m+2\ell} y^{n-2\ell}}{(m+2\ell)!(n-2\ell)!}, \quad (m, n) \in \Lambda_{M+1}^1 \quad (2.7)$$

and

$$Q_{M+1,m,n}(x,y) := \sum_{\ell=1}^{1+\lfloor \frac{n}{2} \rfloor} \frac{(-1)^\ell x^{m+2\ell} y^{n-2\ell+2}}{(m+2\ell)!(n-2\ell+2)!}, \quad (m,n) \in \Lambda_{M-1}. \quad (2.8)$$

From (2.4) we observe that $G_{M+1,m,n}$ is a homogeneous polynomial of total degree $m+n$ for all $(m,n) \in \Lambda_{M+1}^1$, while $Q_{M+1,m,n}$ is a homogeneous polynomial of total degree $m+n+2$ for all $(m,n) \in \Lambda_{M-1}$. For $M=6$, all the polynomials $G_{7,m,n}$, $(m,n) \in \Lambda_7^1$ and $Q_{7,m,n}$, $(m,n) \in \Lambda_5$ are explicitly given by

$$\begin{aligned} G_{7,0,0} &= 1, & G_{7,0,1} &= y, & G_{7,0,2} &= \frac{1}{2}y^2 - \frac{1}{2}x^2, & G_{7,0,3} &= \frac{1}{6}y^3 - \frac{1}{2}x^2y, & G_{7,0,4} &= \frac{1}{24}y^4 + \frac{1}{24}x^4 - \frac{1}{4}x^2y^2, \\ G_{7,0,5} &= \frac{1}{120}y^5 - \frac{1}{12}x^2y^3 + \frac{1}{24}x^4y, & G_{7,0,6} &= \frac{1}{720}y^6 - \frac{1}{720}x^6 - \frac{1}{48}x^2y^4 + \frac{1}{48}x^4y^2, \\ G_{7,0,7} &= \frac{1}{5040}y^7 + \frac{1}{144}x^4y^3 - \frac{1}{720}x^6y - \frac{1}{240}x^2y^5, & G_{7,1,0} &= x, & G_{7,1,1} &= xy, & G_{7,1,2} &= \frac{1}{2}xy^2 - \frac{1}{6}x^3, \\ G_{7,1,3} &= \frac{1}{6}xy^3 - \frac{1}{6}x^3y, & G_{7,1,4} &= \frac{1}{24}xy^4 + \frac{1}{120}x^5 - \frac{1}{12}x^3y^2, & G_{7,1,5} &= \frac{1}{120}xy^5 - \frac{1}{36}x^3y^3 + \frac{1}{120}x^5y, \\ G_{7,1,6} &= \frac{1}{720}xy^6 - \frac{1}{5040}x^7 + \frac{1}{240}x^5y^2 - \frac{1}{144}x^3y^4, \end{aligned}$$

and

$$\begin{aligned} Q_{7,0,0} &= -\frac{1}{2}x^2, & Q_{7,0,1} &= -\frac{1}{2}x^2y, & Q_{7,0,2} &= \frac{1}{24}x^4 - \frac{1}{4}x^2y^2, & Q_{7,0,3} &= -\frac{1}{12}x^2y^3 + \frac{1}{24}x^4y, \\ Q_{7,0,4} &= -\frac{1}{720}x^6 - \frac{1}{48}x^2y^4 + \frac{1}{48}x^4y^2, & Q_{7,0,5} &= \frac{1}{144}x^4y^3 - \frac{1}{720}x^6y - \frac{1}{240}x^2y^5, & Q_{7,1,0} &= -\frac{1}{6}x^3, \\ Q_{7,1,1} &= -\frac{1}{6}x^3y, & Q_{7,1,2} &= \frac{1}{120}x^5 - \frac{1}{12}x^3y^2, & Q_{7,1,3} &= \frac{1}{120}x^5y - \frac{1}{36}x^3y^3, \\ Q_{7,1,4} &= -\frac{1}{5040}x^7 + \frac{1}{240}x^5y^2 - \frac{1}{144}x^3y^4, & Q_{7,2,0} &= -\frac{1}{24}x^4, & Q_{7,2,1} &= -\frac{1}{24}x^4y, & Q_{7,2,2} &= \frac{1}{720}x^6 - \frac{1}{48}x^4y^2, \\ Q_{7,2,3} &= -\frac{1}{144}x^4y^3 + \frac{1}{720}x^6y, & Q_{7,3,0} &= -\frac{1}{120}x^5, & Q_{7,3,1} &= -\frac{1}{120}x^5y, & Q_{7,3,2} &= \frac{1}{5040}x^7 - \frac{1}{240}x^5y^2, \\ Q_{7,4,0} &= -\frac{1}{720}x^6, & Q_{7,4,1} &= -\frac{1}{720}x^6y, & Q_{7,5,0} &= -\frac{1}{5040}x^7. \end{aligned}$$

Hence, by (1.9), the solution u to (2.1) near the base point (x_i^*, y_j^*) can be approximated by

$$u(x+x_i^*, y+y_j^*) = \sum_{(m,n) \in \Lambda_{M+1}^1} u^{(m,n)} G_{M+1,m,n}(x,y) + \sum_{(m,n) \in \Lambda_{M-1}} f^{(m,n)} Q_{M+1,m,n}(x,y) + \mathcal{O}(h^{M+2}), \quad (2.9)$$

for $x, y \in (-2h, 2h)$. We shall use the above identity in (2.9) for finding compact 9-point stencils achieving a desired accuracy order M .

2.2.1 Stencils for regular points

In this subsection, we discuss how to find a compact 9-point scheme centered at a regular point (x_i, y_j) , which has been well studied in the literature. The main purpose of this subsection is to outline the main ideas. For simplicity, we just pick (x_i, y_j) as the base point (x_i^*, y_j^*) , that is, (x_i^*, y_j^*) is defined in (1.6) with $v_0 = w_0 = 0$. Recall that $M \in \mathbb{N}$ stands for the desired accuracy order.

Let us consider the following discretization operator at a regular point (x_i, y_j) :

$$\mathcal{L}_h u := h^{-2} \sum_{k=-1}^1 \sum_{\ell=-1}^1 C_{k,\ell}(h) u(x_i + kh, y_j + \ell h) \quad \text{with} \quad C_{k,\ell}(h) = \sum_{p=0}^{M+1} c_{k,\ell,p} h^p, \quad (2.10)$$

with all $c_{k,\ell,p}$ being to-be-determined constants. We say that the coefficients of the above compact 9-point stencil are nontrivial if $C_{k,\ell}(0) \neq 0$ for at least some $k, \ell = -1, 0, 1$, that is, $c_{k,\ell,0} \neq 0$ for at least some $k, \ell = -1, 0, 1$. Substituting (2.9) into (2.10), we obtain

$$\begin{aligned} \mathcal{L}_h u &= h^{-2} \sum_{k=-1}^1 \sum_{\ell=-1}^1 C_{k,\ell}(h) \left(\sum_{(m,n) \in \Lambda_{M+1}^1} u^{(m,n)} G_{M+1,m,n}(kh, \ell h) \right. \\ &\quad \left. + \sum_{(m,n) \in \Lambda_{M-1}} f^{(m,n)} Q_{M+1,m,n}(kh, \ell h) \right) + \mathcal{O}(h^M) \\ &= \sum_{(m,n) \in \Lambda_{M+1}^1} u^{(m,n)} h^{-2} I_{m,n}(h) + \sum_{(m,n) \in \Lambda_{M-1}} f^{(m,n)} J_{m,n}(h) + \mathcal{O}(h^M), \quad h \rightarrow 0, \end{aligned} \quad (2.11)$$

where the polynomials $G_{M+1,m,n}(x, y)$ and $Q_{M+1,m,n}(x, y)$ are defined (2.7) and (2.8), and

$$I_{m,n}(h) := \sum_{k=-1}^1 \sum_{\ell=-1}^1 C_{k,\ell}(h) G_{M+1,m,n}(kh, \ell h) \quad \text{and} \quad J_{m,n}(h) := \sum_{k=-1}^1 \sum_{\ell=-1}^1 C_{k,\ell}(h) h^{-2} Q_{M+1,m,n}(kh, \ell h), \quad (2.12)$$

for $m, n \in \mathbb{N}_0$. Note that both $I_{m,n}(h)$ and $J_{m,n}(h)$ are polynomials of h because every coefficient of $x^j y^k$ in the polynomial $Q_{M+1,m,n}(x, y)$ vanishes for all $j + k < 2$. Therefore, the following compact 9-point finite difference scheme for $-\nabla^2 u = f$ at the regular point (x_i, y_j) :

$$\mathcal{L}_h u_h := h^{-2} \sum_{k=-1}^1 \sum_{\ell=-1}^1 C_{k,\ell}(h) (u_h)_{i+k, j+\ell} = \sum_{(m,n) \in \Lambda_{M-1}} f^{(m,n)} J_{m,n}(h), \quad (2.13)$$

has the accuracy order M for the numerically approximated solution u_h satisfying (2.13), i.e.,

$$\mathcal{L}_h(u - u_h) = \mathcal{L}_h u - \sum_{(m,n) \in \Lambda_{M-1}} f^{(m,n)} J_{m,n}(h) = \mathcal{O}(h^M), \quad h \rightarrow 0, \quad (2.14)$$

if the following conditions in (2.11) are satisfied:

$$I_{m,n}(h) = \mathcal{O}(h^{M+2}), \quad h \rightarrow 0, \quad \text{for all } (m, n) \in \Lambda_{M+1}^1. \quad (2.15)$$

Note that the solutions of $\{C_{k,\ell}(h)\}_{k,\ell=-1,0,1}$ to (2.15) are homogeneous in terms of its un-

knowns, that is, a solution multiplied with a given polynomial of h to all coefficients is still a solution. Hence, we say that a solution for the coefficients in a compact 9-point stencil is nontrivial if $C_{k,\ell}(0) \neq 0$ for at least some $k, \ell = -1, 0, 1$. Since $G_{M+1,m,n}$ is a homogeneous polynomial of degree $m+n$, we can write $G_{M+1,m,n}(kh, \ell h) = g_{M+1,m,n,k,\ell} h^{m+n}$ for some constants $g_{M+1,m,n,k,\ell}$. Hence, (2.15) becomes

$$\sum_{k=-1}^1 \sum_{\ell=-1}^1 C_{k,\ell}(h) g_{M+1,m,n,k,\ell} = \mathcal{O}(h^{M+2-m-n}), \quad h \rightarrow 0, \quad \text{for all } (m,n) \in \Lambda_{M+1}^1. \quad (2.16)$$

Because $M+2-m-n \geq 1$ for all $(m,n) \in \Lambda_{M+1}^1$, the identities in (2.16) automatically imply

$$\sum_{k=-1}^1 \sum_{\ell=-1}^1 C_{k,\ell}(0) g_{M+1,m,n,k,\ell} = 0, \quad \text{for all } (m,n) \in \Lambda_{M+1}^1. \quad (2.17)$$

By calculation, the maximum integer M for the linear system in (2.17) to have a nontrivial solution $\{C_{k,\ell}(0)\}_{k,\ell=-1,0,1}$ is $M = 6$. More precisely, the rank of the matrix in (2.17)

$$(g_{M+1,m,n,k,\ell})_{(m,n) \in \Lambda_{M+1}^1, (k,\ell) \in \{-1,0,1\}^2},$$

is nine for $M = 7$ (hence (2.17) has only the trivial solution for $M = 7$) and its rank is 8 for $M = 6$. Therefore, for a compact 9-point stencil using Taylor expansion and our sort of technique, the maximum accuracy order M that we can achieve is $M = 6$. Moreover, up to a multiplicative constant, such a nontrivial solution $\{C_{k,\ell}(0)\}_{k,\ell=-1,0,1}$ to (2.17) is uniquely given by

$$C_{0,0} = -20, \quad C_{-1,0} = C_{1,0} = C_{0,-1} = C_{0,1} = 4, \quad C_{-1,-1} = C_{-1,1} = C_{1,-1} = C_{1,1} = 1. \quad (2.18)$$

For a constant solution of $\{C_{k,\ell}(0)\}_{k,\ell=-1,0,1}$ satisfying (2.17), such a constant solution obviously satisfies also (2.16) and therefore, it is a nontrivial solution to (2.15).

Since $Q_{M+1,m,n}$ is a homogeneous polynomial of degree $m+n+2$, we can write

$$Q_{M+1,m,n}(kh, \ell h) = q_{M+1,m,n,k,\ell} h^{m+n+2},$$

for some constants $q_{M+1,m,n,k,\ell}$. Now plugging (2.18) into the definition of $J_{m,n}(h)$ in (2.12), we easily deduce that

$$J_{0,0}(h) := -6, \quad J_{0,2}(h) = J_{2,0}(h) := -\frac{1}{2}h^2, \quad J_{0,4}(h) = J_{4,0}(h) := -\frac{1}{60}h^4, \quad J_{2,2}(h) := -\frac{1}{15}h^4,$$

and all other coefficients $J_{m,n}(h) = 0$. In summary, for a regular point (x_i, y_j) , we obtain the

following theorem which is well known in the literature (e.g., see [98, 114, 109]).

Theorem 2.3. *Let a grid point (x_i, y_j) be a regular point, i.e., either $d_{i,j}^+ = \emptyset$ or $d_{i,j}^- = \emptyset$. Let $(u_h)_{i,j}$ be the numerically approximated solution of the exact solution u of the partial differential equation (2.1) at a regular point (x_i, y_j) . Then the compact 9-point scheme:*

$$\begin{aligned} \mathcal{L}_h u_h := & \frac{1}{h^2} \left((u_h)_{i-1,j-1} + 4(u_h)_{i,j-1} + (u_h)_{i+1,j-1} \right. \\ & + 4(u_h)_{i-1,j} - 20(u_h)_{i,j} + 4(u_h)_{i+1,j} \\ & \left. + (u_h)_{i-1,j+1} + 4(u_h)_{i,j+1} + (u_h)_{i+1,j+1} \right) \\ & = -6f^{(0,0)} - \frac{1}{2}h^2(f^{(0,2)} + f^{(2,0)}) - \frac{1}{60}h^4(f^{(0,4)} + f^{(4,0)}) - \frac{1}{15}h^4f^{(2,2)}, \end{aligned} \quad (2.19)$$

achieves sixth order accuracy for $-\nabla^2 u = f$ at the regular point (x_i, y_j) , where $f^{(m,n)} := \frac{\partial^{m+n} f}{\partial^m x \partial^n y}(x_i, y_j)$. Moreover, the compact 9-point finite difference scheme of order four can be obtained from (2.19) by dropping the terms $-\frac{1}{60}h^4(f^{(0,4)} + f^{(4,0)})$ and $-\frac{1}{15}h^4f^{(2,2)}$.

The maximum accuracy order M for a compact 9-point finite difference scheme which is based on Taylor expansion and our sort of technique is $M = 6$.

2.2.2 Stencils for irregular points

Let (x_i, y_j) be an irregular point, that is, both $d_{i,j}^+ \neq \emptyset$ and $d_{i,j}^- \neq \emptyset$. In this subsection, we shall find a compact 9-point stencil at an irregular point (x_i, y_j) for a given accuracy order M . The idea is essentially the same, although the technicalities are much more complicated. Let (x_i, y_j) be an irregular point and we shall take a base point $(x_i^*, y_j^*) \in \Gamma \cap (x_i - h, x_i + h) \times (y_j - h, y_j + h)$ on the interface Γ and inside $(x_i - h, x_i + h) \times (y_j - h, y_j + h)$. That is, as in (1.6),

$$x_i^* = x_i - v_0 h \quad \text{and} \quad y_j^* = y_j - w_0 h \quad \text{with} \quad -1 < v_0, w_0 < 1 \quad \text{and} \quad (x_i^*, y_j^*) \in \Gamma. \quad (2.20)$$

Let u_{\pm} and f_{\pm} represent the solution u and source term f in Ω_+ or Ω_- , respectively. As in (1.7), we define

$$u_{\pm}^{(m,n)} := \frac{\partial^{m+n} u_{\pm}}{\partial^m x \partial^n y}(x_i^*, y_j^*), \quad f_{\pm}^{(m,n)} := \frac{\partial^{m+n} f_{\pm}}{\partial^m x \partial^n y}(x_i^*, y_j^*).$$

Since the base point (x_i^*, y_j^*) is now on the interface Γ , the equation $-\nabla^2 u = f$ is no longer valid at the base point (x_i^*, y_j^*) . However, the curve Γ is smooth and we assumed that the solution u and f are piecewise smooth. More precisely, u_+ and f_+ on Ω_+ can be extended

into smooth functions in a neighborhood of (x_i^*, y_j^*) , while u_- and f_- on Ω_- can be extended into smooth functions in a neighborhood of (x_i^*, y_j^*) . Therefore, Lemma 2.2 still holds for u_\pm and f_\pm . In other words, the identities in (2.4) hold by replacing u and f by u_\pm and f_\pm , respectively. Consequently, the key identity in (2.9) still holds by replacing u and f with u_\pm and f_\pm , respectively. Explicitly,

$$u_\pm(x+x_i^*, y+y_j^*) = \sum_{(m,n) \in \Lambda_{M+1}^1} u_\pm^{(m,n)} G_{M+1,m,n}(x, y) + \sum_{(m,n) \in \Lambda_{M-1}} f_\pm^{(m,n)} Q_{M+1,m,n}(x, y) + \mathcal{O}(h^{M+2}), \quad (2.21)$$

for $x, y \in (-2h, 2h)$, where the index sets Λ_{M+1}^1 and Λ_{M-1} are defined in (2.5) and (1.8), respectively, while the polynomials $G_{M+1,m,n}(x, y)$ and $Q_{M+1,m,n}(x, y)$ are defined in (2.7) and (2.8), respectively.

Because (x_i, y_j) is an irregular point, instead of using only $-\nabla^2 u = f$ in Section 2.2.1 to set a compact 9-point stencil, in this subsection we shall use the two jump conditions (2.2) and (2.3) to set up the following compact 9-point stencil at an irregular point (x_i, y_j) :

$$\mathcal{L}_h^\Gamma u := h^{-1} \sum_{k=-1}^1 \sum_{\ell=-1}^1 C_{k,\ell}(h) u(x_i + kh, y_j + \ell h) \quad \text{with} \quad C_{k,\ell}(h) = \sum_{p=0}^M c_{k,\ell,p} h^p, \quad (2.22)$$

with all $c_{k,\ell,p}$ being to-be-determined constants. Because the set $\{-1, 0, 1\}^2$ is the disjoint union of $d_{i,j}^+$ and $d_{i,j}^-$, we have

$$\begin{aligned} h\mathcal{L}_h^\Gamma u &= \sum_{k=-1}^1 \sum_{\ell=-1}^1 C_{k,\ell}(h) u(x_i + kh, y_j + \ell h) = \sum_{(k,\ell) \in d_{i,j}^+} C_{k,\ell}(h) u(x_i^* + (v_0 + k)h, y_j^* + (w_0 + \ell)h) \\ &\quad + \sum_{(k,\ell) \in d_{i,j}^-} C_{k,\ell}(h) u(x_i^* + (v_0 + k)h, y_j^* + (w_0 + \ell)h). \end{aligned}$$

By (2.21) with M being replaced by $M-1$, we have

$$\begin{aligned} \sum_{(k,\ell) \in d_{i,j}^\pm} C_{k,\ell}(h) u(x_i^* + (v_0 + k)h, y_j^* + (w_0 + \ell)h) &= \sum_{(m,n) \in \Lambda_M^1} u_\pm^{(m,n)} I_{m,n}^\pm(h) \\ &\quad + h^2 \sum_{(m,n) \in \Lambda_{M-2}} f_\pm^{(m,n)} J_{m,n}^{\pm,0}(h) + \mathcal{O}(h^{M+1}), \end{aligned}$$

where

$$\begin{aligned} I_{m,n}^\pm(h) &:= \sum_{(k,\ell) \in d_{i,j}^\pm} C_{k,\ell}(h) G_{M,m,n}((v_0 + k)h, (w_0 + \ell)h), \\ J_{m,n}^{\pm,0}(h) &:= \sum_{(k,\ell) \in d_{i,j}^\pm} C_{k,\ell}(h) h^{-2} Q_{M,m,n}((v_0 + k)h, (w_0 + \ell)h). \end{aligned} \quad (2.23)$$

Note that both $I_{m,n}^\pm(h)$ and $J_{m,n}^{\pm,0}(h)$ are polynomials of h , because $G_{M,m,n}(x, y)$ and $Q_{M,m,n}(x, y)$ are bivariate polynomials and every coefficient of $x^j y^k$ of $Q_{M,m,n}(x, y)$ vanishes for all $j+k < 2$.

Using the interface conditions in (2.1), we now link the two sets $\{u_-^{(m,n)} : (m, n) \in \Lambda_M^1\}$ and $\{u_+^{(m,n)} : (m, n) \in \Lambda_M^1\}$ through the following result, whose proof is given in Section 2.5.

Theorem 2.4. *Let u be the solution to the Poisson interface problem in (2.1) and the base point $(x_i^*, y_j^*) \in \Gamma$, which is parameterized near (x_i^*, y_j^*) by (1.5). Then*

$$\begin{aligned} u_-^{(m',n')} &= u_+^{(m',n')} + \sum_{(m,n) \in \Lambda_{M-2}} \left(T_{m',n',m,n}^+ f_+^{(m,n)} + T_{m',n',m,n}^- f_-^{(m,n)} \right) \\ &+ \sum_{p=0}^M T_{m',n',p}^{g_0^\Gamma} g_{0,p}^\Gamma + \sum_{p=0}^{M-1} T_{m',n',p}^{g_1^\Gamma} g_{1,p}^\Gamma, \quad \forall (m', n') \in \Lambda_M^1, \end{aligned} \quad (2.24)$$

where

$$g_{0,p}^\Gamma := \frac{1}{p!} \frac{d^p}{dt^p} \left[g_0^\Gamma(r(t) + x_i^*, s(t) + y_j^*) \right] \Big|_{t=0}, \quad p = 0, 1, \dots, M,$$

$$g_{1,p}^\Gamma := \frac{1}{p!} \frac{d^p}{dt^p} \left[g_1^\Gamma(r(t) + x_i^*, s(t) + y_j^*) \sqrt{(r'(t))^2 + (s'(t))^2} \right] \Big|_{t=0}, \quad p = 0, 1, \dots, M-1,$$

and all the transmission coefficients $T^\pm, T^{g_0^\Gamma}, T^{g_1^\Gamma}$ are uniquely determined by $r^{(k)}(0)$ and $s^{(k)}(0)$ for $k = 0, \dots, M$ and can be easily obtained by recursively calculating $U^{(m',n')} := u_+^{(m',n')} - u_-^{(m',n')}$, $(m', n') \in \Lambda_M^1$ through the recursive formulas given in (2.38) and (2.55).

Using (2.24) in Theorem 2.4, we obtain

$$\begin{aligned} \sum_{(m',n') \in \Lambda_M^1} u_-^{(m',n')} I_{m',n'}^-(h) &= \sum_{(m',n') \in \Lambda_M^1} u_+^{(m',n')} I_{m',n'}^-(h) + h^2 \sum_{(m,n) \in \Lambda_{M-2}} \left(f_+^{(m,n)} J_{m,n}^{+,T}(h) \right. \\ &\left. + f_-^{(m,n)} J_{m,n}^{-,T}(h) \right) + \sum_{p=0}^M g_{0,p}^\Gamma J_p^{g_0^\Gamma}(h) + \sum_{p=0}^{M-1} g_{1,p}^\Gamma J_p^{g_1^\Gamma}(h), \end{aligned}$$

where

$$\begin{aligned} J_{m,n}^{\pm,T}(h) &:= \sum_{(m',n') \in \Lambda_M^1} I_{m',n'}^-(h) h^{-2} T_{m',n',m,n}^\pm, \\ J_p^{g_0^\Gamma}(h) &:= \sum_{(m',n') \in \Lambda_M^1} I_{m',n'}^-(h) T_{m',n',p}^{g_0^\Gamma}, \quad J_p^{g_1^\Gamma}(h) := \sum_{(m',n') \in \Lambda_M^1} I_{m',n'}^-(h) T_{m',n',p}^{g_1^\Gamma}. \end{aligned} \quad (2.25)$$

In the proof of Theorem 2.4 in Section 2.5, we shall prove that $T_{m',n',m,n}^\pm = 0$ in (2.24) for $(m', n') \in \Lambda_M^1$ with $m' + n' < 2$. So (2.23) implies that every coefficient of h^k of $J_{m,n}^{\pm,T}(h)$ in

(2.25) vanishes for all $k < 0$. Consequently, for the stencil operator \mathcal{L}_h^Γ defined in (2.22), we obtain

$$\mathcal{L}_h^\Gamma u = \sum_{(m,n) \in \Lambda_M^1} u_+^{(m,n)} h^{-1} I_{m,n}(h) + h F_{M,f}(h) + G_{M,g_0^\Gamma, g_1^\Gamma}(h) + \mathcal{O}(h^M), \quad h \rightarrow 0, \quad (2.26)$$

with

$$\begin{aligned} F_{M,f}(h) &:= \sum_{(m,n) \in \Lambda_{M-2}} \left(f_-^{(m,n)} J_{m,n}^-(h) + f_+^{(m,n)} J_{m,n}^+(h) \right), \\ G_{M,g_0^\Gamma, g_1^\Gamma}(h) &:= h^{-1} \left(\sum_{p=0}^M g_{0,p}^\Gamma J_p^{g_0^\Gamma}(h) + \sum_{p=0}^{M-1} g_{1,p}^\Gamma J_p^{g_1^\Gamma}(h) \right), \end{aligned} \quad (2.27)$$

where

$$I_{m,n}(h) := I_{m,n}^+(h) + I_{m,n}^-(h), \quad J_{m,n}^\pm(h) := J_{m,n}^{\pm,0}(h) + J_{m,n}^{\pm,T}(h). \quad (2.28)$$

Now the following compact 9-point finite difference scheme at the irregular point (x_i, y_j) :

$$\mathcal{L}_h^\Gamma u_h := h^{-1} \sum_{k=-1}^1 \sum_{\ell=-1}^1 C_{k,\ell}(h) (u_h)_{i+k, j+\ell} = h F_{M,f}(h) + G_{M,g_0^\Gamma, g_1^\Gamma}(h), \quad (2.29)$$

has the accuracy order M for the numerically approximated solution u_h satisfying (2.29), i.e.,

$$\mathcal{L}_h^\Gamma(u - u_h) = \mathcal{L}_h^\Gamma u - h F_{M,f}(h) - G_{M,g_0^\Gamma, g_1^\Gamma}(h) = \mathcal{O}(h^M), \quad h \rightarrow 0, \quad (2.30)$$

if $I_{m,n}(h)$ in (2.28) satisfies

$$I_{m,n}(h) = \mathcal{O}(h^{M+1}), \quad h \rightarrow 0, \quad \text{for all } (m, n) \in \Lambda_M^1. \quad (2.31)$$

Due to the relations in (2.24) of Theorem 2.4, we observe that the solution $\{C_{k,\ell}(h)\}_{k,\ell=-1,0,1}$ in (2.18) is also a solution to (2.31) with $M = 7$.

In summary, we obtain the following theorem for compact 9-point stencils at irregular points.

Theorem 2.5. *Let $(u_h)_{i,j}$ be the numerical solution of (2.1) at an irregular point (x_i, y_j) . Pick a base point (x_i^*, y_j^*) as in (2.20). Then the following compact 9-point scheme centered*

at the irregular point (x_i, y_j) :

$$\begin{aligned} \mathcal{L}_h^\Gamma u_h := & \frac{1}{h} \left((u_h)_{i-1,j-1} + 4(u_h)_{i,j-1} + (u_h)_{i+1,j-1} \right. \\ & + 4(u_h)_{i-1,j} - 20(u_h)_{i,j} + 4(u_h)_{i+1,j} \\ & \left. + (u_h)_{i-1,j+1} + 4(u_h)_{i,j+1} + (u_h)_{i+1,j+1} \right) = hF_{7,f}(h) + G_{7,g_0^\Gamma, g_1^\Gamma}(h), \end{aligned} \quad (2.32)$$

achieves seventh order of accuracy at the irregular point (x_i, y_j) , where the quantities $F_{7,f}(h)$ and $G_{7,g_0^\Gamma, g_1^\Gamma}(h)$ are given in (2.27). Moreover, the stencils for the accuracy order $P = 3, 4, 5, 6$ can be easily obtained from the stencil in (2.32) by dropping $G_{7,m,n}$ with $m + n > P + 1$ and $Q_{7,m,n}$ with $m + n > P - 1$.

Remark 2.6. (1) If one of the values $f_+(x_i^*, y_j^*)$ and $f_-(x_i^*, y_j^*)$ is very large at some $(x_i^*, y_j^*) \in \Gamma$ while the other value is small, it is important to accurately determine the membership of the nine points $\{(x_{i+k}, y_{j+\ell}) : k, \ell \in \{-1, 0, 1\}\}$ in Ω_+ or Ω_- . In particular, for the general elliptic interface problem with discontinuous and high-contrast coefficients in Remark 2.1 and Chapter 3, the solution could be sensitive near the interface curve where the coefficient a has high-contrast ratios.

(2) For the parametric equation of Γ , $(x(t), y(t)) = (t + x_i^*, r(t) + y_j^*)$ or $(r(t) + x_i^*, t + y_j^*)$ in (1.4). If $|x'(0)|$ is relatively large, we should use $(x(t), y(t)) = (t + x_i^*, r(t) + y_j^*)$ in (1.4).

Similarly, if $|y'(0)|$ is relatively large, we should use $(x(t), y(t)) = (r(t) + x_i^*, t + y_j^*)$ in (1.4).

(3) By (2.24), the sixth order compact 9-point finite difference scheme uses $\frac{d^k(x(t))}{dt^k}\big|_{t=0}$ and $\frac{d^k(y(t))}{dt^k}\big|_{t=0}$ for $k = 0, 1, \dots, 7$ and $(x(t), y(t)) \in \Gamma$ which would make $T_{m',n',m,n}^\pm$, $T_{m',n',p}^{g_0^\Gamma}$ and $T_{m',n',p}^{g_1^\Gamma}$ complicated in (2.24). While, after normalizing each entry of $T_{m',n',m,n}^\pm$, $T_{m',n',p}^{g_0^\Gamma}$ and $T_{m',n',p}^{g_1^\Gamma}$, we find that there exist many common factors. By using these factors, we can significantly reduce the length of (2.24).

2.2.3 Convergence analysis

We now prove the following convergence result for the sixth order compact 9-point finite difference scheme developed in Sections 2.2.1 and 2.2.2.

Theorem 2.7. *Under the assumptions (A1)–(A3) in Section 2.1, the sixth and seventh order compact 9-point finite difference schemes in Sections 2.2.1 and 2.2.2 for the Poisson interface problem with singular source in (2.1) has the convergence rate of order 6, that is, there exists a positive constant C independent of h such that*

$$\|u - u_h\|_\infty \leq Ch^6,$$

where u and u_h are the exact solution and the numerical solution of (2.1), respectively.

Proof. For simplicity of discussion, we assume $\Omega = (0, 1)^2$ and let $h = 1/N$ be the mesh size with $N \in \mathbb{N}$. We define $\Omega_h := \Omega \cap (h\mathbb{Z}^2)$, $\partial\Omega_h := \partial\Omega \cap (h\mathbb{Z}^2)$, $\bar{\Omega}_h := \bar{\Omega} \cap (h\mathbb{Z}^2)$, and $(x_i, y_j) := (ih, jh)$. So $\bar{\Omega}_h := \{(x_i, y_j) : 0 \leq i, j \leq N\}$ and we also define that $V(\bar{\Omega}_h) := \{(v)_{i,j} : 0 \leq i, j \leq N\}$ with $(v)_{i,j} \in \mathbb{R}$. To be consistent with the notation before, we define that for any $v \in V(\bar{\Omega}_h)$, $(v)_{i,j}$ represents the real value for v at the point (x_i, y_j) . By Theorems 2.3 and 2.5, the compact 9-point finite difference scheme in Section 2.2 can be equivalently expressed as: Find $u_h \in V(\bar{\Omega}_h)$ satisfying

$$\Delta_h u_h = F \quad \text{on} \quad \Omega_h, \quad u_h = g \quad \text{on} \quad \partial\Omega_h,$$

where

$$(\Delta_h u_h)_{i,j} := \frac{1}{h^2} \left(-20(u_h)_{i,j} + 4[(u_h)_{i-1,j} + (u_h)_{i+1,j} + (u_h)_{i,j-1} + (u_h)_{i,j+1}] + [(u_h)_{i-1,j-1} + (u_h)_{i+1,j-1} + (u_h)_{i-1,j+1} + (u_h)_{i+1,j+1}] \right), \quad \text{at the regular point } (x_i, y_j),$$

$$(\Delta_h u_h)_{i,j} := \frac{1}{h} \left(-20(u_h)_{i,j} + 4[(u_h)_{i-1,j} + (u_h)_{i+1,j} + (u_h)_{i,j-1} + (u_h)_{i,j+1}] + [(u_h)_{i-1,j-1} + (u_h)_{i+1,j-1} + (u_h)_{i-1,j+1} + (u_h)_{i+1,j+1}] \right), \quad \text{at the irregular point } (x_i, y_j),$$

and F at the regular point (x_i, y_j) is given in (2.19) by

$$(F)_{i,j} := \left[-6f^{(0,0)} - \frac{1}{2}h^2(f^{(0,2)} + f^{(2,0)}) - \frac{1}{60}h^4(f^{(0,4)} + f^{(4,0)}) - \frac{1}{15}h^4f^{(2,2)} \right] \Big|_{(ih,jh)},$$

and F at the irregular point (x_i, y_j) is similarly given in (2.32). Let $u(x, y)$ be the exact solution and $U_h := \{u(x_i, y_j) : 0 \leq i, j \leq N\}$. By Theorems 2.3 and 2.5, there must exist a positive constant C independent of h (C only depends on u , the data $f, g_0^\Gamma, g_1^\Gamma$ and the interface curve Γ) such that

$$\Delta_h U_h = F + R \quad \text{with} \quad U_h, F \text{ and } R \in V(\bar{\Omega}_h), \quad \|R\|_\infty \leq C \max(h^6, h^7) = Ch^6.$$

More precisely, R represents the truncation error in our compact 9-point finite difference scheme. Using the standard argument, we now prove the discrete maximum principle: for any $v \in V(\bar{\Omega}_h)$ satisfying $\Delta_h v \geq 0$ on Ω_h , we must have $\max_{(x_i, y_j) \in \Omega_h} (v)_{i,j} \leq \max_{(x_i, y_j) \in \partial\Omega_h} (v)_{i,j}$.

Suppose that $\max_{(x_i, y_j) \in \Omega_h} (v)_{i,j} > \max_{(x_i, y_j) \in \partial\Omega_h} (v)_{i,j}$. Take $(x_m, y_n) \in \Omega_h$ where v achieves its

maximum in Ω_h . So

$$4[(v)_{m-1,n} + (u_h)_{m+1,n} + (v)_{m,n-1} + (v)_{m,n+1}] \\ + [(v)_{m-1,n-1} + (v)_{m+1,n-1} + (v)_{m-1,n+1} + (v)_{m+1,n+1}] \leq 20(v)_{m,n}.$$

By $(\Delta_h v)_{m,n} \geq 0$, we have $-h^s(\Delta_h v)_{m,n} \leq 0$ for $s = 1, 2$ and

$$20(v)_{m,n} = 4[(v)_{m-1,n} + (u_h)_{m+1,n} + (v)_{m,n-1} + (v)_{m,n+1}] \\ + [(v)_{m-1,n-1} + (v)_{m+1,n-1} + (v)_{m-1,n+1} + (v)_{m+1,n+1}] - h^s(\Delta_h v)_{m,n} \leq 20(v)_{m,n},$$

where $s = 2$ at the regular point and $s = 1$ at the irregular point. Thus, equality holds throughout and v achieves its maximum at all its nearest neighbors of (x_m, y_n) . Applying the same argument to the neighbors in Ω_h and repeat this argument, we conclude that v must be a constant contradicting our assumption. This proves the discrete maximum principle.

Define $E_h := U_h - u_h$ on $\bar{\Omega}_h$. Then we have

$$\Delta_h E_h = \Delta_h U_h - \Delta_h u_h = (F + R) - F = R \quad \text{on } \Omega_h \quad \text{with } E_h = 0 \quad \text{on } \partial\Omega_h.$$

Now we consider the comparison function $\phi(x, y) := \frac{1}{24}[(x - 1/2)^2 + (y - 1/2)^2]$ and $\Phi = \{\phi(x_i, y_j) : 0 \leq i, j \leq N\}$. Then we can directly check that $\Delta_h \Phi = w$ on Ω_h and $0 \leq \phi \leq \frac{1}{48}$ on $[0, 1]^2$, where $w = 1$ on Ω_h . Then by $\|R\|_\infty \leq Ch^6$, we have

$$\Delta_h(E_h + Ch^6\Phi) = \Delta_h E_h + Ch^6w = R + Ch^6w \geq 0 \quad \text{on } \Omega_h.$$

Therefore, by the discrete maximum principle, we have

$$\max_{(x_i, y_j) \in \Omega_h} (E_h)_{i,j} \leq \max_{(x_i, y_j) \in \Omega_h} (E_h + Ch^6\Phi)_{i,j} \leq \max_{(x_i, y_j) \in \partial\Omega_h} (E_h + Ch^6\Phi)_{i,j} \\ \leq \max_{(x_i, y_j) \in \partial\Omega_h} (E_h)_{i,j} + Ch^6/48 = Ch^6/48.$$

A similar argument can be applied to $-E_h$. Hence, $\|u - u_h\|_\infty = \|E_h\|_\infty \leq \frac{C}{48}h^6$. This proves the convergence rate of the compact 9-point finite difference scheme developed in Sections [2.2.1](#) and [2.2.2](#). \square

2.3 Numerical experiments

In addition, κ denotes the condition number of the coefficient matrix. According to Theorems 2.3 and 2.5, (2.1) has the same coefficient matrix. So we only provide the values of κ in Table 2.1. For simplicity of presentation, we shall state both g_0^Γ and g_1^Γ in (2.1) as functions of x and y in our numerical examples, though as discussed in Section 2.5 we only use the fact that both g_0^Γ, g_1^Γ are functions defined on the interface curve Γ .

2.3.1 Numerical examples with known u , smooth Γ and $\Gamma \cap \partial\Omega = \emptyset$

In this subsection, we provide a few numerical experiments such that the exact solution u of (2.1) is known, the interface curve Γ is smooth and Γ does not touch the boundary of Ω .

Example 2.1. Let $\Omega = (-\pi, \pi)^2$ and the interface curve be given by $\Gamma := \{(x, y) \in \Omega : \psi(x, y) = 0\}$ with $\psi(x, y) = x^2 + y^2 - 2$. Note that $\Gamma \cap \partial\Omega = \emptyset$ and the exact solution u of (2.1) is given by

$$u_+ = u\chi_{\Omega_+} = \sin(4x)(2 - (x^2 + y^2))^2, \quad u_- = u\chi_{\Omega_-} = \cos(4y)(2 - (x^2 + y^2))^2 + 100.$$

All the functions $f, g_0^\Gamma, g_1^\Gamma, g$ in (2.1) can be obtained by plugging the above exact solution into (2.1). In particular, $g_0^\Gamma = -100$ and $g_1^\Gamma = 0$. The numerical results are presented in Table 2.1 and Fig. 2.3.

Table 2.1: Performance in Example 2.1 of the proposed sixth order compact 9-point finite difference scheme in Theorems 2.3 and 2.5 on uniform Cartesian meshes with $h = 2^{-J} \times 2\pi$. κ is the condition number of the coefficient matrix.

J	$\frac{\ u_h - u\ _2}{\ u\ _2}$	order	$\ u_h - u\ _\infty$	order	$\ u_h - u_{h/2}\ _2$	order	$\ u_h - u_{h/2}\ _\infty$	order	κ
3	3.65E+00	0	3.55E+02	0	4.13E+02	0	3.40E+02	0	3.14E+01
4	1.25E-01	4.868	1.90E+01	4.224	2.02E+01	4.352	1.89E+01	4.165	1.26E+02
5	6.60E-04	7.566	1.03E-01	7.529	1.16E-01	7.452	1.03E-01	7.528	5.03E+02
6	3.38E-06	7.610	5.87E-04	7.456	6.08E-04	7.571	5.83E-04	7.459	2.01E+03
7	2.55E-08	7.048	4.27E-06	7.103	4.63E-06	7.036	4.24E-06	7.104	8.05E+03
8	2.40E-10	6.733	3.50E-08	6.928	6.60E-08	6.133	8.04E-08	5.720	3.22E+04

Example 2.2. Let $\Omega = (-\frac{1}{2}, \frac{1}{2})^2$ and the interface curve be given by $\Gamma := \{(x, y) \in \Omega : \psi(x, y) = 0\}$ with $\psi(x, y) = \frac{y^2}{2} + \frac{x^2}{1+x^2} - \frac{1}{10}$. Note that $\Gamma \cap \partial\Omega = \emptyset$ and the exact solution u of (2.1) is given by

$$u_+ = u\chi_{\Omega_+} = \sin(Kx) \sin(Ky), \quad u_- = u\chi_{\Omega_-} = \sin(Kx) \sin(Ky) + 3, \quad \text{with } K = 5, 50, 500.$$

All the functions $f, g_0^\Gamma, g_1^\Gamma, g$ in (2.1) can be obtained by plugging the above exact solution into (2.1). In particular, $g_0^\Gamma = -3$ and $g_1^\Gamma = 0$. The numerical results are provided in Table 2.2 and Fig. 2.3.

Table 2.2: Performance in Example 2.2 of the proposed sixth order compact 9-point finite difference scheme in Theorems 2.3 and 2.5 on uniform Cartesian meshes with $h = 2^{-J} \times 1$.

J	$K = 5$				$K = 50$				$K = 500$			
	$\frac{\ u_h - u\ _2}{\ u\ _2}$	order	$\ u_h - u\ _\infty$	order	$\frac{\ u_h - u\ _2}{\ u\ _2}$	order	$\ u_h - u\ _\infty$	order	$\frac{\ u_h - u\ _2}{\ u\ _2}$	order	$\ u_h - u\ _\infty$	order
3	1.6E-04	0	9.8E-04	0	4.4E+03	0	3.4E+04	0	4.2E+10	0	3.1E+11	0
4	1.7E-06	6.55	8.9E-06	6.77	2.2E+01	7.66	1.6E+02	7.75	6.0E+08	6.14	5.3E+09	5.88
5	1.5E-08	6.81	8.1E-08	6.78	3.6E-01	5.92	2.8E+00	5.82	3.7E+06	7.33	4.2E+07	6.99
6	1.5E-10	6.65	8.1E-10	6.64	3.0E-03	6.91	3.2E-02	6.41	1.0E+05	5.20	9.6E+05	5.44
7	1.5E-12	6.69	7.7E-12	6.72	2.2E-05	7.12	2.1E-04	7.29	2.6E+02	8.61	3.7E+03	8.00
8					2.0E-07	6.77	2.2E-06	6.54	1.7E+00	7.22	4.2E+01	6.49
9					1.5E-09	6.99	1.7E-08	7.01	1.3E-02	7.02	3.5E-01	6.88
10									1.4E-04	6.53	3.3E-03	6.75
11									1.4E-06	6.69	2.8E-05	6.86
12									9.4E-09	7.22	2.1E-07	7.06

2.3.2 Numerical examples with known u , smooth Γ and $\Gamma \cap \partial\Omega \neq \emptyset$

In this subsection, we provide a few numerical experiments such that the exact solution u of (2.1) is known, the interface curve Γ is smooth and Γ touches the boundary of Ω .

Example 2.3. Let $\Omega = (-\frac{3}{2}\pi, \frac{3}{2}\pi)^2$ and the interface curve be given by $\Gamma := \{(x, y) \in \Omega : \psi(x, y) = 0\}$ with $\psi(x, y) = y - \cos(x)$. Note that $\Gamma \cap \partial\Omega \neq \emptyset$ and the exact solution u of (2.1) is given by

$$u_+ = u\chi_{\Omega_+} = -\sin(x)(y - \cos(x))^2, \quad u_- = u\chi_{\Omega_-} = -\cos(y)(y - \cos(x))^2 - 10.$$

All the associated functions $f, g_0^\Gamma, g_1^\Gamma, g$ can be obtained by plugging the above exact solution into (2.1). In particular, $g_0^\Gamma = 10$ and $g_1^\Gamma = 0$. The numerical results are provided in Table 2.3 and Fig. 2.4.

Example 2.4. Let $\Omega = (0, 1)^2$ and the interface curve be given by $\Gamma := \{(x, y) \in \Omega : \psi(x, y) = 0\}$ with $\psi(x, y) = y - \frac{\cos(5x)}{5} - \frac{1}{2}$. Note that $\Gamma \cap \partial\Omega \neq \emptyset$ and the exact solution u of (2.1) is given by

$$u_+ = u\chi_{\Omega_+} = \sin(Kx), \quad u_- = u\chi_{\Omega_-} = \cos(Ky) - 3 \quad \text{with } K = 5, 50, 500.$$

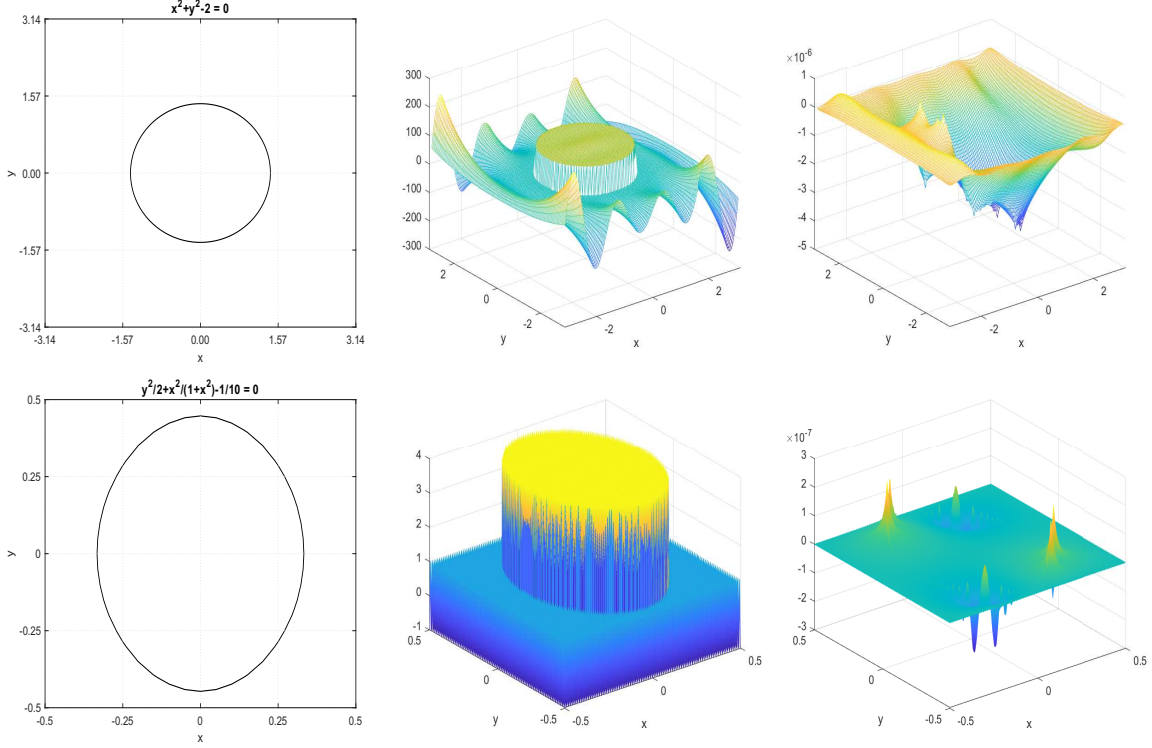


Figure 2.3: Top row for Example [2.1](#): the interface curve Γ (left), the numerical solution u_h (middle) and the error $u - u_h$ (right) with $h = 2^{-7} \times 2\pi$. Bottom row for Example [2.2](#) with $K = 500$: the interface curve Γ (left), the numerical solution u_h (middle) and the error $u - u_h$ (right) with $h = 2^{-12} \times 1$.

Table 2.3: Performance in Example [2.3](#) of the proposed sixth order compact 9-point finite difference scheme in Theorems [2.3](#) and [2.5](#) on uniform Cartesian meshes with $h = 2^{-J} \times 3\pi$.

J	$\frac{\ u_h - u\ _2}{\ u\ _2}$	order	$\ u_h - u\ _\infty$	order	$\ u_h - u_{h/2}\ _2$	order	$\ u_h - u_{h/2}\ _\infty$	order
3	1.72E-01	0	3.28E+00	0	4.81E+00	0	3.22E+00	0
4	3.78E-03	5.508	7.36E-02	5.476	1.20E-01	5.330	7.34E-02	5.454
5	1.28E-05	8.206	2.46E-04	8.224	4.29E-04	8.124	2.42E-04	8.244
6	1.97E-07	6.024	4.25E-06	5.856	6.88E-06	5.962	4.23E-06	5.839
7	1.03E-09	7.577	2.19E-08	7.603	3.64E-08	7.561	2.16E-08	7.611
8	1.17E-11	6.462	2.68E-10	6.348	4.53E-10	6.328	2.81E-10	6.265

All the associated functions $f, g_0^\Gamma, g_1^\Gamma, g$ can be obtained by plugging the above exact solution into (2.1). Clearly, g_0^Γ and g_1^Γ are neither constants. The numerical results are provided in Table 2.4 and Fig. 2.4.

Table 2.4: Performance in Example 2.4 of the proposed sixth order compact 9-point finite difference scheme in Theorems 2.3 and 2.5 on uniform Cartesian meshes with $h = 2^{-J} \times 1$.

J	$K = 5$				$K = 50$				$K = 500$			
	$\frac{\ u_h - u\ _2}{\ u\ _2}$	order	$\ u_h - u\ _\infty$	order	$\frac{\ u_h - u\ _2}{\ u\ _2}$	order	$\ u_h - u\ _\infty$	order	$\frac{\ u_h - u\ _2}{\ u\ _2}$	order	$\ u_h - u\ _\infty$	order
3	7.5E-05	0	4.7E-04	0	2.2E+03	0	1.0E+04	0	3.2E+10	0	2.0E+11	0
4	3.3E-07	7.81	3.3E-06	7.15	1.1E+01	7.73	1.1E+02	6.56	2.5E+08	7.00	2.1E+09	6.57
5	3.9E-09	6.43	3.0E-08	6.78	1.2E-01	6.46	1.7E+00	5.97	2.4E+06	6.70	3.7E+07	5.86
6	3.0E-11	7.01	2.5E-10	6.92	4.4E-04	8.09	1.0E-02	7.41	3.1E+04	6.26	5.7E+05	6.02
7	2.6E-13	6.87	1.7E-12	7.15	2.0E-06	7.78	3.6E-05	8.15	1.3E+02	7.87	1.9E+03	8.25
8					3.0E-08	6.05	5.4E-07	6.04	1.6E+00	6.41	1.8E+01	6.67
9					4.8E-10	5.96	8.0E-09	6.08	8.1E-03	7.59	1.6E-01	6.83
10									7.2E-05	6.81	1.4E-03	6.84
11									3.6E-07	7.65	7.8E-06	7.51
12									1.9E-09	7.60	4.4E-08	7.45

2.3.3 One numerical example with known u , sharp-edged Γ and $\Gamma \cap \partial\Omega = \emptyset$

In this subsection, we provide one numerical experiment such that the exact solution u of (2.1) is known, the interface curve Γ is sharp-edged and Γ does not touch the boundary of Ω .

Example 2.5. Let $\Omega = (-\frac{3\pi}{2}, \frac{3\pi}{2})^2$ and the interface curve be given by $\Gamma := \{(x, y) \in \Omega : \psi(x, y) = 0\}$ which is shown in Fig. 2.5. More precisely, the sharp-edged interface is a square with 4 corner points $(-2, 0)$, $(0, 2)$, $(2, 0)$ and $(0, -2)$. Note that $\Gamma \cap \partial\Omega = \emptyset$ and the exact solution u of (2.1) is given by

$$u_+ = u\chi_{\Omega_+} = \sin(2x)\sin(3y), \quad u_- = u\chi_{\Omega_-} = \cos(2x)\cos(2y) + 3.$$

All the functions $f, g_0^\Gamma, g_1^\Gamma, g$ in (2.1) can be obtained by plugging the above exact solution into (2.1). Clearly, g_0^Γ and g_1^Γ are neither constants. The numerical results are presented in Table 2.5 and Fig. 2.5.

In order to make the programming easy, (x_i^*, y_j^*) should not be the 4 corner points $(-2, 0)$, $(0, 2)$, $(2, 0)$ and $(0, -2)$ in Example 2.5 and Example 2.14. Thus, for the complicated sharp-edged interfaces in [113], more work should be done in the future.

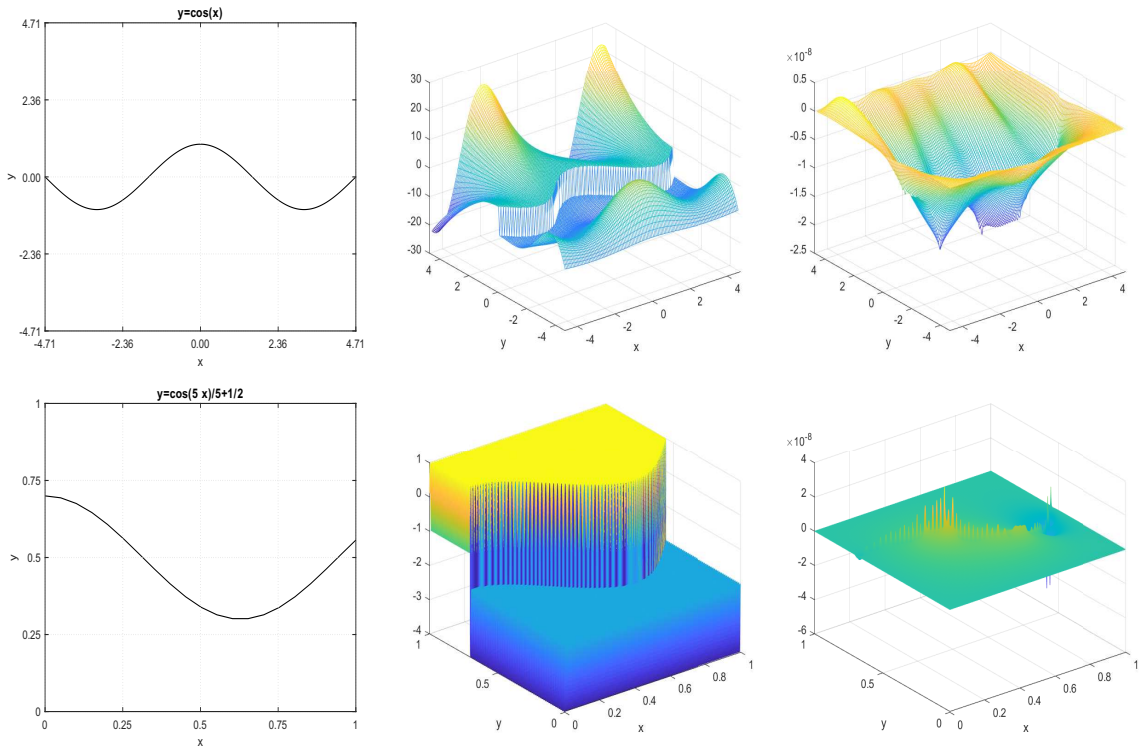


Figure 2.4: Top row for Example [2.3](#): the interface curve Γ (left), the numerical solution u_h (middle) and the error $u - u_h$ (right) with $h = 2^{-7} \times 3\pi$. Bottom row for Example [2.4](#) with $K = 500$: the interface curve Γ (left), the numerical solution u_h (middle) and the error $u - u_h$ (right) with $h = 2^{-12} \times 1$.

Table 2.5: Performance in Example [2.5](#) of the proposed sixth order compact 9-point finite difference scheme in Theorems [2.3](#) and [2.5](#) on uniform Cartesian meshes with $h = 2^{-J} \times 3\pi$.

J	$\frac{\ u_h - u\ _2}{\ u\ _2}$	order	$\ u_h - u\ _\infty$	order	$\ u_h - u_{h/2}\ _2$	order	$\ u_h - u_{h/2}\ _\infty$	order
3	3.45E+01	0	8.90E+01	0	1.42E+02	0	8.84E+01	0
4	3.57E-01	6.596	1.36E+00	6.028	1.65E+00	6.420	1.36E+00	6.025
5	3.58E-03	6.640	8.97E-03	7.247	1.59E-02	6.698	8.92E-03	7.248
6	1.82E-05	7.622	6.10E-05	7.201	8.30E-05	7.584	6.03E-05	7.209
7	1.22E-07	7.219	6.72E-07	6.504	5.63E-07	7.203	6.67E-07	6.499
8	9.41E-10	7.017	4.53E-09	7.213	4.31E-09	7.031	4.49E-09	7.217

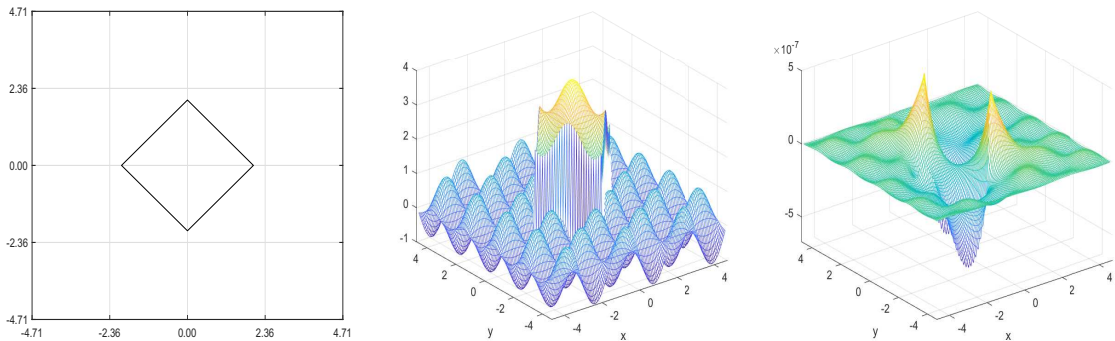


Figure 2.5: Example [2.5](#): the interface curve Γ (left), the numerical solution u_h (middle) and the error $u - u_h$ (right) with $h = 2^{-7} \times 3\pi$.

2.3.4 Numerical examples with unknown u , smooth Γ and $\Gamma \cap \partial\Omega = \emptyset$

In this subsection, we provide a few numerical experiments such that the exact solution u of (2.1) is unknown, the interface curve Γ is smooth and Γ does not touch the boundary of Ω .

Example 2.6. Let $\Omega = (-\pi, \pi)^2$ and the interface curve be given by $\Gamma := \{(x, y) \in \Omega : \psi(x, y) = 0\}$ with $\psi(x, y) = \frac{x^2}{2} + \frac{y^2}{2} - 1$. Note that $\Gamma \cap \partial\Omega = \emptyset$ and the coefficients of (2.1) are given by

$$\begin{aligned} f_+ &= f\chi_{\Omega_+} = \sin(3x) \sin(3y), & f_- &= f\chi_{\Omega_-} = \cos(3x) \cos(3y), \\ g_0^\Gamma &= -\exp(x - y) \sin(x + y), & g_1^\Gamma &= -\exp(x + y) \cos(x - y), & g &= 0. \end{aligned}$$

The numerical results are provided in Table 2.6 and Fig. 2.6.

Example 2.7. Let $\Omega = (-\pi, \pi)^2$ and the interface curve be given by $\Gamma := \{(x, y) \in \Omega : \psi(x, y) = 0\}$ with $\psi(x, y) = \frac{y^2}{2} + \frac{x^2}{1+x^2} - \frac{1}{2}$. Note that $\Gamma \cap \partial\Omega = \emptyset$ and the coefficients of (2.1) are given by

$$\begin{aligned} f_+ &= f\chi_{\Omega_+} = \sin(3x) \sin(2y), & f_- &= f\chi_{\Omega_-} = \cos(2x) \cos(2y), \\ g_0^\Gamma &= -\sin(x) \sin(y), & g_1^\Gamma &= -\cos(x) \sin(y), & g &= 0. \end{aligned}$$

The numerical results are provided in Table 2.6 and Fig. 2.6.

Table 2.6: Performance in Examples 2.6 and 2.7 of the proposed sixth order compact 9-point finite difference scheme in Theorems 2.3 and 2.5 on uniform Cartesian meshes with the same mesh size $h = 2^{-J} \times 2\pi$.

J	Example 2.6				Example 2.7			
	$\ u_h - u_{h/2}\ _2$	order	$\ u_h - u_{h/2}\ _\infty$	order	$\ u_h - u_{h/2}\ _2$	order	$\ u_h - u_{h/2}\ _\infty$	order
3	1.20E+00	0	1.48E+00	0	2.33E+02	0	4.01E+02	0
4	1.29E-01	3.222	9.76E-02	3.919	3.01E-02	12.922	6.00E-02	12.705
5	1.40E-03	6.519	1.01E-03	6.589	3.63E-04	6.371	9.18E-04	6.032
6	1.22E-05	6.847	1.01E-05	6.647	5.78E-06	5.973	1.44E-05	5.992
7	1.67E-07	6.195	4.52E-07	4.483	9.24E-08	5.968	2.61E-07	5.789

Example 2.8. Let $\Omega = (-\pi, \pi)^2$ and the interface curve be given by $\Gamma := \{(x, y) \in \Omega : \psi(x, y) = 0\}$ with $\psi(x, y) = x^4 + 2y^4 - 2$. Note that $\Gamma \cap \partial\Omega = \emptyset$ and the coefficients of (2.1) are given by

$$f_+ = f\chi_{\Omega_+} = \sin(2x) \sin(2y), \quad f_- = f\chi_{\Omega_-} = \cos(2x - 2y),$$

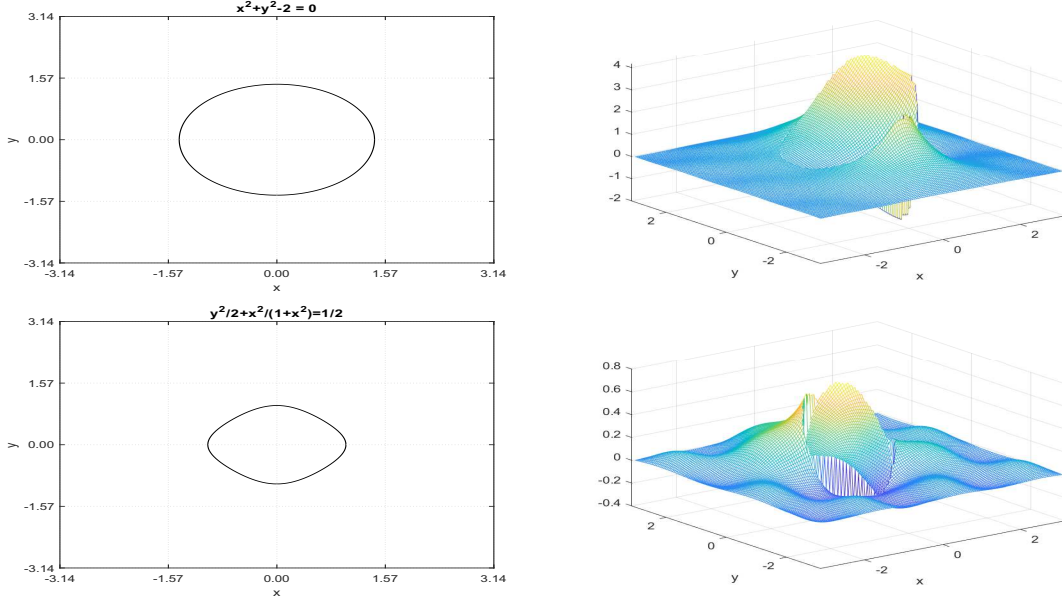


Figure 2.6: Top row for Example [2.6](#): the interface curve Γ (left) and the numerical solution u_h (right) with $h = 2^{-7} \times 2\pi$. Bottom row for Example [2.7](#): the interface curve Γ (left) and the numerical solution u_h (right) with $h = 2^{-7} \times 2\pi$.

$$g_0^\Gamma = -x^2, \quad g_1^\Gamma = -y^2, \quad g = 0.$$

The numerical results are provided in Table [2.7](#) and Fig. [2.7](#).

Example 2.9. Let $\Omega = (-\pi, \pi)^2$ and the interface curve be given by $\Gamma := \{(x, y) \in \Omega : \psi(x, y) = 0\}$ with $\psi(x, y) = y^2 - 2x^2 + x^4 - 1$. Note that $\Gamma \cap \partial\Omega = \emptyset$ and the coefficients of [\(2.1\)](#) are given by

$$\begin{aligned} f_+ &= f\chi_{\Omega_+} = \sin(2x)\sin(3y), & f_- &= f\chi_{\Omega_-} = \cos(2x)\sin(2y), \\ g_0^\Gamma &= 0, & g_1^\Gamma &= -\exp(x-2y), & g &= 0. \end{aligned}$$

Because $g_0^\Gamma = 0$, the Poisson interface problem in [\(2.1\)](#) simply becomes $-\nabla^2 u = f - g_1^\Gamma \delta_\Gamma$ in Ω with the Dirichlet boundary condition $u|_{\partial\Omega} = g$. The numerical results are provided in Table [2.7](#) and Fig. [2.7](#).

Example 2.10. Let $\Omega = (0, 1)^2$ and the interface curve be given by $\Gamma := \{(x, y) \in \Omega : \psi(x, y) = 0\}$ with $\psi(x, y) = (x - 1/2)^2 + 2(y - 1/2)^2 - 1/20$. Note that $\Gamma \cap \partial\Omega = \emptyset$ and the coefficients of [\(2.1\)](#) are given by

$$f_+ = f\chi_{\Omega_+} = 2 \left(\frac{2\pi}{5} K \right)^2 \sin \left(\frac{2\pi}{5} Kx \right) \sin \left(\frac{2\pi}{5} Ky \right), \quad f_- = f\chi_{\Omega_-} = 2K^2 \cos(Kx) \cos(Ky),$$

Table 2.7: Performance in Examples 2.8 and 2.9 of the proposed sixth order compact 9-point finite difference scheme in Theorems 2.3 and 2.5 on uniform Cartesian meshes with the same mesh size $h = 2^{-J} \times 2\pi$.

J	Example 2.8				Example 2.9			
	$\ u_h - u_{h/2}\ _2$	order	$\ u_h - u_{h/2}\ _\infty$	order	$\ u_h - u_{h/2}\ _2$	order	$\ u_h - u_{h/2}\ _\infty$	order
3	1.11E+01	0	8.15E+00	0	3.60E+02	0	5.64E+02	0
4	1.27E-01	6.443	1.01E-01	6.329	8.36E+00	5.428	1.92E+01	4.878
5	3.11E-03	5.350	2.97E-03	5.092	4.85E-01	4.108	1.47E+00	3.708
6	6.20E-05	5.650	8.57E-05	5.116	2.85E-03	7.413	9.31E-03	7.300
7	3.46E-07	7.487	6.83E-07	6.971	1.79E-05	7.313	5.83E-05	7.320

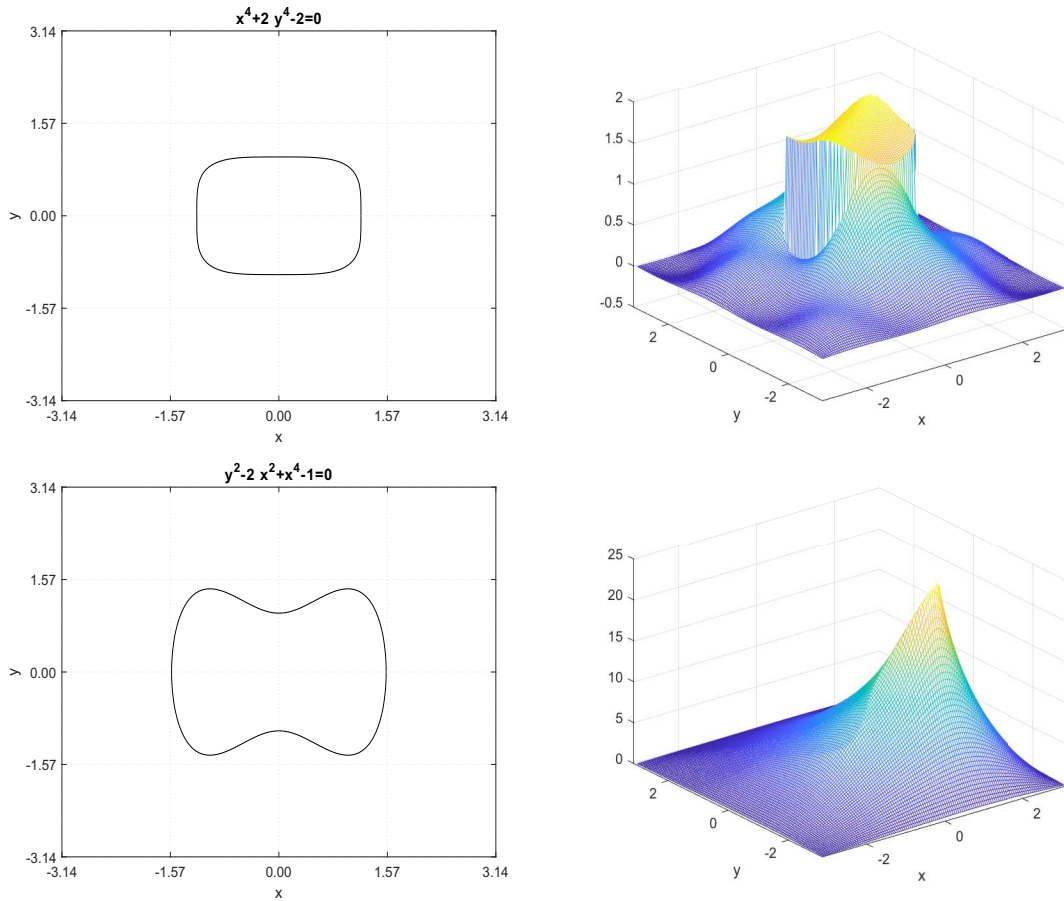


Figure 2.7: Top row for Example 2.8: the interface curve Γ (left) and the numerical solution u_h (right) with $h = 2^{-7} \times 2\pi$. Bottom row for Example 2.9: the interface curve Γ (left) and the numerical solution u_h (right) with $h = 2^{-7} \times 2\pi$.

$$g_0^\Gamma = \sin(x) - 10, \quad g_1^\Gamma = \cos(y), \quad g = 0, \quad \text{with } K = 5, 50, 500.$$

The numerical results are provided in Table 2.8 and Fig. 2.8.

Table 2.8: Performance in Example 2.10 of the proposed sixth order compact 9-point finite difference scheme in Theorems 2.3 and 2.5 on uniform Cartesian meshes with $h = 2^{-J} \times 1$.

J	$K = 5$				$K = 50$				$K = 500$			
	$\ u_h - u_{h/2}\ _2$	order	$\ u_h - u_{h/2}\ _\infty$	order	$\ u_h - u_{h/2}\ _2$	order	$\ u_h - u_{h/2}\ _\infty$	order	$\ u_h - u_{h/2}\ _2$	order	$\ u_h - u_{h/2}\ _\infty$	order
3	1.5E-02	0	1.4E-01	0	6.3E+03	0	4.1E+04	0	9.2E+09	0	6.3E+10	0
4	9.0E-05	7.42	1.1E-03	6.95	1.6E+02	5.27	1.3E+03	5.03	1.3E+08	6.15	1.2E+09	5.76
5	2.5E-06	5.15	3.3E-05	5.07	2.2E+00	6.20	1.9E+01	6.07	1.4E+06	6.51	1.7E+07	6.13
6	3.2E-08	6.33	4.2E-07	6.29	3.8E-02	5.87	3.7E-01	5.67	2.4E+04	5.88	3.8E+05	5.48
7					6.1E-04	5.97	7.5E-03	5.61	5.0E+02	5.59	7.2E+03	5.69
8					7.4E-06	6.36	9.4E-05	6.32	8.3E+00	5.91	1.5E+02	5.58
9									4.4E-01	4.24	6.0E+00	4.66
10									8.2E-03	5.75	1.1E-01	5.78
11									5.8E-05	7.13	1.5E-03	6.19

2.3.5 Numerical examples with unknown u , smooth Γ and $\Gamma \cap \partial\Omega \neq \emptyset$

In this subsection, we provide a few numerical experiments such that the exact solution u of (2.1) is unknown, the interface curve Γ is smooth and Γ touches the boundary of Ω .

Example 2.11. Let $\Omega = (-\pi, \pi)^2$ and the interface curve be given by $\Gamma := \{(x, y) \in \Omega : \psi(x, y) = 0\}$ with $\psi(x, y) = y - \cos(x)$. Note that $\Gamma \cap \partial\Omega \neq \emptyset$ and the coefficients of (2.1) are given by

$$f_+ = f\chi_{\Omega_+} = -\sin(x)\sin(3y), \quad f_- = f\chi_{\Omega_-} = -\sin(2x)\sin(y),$$

$$g_0^\Gamma = 0, \quad g_1^\Gamma = \sin(x), \quad g = 0.$$

Because $g_0^\Gamma = 0$, the Poisson interface problem in (2.1) simply becomes $-\nabla^2 u = f - g_1^\Gamma \delta_\Gamma$ in Ω with the Dirichlet boundary condition $u|_{\partial\Omega} = g$. The numerical results are provided in Table 2.9 and Fig. 2.9.

Example 2.12. Let $\Omega = (0, 3.5)^2$ and the interface curve be given by $\Gamma := \{(x, y) \in \Omega : \psi(x, y) = 0\}$ with $\psi(x, y) = \frac{x^2}{2} + \frac{y^2}{2} - 2$. Note that $\Gamma \cap \partial\Omega \neq \emptyset$ and the coefficients of (2.1) are given by

$$f_+ = f\chi_{\Omega_+} = \sin(\pi x)\sin(2\pi y), \quad f_- = f\chi_{\Omega_-} = \sin(2\pi x)\sin(\pi y),$$

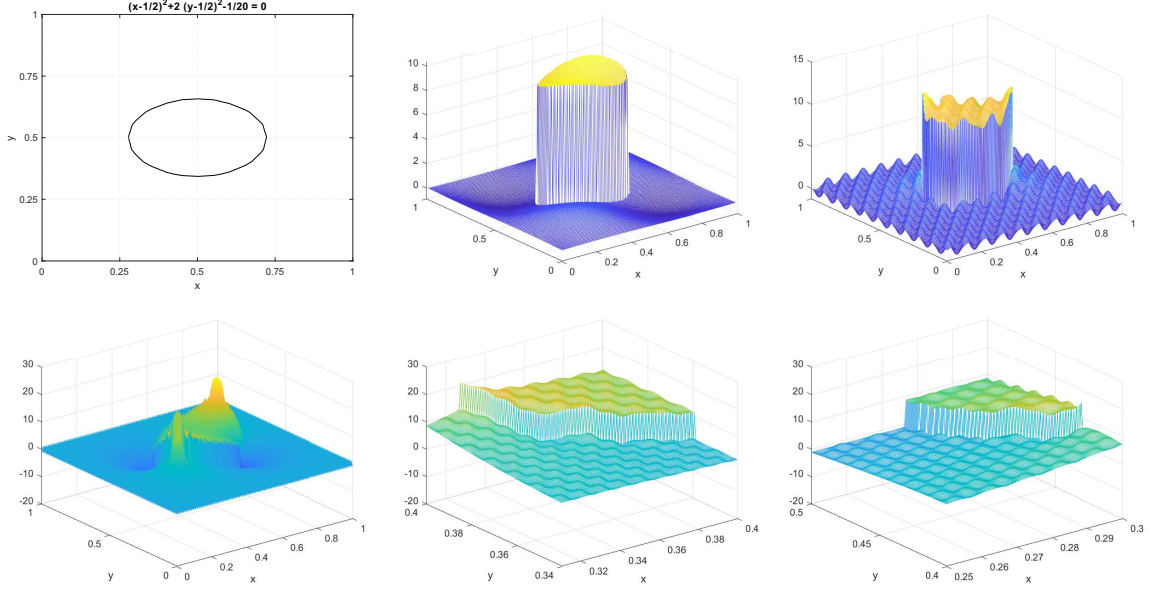


Figure 2.8: Top row for Example [2.10](#): the interface curve Γ (left), the numerical solution u_h with $K = 5$, $h = 2^{-7} \times 1$ (middle) and the numerical solution u_h with $K = 50$, $h = 2^{-8} \times 1$ (right). Bottom row for Example [2.10](#) with $K = 500$ and $h = 2^{-11} \times 1$: the numerical solution u_h in $(0, 1)^2$ (left), the numerical solution u_h in $(0.32, 0.4) \times (0.34, 0.4)$ (middle) and the numerical solution u_h in $(0.25, 0.3) \times (0.4, 0.5)$ (right).

$$g_0^\Gamma = 0, \quad g_1^\Gamma = -\sin(2\pi x) \sin(2\pi y), \quad g = 0.$$

Because $g_0^\Gamma = 0$, the Poisson interface problem in [\(2.1\)](#) simply becomes $-\nabla^2 u = f - g_1^\Gamma \delta_\Gamma$ in Ω with the Dirichlet boundary condition $u|_{\partial\Omega} = g$. The numerical results are provided in [Table 2.9](#) and [Fig. 2.9](#).

Example 2.13. Let $\Omega = (-\pi, \pi)^2$ and the interface curve be given by $\Gamma := \{(x, y) \in \Omega : \psi(x, y) = 0\}$ with $\psi(x, y) = y - \sin(x) - \frac{3}{10}$. Note that $\Gamma \cap \partial\Omega \neq \emptyset$ and the coefficients of [\(2.1\)](#) are given by

$$\begin{aligned} f_+ &= f\chi_{\Omega_+} = \sin(x) \sin(3y), & f_- &= f\chi_{\Omega_-} = \sin(2x) \sin(y), \\ g_0^\Gamma &= 0, & g_1^\Gamma &= -\sin(2x), & g &= 0. \end{aligned}$$

Because $g_0^\Gamma = 0$, the Poisson interface problem in [\(2.1\)](#) simply becomes $-\nabla^2 u = f - g_1^\Gamma \delta_\Gamma$ in Ω with the Dirichlet boundary condition $u|_{\partial\Omega} = g$. The numerical results are provided in [Table 2.10](#) and [Fig. 2.10](#).

Table 2.9: Performance in Examples 2.11 and 2.12 of the proposed sixth order compact 9-point finite difference scheme in Theorems 2.3 and 2.5 on uniform Cartesian meshes with $h = 2^{-J} \times 2\pi$ and $h = 2^{-J} \times 3.5$ respectively.

J	Example 2.11				Example 2.12			
	$\ u_h - u_{h/2}\ _2$	order	$\ u_h - u_{h/2}\ _\infty$	order	$\ u_h - u_{h/2}\ _2$	order	$\ u_h - u_{h/2}\ _\infty$	order
3	1.82E+00	0	2.71E+00	0	2.11E-01	0	3.94E-01	0
4	1.52E-02	6.900	2.37E-02	6.840	1.96E-03	6.745	4.65E-03	6.406
5	1.09E-04	7.128	1.83E-04	7.017	1.73E-05	6.828	3.43E-05	7.085
6	7.03E-07	7.272	1.23E-06	7.211	1.39E-07	6.959	3.13E-07	6.773
7	4.11E-09	7.418	7.61E-09	7.340	8.11E-09	4.098	6.00E-08	2.383

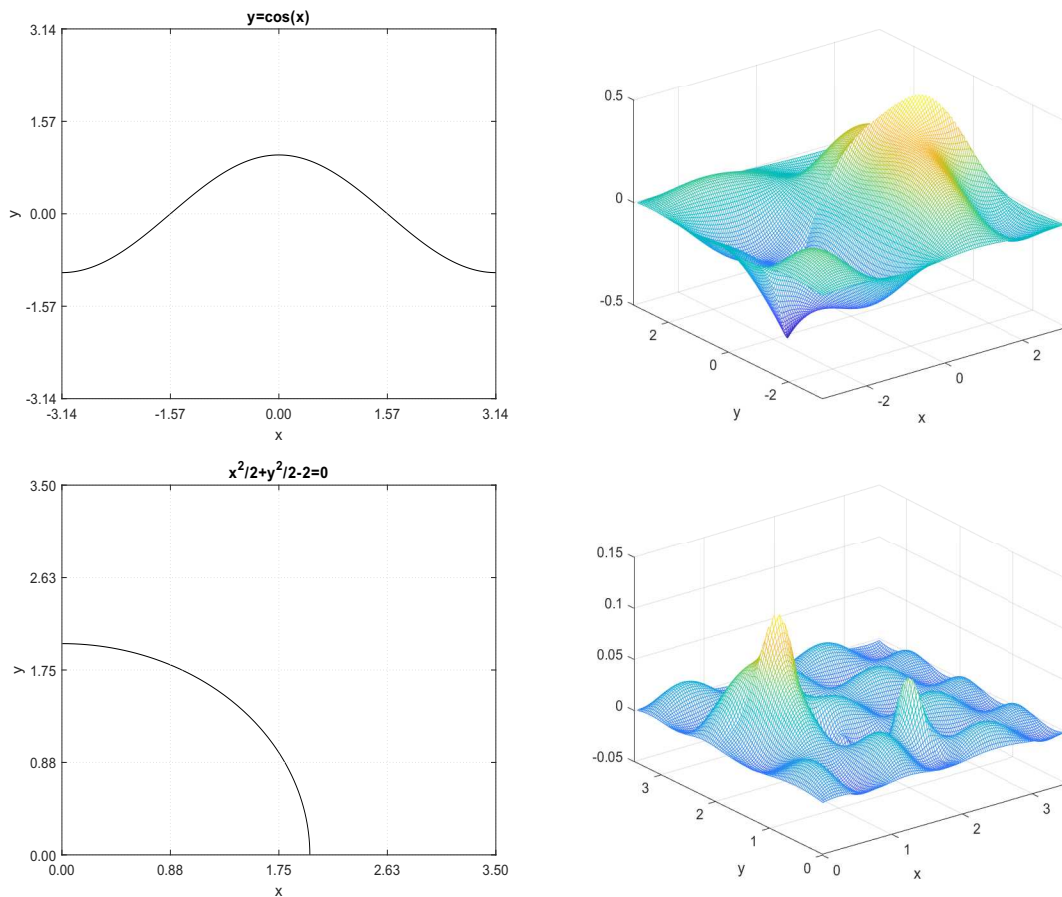


Figure 2.9: Top row for Example 2.11: the interface curve Γ (left) and the numerical solution u_h (right) with $h = 2^{-7} \times 2\pi$. Bottom row for Example 2.12: the interface curve Γ (left) and the numerical solution u_h (right) with $h = 2^{-7} \times 3.5$.

2.3.6 One numerical example with unknown u , sharp-edged Γ and $\Gamma \cap \partial\Omega = \emptyset$

In this subsection, we provide one numerical experiment such that the exact solution u of (2.1) is unknown, the interface curve Γ is sharp-edged and Γ does not touch the boundary of Ω .

Example 2.14. Let $\Omega = (-\frac{3\pi}{2}, \frac{3\pi}{2})^2$ and the interface curve be given by $\Gamma := \{(x, y) \in \Omega : \psi(x, y) = 0\}$ which is shown in Fig. 2.10. More precisely, the sharp-edged interface is a square with 4 corner points $(-2, 0)$, $(0, 2)$, $(2, 0)$ and $(0, -2)$. Note that $\Gamma \cap \partial\Omega = \emptyset$ and the coefficients of (2.1) are given by

$$\begin{aligned} f_+ &= f\chi_{\Omega_+} = 8 \sin(2x) \sin(2y), & f_- &= f\chi_{\Omega_-} = 8 \cos(2x) \cos(2y), \\ g_0^\Gamma &= -3, & g_1^\Gamma &= 0, & g &= 0. \end{aligned}$$

The numerical results are provided in Table 2.10 and Fig. 2.10.

Table 2.10: Performance in Examples 2.13 and 2.14 of the proposed sixth order compact 9-point finite difference scheme in Theorems 2.3 and 2.5 on uniform Cartesian meshes with $h = 2^{-J} \times 2\pi$ and $h = 2^{-J} \times 3\pi$ respectively.

J	Example 2.13				Example 2.14			
	$\ u_h - u_{h/2}\ _2$	order	$\ u_h - u_{h/2}\ _\infty$	order	$\ u_h - u_{h/2}\ _2$	order	$\ u_h - u_{h/2}\ _\infty$	order
3	8.61E-01	0	9.54E-01	0	7.44E+00	0	8.73E+00	0
4	1.47E-03	9.196	2.36E-03	8.662	1.22E+00	2.614	6.12E-01	3.835
5	3.11E-05	5.559	8.19E-05	4.846	3.88E-01	1.646	2.57E-01	1.254
6	2.81E-06	3.468	1.57E-05	2.382	5.30E-02	2.874	4.01E-02	2.679
7	5.71E-07	2.301	6.39E-06	1.299	6.58E-03	3.010	5.31E-03	2.917

Remark 2.8. The interfaces of Examples 2.13 and 2.14 are shown in Fig. 2.10. Note that $\Gamma \cap \partial\Omega \neq \emptyset$ and the angle between Γ and $\partial\Omega$ is not $\pi/2$ in Example 2.13 and the interface is sharp-edged in Example 2.14. Thus, the solutions of Examples 2.13 and 2.14 would both contain singular functions which will affect the convergence rate (see Table 2.10 for details).

2.4 Conclusion

To our best knowledge, so far there were no compact 9-point finite difference schemes available in the literature, that can achieve fifth or sixth order for Poisson interface problems

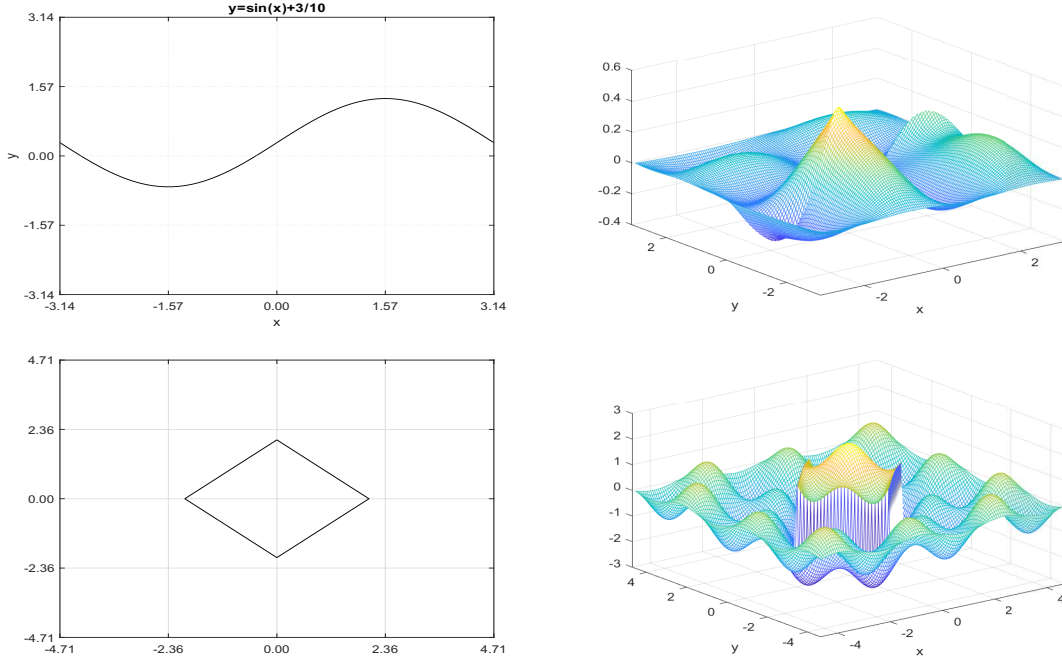


Figure 2.10: Top row for Example [2.13](#): the interface curve Γ (left) and the numerical solution u_h (right) with $h = 2^{-7} \times 2\pi$. Bottom row for Example [2.14](#): the interface curve Γ (left) and the numerical solution u_h (right) with $h = 2^{-7} \times 3\pi$.

with singular source terms [\(2.1\)](#). Our contribution of this chapter is that, we construct the sixth order compact 9-point finite difference schemes on uniform meshes for [\(2.1\)](#) with two non-homogeneous jump conditions and provide explicit formulas for the coefficients of the linear equations. The explicit formulas are independent on how the interface curve partitions the nine points in a stencil, so one can handle the 72 different cases configurations of the nine-point stencil with respect to the interface. The matrix A of the linear equations $Ax = b$, appearing after the discretization, is fixed for any source terms, two jump conditions and interface curves, and this allows for an easy design of preconditioners if iterative methods are used for the solution of the linear system associated with interface problems. The independence of A also allows us to directly use the zero extension and the FFT acceleration in [\[39\]](#) to solve $Ax = b$ without adding new unknown variables to obtain the augmented system and using the Schur complement to solve it. This is particularly useful in case of moving boundary problems. Furthermore, we prove the order 6 convergence for the proposed scheme using the discrete maximum principle. Our numerical experiments confirm the flexibility and the sixth order accuracy in l_2 and l_∞ norms of the proposed schemes.

2.5 Proof of Theorem 2.4

Proof. Since the tangent vector at t of the curve Γ parameterized by (1.5) is given by $(x', y') = (r'(t), s'(t))$, the unit normal vector $\vec{n}(r(t) + x_i^*, s(t) + y_j^*)$ at the point $(r(t) + x_i^*, s(t) + y_j^*)$ pointing from Ω_- to Ω_+ is given by one of

$$\vec{n}(r(t) + x_i^*, s(t) + y_j^*) = \pm \frac{(y', -x')}{\sqrt{(r'(t))^2 + (s'(t))^2}} = \pm \frac{(s'(t), -r'(t))}{\sqrt{(r'(t))^2 + (s'(t))^2}}.$$

Let us firstly consider

$$\vec{n}(r(t) + x_i^*, s(t) + y_j^*) = \frac{(s'(t), -r'(t))}{\sqrt{(r'(t))^2 + (s'(t))^2}}. \quad (2.33)$$

Now we shall use the interface conditions in (2.1). Plugging the parametric equation in (1.5) into the interface condition $[u] = g_0^\Gamma$ on Γ , near the base point (x_i^*, y_j^*) we have

$$u_+(r(t) + x_i^*, s(t) + y_j^*) - u_-(r(t) + x_i^*, s(t) + y_j^*) = g_0^\Gamma(r(t) + x_i^*, s(t) + y_j^*), \quad (2.34)$$

for $t \in (-\epsilon, \epsilon)$. Similarly, for flux, we have

$$\begin{aligned} (\nabla u_+)(r(t) + x_i^*, s(t) + y_j^*) \cdot \vec{n}(r(t) + x_i^*, s(t) + y_j^*) - (\nabla u_-)(r(t) + x_i^*, s(t) + y_j^*) \cdot \vec{n}(r(t) + x_i^*, s(t) + y_j^*) \\ = g_1^\Gamma(r(t) + x_i^*, s(t) + y_j^*), \end{aligned}$$

for $t \in (-\epsilon, \epsilon)$. Using the unit norm vector in (2.33), the above relation becomes

$$\begin{aligned} ((\nabla u_+)(r(t) + x_i^*, s(t) + y_j^*) - (\nabla u_-)(r(t) + x_i^*, s(t) + y_j^*)) \cdot (s'(t), -r'(t)) \\ = g_1^\Gamma(r(t) + x_i^*, s(t) + y_j^*) \sqrt{(r'(t))^2 + (s'(t))^2}, \end{aligned} \quad (2.35)$$

for $t \in (-\epsilon, \epsilon)$. Since all involved functions in (2.34) and (2.35) are assumed to be smooth, to link the two sets $u_+^{(m,n)}$ and $u_-^{(m,n)}$ for $(m, n) \in \Lambda_M^1$, we now take the Taylor approximation of the above functions near the base parameter $t = 0$. By (2.21) with M being replaced by $M - 1$, we have

$$\begin{aligned} u_\pm(r(t) + x_i^*, s(t) + y_j^*) \\ = \sum_{(m,n) \in \Lambda_M^1} u_\pm^{(m,n)} G_{M,m,n}(r(t), s(t)) + \sum_{(m,n) \in \Lambda_{M-2}} f_\pm^{(m,n)} Q_{M,m,n}(r(t), s(t)) + \mathcal{O}(t^{M+1}) \\ = \sum_{p=0}^M \left(\sum_{(m,n) \in \Lambda_M^1} u_\pm^{(m,n)} g_{m,n,p} + \sum_{(m,n) \in \Lambda_{M-2}} f_\pm^{(m,n)} q_{m,n,p} \right) t^p + \mathcal{O}(t^{M+1}), \end{aligned}$$

where the constants $g_{m,n,p}$ and $q_{m,n,p}$ only depend on $r^{(\ell)}(0)$ and $s^{(\ell)}(0)$ for $\ell = 0, \dots, M$, and are uniquely determined by

$$G_{M,m,n}(r(t), s(t)) - \sum_{p=0}^M g_{m,n,p} t^p = \mathcal{O}(t^{M+1}) \quad \text{and} \quad Q_{M,m,n}(r(t), s(t)) - \sum_{p=0}^M q_{m,n,p} t^p = \mathcal{O}(t^{M+1}), \quad t \rightarrow 0.$$

More precisely,

$$g_{m,n,p} := \frac{1}{p!} \left. \frac{d^p (G_{M,m,n}(r(t), s(t)))}{dt^p} \right|_{t=0}, \quad q_{m,n,p} := \frac{1}{p!} \left. \frac{d^p (Q_{M,m,n}(r(t), s(t)))}{dt^p} \right|_{t=0}, \quad p = 0, \dots, M. \quad (2.36)$$

Similarly, we have

$$g_0^\Gamma(r(t) + x_i^*, s(t) + y_j^*) = \sum_{p=0}^M g_{0,p}^\Gamma t^p + \mathcal{O}(t^{M+1}),$$

where the constants $g_{0,p}^\Gamma := \frac{1}{p!} \left. \frac{d^p (g_0^\Gamma(r(t) + x_i^*, s(t) + y_j^*))}{dt^p} \right|_{t=0}$ for $p = 0, \dots, M$. Since $G_{M,m,n}$ is a homogeneous polynomial of degree $m + n$ and because $r(0) = s(0) = 0$, we must have $g_{m,n,p} = 0$ for all $0 \leq p < m + n$ by (2.36). Define

$$U^{(m,n)} := u_+^{(m,n)} - u_-^{(m,n)}, \quad (m, n) \in \Lambda_M^1.$$

Consequently, we deduce from (2.34) that

$$\sum_{(m,n) \in \Lambda_M^1} U^{(m,n)} g_{m,n,p} = \sum_{(m,n) \in \Lambda_M^1} (u_+^{(m,n)} - u_-^{(m,n)}) g_{m,n,p} = F_p, \quad p = 0, \dots, M, \quad (2.37)$$

where $F_0 := g_{0,0}^\Gamma$ and

$$F_p := \sum_{(m,n) \in \Lambda_{M-2}} (f_-^{(m,n)} - f_+^{(m,n)}) q_{m,n,p} + g_{0,p}^\Gamma, \quad p = 1, \dots, M.$$

Note that $g_{0,0,0} = 1$ and $g_{m,n,p} = 0$ for all $0 \leq p < m + n$. We observe that the identities in (2.37) can be equivalently rewritten as

$$U^{(0,0)} = F_0 = g_{0,0}^\Gamma, \quad (2.38)$$

and

$$U^{(0,p)} g_{0,p,p} + U^{(1,p-1)} g_{1,p-1,p} = F_p - \sum_{(m,n) \in \Lambda_M^1, m+n < p} U^{(m,n)} g_{m,n,p}, \quad p = 1, \dots, M. \quad (2.39)$$

On the other hand, (2.21) with M being replaced by $M - 1$ implies that

$$\nabla u_{\pm}(x+x_i^*, y+y_j^*) = \sum_{(m,n) \in \Lambda_M^1} u_{\pm}^{(m,n)} \nabla G_{M,m,n}(x, y) + \sum_{(m,n) \in \Lambda_{M-2}} f_{\pm}^{(m,n)} \nabla Q_{M,m,n}(x, y) + \mathcal{O}(h^M), \quad (2.40)$$

for $x, y \in (-2h, 2h)$. Using (2.40) and a similar argument, we have

$$\begin{aligned} & \nabla u_{\pm}(r(t) + x_i^*, s(t) + y_j^*) \cdot (s'(t), -r'(t)) \\ &= \sum_{(m,n) \in \Lambda_M^1} u_{\pm}^{(m,n)} \nabla G_{M,m,n}(r(t), s(t)) \cdot (s'(t), -r'(t)) \\ &+ \sum_{(m,n) \in \Lambda_{M-2}} f_{\pm}^{(m,n)} \nabla Q_{M,m,n}(r(t), s(t)) \cdot (s'(t), -r'(t)) \\ &= \sum_{p=0}^{M-1} \left(\sum_{(m,n) \in \Lambda_M^1} u_{\pm}^{(m,n)} \tilde{g}_{m,n,p} + \sum_{(m,n) \in \Lambda_{M-2}} f_{\pm}^{(m,n)} \tilde{q}_{m,n,p} \right) t^p + \mathcal{O}(t^M), \end{aligned}$$

where the constants $\tilde{g}_{m,n,p}$ and $\tilde{q}_{m,n,p}$ are uniquely determined by

$$\begin{aligned} \nabla G_{M,m,n}(r(t), s(t)) \cdot (s'(t), -r'(t)) - \sum_{p=0}^{M-1} \tilde{g}_{m,n,p} t^p &= \mathcal{O}(t^M), \quad t \rightarrow 0, \\ \nabla Q_{M,m,n}(r(t), s(t)) \cdot (s'(t), -r'(t)) - \sum_{p=0}^{M-1} \tilde{q}_{m,n,p} t^p &= \mathcal{O}(t^M), \quad t \rightarrow 0. \end{aligned}$$

More precisely, for $p = 0, \dots, M - 1$,

$$\tilde{g}_{m,n,p} := \frac{1}{p!} \frac{d^p (\nabla G_{M,m,n}(r(t), s(t)) \cdot (s'(t), -r'(t)))}{dt^p} \Big|_{t=0}, \quad (2.41)$$

and

$$\tilde{q}_{m,n,p} := \frac{1}{p!} \frac{d^p (\nabla Q_{M,m,n}(r(t), s(t)) \cdot (s'(t), -r'(t)))}{dt^p} \Big|_{t=0}.$$

Note that each entry of $\nabla G_{M,m,n}(x, y)$ is a homogeneous polynomial of degree $m + n - 1$. By $r(0) = s(0) = 0$ and (2.41), we observe that $\tilde{g}_{m,n,p} = 0$ for all $0 \leq p < m + n - 1$. Similarly, we have

$$g_1^{\Gamma}(r(t) + x_i^*, s(t) + y_j^*) \sqrt{(r'(t))^2 + (s'(t))^2} = \sum_{p=0}^{M-1} g_{1,p}^{\Gamma} t^p + \mathcal{O}(t^M),$$

as $t \rightarrow 0$, where the constants $g_{1,p}^\Gamma$ for $p = 0, \dots, M-1$ are uniquely determined by

$$g_{1,p}^\Gamma := \frac{1}{p!} \frac{d^p}{dt^p} \left[g_1^\Gamma(r(t) + x_i^*, s(t) + y_j^*) \sqrt{(r'(t))^2 + (s'(t))^2} \right] \Big|_{t=0}, \quad p = 0, \dots, M-1.$$

Consequently, (2.35) implies that for all $p = 0, \dots, M-1$,

$$\sum_{(m,n) \in \Lambda_M^1} U^{(m,n)} \tilde{g}_{m,n,p} = \sum_{(m,n) \in \Lambda_M^1} \left(u_+^{(m,n)} - u_-^{(m,n)} \right) \tilde{g}_{m,n,p} = G_p, \quad p = 0, \dots, M-1, \quad (2.42)$$

where

$$G_p := \sum_{(m,n) \in \Lambda_{M-2}} \left(f_-^{(m,n)} - f_+^{(m,n)} \right) \tilde{q}_{m,n,p} + g_{1,p}^\Gamma.$$

Note that $\tilde{g}_{0,0,0} = 0$ and $\tilde{g}_{m,n,p} = 0$ for all $0 \leq p < m+n-1$. We observe that the identities in (2.42) can be equivalently rewritten as

$$U^{(0,p)} \tilde{g}_{0,p,p-1} + U^{(1,p-1)} \tilde{g}_{1,p-1,p-1} = G_{p-1} - \sum_{(m,n) \in \Lambda_M^1, m+n < p} U^{(m,n)} \tilde{g}_{m,n,p-1}, \quad p = 1, \dots, M. \quad (2.43)$$

Using our assumption $(r'(0))^2 + (s'(0))^2 > 0$ in (1.5), we now claim that

$$g_{0,p,p} \tilde{g}_{1,p-1,p-1} - g_{1,p-1,p} \tilde{g}_{0,p,p-1} > 0, \quad \forall p = 1, \dots, M.$$

Since the polynomial $G_{M,m,n}(x, y)$ in (2.7) is a homogeneous polynomial of degree $m+n$, we observe

$$g_{m,n,m+n} = G_{M,m,n}(r'(0), s'(0)), \quad (m, n) \in \Lambda_M^1.$$

From the definition of $G_{M,m,n}(x, y)$ in (2.7), we particularly have

$$g_{0,p,p} = \sum_{\ell=0}^{\lfloor \frac{p}{2} \rfloor} (-1)^\ell \frac{(r'(0))^{2\ell} (s'(0))^{p-2\ell}}{(2\ell)!(p-2\ell)!} \quad \text{and} \quad g_{1,p-1,p} = \sum_{\ell=0}^{\lfloor \frac{p-1}{2} \rfloor} (-1)^\ell \frac{(r'(0))^{1+2\ell} (s'(0))^{p-1-2\ell}}{(1+2\ell)!(p-1-2\ell)!}. \quad (2.44)$$

Clearly,

$$\left\lfloor \frac{p}{2} \right\rfloor = \begin{cases} \left\lfloor \frac{p-1}{2} \right\rfloor + 1, & \text{if } p \text{ is even,} \\ \left\lfloor \frac{p-1}{2} \right\rfloor, & \text{if } p \text{ is odd,} \end{cases} \quad \text{and} \quad 2 \left\lfloor \frac{p-1}{2} \right\rfloor + 1 = p, \quad \text{if } p \text{ is odd.} \quad (2.45)$$

Similarly, we also have

$$\tilde{g}_{m,n,m+n-1} = \nabla G_{M,m,n}(r'(0), s'(0)) \cdot (s'(0), -r'(0)), \quad (m, n) \in \Lambda_M^1.$$

From the definition of $G_{M,m,n}(x, y)$ in (2.7), we deduce that

$$\begin{aligned}
\tilde{g}_{0,p,p-1} &= \nabla G_{M,0,p}(r'(0), s'(0)) \cdot (s'(0), -r'(0)) \\
&= \sum_{\ell=1}^{\lfloor \frac{p}{2} \rfloor} (-1)^\ell \frac{(r'(0))^{2\ell-1} (s'(0))^{p+1-2\ell}}{(2\ell-1)!(p-2\ell)!} - \sum_{\ell=0}^{\lfloor \frac{p-1}{2} \rfloor} (-1)^\ell \frac{(r'(0))^{2\ell+1} (s'(0))^{p-2\ell-1}}{(2\ell)!(p-2\ell-1)!} \\
&= - \sum_{\ell=0}^{\lfloor \frac{p}{2} \rfloor - 1} (-1)^\ell \frac{(r'(0))^{2\ell+1} (s'(0))^{p-2\ell-1}}{(2\ell+1)!(p-2\ell-2)!} - \sum_{\ell=0}^{\lfloor \frac{p-1}{2} \rfloor} (-1)^\ell \frac{(r'(0))^{2\ell+1} (s'(0))^{p-2\ell-1}}{(2\ell)!(p-2\ell-1)!}.
\end{aligned} \tag{2.46}$$

By (2.44), (2.45) and (2.46), we conclude that

$$\tilde{g}_{0,p,p-1} = -p \sum_{\ell=0}^{\lfloor \frac{p-1}{2} \rfloor} (-1)^\ell \frac{(r'(0))^{2\ell+1} (s'(0))^{p-2\ell-1}}{(2\ell+1)!(p-2\ell-1)!} = -pg_{1,p-1,p}. \tag{2.47}$$

Similarly,

$$\begin{aligned}
\tilde{g}_{1,p-1,p-1} &= \nabla G_{M,1,p-1}(r'(0), s'(0)) \cdot (s'(0), -r'(0)) \\
&= \sum_{\ell=0}^{\lfloor \frac{p-1}{2} \rfloor} (-1)^\ell \frac{(r'(0))^{2\ell} (s'(0))^{p-2\ell}}{(2\ell)!(p-1-2\ell)!} - \sum_{\ell=0}^{\lfloor \frac{p}{2} \rfloor - 1} (-1)^\ell \frac{(r'(0))^{2\ell+2} (s'(0))^{p-2\ell-2}}{(2\ell+1)!(p-2\ell-2)!} \\
&= \sum_{\ell=0}^{\lfloor \frac{p-1}{2} \rfloor} (-1)^\ell \frac{(r'(0))^{2\ell} (s'(0))^{p-2\ell}}{(2\ell)!(p-1-2\ell)!} + \sum_{\ell=1}^{\lfloor \frac{p}{2} \rfloor} (-1)^\ell \frac{(r'(0))^{2\ell} (s'(0))^{p-2\ell}}{(2\ell-1)!(p-2\ell)!}.
\end{aligned} \tag{2.48}$$

By (2.44), (2.45) and (2.48), we deduce that

$$\tilde{g}_{1,p-1,p-1} = p \sum_{\ell=0}^{\lfloor \frac{p}{2} \rfloor} (-1)^\ell \frac{(r'(0))^{2\ell} (s'(0))^{p-2\ell}}{(2\ell)!(p-2\ell)!} = pg_{0,p,p}. \tag{2.49}$$

By (2.47) and (2.49),

$$g_{0,p,p} \tilde{g}_{1,p-1,p-1} - g_{1,p-1,p} \tilde{g}_{0,p,p-1} = p(g_{0,p,p})^2 + p(g_{1,p-1,p})^2, \quad \forall p = 1, \dots, M. \tag{2.50}$$

Let

$$W := (p!)^2 (g_{0,p,p})^2 + (p!)^2 (g_{1,p-1,p})^2, \quad a := (r'(0))^2 \quad \text{and} \quad b := (s'(0))^2. \tag{2.51}$$

Then

$$\begin{aligned}
W &= \left(\sum_{\ell=0}^{\lfloor \frac{p}{2} \rfloor} (-1)^\ell \binom{p}{2\ell} a^\ell b^{p/2-\ell} \right)^2 + \left(\sum_{\ell=0}^{\lfloor \frac{p-1}{2} \rfloor} (-1)^\ell \binom{p}{2\ell+1} a^{1/2+\ell} b^{(p-1)/2-\ell} \right)^2 \\
&= \sum_{i=0}^{\lfloor \frac{p}{2} \rfloor} \sum_{j=0}^{\lfloor \frac{p}{2} \rfloor} (-1)^{i+j} \binom{p}{2i} \binom{p}{2j} a^{i+j} b^{p-i-j} + \sum_{i=0}^{\lfloor \frac{p-1}{2} \rfloor} \sum_{j=0}^{\lfloor \frac{p-1}{2} \rfloor} (-1)^{i+j} \binom{p}{2i+1} \binom{p}{2j+1} a^{1+i+j} b^{p-1-i-j} \\
&= \sum_{\ell=0}^{2\lfloor \frac{p}{2} \rfloor} \sum_{i=\max(0, \ell-\lfloor \frac{p}{2} \rfloor)}^{\min(\ell, \lfloor \frac{p}{2} \rfloor)} (-1)^\ell \binom{p}{2i} \binom{p}{2(\ell-i)} a^\ell b^{p-\ell} \\
&\quad - \sum_{\ell=0}^{2\lfloor \frac{p-1}{2} \rfloor+1} \sum_{i=\max(0, \ell-\lfloor \frac{p+1}{2} \rfloor)}^{\min(\ell-1, \lfloor \frac{p-1}{2} \rfloor)} (-1)^\ell \binom{p}{2i+1} \binom{p}{2(\ell-i)-1} a^\ell b^{p-\ell}.
\end{aligned} \tag{2.52}$$

Let us consider the first case: p is even and $\ell \leq \lfloor \frac{p}{2} \rfloor$. Then

$$\begin{aligned}
&\sum_{i=\max(0, \ell-\lfloor \frac{p}{2} \rfloor)}^{\min(\ell, \lfloor \frac{p}{2} \rfloor)} (-1)^\ell \binom{p}{2i} \binom{p}{2(\ell-i)} - \sum_{i=\max(0, \ell-\lfloor \frac{p+1}{2} \rfloor)}^{\min(\ell-1, \lfloor \frac{p-1}{2} \rfloor)} (-1)^\ell \binom{p}{2i+1} \binom{p}{2(\ell-i)-1} \\
&= \sum_{i=0}^{\ell} (-1)^\ell \binom{p}{2i} \binom{p}{2(\ell-i)} - \sum_{i=0}^{\ell-1} (-1)^\ell \binom{p}{2i+1} \binom{p}{2(\ell-i)-1} \\
&= (-1)^\ell \sum_{i=0,2,4}^{2\ell} \binom{p}{i} \binom{p}{2\ell-i} - (-1)^\ell \sum_{i=1,3,5}^{2\ell-1} \binom{p}{i} \binom{p}{2\ell-i} = (-1)^\ell \sum_{i=0}^{2\ell} (-1)^i \binom{p}{i} \binom{p}{2\ell-i} \\
&= (-1)^\ell \sum_{i=0}^{2\ell} \text{coeff}((1-x)^p, x^i) \text{coeff}((1+x)^p, x^{2\ell-i}) = (-1)^\ell \text{coeff}((1-x^2)^p, x^{2\ell}) = \binom{p}{\ell},
\end{aligned} \tag{2.53}$$

where the $\text{coeff}(f(x), x^n)$ function extracts the coefficient of x^n in the polynomial $f(x)$. Similarly, we can prove that other cases can obtain the same result. By (2.51), (2.52) and (2.53),

$$W = \sum_{\ell=0}^p \binom{p}{\ell} a^\ell b^{p-\ell} = (a+b)^p = \left((r'(0))^2 + (s'(0))^2 \right)^p. \tag{2.54}$$

According to (2.50), (2.51), (2.54) and (1.5),

$$g_{0,p,p} \tilde{g}_{1,p-1,p-1} - g_{1,p-1,p} \tilde{g}_{0,p,p-1} > 0, \quad \forall p = 1, \dots, M.$$

Consequently, the associated 2×2 coefficient matrix in the linear system in (2.39) and (2.43) is invertible and its inverse is given by

$$Q_p := \frac{1}{g_{0,p,p}\tilde{g}_{1,p-1,p-1} - g_{1,p-1,p}\tilde{g}_{0,p,p-1}} \begin{bmatrix} \tilde{g}_{1,p-1,p-1} & -g_{1,p-1,p} \\ -\tilde{g}_{0,p,p-1} & g_{0,p,p} \end{bmatrix}.$$

Hence, the linear equations in (2.39) and (2.43) must have a unique solution $\{U^{(0,p)}, U^{(1,p-1)}\}$ with $p = 1, \dots, M$, which can be recursively computed from $p = 1$ to $p = M$ by $U^{(0,0)} = g_{0,0}^\Gamma$ due to (2.38) and

$$\begin{bmatrix} U^{(0,p)} \\ U^{(1,p-1)} \end{bmatrix} = Q_p \begin{bmatrix} F_p \\ G_{p-1} \end{bmatrix} - \sum_{n=1}^{p-1} Q_p \begin{bmatrix} U^{(0,n)}g_{0,n,p} + U^{(1,n-1)}g_{1,n-1,p} \\ U^{(0,n)}\tilde{g}_{0,n,p-1} + U^{(1,n-1)}\tilde{g}_{1,n-1,p-1} \end{bmatrix}, \quad p = 1, \dots, M. \quad (2.55)$$

Note that for $p = 1$, the above summation $\sum_{n=1}^{p-1}$ is empty.

If the normal vector \vec{n} in (2.33) gives the direction from Ω_+ to Ω_- , then we only need to add a negative sign to all $\tilde{r}_{m,n,p}$. Since $U^{(m,n)} = u_+^{(m,n)} - u_-^{(m,n)}$, the identities in (2.55) and (2.38) prove all the claims. \square

Chapter 3

A High Order Compact 9-Point Finite Difference Scheme for Elliptic Interface Problems with Discontinuous and High-Contrast Coefficients

3.1 Introduction and problem formulation

Elliptic interface problems with discontinuous coefficients appear in many real-world applications: composite materials, fluid mechanics, nuclear waste disposal, and many others. In Chapter 2, we derived a sixth order compact 9-point finite difference scheme for the Poisson equation with singular sources, whose solution has a discontinuity across a smooth interface. The most important feature of the scheme in Chapter 2 is that the matrix of the resulting linear system is independent of the location of the singularity in the source term. In this chapter, we consider the more general case of an elliptic interface problem with a discontinuous, piecewise smooth, and high-contrast coefficient, and a discontinuous source term. The problem involves two non-homogeneous jump conditions across an interface curve, one on the solution, and the other on the normal component of its gradient. In summary, the goal of this chapter is to derive a high order compact 9-point finite difference scheme for the

elliptic interface problem with piecewise smooth coefficients and sources:

$$\begin{cases} -\nabla \cdot (a\nabla u) = f & \text{in } \Omega \setminus \Gamma, \\ [u] = g_0^\Gamma & \text{on } \Gamma, \\ [a\nabla u \cdot \vec{n}] = g_1^\Gamma & \text{on } \Gamma, \\ u = g & \text{on } \partial\Omega. \end{cases} \quad (3.1)$$

Here \vec{n} is the unit normal vector of Γ pointing towards Ω_+ , and for a point $(x_0, y_0) \in \Gamma$,

$$[u](x_0, y_0) := \lim_{\substack{(x,y) \in \Omega_+ \\ (x,y) \rightarrow (x_0, y_0)}} u(x, y) - \lim_{\substack{(x,y) \in \Omega_- \\ (x,y) \rightarrow (x_0, y_0)}} u(x, y), \quad (3.2)$$

$$[a\nabla u \cdot \vec{n}](x_0, y_0) := \lim_{\substack{(x,y) \in \Omega_+ \\ (x,y) \rightarrow (x_0, y_0)}} a(x, y) \nabla u(x, y) \cdot \vec{n} - \lim_{\substack{(x,y) \in \Omega_- \\ (x,y) \rightarrow (x_0, y_0)}} a(x, y) \nabla u(x, y) \cdot \vec{n}. \quad (3.3)$$

For the convenience of readers, an example for (3.1) with $\psi(x, y) = x^2 + y^2 - 2$ is illustrated in Fig. 3.1.

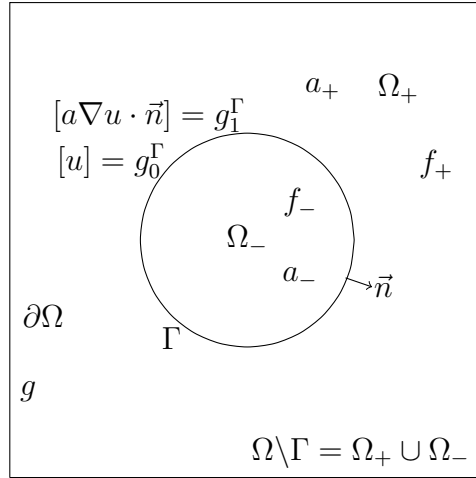


Figure 3.1: The problem region $\Omega = (-\pi, \pi)^2$ and the two subregions $\Omega_+ = \{(x, y) \in \Omega : \psi(x, y) > 0\}$ and $\Omega_- = \{(x, y) \in \Omega : \psi(x, y) < 0\}$ partitioned by the interface curve $\Gamma = \{(x, y) \in \Omega : \psi(x, y) = 0\}$ with the function $\psi(x, y) = x^2 + y^2 - 2$.

In this chapter we consider the elliptic interface problem in (3.1) under the following assumptions (Note that the main results in this chapter have been written in [33]):

(A1) The coefficient a is positive, piecewise smooth and has uniformly continuous partial derivatives of (total) orders up to four in each of the subregions Ω_+ and Ω_- . Note that a can be discontinuous across the interface Γ .

(A2) The solution u and the source term f have uniformly continuous partial derivatives of

(total) orders up to five and three respectively in each of the subregions Ω_+ and Ω_- . Both u and f can be discontinuous across the interface Γ .

- (A3) The interface curve Γ is smooth in the sense that for each $(x^*, y^*) \in \Gamma$, there exists a local parametric equation: $\gamma : (-\epsilon, \epsilon) \rightarrow \Gamma$ with $\epsilon > 0$ such that $\gamma(0) = (x^*, y^*)$ and $\|\gamma'(0)\|_2 \neq 0$. Furthermore, $x(t)$ and $y(t)$ in (1.5) should both have uniformly continuous derivatives of (total) order up to three for the variable $t = 0$.
- (A4) The one-dimensional functions $g_0^\Gamma \circ \gamma$ and $g_1^\Gamma \circ \gamma$ have uniformly continuous derivatives of (total) orders up to three and two respectively on the interface Γ , where γ is given in (A3).

This chapter is organized as follows.

In Section 3.3.1, we construct the fourth order compact 9-point finite difference scheme for the numerical solution at regular points. The explicit formulas at regular points are shown in Theorem 3.2.

In Section 3.3.2, we derive the third order compact 9-point finite difference scheme for the numerical solution at irregular points, and discuss its accuracy order in Theorem 3.4.

In Section 3.3.3, we numerically verify the sign conditions of our proposed compact 9-point finite difference scheme and prove the fourth order convergence rate by the discrete maximum principle in Theorem 3.6.

In Section 3.4, the explicit formulas for the local calculation of the gradient approximation at regular and irregular points are shown in Theorem 3.7 and Theorem 3.8 respectively. Note that the gradient computation is done explicitly.

In Section 3.5, we provide numerical results to verify the convergence rate measured in the l_2 and l_∞ norms for the numerical solution u_h , and the gradient approximation ∇u_h . We consider two test cases: (1) the exact solution is known and Γ does not intersect $\partial\Omega$ and (2) the exact solution is unknown and Γ does not intersect $\partial\Omega$. Note that, we compare our proposed compact 9-point scheme with the second order IIM, EJIIM, MIB, AMIB, and the fourth order IIM in Example 3.1, and choose the coefficient contrast as $\sup(a_+)/\inf(a_-) \approx 10^{-3}$ and 10^6 in Examples 3.2 to 3.6.

In Section 3.6, we summarize the main contributions of this chapter. Finally, in Section 3.7, we present the proof of Theorem 3.3.

3.2 Preliminary

We extend the results in (2.2) of Poisson interface problems to the elliptic interface problems by the following lemma:

Lemma 3.1. *Let u be a function satisfying $-\nabla \cdot (a \nabla u) = f$ in $\Omega \setminus \Gamma$. If a point $(x_i^*, y_j^*) \in \Omega \setminus \Gamma$, then*

$$\begin{aligned} u^{(m', n')} &= (-1)^{\lfloor \frac{m'}{2} \rfloor} u^{(\text{odd}(m'), n' + m' - \text{odd}(m'))} + \sum_{(m, n) \in \Lambda_{m'+n'-1}^1} A_{m', n', m, n}^u u^{(m, n)} \\ &+ \sum_{\ell=1}^{\lfloor \frac{m'}{2} \rfloor} \frac{(-1)^\ell f^{(m'-2\ell, n'+2\ell-2)}}{a^{(0,0)}} + \sum_{(m, n) \in \Lambda_{m'+n'-3}} A_{m', n', m, n}^f f^{(m, n)}, \quad \forall (m', n') \in \Lambda_{M+1}^2, \end{aligned} \quad (3.4)$$

where the subsets Λ_{M+1}^1 and Λ_{M+1}^2 of Λ_{M+1} are defined by

$$\Lambda_{M+1}^2 := \Lambda_{M+1} \setminus \Lambda_{M+1}^1 \quad \text{with} \quad \Lambda_{M+1}^1 := \{(\ell, k - \ell) : k = \ell, \dots, M + 1 - \ell \text{ and } \ell = 0, 1\}, \quad (3.5)$$

and

$$A_{m', n', m, n}^u = \frac{1}{(a^{(0,0)})^{d_{m', n', m, n}^u}} \sum_k C_{m', n', m, n, k}^u \left(\prod_{(i, j) \in \Lambda_{m'+n'-1}} (a^{(i, j)})^{d_{m', n', m, n, i, j, k}^u} \right), \quad (3.6)$$

$$A_{m', n', m, n}^f = \frac{1}{(a^{(0,0)})^{d_{m', n', m, n}^f}} \sum_k C_{m', n', m, n, k}^f \left(\prod_{(i, j) \in \Lambda_{m'+n'-3}} (a^{(i, j)})^{d_{m', n', m, n, i, j, k}^f} \right), \quad (3.7)$$

where all $d_{m', n', m, n}^u$, $d_{m', n', m, n}^f$, $d_{m', n', m, n, i, j, k}^u$ and $d_{m', n', m, n, i, j, k}^f$ are non-negative integers, $C_{m', n', m, n, k}^u$ and $C_{m', n', m, n, k}^f$ are two constants. All above constants are uniquely determined by the identity in (3.8).

See Fig. 3.2 and Fig. 3.3 for an illustration of the quantities $u^{(m, n)}$ with $(m, n) \in \Lambda_{M+1}^1$, $u^{(m, n)}$ with $(m, n) \in \Lambda_{M+1}^2$, $a^{(m, n)}$ with $(m, n) \in \Lambda_M$ and $f^{(m, n)}$ with $(m, n) \in \Lambda_{M-1}$ in Lemma 3.1 with $M = 4$.

Proof. By our assumption, we have $au_{xx} + au_{yy} + a_x u_x + a_y u_y = -f$ in $\Omega \setminus \Gamma$, i.e.,

$$u^{(2,0)} = -\frac{a^{(1,0)}u^{(1,0)} + a^{(0,1)}u^{(0,1)}}{a^{(0,0)}} - u^{(0,2)} - \frac{f^{(0,0)}}{a^{(0,0)}}. \quad (3.8)$$

Then it is clear that for all $2 + n' \leq M + 1$,

$$u^{(2, n')} = -u^{(0, n'+2)} + \sum_{(m, n) \in \Lambda_{n'+1}^1} A_{2, n', m, n}^u u^{(m, n)} - \frac{f^{(0, n')}}{a^{(0,0)}} + \sum_{(m, n) \in \Lambda_{n'-1}} A_{2, n', m, n}^f f^{(m, n)}.$$

where $A_{2, n', m, n}^u$ and $A_{2, n', m, n}^f$ are defined in (3.6) and (3.7) respectively. Similarly to (3.8),

we have $a_x u_{xx} + a u_{xxx} + a_x u_{yy} + a u_{xyy} + a_{xx} u_x + a_x u_{xx} + a_{xy} u_y + a_y u_{xy} = -f_x$ in $\Omega \setminus \Gamma$. So

$$u^{(3,0)} = \frac{2a^{(1,0)}u^{(2,0)} + a^{(1,0)}u^{(0,2)} + a^{(2,0)}u^{(1,0)} + a^{(1,1)}u^{(0,1)} + a^{(0,1)}u^{(1,1)}}{-a^{(0,0)}} - u^{(1,2)} - \frac{f^{(1,0)}}{a^{(0,0)}}. \quad (3.9)$$

Plugging (3.8) into the right-hand side of (3.9), we obtain

$$u^{(3,0)} = -u^{(1,2)} + \sum_{(m,n) \in \Lambda_2^1} A_{3,0,m,n}^u u^{(m,n)} - \frac{f^{(1,0)}}{a^{(0,0)}} + \sum_{(m,n) \in \Lambda_0} A_{3,0,m,n}^f f^{(m,n)}.$$

Then for all $3 + n' \leq M + 1$,

$$u^{(3,n')} = -u^{(1,n'+2)} + \sum_{(m,n) \in \Lambda_{n'+2}^1} A_{3,n',m,n}^u u^{(m,n)} - \frac{f^{(1,n')}}{a^{(0,0)}} + \sum_{(m,n) \in \Lambda_{n'}} A_{3,n',m,n}^f f^{(m,n)}.$$

Calculate the left $u^{(m',n')}$, $(m',n') \in \Lambda_{M+1}^2$ by the order $\{u^{(4,0)}, u^{(4,1)}, \dots, u^{(4,M-3)}\}$, $\{u^{(5,0)}, u^{(5,1)}, \dots, u^{(5,M-4)}\}$, \dots , $\{u^{(M+1,0)}\}$ and use the above identities recursively, to obtain (3.4). \square

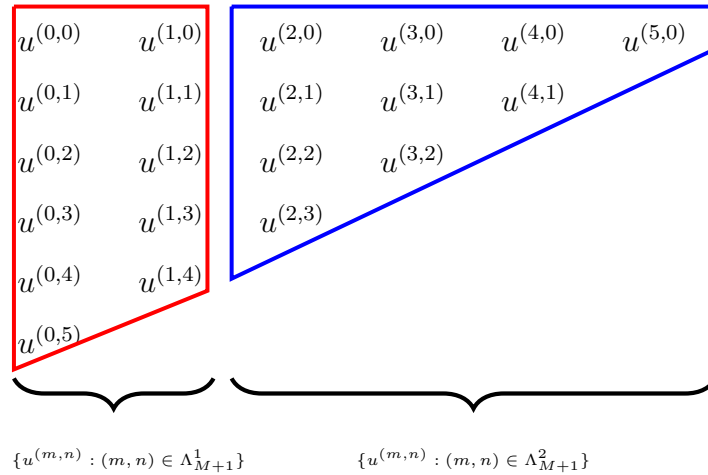


Figure 3.2: Red trapezoid: $\{u^{(m,n)} : (m,n) \in \Lambda_{M+1}^1\}$ with $M = 4$. Blue trapezoid: $\{u^{(m,n)} : (m,n) \in \Lambda_{M+1}^2\}$ with $M = 4$. Note that $\Lambda_{M+1} = \Lambda_{M+1}^1 \cup \Lambda_{M+1}^2$.

Note that $\Lambda_{M+1} = \Lambda_{M+1}^1 \cup \Lambda_{M+1}^2$. The identities in (3.4) of Lemma 3.1 show that every $u^{(m,n)}$ in $\{u^{(m,n)} : (m,n) \in \Lambda_{M+1}\}$ can be written as a combination of the quantities $\{u^{(m,n)} : (m,n) \in \Lambda_{M+1}^1\}$, $\{a^{(m,n)} : (m,n) \in \Lambda_M\}$ and $\{f^{(m,n)} : (m,n) \in \Lambda_{M-1}\}$. As the coefficient a and the source term f are available in (3.1), (3.4) could reduce the number of constraints on $\{u^{(m,n)} : (m,n) \in \Lambda_{M+1}\}$ to $\{u^{(m,n)} : (m,n) \in \Lambda_{M+1}^1\}$. By (2.7), (2.8) and

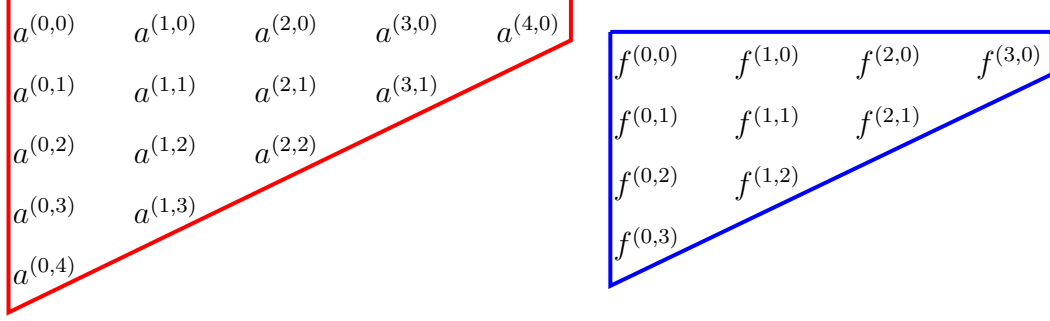


Figure 3.3: Red trapezoid: $\{a^{(m,n)} : (m,n) \in \Lambda_M\}$ with $M = 4$. Blue trapezoid: $\{f^{(m,n)} : (m,n) \in \Lambda_{M-1}\}$ with $M = 4$.

(3.4), the approximation of $u(x + x_i^*, y + y_j^*)$ in (1.9) can be written as

$$\begin{aligned}
& \sum_{(m,n) \in \Lambda_{M+1}} \frac{u^{(m,n)}}{m!n!} x^m y^n = \sum_{(m,n) \in \Lambda_{M+1}^1} \frac{u^{(m,n)}}{m!n!} x^m y^n + \sum_{(m',n') \in \Lambda_{M+1}^2} \frac{u^{(m',n')}}{m'!n'!} x^{m'} y^{n'} \\
&= \sum_{(m',n') \in \Lambda_{M+1}^2} \sum_{(m,n) \in \Lambda_{m'+n'-1}^1} A_{m',n',m,n}^u \frac{x^{m'} y^{n'}}{m'!n'!} + \sum_{(m',n') \in \Lambda_{M+1}^2} \sum_{(m,n) \in \Lambda_{m'+n'-3}} A_{m',n',m,n}^f \frac{x^{m'} y^{n'}}{m'!n'!} \\
&+ \sum_{(m',n') \in \Lambda_{M+1}^2} (-1)^{\lfloor \frac{m'}{2} \rfloor} u^{(\text{odd}(m'), n' + m' - \text{odd}(m'))} \frac{x^{m'} y^{n'}}{m'!n'!} + \sum_{(m',n') \in \Lambda_{M+1}^2} \sum_{\ell=1}^{\lfloor m'/2 \rfloor} \frac{(-1)^\ell f^{(m'-2\ell, n'+2\ell-2)}}{a^{(0,0)}} \frac{x^{m'} y^{n'}}{m'!n'!} \\
&+ \sum_{(m,n) \in \Lambda_{M+1}^1} \frac{u^{(m,n)}}{m!n!} x^m y^n \\
&= \sum_{(m,n) \in \Lambda_M^1} \left(\sum_{\substack{(m',n') \in \Lambda_{M+1}^2 \\ m'+n' \geq m+n+1}} A_{m',n',m,n}^u \frac{x^{m'} y^{n'}}{m'!n'!} \right) u^{(m,n)} + \sum_{(m,n) \in \Lambda_{M-2}} \left(\sum_{\substack{(m',n') \in \Lambda_{M+1}^2 \\ m'+n' \geq m+n+3}} A_{m',n',m,n}^f \frac{x^{m'} y^{n'}}{m'!n'!} \right) f^{(m,n)} \\
&+ \sum_{(m,n) \in \Lambda_{M+1}^1} \left(\sum_{\ell=0}^{\lfloor \frac{n}{2} \rfloor} \frac{(-1)^\ell x^{m+2\ell} y^{n-2\ell}}{(m+2\ell)!(n-2\ell)!} \right) u^{(m,n)} + \sum_{(m,n) \in \Lambda_{M-1}} \left(\sum_{\ell=1-\lfloor \frac{n}{2} \rfloor}^{1+\lfloor \frac{n}{2} \rfloor} \frac{(-1)^\ell x^{m+2\ell} y^{n-2\ell+2}}{(m+2\ell)!(n-2\ell+2)!} \frac{1}{a^{(0,0)}} \right) f^{(m,n)} \\
&= \sum_{(m,n) \in \Lambda_{M+1}^1} u^{(m,n)} G_{M+1,m,n}(x,y) + \sum_{(m,n) \in \Lambda_{M-1}} f^{(m,n)} Q_{M+1,m,n}(x,y),
\end{aligned}$$

where for all $(m,n) \in \Lambda_{M+1}^1$,

$$G_{M+1,m,n}(x,y) := \sum_{\ell=0}^{\lfloor \frac{n}{2} \rfloor} \frac{(-1)^\ell x^{m+2\ell} y^{n-2\ell}}{(m+2\ell)!(n-2\ell)!} + \sum_{(m',n') \in \Lambda_{M+1}^2 \setminus \Lambda_{m+n}^2} A_{m',n',m,n}^u \frac{x^{m'} y^{n'}}{m'!n'!}, \quad (3.10)$$

and for all $(m, n) \in \Lambda_{M-1}$,

$$Q_{M+1,m,n}(x, y) := \sum_{\ell=1}^{1+\lfloor \frac{n}{2} \rfloor} \frac{(-1)^\ell x^{m+2\ell} y^{n-2\ell+2}}{(m+2\ell)!(n-2\ell+2)!} \frac{1}{a^{(0,0)}} + \sum_{(m',n') \in \Lambda_{M+1}^2 \setminus \Lambda_{m+n+2}^2} A_{m',n',m,n}^f \frac{x^{m'} y^{n'}}{m'! n'!}. \quad (3.11)$$

From (3.10) and (3.11), we observe that $G_{M+1,m,n}(x, y)$ and $Q_{M+1,m,n}(x, y)$ are polynomials of total degree $M+1$ for all $(m, n) \in \Lambda_{M+1}^1$ and all $(m, n) \in \Lambda_{M-1}$, respectively. Note that every coefficient of $x^j y^k$ in the polynomial $Q_{M+1,m,n}(x, y)$ vanishes for all $j+k < m+n+2$. Thus, the approximation in (1.9) becomes

$$u(x+x_i^*, y+y_j^*) = \sum_{(m,n) \in \Lambda_{M+1}^1} u^{(m,n)} G_{M+1,m,n}(x, y) + \sum_{(m,n) \in \Lambda_{M-1}} f^{(m,n)} Q_{M+1,m,n}(x, y) + \mathcal{O}(h^{M+2}), \quad (3.12)$$

for $x, y \in (-2h, 2h)$, where u is the exact solution for (3.1) and (x_i^*, y_j^*) is the base point. Note that (3.12) is the key point to derive compact 9-point finite difference schemes for regular and irregular points with the maximum accuracy order.

3.3 A high order compact 9-point finite difference scheme for computing u using uniform Cartesian grids

In this section, we construct a compact 9-point finite difference scheme for numerical solutions of the elliptic equation in (3.1) at regular and irregular points.

3.3.1 Stencils for regular points

In this subsection, we discuss the derivation of the stencil for a compact 9-point finite difference scheme centered at a regular point (x_i, y_j) . For the sake of brevity, we choose $(x_i^*, y_j^*) = (x_i, y_j)$, i.e., (x_i^*, y_j^*) is defined in (1.6) with $v_0 = w_0 = 0$. Similar to Section 2.2.1, we have

$$\begin{aligned} \mathcal{L}_h u &:= h^{-2} \sum_{k=-1}^1 \sum_{\ell=-1}^1 C_{k,\ell}(h) u(x_i + kh, y_j + \ell h) \\ &= \sum_{(m,n) \in \Lambda_{M+1}^1} u^{(m,n)} h^{-2} \sum_{k=-1}^1 \sum_{\ell=-1}^1 C_{k,\ell}(h) G_{M+1,m,n}(kh, \ell h) \\ &\quad + \sum_{(m,n) \in \Lambda_{M-1}} f^{(m,n)} J_{m,n}(h) + \mathcal{O}(h^M), \end{aligned} \quad (3.13)$$

$h \rightarrow 0$, where

$$C_{k,\ell}(h) = \sum_{p=0}^{M+1} c_{k,\ell,p} h^p, \quad J_{m,n}(h) := \sum_{k=-1}^1 \sum_{\ell=-1}^1 C_{k,\ell}(h) h^{-2} Q_{M+1,m,n}(kh, \ell h), \quad (3.14)$$

and the polynomials $G_{M+1,m,n}(x, y)$ and $Q_{M+1,m,n}(x, y)$ are defined (3.10) and (3.11). Then the following compact 9-point finite difference scheme (3.15) for $-\nabla \cdot (a \nabla u) = f$ at the regular point (x_i, y_j) :

$$\mathcal{L}_h u_h := h^{-2} \sum_{k=-1}^1 \sum_{\ell=-1}^1 C_{k,\ell}(h) (u_h)_{i+k, j+\ell} = \sum_{(m,n) \in \Lambda_{M-1}} f^{(m,n)} J_{m,n}(h), \quad (3.15)$$

has the accuracy order M for the numerically approximated solution u_h , i.e., $\mathcal{L}_h(u - u_h) = \mathcal{O}(h^M)$, $h \rightarrow 0$, if

$$\sum_{k=-1}^1 \sum_{\ell=-1}^1 C_{k,\ell}(h) G_{M+1,m,n}(kh, \ell h) = \mathcal{O}(h^{M+2}), \quad h \rightarrow 0, \quad \text{for all } (m, n) \in \Lambda_{M+1}^1. \quad (3.16)$$

By calculation, the largest integer M for the linear system in (3.16) to have a nontrivial solution $\{C_{k,\ell}(h)\}_{k,\ell=-1,0,1}$ is $M = 6$. Define $a_{m,n} := a^{(m,n)}/a^{(0,0)}$ for $m, n \in \mathbb{N}_0$ and $m + n > 0$. Because in this chapter we are only interested in $M = 4$, one nontrivial solution $\{C_{k,\ell}(h)\}_{k,\ell=-1,0,1}$ to (3.16) with $M = 4$ is explicitly given by

$$\begin{aligned} C_{-1,-1}(h) &= 1 - [a_{0,1} + a_{1,0}]h + [\frac{1}{2}(a_{0,1} + a_{1,0})^2]h^2 + [(\frac{3}{4}a_{0,1}^3 + \frac{3}{2}a_{1,0}a_{0,1}^2 + \frac{1}{4}(a_{1,0}^2 - 4a_{0,2} - 5a_{1,1} - a_{2,0})a_{0,1} - \frac{3}{2}a_{1,0}^3 \\ &\quad + \frac{1}{4}(-a_{0,2} + 6a_{2,0} - 3a_{1,1})a_{1,0} + \frac{1}{4}(a_{2,1} + a_{0,3} - a_{3,0} - a_{1,2})]h^3 + [\frac{1}{4}(a_{0,1} + a_{1,0})(a_{0,1}^3 + 3a_{1,0}a_{0,1}^2) \\ &\quad + (7a_{1,0}^2 - 2a_{0,2} - 2a_{1,1} - 3a_{2,0})a_{0,1} + 7a_{1,0}^3 + (-2a_{0,2} - 8a_{2,0} - 3a_{1,1})a_{1,0} + a_{2,1} + a_{0,3} + 2a_{3,0} + 2a_{1,2}]h^4, \\ C_{-1,0}(h) &= 4 - [2a_{0,1} + 4a_{1,0}]h + [2a_{1,0}(a_{0,1} + a_{1,0})]h^2 + [-\frac{3}{2}a_{0,1}^3 - \frac{7}{2}a_{1,0}a_{0,1}^2 + \frac{1}{4}(-10a_{1,0}^2 + 8a_{0,2} + 8a_{1,1} + 2a_{2,0})a_{0,1} + \frac{1}{2}a_{1,0}^3 \\ &\quad + (a_{0,2} - a_{2,0} + \frac{3}{2}a_{1,1})a_{1,0} - \frac{1}{2}(a_{2,1} - a_{0,3})]h^3 + [-\frac{1}{4}a_{0,1}^4 - \frac{3}{4}a_{0,1}^3a_{1,0} + \frac{1}{4}(-7a_{1,0}^2 + 2a_{0,2} + a_{1,1} + 3a_{2,0})a_{0,1}^2 \\ &\quad + \frac{1}{4}(-7a_{1,0}^3 + (3a_{0,2} + 7a_{2,0} + 3a_{1,1})a_{1,0} - a_{2,1} - a_{0,3} - a_{3,0} - a_{1,2})a_{0,1} - \frac{1}{4}a_{1,0}(-a_{1,0}a_{1,1} + a_{0,3} + a_{2,1})]h^4, \\ C_{-1,1}(h) &= 1 - a_{1,0}h + [a_{0,1}a_{1,0} + \frac{1}{2}a_{1,0}^2 - a_{1,1}]h^2 + [-\frac{3}{2}a_{1,0}^3 - \frac{1}{4}a_{0,1}a_{1,0}^2 + \frac{1}{4}(4a_{0,1}^2 - a_{0,2} + a_{1,1} + 6a_{2,0})a_{1,0} \\ &\quad + \frac{3}{4}a_{0,1}^3 + \frac{1}{4}(-4a_{0,2} - a_{2,0} - a_{1,1})a_{0,1} + \frac{1}{4}a_{2,1} + \frac{1}{4}a_{0,3} - \frac{1}{4}a_{3,0} - \frac{1}{4}a_{1,2}]h^3, \\ C_{0,-1}(h) &= 4 - [4a_{0,1} + 2a_{1,0}]h + [\frac{1}{2}a_{0,1}^2 + 2a_{0,1}a_{1,0} + \frac{3}{2}a_{1,0}^2 + a_{0,2} - a_{2,0}]h^2 + [-a_{0,1}^3 - 3a_{1,0}a_{0,1}^2 + \frac{3}{2}a_{1,0}a_{1,1} - \frac{1}{2}a_{2,1} \\ &\quad - \frac{1}{2}a_{0,3} + \frac{1}{4}(-12a_{1,0}^2 + 4a_{0,2} + 8a_{1,1} + 6a_{2,0})a_{0,1}]h^3 + [-\frac{1}{4}a_{0,1}^3a_{1,0} + \frac{1}{4}(-3a_{1,0}^2 + a_{1,1})a_{0,1}^2 + \frac{1}{4}(-7a_{1,0}^3 \\ &\quad + (a_{0,2} + 4a_{2,0} + 2a_{1,1})a_{1,0} - a_{3,0} - a_{1,2})a_{0,1} + \frac{1}{2}a_{1,0}(-\frac{7}{2}a_{1,0}^3 + (a_{0,2} + 4a_{2,0} + a_{1,1})a_{1,0} - a_{3,0} - a_{1,2})]h^4, \\ C_{0,0}(h) &= -20 + [10a_{0,1} + 10a_{1,0}]h + [-7a_{0,1}a_{1,0} - 6a_{1,0}^2 - 2a_{0,2} + 2a_{1,1} + 2a_{2,0}]h^2 + [\frac{5}{2}a_{1,0}^3 + \frac{11}{2}a_{0,1}a_{1,0}^2 \\ &\quad + \frac{1}{2}(8a_{0,1}^2 - a_{0,2} - 5a_{1,1} - 4a_{2,0})a_{1,0} + a_{0,1}^3 + \frac{1}{2}(-2a_{0,2} - 3a_{2,0} - 5a_{1,1})a_{0,1} + \frac{1}{2}(a_{2,1} + a_{0,3} + a_{3,0} + a_{1,2})]h^3, \\ C_{0,1}(h) &= 4 - 2a_{1,0}h + [-\frac{3}{2}a_{0,1}^2 + \frac{3}{2}a_{1,0}^2 + a_{0,2} - a_{2,0}]h^2, \\ C_{1,-1}(h) &= 1 - a_{0,1}h + [\frac{1}{2}a_{0,1}^2 + a_{0,1}a_{1,0} - a_{1,1}]h^2, \quad C_{1,0}(h) = 4 - 2a_{0,1}h, \quad C_{1,1}(h) = 1. \end{aligned} \quad (3.17)$$

Thus, for a regular point (x_i, y_j) , the following theorem proves the fourth order accuracy for the compact 9-point scheme. This result is well known in the literature (e.g., see [98, 114, 109, 106, 81, 79, 80, 115]).

Theorem 3.2. Let (x_i, y_j) be a regular point and $(u_h)_{i,j}$ be the numerical approximation in (3.15) of the exact solution u of the partial differential equation in (3.1) at (x_i, y_j) . Then the compact 9-point scheme centered at the regular point (x_i, y_j) in (3.15) with $M = 4$ has a fourth order consistency error at the regular point (x_i, y_j) , i.e., the accuracy order for u_h is four, where $C_{k,\ell}(h)$ are defined in (3.17), $a^{(m,n)} := \frac{\partial^{m+n} a}{\partial^m x \partial^n y}(x_i, y_j)$ and $f^{(m,n)} := \frac{\partial^{m+n} f}{\partial^m x \partial^n y}(x_i, y_j)$.

Furthermore, the maximum accuracy order M for the numerically approximated solution at the regular point of a compact 9-point finite difference scheme which is based on Taylor expansion and our sort of technique in (3.15) is $M = 6$.

3.3.2 Stencils for irregular points

The derivation of stencils for irregular points is similar to Section 2.2.2, while the discontinuous coefficient $a(x, y)$ causes some difficulties. So in order to help readers understand clearly, we also provide all the details like Section 2.2.2. Let (x_i, y_j) be an irregular point and we can take a base point $(x_i^*, y_j^*) \in \Gamma \cap (x_i - h, x_i + h) \times (y_j - h, y_j + h)$ on the interface Γ and inside $(x_i - h, x_i + h) \times (y_j - h, y_j + h)$. That is, as in (1.6), we have

$$x_i = x_i^* + v_0 h \quad \text{and} \quad y_j = y_j^* + w_0 h \quad \text{with} \quad -1 < v_0, w_0 < 1 \quad \text{and} \quad (x_i^*, y_j^*) \in \Gamma.$$

Let a_{\pm} , u_{\pm} and f_{\pm} represent the coefficient a , the solution u and source term f in Ω_{\pm} . As in (1.7), we define

$$a_{\pm}^{(m,n)} := \frac{\partial^{m+n} a_{\pm}}{\partial^m x \partial^n y}(x_i^*, y_j^*), \quad u_{\pm}^{(m,n)} := \frac{\partial^{m+n} u_{\pm}}{\partial^m x \partial^n y}(x_i^*, y_j^*), \quad f_{\pm}^{(m,n)} := \frac{\partial^{m+n} f_{\pm}}{\partial^m x \partial^n y}(x_i^*, y_j^*). \quad (3.18)$$

Similarly as the discussion for the irregular points in Section 2.2.2, the identities in (3.4) and (3.12) hold by replacing a , u and f by a_{\pm} , u_{\pm} and f_{\pm} , i.e.,

$$u_{\pm}(x + x_i^*, y + y_j^*) = \sum_{(m,n) \in \Lambda_{M+1}^1} u_{\pm}^{(m,n)} G_{M+1,m,n}^{\pm}(x, y) + \sum_{(m,n) \in \Lambda_{M-1}} f_{\pm}^{(m,n)} Q_{M+1,m,n}^{\pm}(x, y) + \mathcal{O}(h^{M+2}), \quad (3.19)$$

for $x, y \in (-2h, 2h)$, where the index sets Λ_{M+1}^1 and Λ_{M-1} are defined in (3.5) and (1.8), respectively, and the polynomials $G_{M+1,m,n}^{\pm}(x, y)$ and $Q_{M+1,m,n}^{\pm}(x, y)$ are defined in (3.10) and (3.11) by replacing a by a_{\pm} .

Similar as Theorem 2.4, according to the two jump conditions for the solution and flux in (3.1), we can link the two sets $\{u_{-}^{(m,n)}\}_{(m,n) \in \Lambda_M^1}$ and $\{u_{+}^{(m,n)}\}_{(m,n) \in \Lambda_M^1}$ by the following theorem, whose proof is given in Section 3.7. Since the coefficient function $a(x, y)$ is discontinuous across the interface curve Γ , we need to add $T_{m',n',m,n}^{u+}$ in the following theorem.

Theorem 3.3. Let u be the exact solution to the elliptic interface problem in (3.1). Assume that the base point $(x_i^*, y_j^*) \in \Gamma$ and Γ is parameterized near (x_i^*, y_j^*) by (1.5). Then

$$\begin{aligned} u_-^{(m',n')} &= \sum_{(m,n) \in \Lambda_M^1} T_{m',n',m,n}^{u_+} u_+^{(m,n)} + \sum_{(m,n) \in \Lambda_{M-2}} \left(T_{m',n',m,n}^+ f_+^{(m,n)} + T_{m',n',m,n}^- f_-^{(m,n)} \right) \\ &\quad + \sum_{p=0}^M T_{m',n',p}^{g_0^\Gamma} g_{0,p}^\Gamma + \sum_{p=0}^{M-1} T_{m',n',p}^{g_1^\Gamma} g_{1,p}^\Gamma, \quad \forall (m', n') \in \Lambda_M^1, \end{aligned} \quad (3.20)$$

where all the transmission coefficients $T^{u_+}, T^\pm, T^{g_0^\Gamma}, T^{g_1^\Gamma}$ are uniquely determined by $r^{(k)}(0), s^{(k)}(0)$ for $k = 0, \dots, M$ and $\{a_\pm^{(m,n)}\}_{(m,n) \in \Lambda_{M-1}}$, and the quantities $g_{1,p}, g_{2,p}$ are defined to be

$$g_{0,p}^\Gamma := \frac{1}{p!} \frac{d^p}{dt^p} \left[g_0^\Gamma(r(t) + x_i^*, s(t) + y_j^*) \right] \Big|_{t=0}, \quad p = 0, 1, \dots, M, \quad (3.21)$$

and

$$g_{1,p}^\Gamma := \frac{1}{p!} \frac{d^p}{dt^p} \left[g_1^\Gamma(r(t) + x_i^*, s(t) + y_j^*) \sqrt{(r'(t))^2 + (s'(t))^2} \right] \Big|_{t=0}, \quad p = 0, 1, \dots, M-1. \quad (3.22)$$

Similar as Section 2.2.2, by (3.19) with M being replaced by $M-1$ and two jump conditions (3.2) and (3.3) at an irregular point (x_i, y_j) , we have

$$\begin{aligned} \mathcal{L}_h^\Gamma u &:= \sum_{k=-1}^1 \sum_{\ell=-1}^1 C_{k,\ell}(h) \frac{1}{h} u(x_i + kh, y_j + \ell h) \\ &= \sum_{(k,\ell) \in d_{i,j}^+} C_{k,\ell}(h) \frac{1}{h} u(x_i^* + (v_0 + k)h, y_j^* + (w_0 + \ell)h) + \sum_{(k,\ell) \in d_{i,j}^-} C_{k,\ell}(h) \frac{1}{h} u(x_i^* + (v_0 + k)h, y_j^* + (w_0 + \ell)h) \\ &= \sum_{(m,n) \in \Lambda_M^1} u_+^{(m,n)} h^{-1} I_{m,n}^+(h) + h \sum_{(m,n) \in \Lambda_{M-2}} f_+^{(m,n)} J_{m,n}^{+,0}(h) + \sum_{(m,n) \in \Lambda_M^1} u_-^{(m,n)} h^{-1} I_{m,n}^-(h) \\ &\quad + h \sum_{(m,n) \in \Lambda_{M-2}} f_-^{(m,n)} J_{m,n}^{-,0}(h) + \mathcal{O}(h^M) \end{aligned} \quad (3.23)$$

where

$$\begin{aligned} C_{k,\ell}(h) &:= \sum_{p=0}^M c_{k,\ell,p} h^p, \quad I_{m,n}^\pm(h) := \sum_{(k,\ell) \in d_{i,j}^\pm} C_{k,\ell}(h) G_{M,m,n}^\pm((v_0 + k)h, (w_0 + \ell)h), \\ J_{m,n}^{\pm,0}(h) &:= \sum_{(k,\ell) \in d_{i,j}^\pm} C_{k,\ell}(h) h^{-2} Q_{M,m,n}^\pm((v_0 + k)h, (w_0 + \ell)h). \end{aligned} \quad (3.24)$$

Note that both $I_{m,n}^\pm(h)$ and $J_{m,n}^{\pm,0}(h)$ are polynomials of h , because $G_{M,m,n}^\pm(x, y)$ (3.10) and

$Q_{M,m,n}^\pm(x, y)$ (3.11) are bivariate polynomials and every coefficient of $x^j y^k$ of $Q_{M,m,n}^\pm(x, y)$ vanishes for all $j + k < 2$. Using (3.20) in Theorem 3.3, we obtain

$$\begin{aligned} \sum_{(m',n') \in \Lambda_M^1} u_-^{(m',n')} h^{-1} I_{m',n'}^-(h) &= \sum_{(m,n) \in \Lambda_M^1} u_+^{(m,n)} h^{-1} J_{m,n}^{u_+,T}(h) + h \sum_{(m,n) \in \Lambda_{M-2}} \left(f_+^{(m,n)} J_{m,n}^{+,T}(h) \right. \\ &\quad \left. + f_-^{(m,n)} J_{m,n}^{-,T}(h) \right) + \sum_{p=0}^M g_{0,p}^\Gamma h^{-1} J_p^{g_0^\Gamma}(h) + \sum_{p=0}^{M-1} g_{1,p}^\Gamma h^{-1} J_p^{g_1^\Gamma}(h), \end{aligned}$$

where

$$\begin{aligned} J_{m,n}^{u_+,T}(h) &:= \sum_{(m',n') \in \Lambda_M^1} I_{m',n'}^-(h) T_{m',n',m,n}^{u_+}, & J_{m,n}^{\pm,T}(h) &:= \sum_{(m',n') \in \Lambda_M^1} I_{m',n'}^-(h) h^{-2} T_{m',n',m,n}^\pm, \\ J_p^{g_0^\Gamma}(h) &:= \sum_{(m',n') \in \Lambda_M^1} I_{m',n'}^-(h) T_{m',n',p}^{g_0^\Gamma}, & J_p^{g_1^\Gamma}(h) &:= \sum_{(m',n') \in \Lambda_M^1} I_{m',n'}^-(h) T_{m',n',p}^{g_1^\Gamma}. \end{aligned} \tag{3.25}$$

In the proof of Theorem 3.3 in Section 3.7, we shall prove that $T_{m',n',m,n}^\pm = 0$ in (3.20) for $(m', n') \in \Lambda_M^1$ with $m' + n' < 2$. So (3.24) implies that every coefficient of h^k of $J_{m,n}^{\pm,T}(h)$ in (3.25) vanishes for all $k < 0$. Similar as Section 2.2.2, let define

$$\begin{aligned} \mathcal{L}_h^\Gamma u_h &:= h^{-1} \sum_{k=-1}^1 \sum_{\ell=-1}^1 C_{k,\ell}(h) (u_h)_{i+k, j+\ell} \\ &= \sum_{(m,n) \in \Lambda_{M-2}} h \left(f_-^{(m,n)} J_{m,n}^-(h) + f_+^{(m,n)} J_{m,n}^+(h) \right) + h^{-1} \left(\sum_{p=0}^M g_{0,p}^\Gamma J_p^{g_0^\Gamma}(h) + \sum_{p=0}^{M-1} g_{1,p}^\Gamma J_p^{g_1^\Gamma}(h) \right), \end{aligned} \tag{3.26}$$

where

$$I_{m,n}(h) := I_{m,n}^+(h) + J_{m,n}^{u_+,T}(h), \quad J_{m,n}^\pm(h) := J_{m,n}^{\pm,0}(h) + J_{m,n}^{\pm,T}(h). \tag{3.27}$$

Then the compact 9-point finite different scheme (3.26) at the irregular point (x_i, y_j) has the accuracy order M for the numerically approximated solution u_h , i.e., $\mathcal{L}_h^\Gamma(u - u_h) = \mathcal{O}(h^M)$, $h \rightarrow 0$, if $I_{m,n}(h)$ in (3.27) satisfies

$$I_{m,n}(h) = \mathcal{O}(h^{M+1}), \quad h \rightarrow 0, \quad \text{for all } (m, n) \in \Lambda_M^1. \tag{3.28}$$

Now we obtain the following theorem for a compact 9-point finite difference scheme at irregular points with the accuracy order M .

Theorem 3.4. *Let (x_i, y_j) be an irregular point and u_h be the numerical approximation in (3.26) of the exact solution u to (3.1) at (x_i, y_j) . Pick a base point $(x_i^*, y_j^*) \in \Gamma$ as in (1.6).*

Then the maximum integer M is 3 for the linear system induced by (3.28) to have a nontrivial solution $\{C_{k,\ell}(h)\}_{k,\ell=-1,0,1}$ and its corresponding compact 9-point finite difference scheme in (3.26) with $M = 3$ at the irregular point (x_i, y_j) has the accuracy order 3.

With the help of free parameters in $\{C_{k,\ell}(h)\}_{k,\ell=-1,0,1}$ in Theorem 3.4, we shall numerically demonstrate in Section 3.3.3 that one can always obtain a compact 9-point finite difference scheme in Theorem 3.4 satisfying the discrete maximum principle for sufficiently small h . Thus, we shall prove in Section 3.3.3 that the compact 9-point finite difference scheme in Theorem 3.4 satisfying the discrete maximum principle must have the convergence rate of order 4.

Theorem 3.5. *The maximum accuracy order for the numerical approximation u_h at an irregular point of a compact 9-point finite difference scheme which is based on Taylor expansion and our sort of technique in (3.26) is three, i.e., the largest M such that the nontrivial solution $\{C_{k,\ell}(h)\}_{k,\ell=-1,0,1}$ exists for (3.28) is $M = 3$.*

Proof. Let us consider the following simple case: $\Gamma = \{(x, y) \in \Omega : \psi(x, y) = 0\}$ with $\psi(x, y) = 2x - y$, $x_i = y_j = 0$, $x_{i-1} = y_{j-1} = -h$, $x_{i+1} = y_{j+1} = h$, $x_i^* = x_i = 0$, $y_j^* = y_j = 0$ and $\vec{n} = \frac{(2, -1)}{\sqrt{5}}$ (see Fig. 3.4 for an illustration). From (3.28), the source term f_{\pm} and the two jump functions g_0^{Γ} and g_1^{Γ} do not affect the existence of the nontrivial solution $\{C_{k,\ell}(h)\}_{k,\ell=-1,0,1}$ of (3.28). To further simplify the calculation, we can assume that $f_{\pm} = g_0^{\Gamma} = g_1^{\Gamma} = 0$. Then it is easy to check that all $\{C_{k,\ell}(h)\}_{k,\ell=-1,0,1}$ of (3.28) are zeros at $h = 0$ for $M = 4$ and $a_-(0, 0) \neq a_+(0, 0)$. So (3.28) only has a trivial solution for $M = 4$. \square

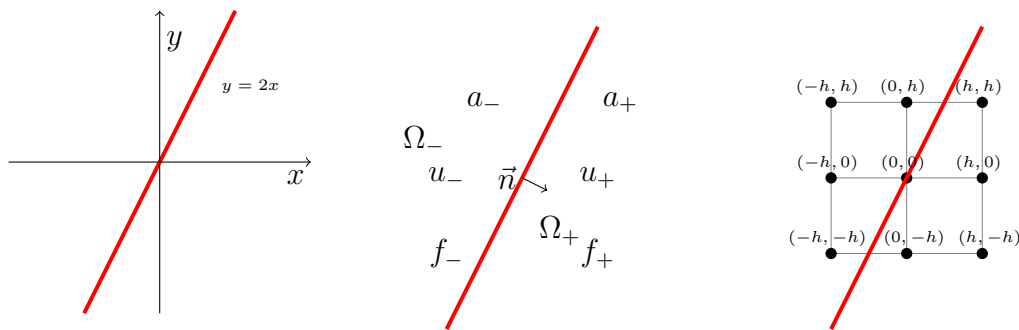


Figure 3.4: One simple example for irregular points. The curve in red color is the interface curve $\Gamma = \{(x, y) \in \Omega : 2x - y = 0\}$, the left of Γ is Ω_- and the right of Γ is Ω_+ .

Finally, for any finite difference schemes of accuracy order M in (3.15) at regular points

and in (3.26) at irregular points, we always have

$$\sum_{k=-1}^1 \sum_{\ell=-1}^1 C_{k,\ell}(h) = 0. \quad (3.29)$$

Indeed, $u = 1$ is the solution to (3.1) with $f = 0$, $g_0^\Gamma = g_1^\Gamma = 0$ and $g = 1$. For regular points, we plug the exact solution $u = 1$ into (3.13) and conclude from (3.16) that $S(h) := \sum_{k=-1}^1 \sum_{\ell=-1}^1 C_{k,\ell}(h) = \mathcal{O}(h^{M+2})$ as $h \rightarrow 0$, which forces $S(h) = 0$ due to $\deg(S) \leq M + 1$ by (3.14). Similarly, for irregular points, we plug $u = 1$ into (3.23) and conclude from (3.28) that $S(h) := \sum_{k=-1}^1 \sum_{\ell=-1}^1 C_{k,\ell}(h) = \mathcal{O}(h^{M+1})$, which forces $S(h) = 0$ due to $\deg(S) \leq M$ by (3.24).

3.3.3 Convergence analysis

For the immersed finite element/volume methods as in [30, 42], when the interface passes through elements, special nodal basis functions are constructed to approximately satisfy the two jump conditions in (3.2) and (3.3). Then the authors form the corresponding immersed finite element/volume space to obtain the error estimates. By using an auxiliary function, [42] could transfer the model problem with nonhomogeneous jump conditions to an equivalent problem with homogeneous jump conditions.

For finite difference schemes, if we have the following sign conditions on the coefficients $C_{k,\ell}(h)$:

$$\begin{cases} C_{k,\ell}(h) < 0, & \text{if } (k, \ell) = (0, 0), \\ C_{k,\ell}(h) > 0, & \text{if } (k, \ell) \neq (0, 0), \end{cases} \quad (3.30)$$

then we can prove the convergence rate using the discrete maximum principle. Theorem 4.1 in [74] theoretically proves that a particular 5-point scheme with the first accuracy order can satisfy the sign conditions (3.30) for any $(x_i^*, y_j^*) \in \Gamma \cap [(x_i, y_j) + (-h, h)^2]$ satisfying $|x_i - x_i^*| + |y_j - y_j^*| < \sqrt{2}h$. Note that the points $(x_i^*, y_j^*) = (x_i + ch, y_j + ch) \in [(x_i, y_j) + (-h, h)^2]$ do not satisfy the last condition if $\frac{\sqrt{2}}{2} \leq c < 1$. Then [74, Theorem 4.4] derives a theoretical proof for the first order convergence rate of the 5-point scheme. While for the second order 9-point scheme, here we provide the following example:

$$\begin{aligned} x_i^* &= x_i + \frac{4}{9}h, & y_j^* &= y_j - \frac{1}{10}h, & r'(0) &= 1, & s'(0) &= -\frac{3}{5}, & a_+ &= 1, & a_- &= 10, \\ (x_i + kh, y_j - h) &\in \Omega_-, & \text{for } k &= -1, 0, 1, \\ (x_i + kh, y_j + \ell h) &\in \Omega_+, & \text{for } k &= -1, 0, 1, & \ell &= 0, 1. \end{aligned} \quad (3.31)$$

We can directly check that for any f , g_0^Γ and g_1^Γ , it is impossible to have a second order 9-point scheme coefficients $\{C_{k,\ell}(h)\}_{k,\ell=-1,0,1}$ satisfying (3.30) for the example in (3.31). Note that (x_i^*, y_j^*) is not the orthogonal projection of (x_i, y_j) in (3.31). For the second order compact 9-point finite difference schemes, [74] and [17] proposed Conjectures 5.1 and 4.1 for the sign restrictions (3.30) and then numerically proved the second order convergence rate by the discrete maximum principle. [74] and [17] also numerically verify the existences of sign conditions (3.30) of the second order 9-point schemes, where (x_i^*, y_j^*) is the orthogonal projection of (x_i, y_j) in [74] and $(x_i^*, y_j^*) = (x_i^*, y_j)$ or (x_i, y_j^*) in [17]. The theoretical proof for the convergence rate of the first order compact 5-point scheme is not complete (due to the required condition $|x_i - x_i^*| + |y_j - y_j^*| < \sqrt{2}h$ which often fails for a general interface Γ) and the convergence rate of the second order compact 9-point scheme is unsolved in [74].

The goal of this subsection is to numerically prove that our proposed compact 9-point finite difference scheme in Sections 3.4.1 and 3.4.2 has the convergence rate of order 4. For any regular point (x_i, y_j) , it is obvious that $\{C_{k,\ell}(h)\}_{k,\ell=-1,0,1}$ in (3.17) satisfies the sign condition in (3.30) for sufficiently small h .

For any irregular point (x_i, y_j) , we now numerically show that one can always obtain a compact 9-point finite difference scheme in Theorem 3.4 satisfying the discrete maximum principle for sufficiently small h . Without loss of generality, we can assume $(x_i, y_j) \in \Omega_+$; otherwise, we can consider the level set function $-\psi$ instead of ψ so that Ω_- for the level set function ψ becomes Ω_+ for the level set function $-\psi$. Up to rotations and symmetry transformations, for any interface curve Γ , we essentially have a total of 5 typical irregular points cases for sufficiently small h , which is illustrated in Fig. 3.5.

When h is sufficiently small, the interface Γ near (x_i^*, y_j^*) essentially behaves like a straight line. For simplicity of discussion, after translation of the irregular point (x_i, y_j) to $(0, 0)$, without loss of generality, we can assume that (x_i^*, y_j^*) is the orthogonal projection of $(x_i, y_j) = (0, 0)$, or $(x_i^*, y_j^*) = (x_i^*, y_j) = (x_i^*, 0)$ or $(x_i^*, y_j^*) = (x_i, y_j^*) = (0, y_j^*)$, $r'(0) = 1$, $s'(0) = k$ and the intersection point of Γ and $x = 0$ is $(0, hb)$. For each of the five cases in Fig. 3.5, to maintain the same set $d_{i,j}^-$, we naturally have restriction conditions on the parameters k and b as follows:

- (1) For $d_{i,j}^- = \{(-1, 1)\}$, we have $k \in (0, \infty)$ and $b \in (\max\{k, 1\}, 1 + k)$.
- (2) For $d_{i,j}^- = \{(-1, 1), (0, 1)\}$, we have $k \in (0, 1)$ and $b \in (\max\{1 - k, k\}, \min\{1, k + 1\})$.
- (3) For $d_{i,j}^- = \{(-1, 0), (-1, 1), (0, 1)\}$, we have $k \in (0, 2)$ and $b \in (\max\{1 - k, k - 1\}, \min\{1, k\})$.
- (4) For $d_{i,k}^- = \{(-1, 1), (0, 1), (1, 1)\}$, we have $k \in (-\frac{1}{2}, \frac{1}{2})$ and $b \in (\max\{0, k\}, 1 - k)$.

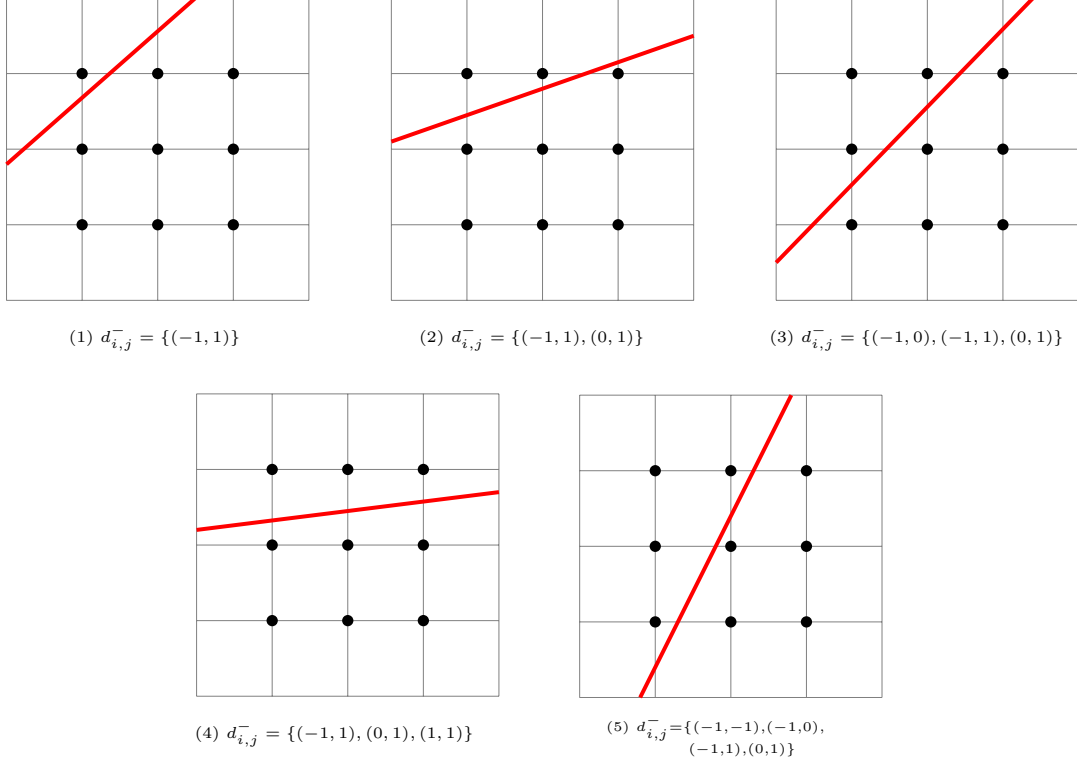


Figure 3.5: Five cases of irregular points when h is sufficiently small. The curve in red color is the interface curve Γ . The center point is the irregular point (x_i, y_j) .

(5) For $d_{i,j}^- = \{(-1, -1), (-1, 0), (-1, 1), (0, 1)\}$, we have $k \in (1, \infty)$ and $\mathbf{b} \in (\max\{0, k - 2\}, \min\{1, k - 1\})$.

For each $q \in \{1, \dots, 5\}$, we define D_q to be the open domain described in the above case (q). For $d_{i,j}^- = \{(-1, 1), (0, 1)\}$ of case (2) in Fig. 3.5, if $k = 1$ and $\mathbf{b} = 1$, then $d_{i,j}^- = \{(-1, 0), (-1, 1), (0, 1)\}$ by (1.2) and (1.3); similarly, if $k = \frac{1}{2}$ and $\mathbf{b} = \frac{1}{2}$, then $d_{i,j}^- = \{(-1, 0), (-1, 1), (0, 1), (1, 1)\}$. These are the special limiting/boundary cases of (2) in Fig. 3.5 and can be easily covered by considering the closure $\overline{D_2}$ of the open region D_2 in case (2), i.e., $k \in [0, 1]$ and $\mathbf{b} \in [\max\{1 - k, k\}, \min\{1, k + 1\}]$. To include all the special limiting cases for cases (1)–(5), our analysis below considers the closure of the open regions in cases (1)–(5).

For each case $q = 1, \dots, 5$, let $\{C_{k,\ell}(h) = \sum_{p=0}^M c_{k,\ell,p} h^p\}_{k,\ell=-1,0,1}$ be a nontrivial solution in Theorem 3.4 for the stencil at the irregular point (x_i, y_j) . If we normalize $C_{0,0}(0) = -20$, then we have

$$C_{k,\ell}(0) = \begin{cases} -20, & \text{if } (k, \ell) = (0, 0), \\ \mathbf{a}_{k,\ell}\mathbf{c} + \mathbf{d}_{k,\ell}, & \text{if } k, \ell = -1, 0, 1 \text{ and } (k, \ell) \neq (0, 0), \end{cases}$$

with \mathbf{c} being a free parameter, where $\mathbf{a}_{k,\ell}$ and $\mathbf{d}_{k,\ell}$ only depend on $a_{\pm}^{(0,0)}$, \mathbf{k} and \mathbf{b} . Moreover, for a particular $(k', \ell') \neq (0, 0)$, $\mathbf{a}_{k',\ell'} = 1$ and $\mathbf{d}_{k',\ell'} = 0$, i.e., $C_{k',\ell'}(0) = \mathbf{c}$. For each case $q = 1, \dots, 5$, it is easy to observe that the sign condition in (3.30) holds for sufficiently small h if and only if there exists a constant \mathbf{c} satisfying all the following conditions:

$$\begin{cases} \mathbf{d}_{k,\ell} > 0, & \text{if } \mathbf{a}_{k,\ell} = 0, \\ \mathbf{c} > -\frac{\mathbf{d}_{k,\ell}}{\mathbf{a}_{k,\ell}}, & \text{if } \mathbf{a}_{k,\ell} > 0, \\ \mathbf{c} < -\frac{\mathbf{d}_{k,\ell}}{\mathbf{a}_{k,\ell}}, & \text{if } \mathbf{a}_{k,\ell} < 0, \end{cases} \quad \forall (k, \ell) \in \{-1, 0, 1\} \setminus \{(0, 0)\}, \quad (3.32)$$

for every given $(\mathbf{k}, \mathbf{b}) \in \overline{D}_q$ in case (q) of Fig. 3.5. Due to the long complicated expressions of $\mathbf{a}_{k,\ell}$ and $\mathbf{d}_{k,\ell}$ for each case $q = 1, \dots, 5$, a theoretical proof of the existence of \mathbf{c} is necessarily complicated and technical and hence we leave this as a future research topic. Here, we numerically verify the condition (3.32). More precisely, for each case $q = 1, \dots, 5$ in Fig. 3.5, we take a dense enough set $S_q \subseteq \overline{D}_q$. We can easily numerically verify that for each $(\mathbf{k}, \mathbf{b}) \in S_q$, there always exists \mathbf{c} satisfying (3.32), where (x_i^*, y_j^*) is the orthogonal projection of (x_i, y_j) and $(x_i^*, y_j^*) = (x_i^*, y_j)$ or (x_i, y_j^*) . This numerically proves that for every irregular point (x_i, y_j) , there always exists $\{C_{k,\ell}(h)\}_{k,\ell=-1,0,1}$ in Theorem 3.4 satisfying the sign condition in (3.30) for sufficiently small h and hence such compact 9-point finite difference scheme satisfies the discrete maximum principle. Thus, we have the following result on the convergence rate of our proposed compact 9-point finite difference scheme in Theorems 3.2 and 3.4:

Theorem 3.6. *Under the assumptions (A1)–(A4) in Section 3.1, we consider the compact 9-point finite difference scheme (3.15) using $\{C_{k,\ell}(h)\}_{k,\ell=-1,0,1}$ in (3.17) for regular points, and the compact 9-point finite difference scheme (3.26) in Theorem 3.4 using the above discussed $\{C_{k,\ell}(h)\}_{k,\ell=-1,0,1}$ satisfying the sign condition in (3.30) for irregular points and sufficiently small h . Then the compact 9-point finite difference scheme for the elliptic interface problem in (3.1) has the convergence rate of order 4 for sufficiently small h , that is, there exists a positive constant C independent of h such that*

$$\|u - u_h\|_{\infty} \leq Ch^4,$$

where u and u_h are the exact solution and the numerical solution of (3.1), respectively.

Proof. For simplicity, we assume $\Omega = (0, 1)^2$ and $h = 1/N$ with $N \in \mathbb{N}$. We define $\Omega_h := \Omega \cap (h\mathbb{Z}^2)$, $\partial\Omega_h := \partial\Omega \cap (h\mathbb{Z}^2)$, $\overline{\Omega}_h := \overline{\Omega} \cap (h\mathbb{Z}^2)$, and $(x_i, y_j) := (ih, jh)$. So $\overline{\Omega}_h := \{(x_i, y_j) : 0 \leq i, j \leq N\}$ and we also define $V(\overline{\Omega}_h) := \{(v)_{i,j} : 0 \leq i, j \leq N\}$ with $(v)_{i,j} \in \mathbb{R}$, and for any $v \in V(\overline{\Omega}_h)$, $(v)_{i,j}$ represents the value of v at the point (x_i, y_j) . Using \mathcal{L}_h in (3.15) at an

regular point (x_i, y_j) , we define

$$(\Delta_h u_h)_{i,j} := \mathcal{L}_h u_h \quad \text{and} \quad F_{i,j} := \sum_{(m,n) \in \Lambda_3} f^{(m,n)} J_{m,n}(h).$$

By Theorem 3.2, we have $\mathcal{L}_h(u - u_h) = \mathcal{O}(h^4)$ as $h \rightarrow 0$. Similarly, using \mathcal{L}_h^Γ in (3.26) at an irregular point (x_i, y_j) , we define

$$(\Delta_h u_h)_{i,j} := \mathcal{L}_h^\Gamma u_h \quad \text{and} \quad F_{i,j} := hF_{3,f}(h) + G_{3,g_0^\Gamma, g_1^\Gamma}(h).$$

By Theorem 3.4, we have $\mathcal{L}_h^\Gamma(u - u_h) = \mathcal{O}(h^3)$ as $h \rightarrow 0$. Therefore, the compact 9-point finite difference scheme in Theorems 3.2 and 3.4 can be equivalently expressed as: Find $u_h \in V(\bar{\Omega}_h)$ satisfying

$$\Delta_h u_h = F \quad \text{on} \quad \Omega_h \quad \text{with} \quad u_h = g \quad \text{on} \quad \partial\Omega_h.$$

Using (3.29) and (3.30), we now prove the discrete maximum principle: for any $v \in V(\bar{\Omega}_h)$ satisfying $\Delta_h v \geq 0$, we must have $\max_{(x_i, y_j) \in \Omega_h} v(x_i, y_j) \leq \max_{(x_i, y_j) \in \partial\Omega_h} v(x_i, y_j)$.

Suppose that $\max_{(x_i, y_j) \in \Omega_h} (v)_{i,j} > \max_{(x_i, y_j) \in \partial\Omega_h} (v)_{i,j}$. Take $(x_m, y_n) \in \Omega_h$ where v achieves its maximum in Ω_h . Because all the stencils satisfying (3.29) and the sign condition in (3.30), we have

$$\sum_{\substack{k, \ell \in \{-1, 0, 1\} \\ k \neq 0, \ell \neq 0}} C_{k, \ell}(h)(v)_{m+k, n+\ell} \leq -C_{0,0}(h)(v)_{m,n}.$$

By

$$0 \leq h^s (\Delta_h v)_{m,n} = C_{0,0}(h)(v)_{m,n} + \sum_{\substack{k, \ell \in \{-1, 0, 1\} \\ k \neq 0, \ell \neq 0}} C_{k, \ell}(h)(v)_{m+k, n+\ell},$$

where $s = 1, 2$, we have

$$-C_{0,0}(h)(v)_{m,n} \leq \sum_{\substack{k, \ell \in \{-1, 0, 1\} \\ k \neq 0, \ell \neq 0}} C_{k, \ell}(h)(v)_{m+k, n+\ell} \leq -C_{0,0}(h)(v)_{m,n}.$$

Thus, equality holds throughout and v achieves its maximum at all its nearest neighbors of (x_m, y_n) . Applying the same argument to the neighbors in Ω_h and repeat this argument, we conclude that v must be a constant contradicting our assumption. This proves the discrete maximum principle.

Define $U_h := \{u(x_i, y_j)\}_{(x_i, y_j) \in \bar{\Omega}_h}$. Our results in Sections 3.3.1 and 3.3.2 (more precisely, (3.15) with $M = 4$ and (3.26) with $M = 3$) show that there exists a positive constant C

independent of h such that

$$\Delta_h U_h = F + R \quad \text{with} \quad \|R|_{\Omega_h \setminus \Omega_{ir}}\|_\infty \leq Ch^4 \quad \text{and} \quad \|R|_{\Omega_{ir}}\|_\infty \leq Ch^3, \quad (3.33)$$

where Ω_{ir} is the set of all irregular points $(x_i, y_j) \in \Omega_h$. Define $E_h := U_h - u_h$ on $\bar{\Omega}_h$. Because $\Delta_h u_h = F$, we have

$$\Delta_h E_h = \Delta_h U_h - \Delta_h u_h = R \quad \text{on} \quad \Omega_h \quad \text{with} \quad E_h = 0 \quad \text{on} \quad \partial\Omega_h.$$

Let η be the unique weak solution to $-\nabla \cdot (a\nabla\eta) = 1$ on Ω with the Dirichlet boundary condition $\eta = 0$ on $\partial\Omega$ and two jump conditions $[\eta] = [a\nabla\eta \cdot \vec{n}] = 0$ on Γ . Then η is continuous and piecewise smooth. Without loss of generality, we assume that the inner region is Ω_- as illustrated by Fig. [3.1](#); otherwise, we can replace the level function ψ with $-\psi$ so that the inner region is Ω_- . We define a function ϕ on Ω such that $\phi = \eta$ on Ω_+ and $\phi = \eta - 1$ on Ω_- . Then it is trivial to observe that ϕ is a solution to

$$\begin{cases} -\nabla \cdot (a\nabla\phi) = 1 & \text{in } \Omega \setminus \Gamma, \\ [\phi] = 1 & \text{on } \Gamma, \\ [a\nabla\phi \cdot \vec{n}] = 0 & \text{on } \Gamma, \\ \phi = 0 & \text{on } \partial\Omega. \end{cases} \quad (3.34)$$

Because ϕ is bounded, there exists a positive constant C_ϕ such that $\Phi := \phi + C_\phi \geq 0$ on Ω . Obviously, $\Phi = C_\phi$ on $\partial\Omega$. From [\(3.29\)](#), we trivially have $\mathcal{L}_h 1 = 0$. By [\(3.15\)](#) and [\(3.14\)](#) with $M = 4$ at any regular points (x_i, y_j) , we have

$$\Delta_h \Phi = \mathcal{L}_h \Phi = \mathcal{L}_h \phi + C_\phi \mathcal{L}_h 1 = \mathcal{L}_h \phi = 1 + \mathcal{O}(h),$$

due to $-\nabla \cdot (a\nabla\phi) = 1$ in [\(3.34\)](#). In particular, for sufficiently small h , we obtain $2C(\Delta_h \Phi)_{i,j} = 2C + 2C\mathcal{O}(h) \geq C$. Now by [\(3.33\)](#), we have

$$(\Delta_h E_h + 2Ch^4 \Delta_h \Phi)_{i,j} = (\Delta_h E_h)_{i,j} + 2Ch^4 (\Delta_h \Phi)_{i,j} \geq R(x_i, y_j) + Ch^4 \geq 0,$$

at any regular points (x_i, y_j) , because $|R(x_i, y_j)| \leq Ch^4$ in [\(3.33\)](#).

Now we consider an irregular point $(x_i, y_j) \in \Omega_{ir}$. By [\(3.29\)](#), we trivially have $\mathcal{L}_h^\Gamma 1 = 0$. Consequently, by [\(3.26\)](#) and [\(3.27\)](#) at an irregular point $(x_i, y_j) \in \Omega_{ir}$, we have

$$\Delta_h \Phi = \mathcal{L}_h^\Gamma \Phi = \mathcal{L}_h^\Gamma \phi + C_\phi \mathcal{L}_h^\Gamma 1 = \mathcal{L}_h^\Gamma \phi = h^{-1} + \mathcal{O}(1),$$

where h^{-1} is from $[\phi] = 1$ in (3.34). In particular, for sufficiently small h , we obtain $2C\Delta_h\Phi = 2Ch^{-1} + 2C\mathcal{O}(1) \geq Ch^{-1}$ at the irregular point (x_i, y_j) . Thus, for sufficiently small h , by (3.33), we have

$$(\Delta_h E_h + 2Ch^4\Delta_h\Phi)_{i,j} = (\Delta_h E_h)_{i,j} + 2Ch^4(\Delta_h\Phi)_{i,j} \geq R(x_i, y_j) + Ch^3 \geq 0,$$

at any $(x_i, y_j) \in \Omega_{ir}$, because $|R(x_i, y_j)| \leq Ch^3$ in (3.33) for irregular points $(x_i, y_j) \in \Omega_{ir}$.

In summary, we proved $\Delta_h(E_h + 2Ch^4\Phi) \geq 0$ on Ω_h . Now by the discrete maximum principle of Δ_h , $\Phi \geq 0$ on Ω , and $E_h = 0$ on $\partial\Omega_h$, we conclude that

$$\begin{aligned} \max_{(x_i, y_j) \in \Omega_h} (E_h)_{i,j} &\leq \max_{(x_i, y_j) \in \Omega_h} (E_h + 2Ch^4\Phi)_{i,j} \leq \max_{(x_i, y_j) \in \partial\Omega_h} (E_h + 2Ch^4\Phi)_{i,j} \\ &\leq \max_{(x_i, y_j) \in \partial\Omega_h} (E_h)_{i,j} + 2Ch^4 \max_{(x_i, y_j) \in \partial\Omega_h} (\Phi)_{i,j} = 2CC_\phi h^4, \end{aligned}$$

where C is the constant in (3.33) and we used $\Phi = C_\phi$ on $\partial\Omega$. This proves $\max_{(x_i, y_j) \in \Omega_h} (E_h)_{i,j} \leq 2CC_\phi h^4$. Similarly, we can consider $-E_h$ to obtain $\max_{(x_i, y_j) \in \Omega_h} (-E_h)_{i,j} \leq 2CC_\phi h^4$. Hence, we proved $\|E_h\|_\infty = \|u - u_h\|_\infty \leq 2CC_\phi h^4$ and established the convergence rate of order 4 of our proposed compact 9-point finite difference scheme. \square

3.4 A high order local approximation for computing ∇u using uniform Cartesian grids

In Section 3.3, we derived a high order compact 9-point finite difference scheme for the elliptic interface problem. After obtaining the numerical solution described by Theorem 3.2 and Theorem 3.4, we can locally compute the gradient approximation without constructing and solving a global linear system. For the convenience of the readers, in this section, we derive a high order approximation for the gradient by using the already computed numerical solution in Section 3.3.

3.4.1 Compute ∇u at regular points

In this subsection, we discuss the derivation of a compact 9-point approximation of the gradient at regular points. The calculation is local and does not require to solve a global linear system. As in Section 3.3.1, we choose $(x_i^*, y_j^*) = (x_i, y_j)$, i.e., $v_0 = w_0 = 0$ in (1.6). For a positive integer \tilde{M} , we consider the following compact 9-point stencil for approximating

the partial derivative $u_x(x_i, y_j)$:

$$\mathcal{L}_{x,h}u := h^{-1} \sum_{k=-1}^1 \sum_{\ell=-1}^1 \tilde{C}_{k,\ell}(h) u(x_i + kh, y_j + \ell h) \quad \text{with} \quad \tilde{C}_{k,\ell}(h) := \sum_{p=0}^{\tilde{M}} \tilde{c}_{k,\ell,p} h^p,$$

where $\tilde{c}_{k,\ell,p}$ are to-be-determined constants. Using (3.12) with $x_i^* = x_i$ and $y_j^* = y_j$ and $M = \tilde{M} - 1$ we have

$$\mathcal{L}_{x,h}u = \sum_{(m,n) \in \Lambda_{\tilde{M}}^1} u^{(m,n)} h^{-1} \tilde{I}_{m,n}(h) + \sum_{(m,n) \in \Lambda_{\tilde{M}-2}} f^{(m,n)} h \tilde{J}_{m,n}(h) + \mathcal{O}(h^{\tilde{M}}),$$

where $u^{(m,n)} := \frac{\partial^{m+n} u}{\partial x^m \partial y^n}(x_i, y_j)$, $f^{(m,n)} := \frac{\partial^{m+n} f}{\partial x^m \partial y^n}(x_i, y_j)$, and the polynomials $\tilde{I}_{m,n}(h)$ and $\tilde{J}_{m,n}(h)$ are

$$\tilde{I}_{m,n}(h) := \sum_{k=-1}^1 \sum_{\ell=-1}^1 \tilde{C}_{k,\ell}(h) G_{\tilde{M},m,n}(kh, \ell h) \quad \text{and} \quad \tilde{J}_{m,n}(h) := \sum_{k=-1}^1 \sum_{\ell=-1}^1 \tilde{C}_{k,\ell}(h) h^{-2} Q_{\tilde{M},m,n}(kh, \ell h).$$

Therefore, we conclude from the above identities that if

$$\tilde{I}_{1,0}(h) = h + \mathcal{O}(h^{\tilde{M}+1}) \quad \text{and} \quad \tilde{I}_{m,n}(h) = \mathcal{O}(h^{\tilde{M}+1}), \quad h \rightarrow 0 \quad \text{for all } (m,n) \in \Lambda_{\tilde{M}}^1 \setminus \{(1,0)\}, \quad (3.35)$$

then we must have the following approximation order (but using the exact solution u):

$$\mathcal{L}_{x,h}u - h \sum_{(m,n) \in \Lambda_{\tilde{M}-2}} f^{(m,n)} \tilde{J}_{m,n}(h) = u^{(1,0)} + \mathcal{O}(h^{\tilde{M}}) = u_x(x_i, y_j) + \mathcal{O}(h^{\tilde{M}}), \quad h \rightarrow 0. \quad (3.36)$$

Now assume that the numerical solution u_h to the exact solution u has an accuracy order M near (x_i, y_j) , i.e.,

$$(u_h)_{i+k, j+\ell} = u(x_i + kh, y_j + \ell h) + \mathcal{O}(h^M), \quad h \rightarrow 0 \quad \text{for all } k, \ell \in \{-1, 0, 1\}. \quad (3.37)$$

Then we trivially have $\mathcal{L}_{x,h}(u - u_h) = \mathcal{O}(h^{M-1})$ as $h \rightarrow 0$. Hence, by (3.36), the following approximation of $u_x(x_i, y_j)$ from the numerical solution u_h must have the approximation order $\min(\tilde{M}, M - 1)$ satisfying

$$D_{x,h}u_h := \mathcal{L}_{x,h}u_h - h \sum_{(m,n) \in \Lambda_{\tilde{M}-2}} f^{(m,n)} \tilde{J}_{m,n}(h) = u_x(x_i, y_j) + \mathcal{O}(h^{\min(\tilde{M}, M-1)}), \quad h \rightarrow 0, \quad (3.38)$$

where

$$\mathcal{L}_{x,h}u_h := h^{-1} \sum_{k=-1}^1 \sum_{\ell=-1}^1 \tilde{C}_{k,\ell}(h)(u_h)_{i+k,j+\ell}.$$

We find that the maximum integer \tilde{M} is 4 for (3.35) to have a solution $\{\tilde{C}_{k,\ell}\}_{k,\ell=-1,0,1}$. Moreover, a particular such solution $\{\tilde{C}_{k,\ell}\}_{k,\ell=-1,0,1}$ to (3.35) with $\tilde{M} = 4$ is given by

$$\begin{aligned} \tilde{C}_{-1,-1}(h) &= 1 - [\frac{13}{12}a_{0,1} + \frac{13}{12}a_{1,0}]h + [-\frac{9}{8}a_{0,1}^2 - \frac{55}{24}a_{0,1}a_{1,0} + \frac{7}{3}a_{1,0}^2 + \frac{13}{12}a_{0,2} - \frac{7}{6}a_{2,0} + \frac{9}{4}a_{1,1}]h^2 + [-\frac{13}{24}a_{0,1}^3 \\ &\quad - \frac{9}{8}a_{0,1}^2a_{1,0} - (\frac{83}{24}a_{1,0}^2 - \frac{13}{12}a_{0,2} - \frac{41}{24}a_{2,0} - \frac{13}{24}a_{1,1})a_{0,1} - \frac{23}{8}a_{1,0}^3 + \frac{13}{24}(a_{0,2} + \frac{54}{13}a_{2,0} + a_{1,1})a_{1,0} \\ &\quad - \frac{13}{24}(a_{2,1} + a_{0,3} + a_{3,0} + a_{1,2})]h^3, \\ \tilde{C}_{-1,0}(h) &= 4 - \frac{13}{3}a_{1,0}h + [\frac{9}{4}a_{0,1}^2 + \frac{14}{3}a_{0,1}a_{1,0} - \frac{13}{12}a_{1,0}^2 - \frac{13}{6}a_{0,2} + \frac{13}{6}a_{2,0} - \frac{7}{3}a_{1,1}]h^2 + [\frac{13}{24}a_{0,1}^3 + \frac{7}{12}a_{0,1}^2a_{1,0} + (\frac{69}{24}a_{1,0}^2 \\ &\quad - \frac{13}{12}a_{0,2} - \frac{41}{24}a_{2,0})a_{0,1} + \frac{13}{24}(-a_{1,0}a_{1,1} + a_{0,3} + a_{2,1})]h^3, \\ \tilde{C}_{-1,1}(h) &= 1 - [\frac{1}{12}a_{0,1} + \frac{13}{12}a_{1,0}]h + [-\frac{9}{8}a_{0,1}^2 - \frac{29}{24}a_{0,1}a_{1,0} + \frac{7}{3}a_{1,0}^2 + \frac{13}{12}a_{0,2} + \frac{1}{12}a_{1,1} - \frac{7}{6}a_{2,0}]h^2, \\ \tilde{C}_{0,-1}(h) &= 4 + \frac{1}{3} - [\frac{13}{6}a_{0,1} + \frac{7}{3}a_{1,0}]h + [\frac{7}{6}a_{0,1}^2 + \frac{14}{3}a_{0,1}a_{1,0} - \frac{7}{3}a_{1,1}]h^2 + [\frac{23}{8}a_{1,0}^3 + \frac{7}{12}a_{0,1}a_{1,0}^2 + (\frac{13}{24}a_{0,1}^2 - \frac{13}{24}a_{0,2} \\ &\quad - \frac{27}{12}a_{2,0})a_{1,0} + \frac{13}{24}(-a_{0,1}a_{1,1} + a_{3,0} + a_{1,2})]h^3, \\ \tilde{C}_{0,0}(h) &= -20 - \frac{5}{3} + [\frac{7}{3}a_{0,1} + \frac{67}{6}a_{1,0}]h + [-\frac{7}{6}a_{0,1}^2 - \frac{35}{6}a_{0,1}a_{1,0} - \frac{43}{12}a_{1,0}^2 + \frac{7}{3}a_{1,1} + \frac{1}{6}a_{2,0}]h^2, \\ \tilde{C}_{0,1}(h) &= 4 + \frac{1}{3} + [\frac{13}{6}a_{0,1} - \frac{7}{3}a_{1,0}]h, \quad \tilde{C}_{1,-1}(h) = 1 + \frac{1}{6} - \frac{7}{6}a_{0,1}h, \quad \tilde{C}_{1,0}(h) = 4 + \frac{2}{3}, \quad \tilde{C}_{1,1}(h) = 1 + \frac{1}{6}, \end{aligned} \tag{3.39}$$

where $a_{m,n} := a^{(m,n)}/a^{(0,0)}$ for $m, n \in \mathbb{N}_0$ and $m + n > 0$. Therefore, we proved the following theorem:

Theorem 3.7. *Let (x_i, y_j) be a regular point and u_h be a numerical solution such that u_h satisfies the approximation order $M = 4$ in (3.37) to the exact solution u (this is guaranteed by our finite difference scheme discussed in Theorem 3.2). Then the local compact 9-point approximation $D_{x,h}u_h$ in (3.38) to the partial derivative u_x of the exact solution u of problem (3.1) at (x_i, y_j) achieves the approximation order 3 with $\{\tilde{C}_{k,\ell}(h)\}_{k,\ell=-1,0,1}$ in (3.39). Furthermore, the local compact 9-point approximation $D_{y,h}u_h$ to u_y with the approximation order 3 can be obtained similarly.*

3.4.2 Compute ∇u at irregular points

In this section, we will discuss the derivation of the local 25-point computation of the gradient approximation at irregular points. As in Section 3.4.1, we choose $(x_i^*, y_j^*) = (x_i, y_j)$, i.e., $v_0 = w_0 = 0$ in (1.6). We assume that (3.18) and (3.19) hold. To simplify the calculation, we also assume that $(x_i, y_j) \in \Omega_+$, and define

$$e_{i,j}^+ := \{(k, \ell) : k, \ell \in \{-2, -1, 0, 1, 2\}, \psi(x_i + kh, y_j + \ell h) > 0\}.$$

For a positive integer \tilde{M} , we consider the following stencil for approximating u_x :

$$\mathcal{L}_{x,h}^\Gamma u := h^{-1} \sum_{(k,\ell) \in e_{i,j}^+} \tilde{C}_{k,\ell}(h)u(x_i + kh, y_j + \ell h) \quad \text{with} \quad \tilde{C}_{k,\ell}(h) := \sum_{p=0}^{\tilde{M}} \tilde{c}_{k,\ell,p}h^p,$$

where $\tilde{c}_{k,\ell,p}$ are to be-determined constants. By the same argument as in Section [3.4.1](#), we obtain

$$\mathcal{L}_{x,h}^\Gamma u = h^{-1} \sum_{(m,n) \in \Lambda_M^1} u_+^{(m,n)} \tilde{I}_{m,n}^+(h) + h \sum_{(m,n) \in \Lambda_{\tilde{M}-2}} f_+^{(m,n)} \tilde{J}_{m,n}^+(h) + \mathcal{O}(h^{\tilde{M}}), \quad h \rightarrow 0,$$

where

$$\tilde{I}_{m,n}^+(h) := \sum_{(k,\ell) \in e_{i,j}^+} \tilde{C}_{k,\ell}(h) G_{\tilde{M},m,n}^+(kh, \ell h),$$

and

$$\tilde{J}_{m,n}^+ := \sum_{(k,\ell) \in e_{i,j}^+} \tilde{C}_{k,\ell}(h) h^{-2} Q_{\tilde{M},m,n}^+(kh, \ell h).$$

Therefore, by the same argument as in Section [3.4.1](#), if

$$\tilde{I}_{1,0}^+(h) = h + \mathcal{O}(h^{\tilde{M}+1}) \quad \text{and} \quad \tilde{I}_{m,n}^+(h) = \mathcal{O}(h^{\tilde{M}+1}), \quad h \rightarrow 0 \text{ for all } (m,n) \in \Lambda_M^1 \setminus \{(1,0)\}, \quad (3.40)$$

then

$$\mathcal{L}_{x,h}^\Gamma u - h \sum_{(m,n) \in \Lambda_{\tilde{M}-2}} f_+^{(m,n)} \tilde{J}_{m,n}^+(h) = u_x(x_i, y_j) + \mathcal{O}(h^{\tilde{M}}), \quad h \rightarrow 0.$$

If a numerical solution u_h has the accuracy order M by satisfying [\(3.37\)](#), then we must have

$$\mathcal{L}_{x,h}^\Gamma u_h - h \sum_{(m,n) \in \Lambda_{\tilde{M}-2}} f_+^{(m,n)} \tilde{J}_{m,n}^+(h) = u_x(x_i, y_j) + \mathcal{O}(h^{\min(\tilde{M}, M-1)}), \quad h \rightarrow 0,$$

where

$$\mathcal{L}_{x,h}^\Gamma u_h := h^{-1} \sum_{(k,\ell) \in e_{i,j}^+} \tilde{C}_{k,\ell}(h) (u_h)_{i+k, j+\ell}.$$

In summary, we have the following result:

Theorem 3.8. *Let (x_i, y_j) be an irregular point and u_h be a numerical approximation of the exact solution u satisfying [\(3.37\)](#) with $M = 4$. Then [\(3.40\)](#) with $\tilde{M} = 3$ always has a solution $\{\tilde{C}_{k,\ell}\}_{(k,\ell) \in e_{i,j}^+}$. Consequently, the following approximation scheme has the approximation order 3:*

$$D_{x,h}^\Gamma u_h := \mathcal{L}_{x,h}^\Gamma u_h - h \sum_{(m,n) \in \Lambda_1} f_+^{(m,n)} \tilde{J}_{m,n}^+(h) = u_x(x_i, y_j) + \mathcal{O}(h^3), \quad h \rightarrow 0.$$

Furthermore, the local approximation $D_{y,h}^\Gamma u_h$ to u_y with the approximation order 3 can be obtained similarly.

3.5 Numerical experiments

3.5.1 Numerical examples with u known

In this subsection, we provide numerical results of 3 test problems with an available exact solution u of (3.1). In Example 3.1, we compare our proposed compact 9-point finite difference scheme with second order IIM [69, 117, 17], second order EJIIM [110], second order MIB [119], second order AMIB with the FFT acceleration [39] and fourth order IIM [117]. The number of points in the left hands of stencils in the above schemes are: 9 points [17, second order IIM], 6 points [69, second order IIM], 4 points [117, second order IIM], 6 points [110, second order EJIIM], 10 points [119, second order MIB], 11 points [39, second order AMIB], and 8 points [117, fourth order IIM].

Example 3.1. Let $\Omega = (-l_1, l_1)^2$ and the interface curve be given by $\Gamma := \{(x, y) \in \Omega : \psi(x, y) = 0\}$ with $\psi(x, y) = x^2 + y^2 - 1/4$. Note that $\Gamma \cap \partial\Omega = \emptyset$ and $r^2 := x^2 + y^2$, the coefficient a and the exact solution u of (3.1) are given by

$$\begin{aligned}
 \text{Case 1: } & a_+ = a\chi_{\Omega_+} = b, \quad a_- = a\chi_{\Omega_-} = x^2 + y^2 + 1, \\
 & u_+ = u\chi_{\Omega_+} = (1 - 9/(8b))/4 + (r^4 + 2r^2)/(2b) + C \log(2r)/b, \\
 & u_- = u\chi_{\Omega_-} = x^2 + y^2. \\
 \text{Case 2: } & a_+ = a\chi_{\Omega_+} = b, \quad a_- = a\chi_{\Omega_-} = 2, \\
 & u_+ = u\chi_{\Omega_+} = (1 - 9/(8b))/4 + (r^4 + 2r^2)/(2b), \quad u_- = u\chi_{\Omega_-} = x^2 + y^2. \\
 \text{Case 3: } & a_+ = a\chi_{\Omega_+} = \cos(x + y) + 2, \quad a_- = a\chi_{\Omega_-} = \sin(x + y) + 2, \\
 & u_+ = u\chi_{\Omega_+} = \log(x^2 + y^2 + 1), \quad u_- = u\chi_{\Omega_-} = \sin(x + y). \\
 \text{Case 4: } & a_+ = a\chi_{\Omega_+} = 100, \quad a_- = a\chi_{\Omega_-} = 1, \\
 & u_+ = u\chi_{\Omega_+} = \sin(3x) \sin(3y), \quad u_- = u\chi_{\Omega_-} = \exp(-x^2 - y^2/2).
 \end{aligned}$$

All the functions $f, g_0^\Gamma, g_1^\Gamma, g$ in (3.1) can be obtained by plugging the above coefficient and exact solution into (3.1). The numerical results are presented in Tables 3.1 to 3.4.

Example 3.2. Let $\Omega = (-\pi, \pi)^2$ and the interface curve be given by $\Gamma := \{(x, y) \in \Omega : \psi(x, y) = 0\}$ with $\psi(x, y) = y^2 - 2x^2 + x^4 - 1/4$. Note that $\Gamma \cap \partial\Omega = \emptyset$, the coefficient a and the exact solution u of (3.1) are given by

$$\begin{aligned}
 a_+ &= a\chi_{\Omega_+} = 10^{-1}(2 + \sin(x) \cos(y)), & a_- &= a\chi_{\Omega_-} = 10^2(2 + \sin(x) \cos(y)), \\
 u_+ &= u\chi_{\Omega_+} = 10 \sin(5x) \sin(5y)(y^2 - 2x^2 + x^4 - 1/4),
 \end{aligned}$$

Table 3.1: Case 1 of Example 3.1 with $b = 10$, $C = 0.1$, $\Omega = (-1, 1)^2$ and $h = 2/N_1$. The ratio r_1 is equal to $\|u_h - u\|_\infty$ of [69, 2nd-IIM] divided by $\|u_h - u\|_\infty$ of our proposed method and the ratio r_2 is equal to $\|u_h - u\|_\infty$ of [110, 2nd-EJIIM] divided by $\|u_h - u\|_\infty$ of our proposed method. In other words, for the same grid size h with $h = 2/N_1$, the errors of [69, 2nd-IIM] and [110, 2nd-EJIIM] are r_1 and r_2 times larger than those of our proposed method, respectively.

	[69, 2nd-IIM]	[110, 2nd-EJIIM]	Proposed		
N_1	$\ u_h - u\ _\infty$	$\ u_h - u\ _\infty$	$\ u_h - u\ _\infty$	r_1	r_2
20	3.5E-03	7.6E-04	4.6E-04	7.6	1.7
40	7.6E-04	2.4E-04	6.5E-05	11.7	3.7
80	1.7E-04	7.9E-05	7.0E-06	24.4	11.4
160	3.6E-05	2.2E-05	8.3E-07	43.5	26.6
320	8.4E-06	5.3E-06	8.8E-08	95.7	60.4

Table 3.2: Case 1 of Example 3.1 with $C = 0.1$, $\Omega = (-1, 1)^2$ and $h = 2/N_1$. The ratio r_1 is equal to $\|u_h - u\|_\infty/|u(1, 1)|$ of [117, 2nd-IIM] divided by $\|u_h - u\|_\infty/|u(1, 1)|$ of our proposed method and the ratio r_2 is equal to $\|u_h - u\|_\infty/|u(1, 1)|$ of [117, 4th-IIM] divided by $\|u_h - u\|_\infty/|u(1, 1)|$ of our proposed method. In other words, for the same grid size h with $h = 2/N_1$, the errors of [117, 2nd-IIM] and [117, 4th-IIM] are r_1 and r_2 times larger than those of our proposed method, respectively.

		$b = 10^{-1}$					$b = 10^{-2}$				
		[117, 2nd-IIM]	[117, 4th-IIM]	Proposed			[117, 2nd-IIM]	[117, 4th-IIM]	Proposed		
N_1		$\frac{\ u_h - u\ _\infty}{ u(1,1) }$	$\frac{\ u_h - u\ _\infty}{ u(1,1) }$	$\frac{\ u_h - u\ _\infty}{ u(1,1) }$	r_1	r_2	$\frac{\ u_h - u\ _\infty}{ u(1,1) }$	$\frac{\ u_h - u\ _\infty}{ u(1,1) }$	$\frac{\ u_h - u\ _\infty}{ u(1,1) }$	r_1	r_2
20		4.66E-03	6.76E-05	6.67E-04	7.0	0.10	2.89E-02	4.94E-04	5.71E-03	5.1	0.09
40		1.94E-03	1.40E-04	7.86E-05	24.6	1.78	1.91E-02	1.05E-03	3.28E-04	58.2	3.2
80		5.29E-04	2.56E-05	9.96E-06	53.1	2.57	5.16E-03	2.44E-04	4.83E-06	1068	50.4
		$b = 10^{-3}$					$b = 10^{-4}$				
		[117, 2nd-IIM]	[117, 4th-IIM]	Proposed			[117, 2nd-IIM]	[117, 4th-IIM]	Proposed		
N_1		$\frac{\ u_h - u\ _\infty}{ u(1,1) }$	$\frac{\ u_h - u\ _\infty}{ u(1,1) }$	$\frac{\ u_h - u\ _\infty}{ u(1,1) }$	r_1	r_2	$\frac{\ u_h - u\ _\infty}{ u(1,1) }$	$\frac{\ u_h - u\ _\infty}{ u(1,1) }$	$\frac{\ u_h - u\ _\infty}{ u(1,1) }$	r_1	r_2
20		9.57E-02	3.64E-03	8.81E-02	1.1	0.04	1.26E-01	1.08E-02	3.36E-01	0.4	0.03
40		6.16E-01	9.16E-03	1.60E-04	3861	57	2.85E-01	4.72E-02	2.98E-02	9.6	1.58
80		8.88E-02	2.43E-03	4.41E-05	2014	55	1.39E-01	2.54E-02	1.81E-03	77	14.1

$$u_- = u\chi_{\Omega_-} = 10^{-2} \sin(5x) \sin(5y)(y^2 - 2x^2 + x^4 - 1/4) + 500.$$

All the functions $f, g_0^\Gamma, g_1^\Gamma, g$ in (3.1) can be obtained by plugging the above coefficient and exact solution into (3.1). In particular, $g_0^\Gamma = -500$ and $g_1^\Gamma = 0$. The numerical results are presented in Table 3.5 and Fig. 3.6.

Example 3.3. Let $\Omega = (-3.5, 3.5)^2$ and the interface curve be given by $\Gamma := \{(x, y) \in \Omega : \psi(x, y) = 0\}$ which is shown in Fig. 3.7. Precisely, the sharp-edged interface is a square with 4 corner points $(-2, 0)$, $(0, 2)$, $(2, 0)$ and $(0, -2)$. Note that $\Gamma \cap \partial\Omega = \emptyset$, the coefficient a and

Table 3.3: Case 2 of Example 3.1 with $b = 10$, $\Omega = (-1, 1)^2$ and $h = 2/N_1$. The ratio r_1 is equal to $\|u_h - u\|_\infty$ of [119, 2nd-MIB] divided by $\|u_h - u\|_\infty$ of our proposed method and the ratio r_2 is equal to $\|u_h - u\|_\infty$ of [69, 2nd-IIM] divided by $\|u_h - u\|_\infty$ of our proposed method. In other words, for the same grid size h with $h = 2/N_1$, the errors of [119, 2nd-MIB] and [69, 2nd-IIM] are r_1 and r_2 times larger than those of our proposed method, respectively.

	[119, 2nd-MIB]	[69, 2nd-IIM]	Proposed		
N_1	$\ u_h - u\ _\infty$	$\ u_h - u\ _\infty$	$\ u_h - u\ _\infty$	r_1	r_2
20	2.852E-04	2.167E-03	4.737E-04	0.60	4.57
40	7.707E-05	5.000E-04	6.228E-05	1.24	8.03
80	2.069E-05	1.131E-04	7.645E-06	2.71	14.79
160	5.131E-06	2.748E-05	9.824E-07	5.22	27.97
320	1.257E-06	6.781E-06	1.111E-07	11.32	61.06

Table 3.4: Case 3 and Case 4 of Example 3.1. The ratio r_1 is equal to $\|u_h - u\|_\infty$ of [17, 2nd-IIM] divided by $\|u_h - u\|_\infty$ of our proposed method and the ratio r_2 is equal to $\|u_h - u\|_\infty$ of [39, 2nd-AMIB] divided by $\|u_h - u\|_\infty$ of our proposed method. In other words, for the same grid size h , the errors of [17, 2nd-IIM] and [39, 2nd-AMIB] are r_1 and r_2 times larger than those of our proposed method, respectively.

Case 3				Case 4							
$\Omega = (-1, 1)^2$ and $h = 2/N_1$				$\Omega = (-\frac{\pi}{3}, \frac{\pi}{3})^2$ and $h = \frac{2\pi}{3N_1}$				$\Omega = (-\frac{\pi}{3.5}, \frac{\pi}{3.5})^2$ and $h = \frac{2\pi}{3.5N_1}$			
	[17, 2nd-IIM]	Proposed			[39, 2nd-AMIB]	Proposed			[39, 2nd-AMIB]	Proposed	
N_1	$\ u_h - u\ _\infty$	$\ u_h - u\ _\infty$	r_1	N_1	$\ u_h - u\ _\infty$	$\ u_h - u\ _\infty$	r_2	N_1	$\ u_h - u\ _\infty$	$\ u_h - u\ _\infty$	r_2
16	1.0E-03	1.4E-03	0.7	32	4.4E-03	7.9E-03	0.6	32	2.7E-03	3.9E-03	0.7
32	3.8E-04	1.4E-04	2.7	64	1.2E-03	1.4E-03	0.9	64	9.5E-04	5.0E-04	1.9
64	8.0E-05	1.5E-05	5.2	128	3.6E-04	1.2E-04	2.9	128	2.0E-04	7.4E-05	2.8
128	2.3E-05	1.8E-06	12.6	256	8.3E-05	2.1E-05	3.9	256	4.5E-05	1.2E-05	3.9
256	5.7E-06	2.2E-07	25.6	512	1.9E-05	2.0E-06	9.6	512	1.2E-05	1.3E-06	8.9
512	1.5E-06	2.8E-08	53.4	1024	4.9E-06	2.5E-07	19.4	1024	3.1E-06	1.5E-07	20.8

Table 3.5: Performance in Example 3.2 of our proposed method on uniform Cartesian meshes with $h = 2^{-J} \times 2\pi$.

J	$\frac{\ u_h - u\ _2}{\ u\ _2}$	order	$\ u_h - u\ _\infty$	order	$\frac{\ \nabla u_h - \nabla u\ _2}{\ \nabla u\ _2}$	order	$\ \nabla u_h - \nabla u\ _\infty$	order
5	1.5785E-02	0	1.8642E+01	0	6.5837E-02	0	4.4162E+02	0
6	1.2083E-03	3.7	1.6060E+00	3.5	3.2683E-03	4.3	2.2133E+01	4.3
7	8.3619E-05	3.9	1.2258E-01	3.7	2.0640E-04	4.0	2.6279E+00	3.1
8	4.7447E-06	4.1	8.4474E-03	3.9	1.3500E-05	3.9	2.6734E-01	3.3
9	3.2341E-07	3.9	5.9899E-04	3.8	9.4036E-07	3.8	3.5506E-02	2.9
10	1.9622E-08	4.0	4.1601E-05	3.8	7.0430E-08	3.7	4.8334E-03	2.9

the exact solution u of (3.1) are given by

$$a_+ = 10^3, \quad a_- = 10^{-3}, \quad u_+ = 10^{-3} \sin(4x - 4y), \quad u_- = 10^3 \cos(4x) \cos(4y) + 1000.$$

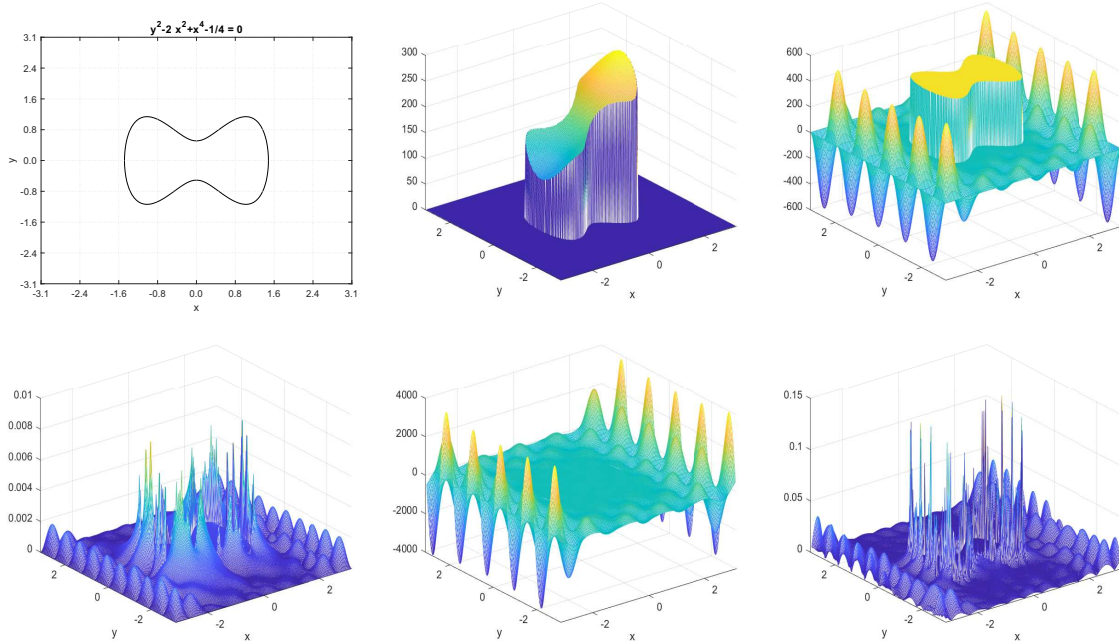


Figure 3.6: Top row for Example 3.2: the interface curve Γ (left), the coefficient $a(x, y)$ (middle) and the numerical solution u_h (right) with $h = 2^{-8} \times 2\pi$. Bottom row for Example 3.2: the error $|u_h - u|$ (left), the numerical $(u_h)_x$ (middle) and the error $|(u_h)_x - u_x|$ (right) with $h = 2^{-8} \times 2\pi$.

All the functions $f, g_0^\Gamma, g_1^\Gamma, g$ in (3.1) can be obtained by plugging the above coefficient and exact solution into (3.1). Clearly, g_0^Γ and g_1^Γ are not constants. The numerical results are presented in Table 3.6 and Fig. 3.7.

Table 3.6: Performance in Example 3.3 of our proposed method on uniform Cartesian meshes with $h = 2^{-J} \times 7$.

J	$\frac{\ u_h - u\ _2}{\ u\ _2}$	order	$\ u_h - u\ _\infty$	order	$\frac{\ \nabla u_h - \nabla u\ _2}{\ \nabla u\ _2}$	order	$\ \nabla u_h - \nabla u\ _\infty$	order
5	8.8954E-02	0	2.1581E+02	0	2.4814E-01	0	3.2146E+03	0
6	3.7639E-03	4.6	1.3830E+01	4.0	1.3965E-02	4.2	2.7688E+02	3.5
7	1.7450E-04	4.4	6.8185E-01	4.3	7.2657E-04	4.3	1.5547E+01	4.2
8	1.1627E-05	3.9	5.2208E-02	3.7	3.9462E-05	4.2	8.8775E-01	4.1
9	8.6688E-07	3.7	3.8840E-03	3.7	2.4032E-06	4.0	5.2936E-02	4.1

3.5.2 Numerical examples with u unknown

In this subsection, we provide 3 numerical experiments such that the exact solution u of (3.1) is unknown.

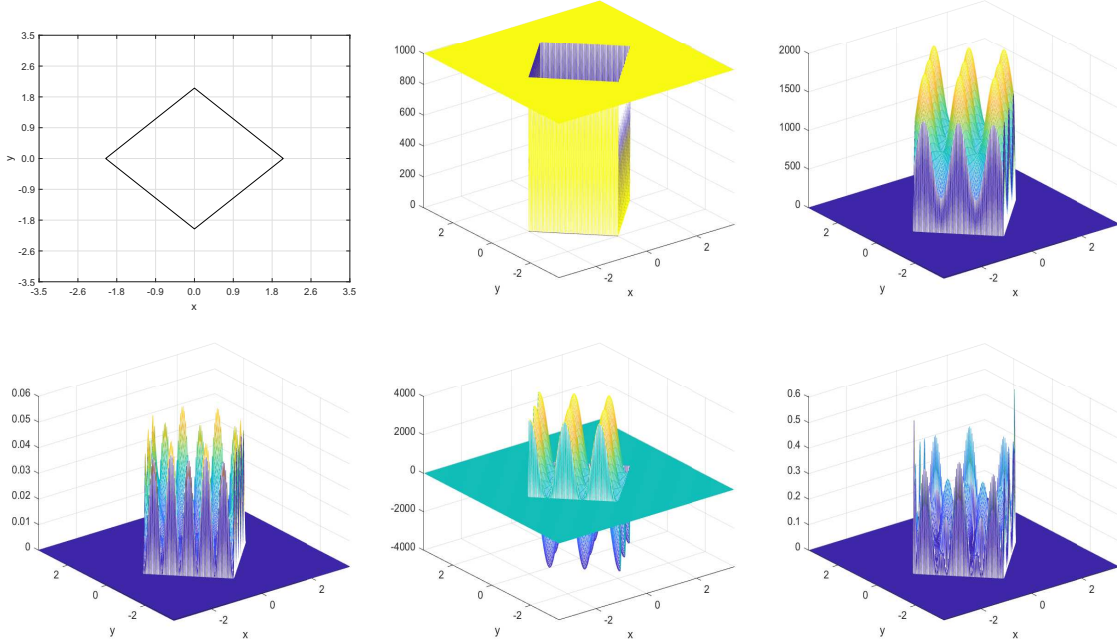


Figure 3.7: Top row for Example 3.3: the interface curve Γ (left), the coefficient $a(x, y)$ (middle) and the numerical solution u_h (right) with $h = 2^{-8} \times 7$. Bottom row for Example 3.3: the error $|u_h - u|$ (left), the numerical $(u_h)_x$ (middle) and the error $|(u_h)_x - u_x|$ (right) with $h = 2^{-8} \times 7$.

Example 3.4. Let $\Omega = (-2\pi/3, 2\pi/3)^2$ and the interface curve be given by $\Gamma := \{(x, y) \in \Omega : \psi(x, y) = 0\}$ with $\psi(x, y) = x^4 + 2y^4 - 2$. Note that $\Gamma \cap \partial\Omega = \emptyset$ and (3.1) is given by

$$\begin{aligned}
 a_+ &= a\chi_{\Omega_+} = 2 + \cos(x - y), & a_- &= a\chi_{\Omega_-} = 10^3(2 + \sin(x) \cos(y)), \\
 f_+ &= f\chi_{\Omega_+} = \sin(3x) \sin(3y), & f_- &= f\chi_{\Omega_-} = \cos(3x) \cos(3y), \\
 g_0^\Gamma &= \sin(x), & g_1^\Gamma &= \cos(y), & g &= 0.
 \end{aligned}$$

The numerical results are provided in Table 3.7 and Fig. 3.8.

Table 3.7: Performance in Example 3.4 of our proposed method on uniform Cartesian meshes with $h = 2^{-J} \times 4\pi/3$.

J	$\ u_h - u_{h/2}\ _2$	order	$\ u_h - u_{h/2}\ _\infty$	order	$\ \nabla u_h - \nabla u_{h/2}\ _2$	order	$\ \nabla u_h - \nabla u_{h/2}\ _\infty$	order
5	4.7877E-01	0	1.7752E-01	0	5.2967E-01	0	4.3910E-01	0
6	5.4887E-02	3.1	1.9966E-02	3.2	6.1966E-02	3.1	5.0909E-02	3.1
7	3.8920E-03	3.8	1.4235E-03	3.8	4.4494E-03	3.8	4.9900E-03	3.4
8	2.4772E-04	4.0	9.0274E-05	4.0	2.8557E-04	4.0	7.6614E-04	2.7

Example 3.5. Let $\Omega = (-2.5, 2.5)^2$ and the interface curve be given by $\Gamma := \{(x, y) \in \Omega :$

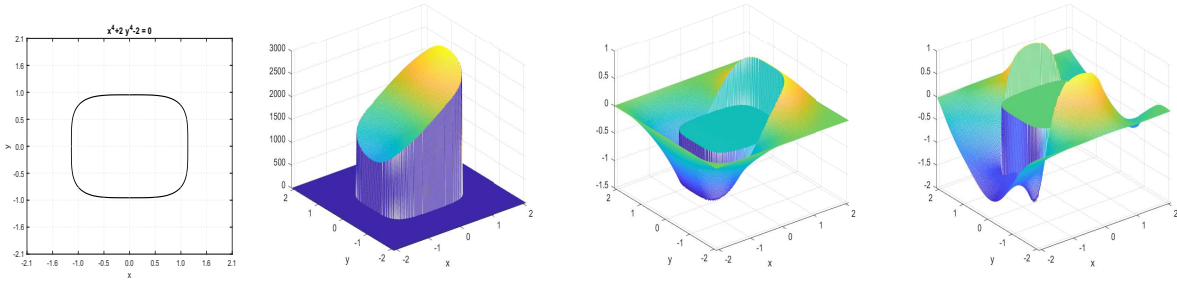


Figure 3.8: Example [3.4](#): the interface curve Γ (first panel), the coefficient $a(x, y)$ (second panel), the numerical solution u_h (third panel), and the numerical $(u_h)_x$ (fourth panel) with $h = 2^{-8} \times 4\pi/3$.

$\psi(x, y) = 0\}$ with $\psi(x, y) = y^2 - 2x^2 + x^4 - 1/4$. Note that $\Gamma \cap \partial\Omega = \emptyset$ and [\(3.1\)](#) is given by

$$\begin{aligned} a_+ &= a\chi_{\Omega_+} = 10^3(2 + \cos(x - y)), & a_- &= a\chi_{\Omega_-} = 10^{-3}(2 + \sin(x + y)), \\ f_+ &= f\chi_{\Omega_+} = \sin(4\pi x) \sin(4\pi y), & f_- &= f\chi_{\Omega_-} = \cos(4\pi(x - y)), \\ g_0^\Gamma &= \cos(x) \cos(y) - 1, & g_1^\Gamma &= \sin(x) \sin(y), & g &= 0. \end{aligned}$$

The numerical results are provided in Table [3.8](#) and Fig. [3.9](#).

Table 3.8: Performance in Example [3.5](#) of our proposed method on uniform Cartesian meshes with $h = 2^{-J} \times 5$.

J	$\ u_h - u_{h/2}\ _2$	order	$\ u_h - u_{h/2}\ _\infty$	order	$\ \nabla u_h - \nabla u_{h/2}\ _2$	order	$\ \nabla u_h - \nabla u_{h/2}\ _\infty$	order
6	2.4131E+00	0	7.9478E+00	0	2.4730E+01	0	1.5123E+02	0
7	1.6162E-01	3.9	5.8890E-01	3.8	1.5033E+00	4.0	1.2649E+01	3.6
8	7.8706E-03	4.4	3.4649E-02	4.1	1.0738E-01	3.8	1.4253E+00	3.1
9	4.9064E-04	4.0	2.1766E-03	4.0	8.1468E-03	3.7	1.9083E-01	2.9

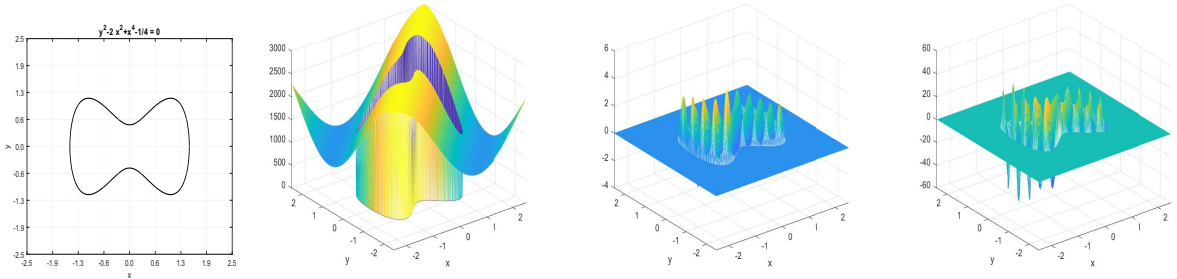


Figure 3.9: Example [3.5](#): the interface curve Γ (first panel), the coefficient $a(x, y)$ (second panel), the numerical solution u_h (third panel), and the numerical $(u_h)_x$ (fourth panel) with $h = 2^{-8} \times 5$.

Example 3.6. Let $\Omega = (-1.5, 1.5)^2$ and the interface curve be given by $\Gamma := \{(x, y) \in \Omega : \psi(x, y) = 0\}$ with $\psi(x, y) = 2x^4 + y^2 - 1/2$. Note that $\Gamma \cap \partial\Omega = \emptyset$ and (3.1) is given by

$$\begin{aligned} a_+ &= a\chi_{\Omega_+} = 10^3(2 + \sin(x)\sin(y)), & a_- &= a\chi_{\Omega_-} = 10^{-3}(2 + \cos(x)\cos(y)), \\ f_+ &= f\chi_{\Omega_+} = \sin(4\pi x)\sin(4\pi y), & f_- &= f\chi_{\Omega_-} = \cos(4\pi x)\cos(4\pi y), \\ g_0^\Gamma &= \sin(x+y) - 10^6, & g_1^\Gamma &= \cos(x-y), & g &= 0. \end{aligned}$$

The numerical results are provided in Table 3.9 and Fig. 3.10.

Table 3.9: Performance in Example 3.6 of our proposed method on uniform Cartesian meshes with $h = 2^{-J} \times 3$.

J	$\ u_h - u_{h/2}\ _2$	order	$\ u_h - u_{h/2}\ _\infty$	order	$\ \nabla u_h - \nabla u_{h/2}\ _2$	order	$\ \nabla u_h - \nabla u_{h/2}\ _\infty$	order
5	1.0037E+00	0	2.2166E+00	0	1.1762E+01	0	3.9078E+01	0
6	6.5117E-02	3.9	1.2140E-01	4.2	5.8901E-01	4.3	3.4589E+00	3.5
7	3.3958E-03	4.3	7.7527E-03	4.0	4.5420E-02	3.7	5.1817E-01	2.7
8	2.0302E-04	4.1	4.8001E-04	4.0	3.2275E-03	3.8	4.7358E-02	3.5
9	9.5975E-06	4.4	3.1181E-05	3.9	2.3421E-04	3.8	4.3064E-03	3.5

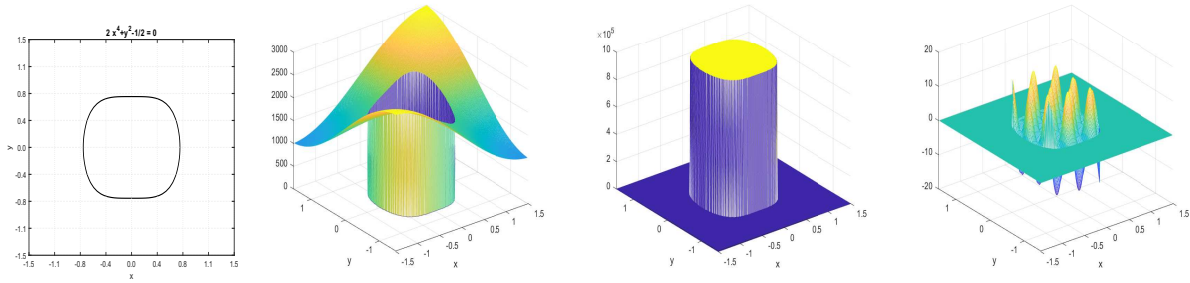


Figure 3.10: Example 3.6: the interface curve Γ (first panel), the coefficient $a(x, y)$ (second panel), the numerical solution u_h (third panel), and the numerical $(u_h)_x$ (fourth panel) with $h = 2^{-8} \times 3$.

3.6 Conclusion

To our best knowledge, so far there were no compact 9-point finite difference schemes available in the literature, that can achieve third or fourth order for the elliptic interface problems with piecewise smooth coefficients on uniform meshes. The third or fourth order compact 9-point IIM methods for the elliptic interface problems with discontinuous constant coefficients on uniform meshes are derived in [89, 75].

Our contributions of this chapter are as follows:

- (1) We construct a high order compact 9-point finite difference scheme for the numerical solution on uniform meshes for (3.1) with discontinuous, piecewise smooth and high-contrast coefficients (the ratio $\sup(a_+)/\inf(a_-) \approx 10^{-3}$ and 10^6 in Examples 3.2 to 3.6), discontinuous source terms and two non-homogeneous jump conditions.
- (2) In Tables 3.1 to 3.4 of Example 3.1, we compare our proposed compact 9-point finite difference scheme with the second order IIM, EJIIM, MIB and AMIB. Since the accuracy order in irregular points of our proposed scheme is three, the numerical results in Tables 3.1 to 3.4 show that our proposed compact 9-point scheme produces smaller errors than the second order IIM, EJIIM, MIB and AMIB.
- (3) In the Table 3.2 of Example 3.1, we also compare our proposed compact 9-point finite difference scheme with the fourth order IIM, the numerical results in Table 3.2 show that our proposed compact 9-point scheme also produces smaller errors than the fourth order IIM.
- (4) Since our proposed scheme does not require to change coordinates into the local coordinates and solve an optimization problem which are two basic steps for IIM, it is simpler for readers to derive our schemes, and perform the corresponding implementations.
- (5) MIB methods do not use the high order jump conditions, so our method could derive a higher order scheme than MIB methods in the same number of points of the stencils. Conversely, for the same accuracy order, our method could form a sparser matrix of the global corresponding linear system than the MIB methods.
- (6) For the irregular points case, Eq.(7.73) in [75, Section 7.2.7] expands the Taylor series of $u(x, y)$ to $\mathcal{O}(h^5)$, while we only need to expand the Taylor series of $u(x, y)$ to $\mathcal{O}(h^4)$, which significantly reduces the computational costs to calculate the coefficients of the proposed schemes.
- (7) We numerically verify the sign conditions of our proposed compact 9-point finite difference scheme and prove the fourth order convergence rate by the discrete maximum principle in Theorem 3.6.
- (8) Our numerical experiments confirm the flexibility and the fourth order accuracy for the numerically approximated solutions u_h in both l_2 and l_∞ norms, and the fourth/third order accuracy for the numerically approximated gradients $((u_h)_x, (u_h)_y)$ in the l_2/l_∞ norm.

3.7 Proof of Theorem 3.3

Proof of Theorem 3.3. Similar as the proof of Theorem 2.4 by the parametric equation in (1.5) for the interface Γ near (x_i^*, y_j^*) , the two jump conditions in (3.1) can be rewritten as

$$u_+(r(t) + x_i^*, s(t) + y_j^*) - u_-(r(t) + x_i^*, s(t) + y_j^*) = g_0^\Gamma(r(t) + x_i^*, s(t) + y_j^*), \quad (3.41)$$

$$\begin{aligned} & ((a_+ \nabla u_+)(r(t) + x_i^*, s(t) + y_j^*) - (a_- \nabla u_-)(r(t) + x_i^*, s(t) + y_j^*)) \cdot (s'(t), -r'(t)) \\ &= g_1^\Gamma(r(t) + x_i^*, s(t) + y_j^*) \sqrt{(r'(t))^2 + (s'(t))^2}, \end{aligned} \quad (3.42)$$

for $t \in (-\epsilon, \epsilon)$. Because all involved functions in (3.41) and (3.42) are assumed to be smooth, to link the two sets $\{u_+^{(m,n)} : (m,n) \in \Lambda_M^1\}$ and $\{u_-^{(m,n)} : (m,n) \in \Lambda_M^1\}$, we now take the Taylor approximation of the above functions near the base parameter $t = 0$. (3.19) with M being replaced by $M - 1$ implies

$$\begin{aligned} & u_\pm(r(t) + x_i^*, s(t) + y_j^*) \\ &= \sum_{(m,n) \in \Lambda_M^1} u_\pm^{(m,n)} G_{M,m,n}^\pm(r(t), s(t)) + \sum_{(m,n) \in \Lambda_{M-2}} f_\pm^{(m,n)} Q_{M,m,n}^\pm(r(t), s(t)) + \mathcal{O}(t^{M+1}) \\ &= \sum_{p=0}^M \left(\sum_{(m,n) \in \Lambda_M^1} u_\pm^{(m,n)} g_{m,n,p}^\pm + \sum_{(m,n) \in \Lambda_{M-2}} f_\pm^{(m,n)} q_{m,n,p}^\pm \right) t^p + \mathcal{O}(t^{M+1}), \end{aligned}$$

where

$$g_{m,n,p}^\pm := \frac{1}{p!} \frac{d^p(G_{M,m,n}^\pm(r(t), s(t)))}{dt^p} \Big|_{t=0}, \quad q_{m,n,p}^\pm := \frac{1}{p!} \frac{d^p(Q_{M,m,n}^\pm(r(t), s(t)))}{dt^p} \Big|_{t=0}, \quad p = 0, \dots, M. \quad (3.43)$$

By the definition of $g_{0,p}^\Gamma$ in (3.21), we have $g_0^\Gamma(r(t) + x_i^*, s(t) + y_j^*) = \sum_{p=0}^M g_{0,p}^\Gamma t^p + \mathcal{O}(t^{M+1})$ as $h \rightarrow 0$. Since every coefficients of $x^j y^k$ of the bivariate polynomial $G_{M,m,n}^\pm(x, y)$ vanishes for all $j + k < m + n$ and $r(0) = s(0) = 0$, we have $g_{m,n,p}^\pm = 0$ for all $0 \leq p < m + n$ by (3.43). Thus, (3.41) leads to

$$\sum_{(m,n) \in \Lambda_M^1} u_+^{(m,n)} g_{m,n,p}^+ - u_-^{(m,n)} g_{m,n,p}^- = F_p, \quad p = 0, \dots, M, \quad (3.44)$$

where $F_0 := g_{0,0}^\Gamma$ and

$$F_p := g_{0,p}^\Gamma + \sum_{(m,n) \in \Lambda_{M-2}} f_-^{(m,n)} q_{m,n,p}^- - f_+^{(m,n)} q_{m,n,p}^+, \quad p = 1, \dots, M.$$

Note that $g_{0,0}^\pm = 1$ and $g_{m,n,p}^\pm = 0$ for all $0 \leq p < m + n$. We observe that the identities in (3.44) become

$$u_-^{(0,0)} = u_+^{(0,0)} - g_{0,0}^\Gamma, \quad (3.45)$$

and

$$\begin{aligned} u_-^{(0,p)} g_{0,p,p}^- + u_-^{(1,p-1)} g_{1,p-1,p}^- &= u_+^{(0,p)} g_{0,p,p}^+ + u_+^{(1,p-1)} g_{1,p-1,p}^+ - F_p \\ &+ \sum_{(m,n) \in \Lambda_{p-1}^1} u_+^{(m,n)} g_{m,n,p}^+ - u_-^{(m,n)} g_{m,n,p}^-, \quad p = 1, \dots, M. \end{aligned} \quad (3.46)$$

By (3.10) with M being replaced by $M - 1$,

$$G_{M,m,n}^\pm(x, y) := G_{M,m,n}^{\pm,1}(x, y) + G_{M,m,n}^{\pm,2}(x, y), \quad (3.47)$$

where

$$G_{M,m,n}^{\pm,1}(x, y) := \sum_{\ell=0}^{\lfloor \frac{n}{2} \rfloor} \frac{(-1)^\ell x^{m+2\ell} y^{n-2\ell}}{(m+2\ell)!(n-2\ell)!}, \quad (3.48)$$

$$G_{M,m,n}^{\pm,2}(x, y) := \sum_{(m',n') \in \Lambda_M^2 \setminus \Lambda_{m+n}^2} A_{m',n',m,n}^u \frac{x^{m'} y^{n'}}{m'! n'!}, \quad \forall (m, n) \in \Lambda_M^1. \quad (3.49)$$

Since every coefficient of $x^j y^k$ of $G_{M,m,n}^{\pm,2}(x, y)$ vanishes for all $j + k < m + n + 1$ and $s(0) = r(0) = 0$, (3.43) leads to

$$g_{m,n,p}^\pm = \frac{1}{p!} \left. \frac{d^p (G_{M,m,n}^{\pm,1}(r(t), s(t)))}{dt^p} \right|_{t=0}, \quad (m, n) \in \{(0, p), (1, p-1)\}. \quad (3.50)$$

For the flux jump condition (3.42), (3.19) with M being replaced by $M - 1$ implies

$$\nabla(u_\pm(x + x_i^*, y + y_j^*)) = \sum_{(m,n) \in \Lambda_M^1} u_\pm^{(m,n)} \nabla(G_{M,m,n}^\pm(x, y)) + \sum_{(m,n) \in \Lambda_{M-2}} f_\pm^{(m,n)} \nabla(Q_{M,m,n}^\pm(x, y)) + \mathcal{O}(h^M), \quad (3.51)$$

for $x, y \in (-2h, 2h)$ and clearly

$$a_\pm(x + x_i^*, y + y_j^*) = \sum_{(m,n) \in \Lambda_{M-1}} \frac{a_\pm^{(m,n)}}{m! n!} x^m y^n + \mathcal{O}(h^M), \quad (3.52)$$

for $x, y \in (-2h, 2h)$. By (3.51) and (3.52),

$$a_\pm(x + x_i^*, y + y_j^*) \nabla u_\pm(r(t) + x_i^*, s(t) + y_j^*) \cdot (s'(t), -r'(t))$$

$$\begin{aligned}
&= \sum_{(m,n) \in \Lambda_M^1} u_{\pm}^{(m,n)} \tilde{G}_{M,m,n}^{\pm}(r(t), s(t)) \cdot (s'(t), -r'(t)) + \sum_{(m,n) \in \Lambda_{M-2}} f_{\pm}^{(m,n)} \tilde{Q}_{M,m,n}^{\pm}(r(t), s(t)) \cdot (s'(t), -r'(t)) \\
&= \sum_{p=0}^{M-1} \left(\sum_{(m,n) \in \Lambda_M^1} u_{\pm}^{(m,n)} \tilde{g}_{m,n,p}^{\pm} + \sum_{(m,n) \in \Lambda_{M-2}} f_{\pm}^{(m,n)} \tilde{q}_{m,n,p}^{\pm} \right) t^p + \mathcal{O}(t^M),
\end{aligned}$$

where

$$\begin{aligned}
\tilde{G}_{M,m,n}^{\pm}(x, y) &= \nabla G_{M,m,n}^{\pm}(x, y) \left(\sum_{(m,n) \in \Lambda_{M-1}} \frac{a_{\pm}^{(m,n)}}{m!n!} x^m y^n \right), \\
\tilde{Q}_{M,m,n}^{\pm}(x, y) &= \nabla Q_{M,m,n}^{\pm}(x, y) \left(\sum_{(m,n) \in \Lambda_{M-1}} \frac{a_{\pm}^{(m,n)}}{m!n!} x^m y^n \right),
\end{aligned}$$

$$\tilde{g}_{m,n,p}^{\pm} := \frac{d^p (\tilde{G}_{M,m,n}^{\pm}(r(t), s(t)) \cdot (s'(t), -r'(t)))}{p! dt^p} \Big|_{t=0}, \quad \tilde{q}_{m,n,p}^{\pm} := \frac{d^p (\tilde{Q}_{M,m,n}^{\pm}(r(t), s(t)) \cdot (s'(t), -r'(t)))}{p! dt^p} \Big|_{t=0}. \quad (3.53)$$

Note that each entry of $\tilde{G}_{M,m,n}^{\pm}$ is a homogeneous polynomial of degree $\geq m + n - 1$. By $r(0) = s(0) = 0$ and (3.53), we can say that $\tilde{g}_{m,n,p}^{\pm} = 0$ for all $0 \leq p < m + n - 1$. Similarly, by the definition of $g_{2,p}$ in (3.22), we have

$$g_1^{\Gamma}(r(t) + x_i^*, s(t) + y_j^*) \sqrt{(r'(t))^2 + (s'(t))^2} = \sum_{p=0}^{M-1} g_{1,p}^{\Gamma} t^p + \mathcal{O}(t^M), \quad h \rightarrow 0.$$

Therefore, (3.42) implies

$$\sum_{(m,n) \in \Lambda_M^1} u_+^{(m,n)} \tilde{g}_{m,n,p}^+ - u_-^{(m,n)} \tilde{g}_{m,n,p}^- = G_p, \quad p = 0, \dots, M-1, \quad (3.54)$$

where

$$G_p := g_{1,p}^{\Gamma} + \sum_{(m,n) \in \Lambda_{M-2}} f_-^{(m,n)} \tilde{q}_{m,n,p}^- - f_+^{(m,n)} \tilde{q}_{m,n,p}^+.$$

Clearly, $\tilde{g}_{0,0,0}^{\pm} = 0$ and $\tilde{g}_{m,n,p}^{\pm} = 0$ for all $0 \leq p < m + n - 1$. We observe that (3.54) become

$$\begin{aligned}
u_-^{(0,p)} \tilde{g}_{0,p,p-1}^- + u_-^{(1,p-1)} \tilde{g}_{1,p-1,p-1}^- &= u_+^{(0,p)} \tilde{g}_{0,p,p-1}^+ + u_+^{(1,p-1)} \tilde{g}_{1,p-1,p-1}^+ - G_{p-1} \\
&+ \sum_{(m,n) \in \Lambda_{p-1}^1} u_+^{(m,n)} \tilde{g}_{m,n,p-1}^+ - u_-^{(m,n)} \tilde{g}_{m,n,p-1}^-, \quad p = 1, \dots, M. \quad (3.55)
\end{aligned}$$

Since each entry of $G_{M,m,n}^{\pm,2}(x,y)$ is a homogeneous polynomial of degree $\geq m+n+1$ and $s(0) = r(0) = 0$, (3.53) (3.47), (3.48) and (3.49) leads to

$$\tilde{g}_{m,n,p-1}^{\pm} := \frac{a_{\pm}^{(0,0)}}{(p-1)!} \left. \frac{d^{p-1}(\nabla G_{M,m,n}^{\pm,1}(x,y) \cdot (s'(t), -r'(t)))}{dt^{p-1}} \right|_{t=0}, \quad (m,n) \in \{(0,p), (1,p-1)\}. \quad (3.56)$$

According to the assumption $(r'(0))^2 + (s'(0))^2 > 0$ in (1.5), $a_{\pm}^{(0,0)} \neq 0$ in (3.1) and the proof of Theorem 2.4 (3.48), (3.50) and (3.56) imply

$$g_{0,p,p}^{\pm} \tilde{g}_{1,p-1,p-1}^{\pm} - g_{1,p-1,p}^{\pm} \tilde{g}_{0,p,p-1}^{\pm} > 0, \quad \forall p = 1, \dots, M. \quad (3.57)$$

Let

$$W_p^{\pm} = \begin{bmatrix} g_{0,p,p}^{\pm} & g_{1,p-1,p}^{\pm} \\ \tilde{g}_{0,p,p-1}^{\pm} & \tilde{g}_{1,p-1,p-1}^{\pm} \end{bmatrix} \quad \text{and} \quad Q_p^{\pm} := \frac{1}{g_{0,p,p}^{\pm} \tilde{g}_{1,p-1,p-1}^{\pm} - g_{1,p-1,p}^{\pm} \tilde{g}_{0,p,p-1}^{\pm}} \begin{bmatrix} \tilde{g}_{1,p-1,p-1}^{\pm} & -g_{1,p-1,p}^{\pm} \\ -\tilde{g}_{0,p,p-1}^{\pm} & g_{0,p,p}^{\pm} \end{bmatrix}.$$

Then, by (3.57), we have $W_p^{\pm} Q_p^{\pm} = I_2$, where I_2 is a 2 by 2 identity matrix.

Therefore, the solution $\{u_{-}^{(0,p)}, u_{-}^{(1,p-1)}\}_{p=1, \dots, M}$ of the linear equations in (3.46) and (3.55) can be recursively and uniquely calculated from $p = 1$ to $p = M$ by $u_{-}^{(0,0)} = u_{+}^{(0,0)} - g_{0,0}^{\Gamma}$ due to (3.45) and

$$\begin{aligned} \begin{bmatrix} u_{-}^{(0,p)} \\ u_{-}^{(1,p-1)} \end{bmatrix} &= Q_p^{-} W_p^{+} \begin{bmatrix} u_{+}^{(0,p)} \\ u_{+}^{(1,p-1)} \end{bmatrix} - Q_p^{-} \begin{bmatrix} F_p \\ G_{p-1} \end{bmatrix} + \sum_{n=1}^{p-1} Q_p^{-} \begin{bmatrix} u_{+}^{(0,n)} g_{0,n,p}^{+} + u_{+}^{(1,n-1)} g_{1,n-1,p}^{+} \\ u_{+}^{(0,n)} \tilde{g}_{0,n,p-1}^{+} + u_{+}^{(1,n-1)} \tilde{g}_{1,n-1,p-1}^{+} \end{bmatrix} \\ &\quad - \sum_{n=1}^{p-1} Q_p^{-} \begin{bmatrix} u_{-}^{(0,n)} g_{0,n,p}^{-} + u_{-}^{(1,n-1)} g_{1,n-1,p}^{-} \\ u_{-}^{(0,n)} \tilde{g}_{0,n,p-1}^{-} + u_{-}^{(1,n-1)} \tilde{g}_{1,n-1,p-1}^{-} \end{bmatrix}, \end{aligned} \quad (3.58)$$

for $p = 1, \dots, M$. Note that for $p = 1$, the above summation $\sum_{n=1}^{p-1}$ is empty. \square

Chapter 4

Hybrid Finite Difference Schemes for Elliptic Interface Problems with Discontinuous and High-Contrast Variable Coefficients

4.1 Introduction and problem formulation

In Chapter [3](#), we developed a compact 9-point finite difference scheme for elliptic problems, that is formally fourth order accurate away from the interface of singularity of the solution (regular points), and third order accurate in the vicinity of this interface (irregular points). The numerical experiments in Chapter [3](#) demonstrate that the proposed scheme is fourth order accuracy in the l_2 norm. Using Taylor expansion and our sort of technique, the maximum accuracy for compact 9-point finite difference stencil at regular points is six, and a 13-point stencil at irregular points can achieve a fifth order of accuracy, so in the present chapter we derive a hybrid scheme that utilizes a 9-point stencil for regular points and a 13-point stencil for irregular points, for the case of elliptic problems with discontinuous scalar coefficients. In Chapter [2](#), we demonstrated that if the coefficient of the problem is continuous the stencil of a 9-point scheme in 2D can be partitioned into 72 different configurations by the interface of singularity of the solution. In the case of discontinuous coefficients, we need to use a 13-point stencil at irregular points and this results in more possibilities for the stencil partitioning (see figure [Fig. 4.1](#)). Thus, in this chapter, we also derive an efficient way to achieve the implementation of the proposed hybrid scheme. In Chapter [5](#), we discussed the 6-point and 4-point finite difference schemes with sixth order

accuracy for the side points and corner points of the Helmholtz equations respectively with a constant wave number k in a rectangle. In this chapter, we also extend the above results in Chapter 5 to the elliptic equations with variable coefficients and mixed combinations of Dirichlet $u = g_i$ in $\partial\Omega|_i$, Neumann $\frac{\partial u}{\partial \vec{n}} = g_j$ in $\partial\Omega|_j$ and Robin $\frac{\partial u}{\partial \vec{n}} + \alpha u = g_k$ in $\partial\Omega|_k$ with smooth functions α , g_i , g_j and g_k , where $\partial\Omega|_i$, $\partial\Omega|_j$, $\partial\Omega|_k$ for $i, j, k = 1, 2, 3, 4$ is one side of the rectangle (see Fig. 4.2 for an example of the mixed boundary conditions).

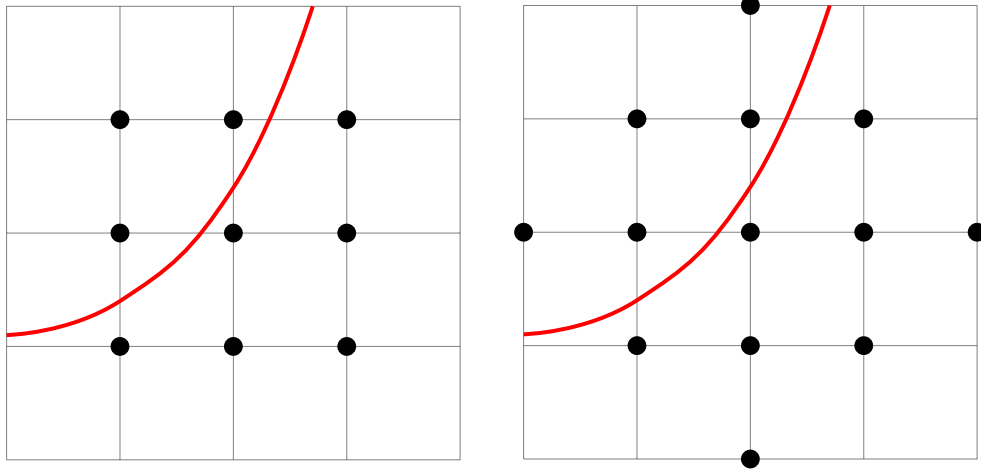


Figure 4.1: For irregular points, the 9-point scheme (left) and the 13-point scheme (right). The curve in red color is the interface curve Γ .

Let $\Omega = (l_1, l_2) \times (l_3, l_4)$ and ψ be a smooth two-dimensional function. Consider a smooth curve $\Gamma := \{(x, y) \in \Omega : \psi(x, y) = 0\}$, which partitions Ω into two subregions: $\Omega_+ := \{(x, y) \in \Omega : \psi(x, y) > 0\}$ and $\Omega_- := \{(x, y) \in \Omega : \psi(x, y) < 0\}$. We also define $a_{\pm} := a\chi_{\Omega_{\pm}}$, $f_{\pm} := f\chi_{\Omega_{\pm}}$ and $u_{\pm} := u\chi_{\Omega_{\pm}}$. The model problem in this chapter is defined as follows:

$$\begin{cases} -\nabla \cdot (a\nabla u) = f & \text{in } \Omega \setminus \Gamma, \\ [u] = g_0^{\Gamma}, \quad [a\nabla u \cdot \vec{n}] = g_1^{\Gamma} & \text{on } \Gamma, \\ \mathcal{B}_1 u = g_1 \text{ on } \partial\Omega|_1 := \{l_1\} \times (l_3, l_4), \quad \mathcal{B}_2 u = g_2 \text{ on } \partial\Omega|_2 := \{l_2\} \times (l_3, l_4), \\ \mathcal{B}_3 u = g_3 \text{ on } \partial\Omega|_3 := (l_1, l_2) \times \{l_3\}, \quad \mathcal{B}_4 u = g_4 \text{ on } \partial\Omega|_4 := (l_1, l_2) \times \{l_4\}, \end{cases} \quad (4.1)$$

where f is the source term, and for any point $(x_0, y_0) \in \Gamma$,

$$\begin{aligned} [u](x_0, y_0) &:= \lim_{(x,y) \in \Omega_+, (x,y) \rightarrow (x_0, y_0)} u(x, y) - \lim_{(x,y) \in \Omega_-, (x,y) \rightarrow (x_0, y_0)} u(x, y), \\ [a\nabla u \cdot \vec{n}](x_0, y_0) &:= \lim_{(x,y) \in \Omega_+, (x,y) \rightarrow (x_0, y_0)} a\nabla u(x, y) \cdot \vec{n} - \lim_{(x,y) \in \Omega_-, (x,y) \rightarrow (x_0, y_0)} a\nabla u(x, y) \cdot \vec{n}, \end{aligned}$$

where \vec{n} is the unit normal vector of Γ pointing towards Ω_+ . In (4.1), the boundary operators $\mathcal{B}_1, \dots, \mathcal{B}_4 \in \{\mathbf{I}_d, \frac{\partial}{\partial \vec{n}} + \alpha \mathbf{I}_d\}$, where \mathbf{I}_d represents the Dirichlet boundary condition, when $\alpha = 0$, $\frac{\partial}{\partial \vec{n}}$ represents the Neumann boundary condition, when α is a smooth 1D function, $\frac{\partial}{\partial \vec{n}} + \alpha \mathbf{I}_d$ represents the Robin boundary condition. An example for the boundary conditions of (4.1) is shown in Fig. 4.2.

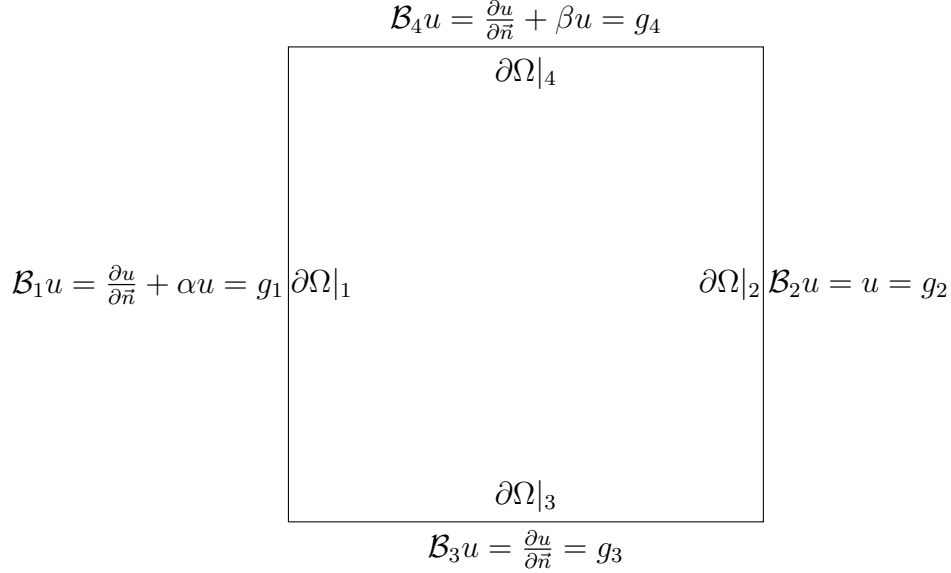


Figure 4.2: An example for the boundary configuration in (4.1), where α and β are two smooth 1D functions in y and x directions respectively.

We derive a hybrid finite difference scheme to solve (4.1) given the following assumptions (Note that the main results in this chapter have been written in [34]):

- (A1) The coefficient a is positive, piecewise smooth and has uniformly continuous partial derivatives of (total) orders up to six in each of the subregions Ω_+ and Ω_- . The coefficient a is discontinuous across the interface Γ .
- (A2) The solution u and the source term f have uniformly continuous partial derivatives of (total) orders up to seven and five respectively in each of the subregions Ω_+ and Ω_- . Both u and f can be discontinuous across the interface Γ .
- (A3) The interface curve Γ is smooth in the sense that for each $(x^*, y^*) \in \Gamma$, there exists a local parametric equation: $\gamma : (-\epsilon, \epsilon) \rightarrow \Gamma$ with $\epsilon > 0$ such that $\gamma(0) = (x^*, y^*)$ and $\|\gamma'(0)\|_2 \neq 0$. Furthermore, $x(t)$ and $y(t)$ in (1.5) should both have uniformly continuous derivatives of (total) order up to five for the variable $t = 0$.
- (A4) The 1D interface functions $g_0^\Gamma \circ \gamma$ and $g_1^\Gamma \circ \gamma$ have uniformly continuous derivatives of

(total) orders up to five and four respectively on the interface Γ , where γ is given in (A2).

(A5) Each of the 1D boundary functions g_1, \dots, g_4 in (4.1) and α in the Robin boundary conditions has uniformly continuous derivatives of (total) order up to five on the boundary Γ_j .

The organization of this chapter is as follows.

In Section 4.2.1, we derive the compact 9-point finite difference scheme with sixth order accuracy for regular points in Theorem 4.1.

In Section 4.2.2.1, we propose the 6-point schemes with sixth order accuracy for the side points of the boundary conditions $\frac{\partial u}{\partial \bar{n}} + \alpha u = g_1$ in $\partial\Omega|_1$, $\frac{\partial u}{\partial \bar{n}} = g_3$ in $\partial\Omega|_3$ and $\frac{\partial u}{\partial \bar{n}} + \beta u = g_4$ in $\partial\Omega|_4$ in Theorems 4.2 to 4.4 with two smooth functions α and β .

In Section 4.2.2.2, we construct the 4-point schemes with sixth order accuracy for the corner points of the boundary conditions $\frac{\partial u}{\partial \bar{n}} + \alpha u = g_1$ in $\partial\Omega|_1$, $\frac{\partial u}{\partial \bar{n}} = g_3$ in $\partial\Omega|_3$ and $\frac{\partial u}{\partial \bar{n}} + \beta u = g_4$ in $\partial\Omega|_4$ in Theorems 4.5 and 4.6 with two smooth functions α and β .

In Section 4.2.3, we first propose a simpler version of the transmission equation for the interface curve Γ in Theorem 4.7. Then the 13-point finite difference scheme with fifth order accuracy for irregular points is shown in Theorem 4.8. In order to achieve the implementation effectively for the 13-point scheme, we derive efficient implementation details using (4.31) to (4.40).

In Section 4.3, we present 10 numerical examples, including 5 examples with exact known solutions u , for our proposed hybrid finite difference scheme with contrast ratios $\sup(a_+)/\inf(a_-) = 10^{-3}, 10^{-6}, 10^6, 10^7$. Our numerical experiments confirm the flexibility and the sixth order accuracy in l_2 and l_∞ norms of our proposed hybrid scheme. For the coefficients $a(x, y)$, two jump functions g_0^Γ, g_1^Γ , interface curves Γ and boundary conditions, we test the following cases:

- Either a_+/a_- or a_-/a_+ is very large on the interface Γ for high contrast coefficients a .
- The jump functions g_0^Γ and g_1^Γ are both either constant or non-constant.
- The interface curve Γ is either smooth or sharp-edged.
- 4-side Dirichlet boundary conditions.
- 3-side Dirichlet and 1-side Robin boundary conditions.
- 1-side Dirichlet, 1-side Neumann and 2-side Robin boundary conditions.

In Section 4.4, we summarize the main contributions of this chapter. Finally, in Section 4.5 we present the proofs for results stated in Section 4.2.

4.2 Hybrid finite difference methods using uniform Cartesian grids

Recall $\Omega = (l_1, l_2) \times (l_3, l_4)$ and

$$x_i = l_1 + ih, \quad i = 0, \dots, N_1, \quad \text{and} \quad y_j = l_3 + jh, \quad j = 0, \dots, N_2. \quad (4.2)$$

$$x_i^* = x_i - v_0 h \quad \text{and} \quad y_j^* = y_j - w_0 h \quad \text{with} \quad -1 < v_0, w_0 < 1. \quad (4.3)$$

Throughout the chapter, we shall use the following notations:

$$\begin{aligned} \alpha^{(n)} &:= \frac{d^n \alpha}{dy^n}(y_j^*), & g_1^{(n)} &:= \frac{d^n g_1}{dy^n}(y_j^*), \\ \beta^{(m)} &:= \frac{d^m \beta}{dx^m}(x_i^*), & g_3^{(m)} &:= \frac{d^m g_3}{dx^m}(x_i^*), & g_4^{(m)} &:= \frac{d^m g_4}{dx^m}(x_i^*), \\ a^{(m,n)} &:= \frac{\partial^{m+n} a}{\partial^m x \partial^n y}(x_i^*, y_j^*), & u^{(m,n)} &:= \frac{\partial^{m+n} u}{\partial^m x \partial^n y}(x_i^*, y_j^*), & f^{(m,n)} &:= \frac{\partial^{m+n} f}{\partial^m x \partial^n y}(x_i^*, y_j^*), \end{aligned} \quad (4.4)$$

which are their (m, n) th partial derivatives at the base point (x_i^*, y_j^*) . Recall that

$$\Lambda_{M+1} := \{(m, n - m) : n = 0, \dots, M + 1 \text{ and } m = 0, \dots, n\}, \quad M + 1 \in \mathbb{N}_0, \quad (4.5)$$

$$\Lambda_{M+1}^{V,2} := \Lambda_{M+1} \setminus \Lambda_{M+1}^{V,1} \quad \text{with} \quad \Lambda_{M+1}^{V,1} := \{(\ell, k - \ell) : k = \ell, \dots, M + 1 - \ell \text{ and } \ell = 0, 1\}, \quad (4.6)$$

$$\Lambda_{M+1}^{H,j} := \{(n, m) : (m, n) \in \Lambda_{M+1}^{V,j}, j = 1, 2\}. \quad (4.7)$$

For all $(m, n) \in \Lambda_{M+1}^{V,1}$, we define

$$G_{M+1,m,n}^V(x, y) := \sum_{\ell=0}^{\lfloor \frac{n}{2} \rfloor} \frac{(-1)^\ell x^{m+2\ell} y^{n-2\ell}}{(m+2\ell)!(n-2\ell)!} + \sum_{(m',n') \in \Lambda_{M+1}^{V,2} \setminus \Lambda_{m+n}^{V,2}} A_{m',n',m,n}^{V,u} \frac{x^{m'} y^{n'}}{m'!n'!}, \quad (4.8)$$

and for all $(m, n) \in \Lambda_{M-1}$,

$$Q_{M+1,m,n}^V(x, y) := \sum_{\ell=1}^{1+\lfloor \frac{n}{2} \rfloor} \frac{(-1)^\ell x^{m+2\ell} y^{n-2\ell+2}}{(m+2\ell)!(n-2\ell+2)!} \frac{1}{a^{(0,0)}} + \sum_{(m',n') \in \Lambda_{M+1}^{V,2} \setminus \Lambda_{m+n+2}^{V,2}} A_{m',n',m,n}^{V,f} \frac{x^{m'} y^{n'}}{m'!n'!}, \quad (4.9)$$

where $A_{m',n',m,n}^{V,u}$ and $A_{m',n',m,n}^{V,f}$ are constants which are uniquely determined by $\{a^{(m,n)} : (m, n) \in \Lambda_M\}$, and the floor function $\lfloor x \rfloor$ is defined to be the largest integer less than or

equal to $x \in \mathbb{R}$.

For all $(m, n) \in \Lambda_{M+1}^{H,1}$, we define

$$G_{M+1,m,n}^H(x, y) := \sum_{\ell=0}^{\lfloor \frac{m}{2} \rfloor} \frac{(-1)^\ell y^{n+2\ell} x^{m-2\ell}}{(n+2\ell)!(m-2\ell)!} + \sum_{(m',n') \in \Lambda_{M+1}^{H,2} \setminus \Lambda_{m+n}^{H,2}} A_{m',n',m,n}^{H,u} \frac{x^{m'} y^{n'}}{m'!n'!}, \quad (4.10)$$

and for all $(m, n) \in \Lambda_{M-1}$,

$$Q_{M+1,m,n}^H(x, y) := \sum_{\ell=1}^{1+\lfloor \frac{m}{2} \rfloor} \frac{(-1)^\ell y^{n+2\ell} x^{m-2\ell+2}}{(n+2\ell)!(m-2\ell+2)!} \frac{1}{a^{(0,0)}} + \sum_{(m',n') \in \Lambda_{M+1}^{H,2} \setminus \Lambda_{m+n+2}^{H,2}} A_{m',n',m,n}^{H,f} \frac{x^{m'} y^{n'}}{m'!n'!}, \quad (4.11)$$

where $A_{m',n',m,n}^{H,u}$ and $A_{m',n',m,n}^{H,f}$ are constants which are uniquely determined by $\{a^{(m,n)} : (m, n) \in \Lambda_M\}$, and the floor function $\lfloor x \rfloor$ is defined to be the largest integer less than or equal to $x \in \mathbb{R}$.

Similar to (3.12) and (5.10), we have

$$u(x+x_i^*, y+y_j^*) = \sum_{(m,n) \in \Lambda_{M+1}^{V,1}} u^{(m,n)} G_{M+1,m,n}^V(x, y) + \sum_{(m,n) \in \Lambda_{M-1}} f^{(m,n)} Q_{M+1,m,n}^V(x, y) + \mathcal{O}(h^{M+2}), \quad (4.12)$$

for $x, y \in (-2h, 2h)$, where u is the exact solution for (4.1), the index sets Λ_{M-1} and $\Lambda_{M+1}^{V,1}$ are defined in (4.5) and (4.6) respectively, and the functions $G_{M+1,m,n}^V$ and $Q_{M+1,m,n}^V$ are defined in (4.8) and (4.9) respectively. Similar to (3.12) and (5.11), we also have

$$u(x+x_i^*, y+y_j^*) = \sum_{(m,n) \in \Lambda_{M+1}^{H,1}} u^{(m,n)} G_{M+1,m,n}^H(x, y) + \sum_{(m,n) \in \Lambda_{M-1}} f^{(m,n)} Q_{M+1,m,n}^H(x, y) + \mathcal{O}(h^{M+2}),$$

where the index sets Λ_{M-1} and $\Lambda_{M+1}^{H,1}$ are defined in (4.5) and (4.7) respectively, and the functions $G_{M+1,m,n}^H$ and $Q_{M+1,m,n}^H$ are defined in (4.10) and (4.11) respectively.

For the sake of better readability, all technical proofs of this section are provided in Section 4.5. For simplicity, we cancel the (h) in $I_{m,n}(h)$, $J_{m,n}(h)$, $C_{k,\ell}(h)$ and other related notations.

4.2.1 Stencils for regular points (interior)

We now extend the fourth order compact 9-point scheme in Theorem 3.2 to a sixth order compact 9-point scheme. We only need to choose $M = 6$ and replace $G_{m,n}$, $Q_{m,n}$ and Λ_{M+1}^1

in Chapter 3 by $G_{M+1,m,n}^V$ in (4.8), $Q_{M+1,m,n}^V$ in (4.9), and $\Lambda_{M+1}^{V,1}$ in (4.6). We choose (x_i^*, y_j^*) to be the center point of the 9-point compact scheme, i.e., $(x_i^*, y_j^*) = (x_i, y_j)$ and $v_0 = w_0 = 0$ in (4.3).

Theorem 4.1. *Let a grid point (x_i, y_j) be a regular point, i.e., either $d_{i,j}^+ = \emptyset$ or $d_{i,j}^- = \emptyset$ and $(x_i, y_j) \notin \partial\Omega$. Let $(u_h)_{i,j}$ denote the numerical approximation of the exact solution u of the elliptic interface problem (4.1) at an interior regular point (x_i, y_j) . Then the following difference scheme on a stencil centered at (x_i, y_j) :*

$$\begin{aligned} \mathcal{L}_h u_h := & \frac{1}{h^2} \begin{pmatrix} C_{-1,-1}(u_h)_{i-1,j-1} & +C_{0,-1}(u_h)_{i,j-1} & +C_{1,-1}(u_h)_{i+1,j-1} \\ +C_{-1,0}(u_h)_{i-1,j} & +C_{0,0}(u_h)_{i,j} & +C_{1,0}(u_h)_{i+1,j} \\ +C_{-1,1}(u_h)_{i-1,j+1} & +C_{0,1}(u_h)_{i,j+1} & +C_{1,1}(u_h)_{i+1,j+1} \end{pmatrix} = \sum_{(m,n) \in \Lambda_5} f^{(m,n)} J_{m,n}, \end{aligned}$$

achieves sixth order of accuracy for $-\nabla \cdot (a\nabla u) = f$ at the point (x_i, y_j) , where

$$J_{m,n} := \sum_{k=-1}^1 \sum_{\ell=-1}^1 C_{k,\ell} h^{-2} Q_{7,m,n}^V(kh, \ell h), \quad \text{for all } (m,n) \in \Lambda_5,$$

$$C_{k,\ell}(h) := \sum_{p=0}^{M+1} c_{k,\ell,p} h^p, \quad k, \ell \in \{-1, 0, 1\},$$

and $\{c_{k,\ell,p}\}$ is any non-trivial solution to the linear system induced by (3.15) with $M = 6$.

The maximum accuracy order of a compact 9-point finite difference scheme using Taylor expansion and our sort of technique for $-\nabla \cdot (a\nabla u) = f$ at the point (x_i, y_j) is six. To verify Theorem 4.1 with the numerical experiments in Section 4.3, we use the unique solution $\{c_{k,\ell,p}\}$ to (3.15) with $M = 6$ and the normalization condition $c_{-1,-1,0} = 1$, setting to zero all $c_{-1,0,7}, c_{0,-1,7}, c_{0,0,6}, c_{0,0,7}, c_{-1,1,p_1}, c_{0,1,p_2}, c_{1,-1,p_2}, c_{1,0,p_3}, c_{1,1,p_4}$ for $p_1 = 1, 6, 7$, $p_2 = 5, 6, 7$, $p_3 = 4, 5, 6, 7$ and $p_4 = 2, 3, 4, 5, 6, 7$.

4.2.2 Stencils for boundary and corner points

In this subsection, we extend Section 5.2.2 and discuss how to find compact (6-point, 4-point) finite difference schemes with accuracy order six centered at $(x_i, y_j) \in \partial\Omega$. For clarity of presentation, we consider the following boundary conditions

$$\begin{aligned} \mathcal{B}_1 u &= \frac{\partial u}{\partial \bar{n}} + \alpha u = g_1 \quad \text{on } \partial\Omega|_1, & \mathcal{B}_2 u &= u = g_2 \quad \text{on } \partial\Omega|_2, \\ \mathcal{B}_3 u &= \frac{\partial u}{\partial \bar{n}} = g_3 \quad \text{on } \partial\Omega|_3, & \mathcal{B}_4 u &= \frac{\partial u}{\partial \bar{n}} + \beta u = g_4 \quad \text{on } \partial\Omega|_4, \end{aligned} \tag{4.13}$$

where α and β are two smooth 1D functions in y and x directions. For the 6-point and 4-point schemes in this subsection, we choose $(x_i^*, y_j^*) = (x_i, y_j)$ and $v_0 = w_0 = 0$ in (4.3). An illustration of (4.13) is shown in Fig. 4.2. For the following identities in (4.15) and (4.19), we define

$$\delta_{a,a} := 1 \quad \text{and} \quad \delta_{a,b} := 0 \quad \text{for } a \neq b.$$

4.2.2.1 Side points on the boundary $\partial\Omega$

Theorem 4.2. *Let $(u_h)_{i,j}$ denote the numerical approximation of the exact solution u of the elliptic interface problem (4.1) at the point (x_i, y_j) . The following discretization on a stencil centered at $(x_0, y_j) \in \partial\Omega|_1$:*

$$\begin{aligned} \mathcal{L}_h^{\mathcal{B}_1} u_h := & \frac{1}{h} \left(C_{0,-1}^{\mathcal{B}_1}(u_h)_{0,j-1} + C_{1,-1}^{\mathcal{B}_1}(u_h)_{1,j-1} \right. \\ & + C_{0,0}^{\mathcal{B}_1}(u_h)_{0,j} + C_{1,0}^{\mathcal{B}_1}(u_h)_{1,j} \\ & \left. + C_{0,1}^{\mathcal{B}_1}(u_h)_{0,j+1} + C_{1,1}^{\mathcal{B}_1}(u_h)_{1,j+1} \right) = \sum_{(m,n) \in \Lambda_4} f^{(m,n)} h J_{m,n}^{\mathcal{B}_1} + \sum_{n=0}^5 g_1^{(n)} h^{-1} J_{g_1,n}^{\mathcal{B}_1}, \end{aligned} \quad (4.14)$$

achieves sixth order of accuracy for $\mathcal{B}_1 u = \frac{\partial u}{\partial \bar{n}} + \alpha u = g_1$ at the point $(x_0, y_j) \in \partial\Omega|_1$, where

$$J_{m,n}^{\mathcal{B}_1} := \sum_{k=0}^1 \sum_{\ell=-1}^1 C_{k,\ell}^{\mathcal{B}_1} h^{-2} Q_{6,m,n}^V(kh, \ell h), \quad \text{for all } (m,n) \in \Lambda_4,$$

$$J_{g_1,n}^{\mathcal{B}_1} := - \sum_{k=0}^1 \sum_{\ell=-1}^1 C_{k,\ell}^{\mathcal{B}_1} G_{6,1,n}^V(kh, \ell h), \quad \text{for all } n = 0, \dots, 5,$$

$$C_{k,\ell}^{\mathcal{B}_1}(h) := \sum_{p=0}^6 c_{k,\ell,p}^{\mathcal{B}_1} h^p, \quad k \in \{0, 1\}, \ell \in \{-1, 0, 1\},$$

and $\{c_{k,\ell,p}^{\mathcal{B}_1}\}$ is any non-trivial solution to the linear system induced by

$$\begin{aligned} & \sum_{k=0}^1 \sum_{\ell=-1}^1 C_{k,\ell}^{\mathcal{B}_1} \left(G_{6,0,n}^V(kh, \ell h) + \sum_{i=n}^5 \binom{i}{n} \alpha^{(i-n)} G_{6,1,i}^V(kh, \ell h) (1 - \delta_{n,6}) \right) \\ & = \mathcal{O}(h^7), \quad \text{for all } n = 0, 1, \dots, 6. \end{aligned} \quad (4.15)$$

The maximum accuracy order of a 6-point finite difference scheme using Taylor expansion and our sort of technique for $\mathcal{B}_1 u = \frac{\partial u}{\partial \bar{n}} + \alpha u = g_1$ at the point $(x_0, y_j) \in \partial\Omega|_1$ with two smooth functions $\alpha(y)$ and $a(x, y)$ is six. In our numerical experiments in Section 4.3, we use the unique solution $\{c_{k,\ell,p}^{\mathcal{B}_1}\}$ to (4.15) with the normalization condition $c_{1,1,0}^{\mathcal{B}_1} = 1$, where all $c_{0,0,6}^{\mathcal{B}_1}, c_{0,1,5}^{\mathcal{B}_1}, c_{0,1,6}^{\mathcal{B}_1}, c_{1,-1,p_1}^{\mathcal{B}_1}, c_{1,0,p_2}^{\mathcal{B}_1}, c_{1,1,p_3}^{\mathcal{B}_1}$ for $p_1 = 1, 4, 5, 6, p_2 = 3, 4, 5, 6,$ and $p_3 = 2, 3, 4, 5, 6,$

are set to zero. In particular, if a in (4.1) is a discontinuous constant coefficient and $\mathcal{B}_1 u = \frac{\partial u}{\partial \bar{n}} + \alpha u = g_1$ with a constant α , then the coefficients in (4.14) are

$$\begin{aligned} C_{0,1}^{\mathcal{B}_1} &= \frac{1}{75}\alpha^2 h^2 + \frac{1}{5}\alpha h + 2, & C_{0,0}^{\mathcal{B}_1} &= \frac{8}{675}\alpha^5 h^5 - \frac{16}{675}\alpha^4 h^4 + \frac{16}{225}\alpha^3 h^3 - \frac{8}{25}\alpha^2 h^2 - \frac{34}{5}\alpha h - 10, \\ C_{1,1}^{\mathcal{B}_1} &= 1, & C_{1,0}^{\mathcal{B}_1} &= -\frac{8}{675}\alpha^4 h^4 + \frac{8}{225}\alpha^3 h^3 - \frac{8}{75}\alpha^2 h^2 + \frac{2}{5}\alpha h + 4, & C_{0,-1}^{\mathcal{B}_1} &= C_{0,1}^{\mathcal{B}_1}, & C_{1,-1}^{\mathcal{B}_1} &= C_{1,1}^{\mathcal{B}_1}. \end{aligned}$$

Similarly, we could obtain the following Theorems 4.3 and 4.4.

Theorem 4.3. *Let $(u_h)_{i,j}$ be the numerical approximation of the exact solution u of the elliptic interface problem (4.1) at the point (x_i, y_j) . Then the following discretization stencil centered at $(x_i, y_0) \in \partial\Omega|_3$:*

$$\begin{aligned} \mathcal{L}_h^{\mathcal{B}_3} u_h &:= \frac{1}{h} \left(\begin{array}{ccc} C_{-1,0}^{\mathcal{B}_3}(u_h)_{i-1,0} & + C_{0,0}^{\mathcal{B}_3}(u_h)_{i,0} & + C_{1,0}^{\mathcal{B}_3}(u_h)_{i+1,0} \\ + C_{-1,1}^{\mathcal{B}_3}(u_h)_{i-1,1} & + C_{0,1}^{\mathcal{B}_3}(u_h)_{i,1} & + C_{1,1}^{\mathcal{B}_3}(u_h)_{i+1,1} \end{array} \right) = \sum_{(m,n) \in \Lambda_4} f^{(m,n)} h J_{m,n}^{\mathcal{B}_3} + \sum_{n=0}^5 g_3^{(n)} h^{-1} J_{g_3,n}^{\mathcal{B}_3}, \end{aligned} \quad (4.16)$$

achieves sixth order of accuracy for $\mathcal{B}_3 u = \frac{\partial u}{\partial \bar{n}} = g_3$ at the point $(x_i, y_0) \in \partial\Omega|_3$, where

$$J_{m,n}^{\mathcal{B}_3} := \sum_{k=-1}^1 \sum_{\ell=0}^1 C_{k,\ell}^{\mathcal{B}_3} h^{-2} Q_{6,m,n}^H(kh, \ell h), \quad \text{for all } (m,n) \in \Lambda_4,$$

$$J_{g_3,n}^{\mathcal{B}_3} := - \sum_{k=-1}^1 \sum_{\ell=0}^1 C_{k,\ell}^{\mathcal{B}_3} G_{6,n,1}^H(kh, \ell h), \quad \text{for all } n = 0, \dots, 5,$$

$$C_{k,\ell}^{\mathcal{B}_3}(h) := \sum_{p=0}^6 c_{k,\ell,p}^{\mathcal{B}_3} h^p, \quad k \in \{-1, 0, 1\}, \ell \in \{0, 1\},$$

and $\{c_{k,\ell,p}^{\mathcal{B}_3}\}$ is any non-trivial solution to the linear system induced by

$$\sum_{k=-1}^1 \sum_{\ell=0}^1 C_{k,\ell}^{\mathcal{B}_3} G_{6,n,0}^H(kh, \ell h) = \mathcal{O}(h^7), \quad \text{for all } n = 0, 1, \dots, 6, \quad (4.17)$$

The maximum accuracy order of a 6-point finite difference scheme using Taylor expansion and our sort of technique for $\mathcal{B}_3 u = \frac{\partial u}{\partial \bar{n}} = g_3$ at the point $(x_i, y_0) \in \partial\Omega|_3$ with a smooth function $a(x, y)$ is six. For our numerical experiments in Section 4.3, we use the unique solution $\{c_{k,\ell,p}^{\mathcal{B}_3}\}$ to (4.17) with the normalization condition $c_{1,1,0}^{\mathcal{B}_3} = 1$, presetting to zero all $c_{0,0,6}^{\mathcal{B}_3}, c_{-1,1,p_1}^{\mathcal{B}_3}, c_{0,1,p_2}^{\mathcal{B}_3}, c_{1,0,p_3}^{\mathcal{B}_3}, c_{1,1,p_4}^{\mathcal{B}_3}$ for $p_1 = 1, 5, 6$, $p_2 = 4, 5, 6$, $p_3 = 3, 4, 5, 6$, and $p_4 = 2, 3, 4, 5, 6$. In particular, if a is a discontinuous constant coefficient in (4.1), then the

coefficients in (4.16) are

$$C_{1,0}^{\mathcal{B}_3} = 2, \quad C_{1,1}^{\mathcal{B}_3} = 1, \quad C_{0,0}^{\mathcal{B}_3} = -10, \quad C_{0,1}^{\mathcal{B}_3} = 4, \quad C_{-1,0}^{\mathcal{B}_3} = C_{1,0}^{\mathcal{B}_3}, \quad C_{-1,1}^{\mathcal{B}_3} = C_{1,1}^{\mathcal{B}_3}.$$

Theorem 4.4. *Let $(u_h)_{i,j}$ be the numerical approximation of the exact solution u of the elliptic interface problem (4.1) at the point (x_i, y_j) . Then the following discretization stencil centered at $(x_i, y_{N_2}) \in \partial\Omega|_4$:*

$$\begin{aligned} \mathcal{L}_h^{\mathcal{B}_4} u_h &:= \frac{1}{h} \left(C_{-1,-1}^{\mathcal{B}_4} (u_h)_{i-1,-1} + C_{0,-1}^{\mathcal{B}_4} (u_h)_{i,-1} + C_{1,-1}^{\mathcal{B}_4} (u_h)_{i+1,-1} \right. \\ &\quad \left. + C_{-1,0}^{\mathcal{B}_4} (u_h)_{i-1,0} + C_{0,0}^{\mathcal{B}_4} (u_h)_{i,0} + C_{1,0}^{\mathcal{B}_4} (u_h)_{i+1,0} \right) \\ &= \sum_{(m,n) \in \Lambda_4} f^{(m,n)} h J_{m,n}^{\mathcal{B}_4} + \sum_{n=0}^5 g_4^{(n)} h^{-1} J_{g_4,n}^{\mathcal{B}_4}, \end{aligned} \quad (4.18)$$

achieves sixth order of accuracy for $\mathcal{B}_4 u = \frac{\partial u}{\partial \bar{n}} + \beta u = g_4$ at the point $(x_i, y_{N_2}) \in \partial\Omega|_4$, where

$$J_{m,n}^{\mathcal{B}_4} := \sum_{k=-1}^1 \sum_{\ell=-1}^0 C_{k,\ell}^{\mathcal{B}_4} h^{-2} Q_{6,m,n}^H(kh, \ell h), \quad \text{for all } (m,n) \in \Lambda_4,$$

$$J_{g_4,n}^{\mathcal{B}_4} := \sum_{k=-1}^1 \sum_{\ell=-1}^0 C_{k,\ell}^{\mathcal{B}_4} G_{6,n,1}^H(kh, \ell h), \quad \text{for all } n = 0, \dots, 5,$$

$$C_{k,\ell}^{\mathcal{B}_4}(h) := \sum_{p=0}^6 c_{k,\ell,p}^{\mathcal{B}_4} h^p, \quad k \in \{-1, 0, 1\}, \ell \in \{-1, 0\},$$

and $\{c_{k,\ell,p}^{\mathcal{B}_4}\}$ is any non-trivial solution to the linear system induced by

$$\begin{aligned} &\sum_{k=-1}^1 \sum_{\ell=-1}^0 C_{k,\ell}^{\mathcal{B}_4} \left(G_{6,n,0}^H(kh, \ell h) - \sum_{i=n}^5 \binom{i}{n} \beta^{(i-n)} G_{6,i,1}^H(kh, \ell h) (1 - \delta_{n,6}) \right) \\ &= \mathcal{O}(h^7), \quad \text{for all } n = 0, 1, \dots, 6. \end{aligned} \quad (4.19)$$

The maximum accuracy order of a 6-point finite difference scheme using Taylor expansion and our sort of technique for $\mathcal{B}_4 u = \frac{\partial u}{\partial \bar{n}} + \beta u = g_4$ at the point $(x_i, y_{N_2}) \in \partial\Omega|_4$ with two smooth functions $\beta(x)$ and $a(x, y)$ is six. For our numerical experiments in Section 4.3, we use the unique solution $\{c_{k,\ell,p}^{\mathcal{B}_4}\}$ to (4.19) with the normalization condition $c_{1,-1,0}^{\mathcal{B}_4} = 1$, presetting to zero all $c_{0,-1,6}^{\mathcal{B}_4}, c_{-1,0,5}^{\mathcal{B}_4}, c_{-1,0,6}^{\mathcal{B}_4}, c_{0,0,p_1}^{\mathcal{B}_4}, c_{1,-1,p_2}^{\mathcal{B}_4}, c_{1,0,p_3}^{\mathcal{B}_4}$ with $p_1 = 4, 5, 6, p_2 = 2, 3, 4, 5, 6, p_3 = 1, 3, 4, 5, 6$. In particular, if a is a discontinuous piecewise constant coefficient and $\mathcal{B}_4 u =$

$\frac{\partial u}{\partial \bar{n}} + \beta u = g_4$ with a constant β , then the coefficients in (4.18) are

$$\begin{aligned} C_{1,-1}^{\mathcal{B}_4} &= 1, & C_{0,-1}^{\mathcal{B}_4} &= -\frac{8}{675}\beta^4 h^4 + \frac{8}{225}\beta^3 h^3 - \frac{8}{75}\beta^2 h^2 + \frac{2}{5}\beta h + 4, \\ C_{1,0}^{\mathcal{B}_4} &= \frac{1}{75}\beta^2 h^2 + \frac{1}{5}\beta h + 2, \\ C_{0,0}^{\mathcal{B}_4} &= \frac{8}{675}\beta^5 h^5 - \frac{16}{675}\beta^4 h^4 + \frac{16}{225}\beta^3 h^3 - \frac{8}{25}\beta^2 h^2 - \frac{34}{5}\beta h - 10, \\ C_{-1,-1}^{\mathcal{B}_4} &= C_{1,-1}^{\mathcal{B}_4}, & C_{-1,0}^{\mathcal{B}_4} &= C_{1,0}^{\mathcal{B}_4}. \end{aligned}$$

4.2.2.2 Stencils for corner points

Theorem 4.5. *Let $(u_h)_{i,j}$ be the numerical approximation of the exact solution u of the elliptic interface problem (4.1) at the point (x_i, y_j) . Then the following discretization on a stencil centered at the corner point (x_0, y_0) :*

$$\begin{aligned} \mathcal{L}_h^{\mathcal{R}_1} u_h &:= \frac{1}{h} \left(C_{0,0}^{\mathcal{R}_1}(u_h)_{0,0} + C_{1,0}^{\mathcal{R}_1}(u_h)_{1,0} \right. \\ &\quad \left. + C_{0,1}^{\mathcal{R}_1}(u_h)_{0,1} + C_{1,1}^{\mathcal{R}_1}(u_h)_{1,1} \right) \\ &= \sum_{(m,n) \in \Lambda_4} f^{(m,n)} h J_{m,n}^{\mathcal{R}_1} + \sum_{n=0}^5 g_1^{(n)} h^{-1} J_{g_1,n}^{\mathcal{R}_1} + \sum_{n=0}^5 g_3^{(n)} h^{-1} J_{g_3,n}^{\mathcal{R}_1}, \end{aligned} \quad (4.20)$$

achieves sixth order of accuracy for $\mathcal{B}_1 u = \frac{\partial u}{\partial \bar{n}} + \alpha u = g_1$ and $\mathcal{B}_3 u = \frac{\partial u}{\partial \bar{n}} = g_3$ at the point (x_0, y_0) , where $\{C_{k,\ell}^{\mathcal{R}_1}\}_{k,\ell \in \{0,1\}}$, $\{J_{m,n}^{\mathcal{R}_1}\}_{(m,n) \in \Lambda_4}$, $\{J_{g_1,n}^{\mathcal{R}_1}\}_{n=0}^5$ and $\{J_{g_3,n}^{\mathcal{R}_1}\}_{n=0}^5$ can be calculated by replacing $\mathcal{B}_1 u = \frac{\partial u}{\partial \bar{n}} - iku = g_1$ by $\mathcal{B}_1 u = \frac{\partial u}{\partial \bar{n}} + \alpha u = g_1$ in Theorem 5.4 with $M = M_f = M_{g_1} = M_{g_3} = 6$, and replacing $G_{M,m,n}^V$, $Q_{M,m,n}^V$, $G_{M,m,n}^H$ and $Q_{M,m,n}^H$ in Chapter 5 by (4.8), (4.9), (4.10) and (4.11), respectively.

The maximum accuracy order of a 4-point finite difference scheme using Taylor expansion and our sort of technique for $\mathcal{B}_1 u = \frac{\partial u}{\partial \bar{n}} + \alpha u = g_1$ and $\mathcal{B}_3 u = \frac{\partial u}{\partial \bar{n}} = g_3$ at the point (x_0, y_0) with two smooth functions $\alpha(y)$ and $a(x, y)$ is six. In particular, if a in (4.1) is a discontinuous piecewise constant coefficient, and $\mathcal{B}_1 u = \frac{\partial u}{\partial \bar{n}} + \alpha u = g_1$ with a constant α , then the coefficients in (4.20) are

$$\begin{aligned} C_{0,0}^{\mathcal{R}_1} &= \frac{4}{675}\alpha^5 h^5 - \frac{8}{675}\alpha^4 h^4 + \frac{8}{225}\alpha^3 h^3 - \frac{4}{25}\alpha^2 h^2 - \frac{17}{5}\alpha h - 5, \\ C_{0,1}^{\mathcal{R}_1} &= \frac{1}{75}\alpha^2 h^2 + \frac{1}{5}\alpha h + 2, \\ C_{1,0}^{\mathcal{R}_1} &= -\frac{4}{675}\alpha^4 h^4 + \frac{4}{225}\alpha^3 h^3 - \frac{4}{75}\alpha^2 h^2 + \frac{1}{5}\alpha h + 2, & C_{1,1}^{\mathcal{R}_1} &= 1. \end{aligned}$$

Theorem 4.6. Let $(u_h)_{i,j}$ be the numerical approximation of the exact solution u of the elliptic interface problem (4.1) at the point (x_i, y_j) . Then the following discretization on a stencil centered at the corner point (x_0, y_{N_2}) :

$$\begin{aligned} \mathcal{L}_h^{\mathcal{R}_2} u_h &:= \frac{1}{h} \left(C_{0,-1}^{\mathcal{R}_2}(u_h)_{0,N_2-1} + C_{1,-1}^{\mathcal{R}_2}(u_h)_{1,N_2-1} \right. \\ &\quad \left. + C_{0,0}^{\mathcal{R}_2}(u_h)_{0,N_2} + C_{1,0}^{\mathcal{R}_2}(u_h)_{1,N_2} \right) \\ &= \sum_{(m,n) \in \Lambda_4} f^{(m,n)} h J_{m,n}^{\mathcal{R}_2} + \sum_{n=0}^5 g_1^{(n)} h^{-1} J_{g_1,n}^{\mathcal{R}_2} + \sum_{n=0}^5 g_4^{(n)} h^{-1} J_{g_4,n}^{\mathcal{R}_2}, \end{aligned} \quad (4.21)$$

achieves sixth order of accuracy for $\mathcal{B}_1 u = \frac{\partial u}{\partial \bar{n}} + \alpha u = g_1$ and $\mathcal{B}_4 u = \frac{\partial u}{\partial \bar{n}} + \beta u = g_4$ at the point (x_0, y_{N_2}) , where $\{C_{k,\ell}^{\mathcal{R}_2}\}_{k \in \{0,1\}, \ell \in \{-1,0\}}$, $\{J_{m,n}^{\mathcal{R}_2}\}_{(m,n) \in \Lambda_4}$, $\{J_{g_1,n}^{\mathcal{R}_2}\}_{n=0}^5$ and $\{J_{g_4,n}^{\mathcal{R}_2}\}_{n=0}^5$ can be calculated by replacing $\mathcal{B}_1 u = \frac{\partial u}{\partial \bar{n}} - iku = g_1$ and $\mathcal{B}_4 u = \frac{\partial u}{\partial \bar{n}} - iku = g_4$ by $\mathcal{B}_1 u = \frac{\partial u}{\partial \bar{n}} + \alpha u = g_1$ and $\mathcal{B}_4 u = \frac{\partial u}{\partial \bar{n}} + \beta u = g_4$ respectively in Theorem 5.5 with $M = M_f = M_{g_1} = M_{g_4} = 6$ and replacing $G_{M,m,n}^V$, $Q_{M,m,n}^V$, $G_{M,m,n}^H$ and $Q_{M,m,n}^H$ in Chapter 5 by (4.8), (4.9), (4.10) and (4.11), respectively.

The maximum accuracy order of a 4-point finite difference scheme using Taylor expansion and our sort of technique for $\mathcal{B}_1 u = \frac{\partial u}{\partial \bar{n}} + \alpha u = g_1$ and $\mathcal{B}_4 u = \frac{\partial u}{\partial \bar{n}} + \beta u = g_4$ at the point (x_0, y_{N_2}) with three smooth functions $\alpha(y)$, $\beta(x)$ and $a(x, y)$ is six, where $\alpha(y_{N_2}) \neq \beta(x_0)$. Again, if a in (4.1) is a discontinuous constant coefficient, $\mathcal{B}_1 u = \frac{\partial u}{\partial \bar{n}} + \alpha u = g_1$ and $\mathcal{B}_4 u = \frac{\partial u}{\partial \bar{n}} + \beta u = g_4$ with α and β being constant, then the coefficients on the left hand side in (4.21) are

$$\begin{aligned} C_{0,-1}^{\mathcal{R}_2} &= \frac{1}{675} (4\alpha^5 - 6\alpha^4\beta + 6\alpha^3\beta^2 - 4\alpha^2\beta^3) h^5 + \frac{1}{675} (4\alpha^4 - 6\alpha^3\beta + 6\alpha^2\beta^2 - 4\alpha\beta^3) h^4 \\ &\quad + \frac{1}{675} (9\alpha^2 + 63\alpha\beta - 36\beta^2) h^2 + \frac{1}{675} (135\beta + 135\alpha) h + 2, \\ C_{0,0}^{\mathcal{R}_2} &= \frac{1}{225} (-4\alpha^4 + 6\alpha^3\beta - 6\alpha^2\beta^2 + 4\alpha\beta^3) h^4 + \frac{1}{225} (8\alpha^3 - 18\alpha^2\beta - 30\alpha\beta^2 + 16\beta^3) h^3 \\ &\quad + \frac{1}{225} (-36\alpha^2 - 357\alpha\beta - 36\beta^2) h^2 + \frac{1}{225} (-765\alpha - 765\beta) h - 5, \\ C_{1,-1}^{\mathcal{R}_2} &= \frac{1}{675} (-4\alpha^4 + 6\alpha^3\beta - 6\alpha^2\beta^2 + 4\alpha\beta^3) h^4 + 1, \\ C_{1,0}^{\mathcal{R}_2} &= \frac{1}{225} (4\alpha^3 - 6\alpha^2\beta + 6\alpha\beta^2 - 4\beta^3) h^3 + \frac{1}{225} (-12\alpha^2 + 21\alpha\beta + 3\beta^2) h^2 \\ &\quad + \frac{1}{225} (45\beta + 45\alpha) h + 2. \end{aligned} \quad (4.22)$$

When $\alpha = \beta$, we further have $C_{0,-1}^{\mathcal{R}_2} = C_{1,0}^{\mathcal{R}_2} = \frac{4}{75} \beta^2 h^2 + \frac{2}{5} \beta h + 2$ and $C_{1,-1}^{\mathcal{R}_2} = 1$ in (4.22).

4.2.3 Stencils for irregular points

Let (x_i, y_j) be an irregular point (i.e., both $d_{i,j}^+$ and $d_{i,j}^-$ are nonempty, see Fig. 4.1 for an example) and choose the base point $(x_i^*, y_j^*) \in \Gamma \cap (x_i - h, x_i + h) \times (y_j - h, y_j + h)$. By (4.3), we have

$$x_i^* = x_i - v_0 h \quad \text{and} \quad y_j^* = y_j - w_0 h \quad \text{with} \quad -1 < v_0, w_0 < 1 \quad \text{and} \quad (x_i^*, y_j^*) \in \Gamma. \quad (4.23)$$

Let a_{\pm} , u_{\pm} and f_{\pm} represent the coefficient function a , the solution u and source term f in Ω^{\pm} . Similar to (4.4), we define that

$$a_{\pm}^{(m,n)} := \frac{\partial^{m+n} a_{\pm}}{\partial^m x \partial^n y}(x_i^*, y_j^*), \quad u_{\pm}^{(m,n)} := \frac{\partial^{m+n} u_{\pm}}{\partial^m x \partial^n y}(x_i^*, y_j^*), \quad f_{\pm}^{(m,n)} := \frac{\partial^{m+n} f_{\pm}}{\partial^m x \partial^n y}(x_i^*, y_j^*).$$

Similar to (4.12), we have

$$u_{\pm}(x + x_i^*, y + y_j^*) = \sum_{(m,n) \in \Lambda_{M+1}^{V,1}} u_{\pm}^{(m,n)} G_{M+1,m,n}^{\pm,V}(x, y) + \sum_{(m,n) \in \Lambda_{M-1}} f_{\pm}^{(m,n)} Q_{M+1,m,n}^{\pm,V}(x, y) + \mathcal{O}(h^{M+2}),$$

for $x, y \in (-2h, 2h)$, where Λ_{M-1} and $\Lambda_{M+1}^{V,1}$ are defined in (4.5) and (4.6) respectively, $G_{M+1,m,n}^{\pm,V}(x, y)$ and $Q_{M+1,m,n}^{\pm,V}(x, y)$ are obtained by replacing $\{a^{(m,n)} : (m, n) \in \Lambda_M\}$ by $\{a_{\pm}^{(m,n)} : (m, n) \in \Lambda_M\}$ in (4.8) and (4.9). Similarly to the definition of the 9-point compact stencil in (1.2) and (1.3), we define the following 4-point set for the 13-point scheme:

$$\begin{aligned} e_{i,j}^+ &:= \{(k, \ell) : (k, \ell) \in \{(-2, 0), (0, -2), (0, 2), (2, 0)\}, \psi(x_i + kh, y_j + \ell h) > 0\}, \quad \text{and} \\ e_{i,j}^- &:= \{(k, \ell) : (k, \ell) \in \{(-2, 0), (0, -2), (0, 2), (2, 0)\}, \psi(x_i + kh, y_j + \ell h) \leq 0\}. \end{aligned} \quad (4.24)$$

In the next theorem we present a simplified version of Theorem 3.3, adapted to the aim of developing of a fifth order hybrid 13-point scheme for irregular points.

Theorem 4.7. *Let u be the solution to the elliptic interface problem in (4.1) and let Γ be parameterized near (x_i^*, y_j^*) by (1.5). Then*

$$\begin{aligned} u_-^{(m',n')} &= \sum_{\substack{(m,n) \in \Lambda_M^{V,1} \\ m+n \leq m'+n'}} T_{m',n',m,n}^{u_+} u_+^{(m,n)} + \sum_{(m,n) \in \Lambda_{M-2}} \left(T_{m',n',m,n}^+ f_+^{(m,n)} + T_{m',n',m,n}^- f_-^{(m,n)} \right) \\ &+ \sum_{p=0}^M T_{m',n',p}^{g_0^\Gamma} g_{0,p}^\Gamma + \sum_{p=0}^{M-1} T_{m',n',p}^{g_1^\Gamma} g_{1,p}^\Gamma, \quad \forall (m', n') \in \Lambda_M^{V,1}, \end{aligned} \quad (4.25)$$

where

$$g_{0,p}^\Gamma := \frac{1}{p!} \frac{d^p}{dt^p} [g_0^\Gamma(r(t) + x_i^*, s(t) + y_j^*)] \Big|_{t=0}, \quad p = 0, 1, \dots, M,$$

$$g_{1,p}^\Gamma := \frac{1}{p!} \frac{d^p}{dt^p} \left[g_1^\Gamma(r(t) + x_i^*, s(t) + y_j^*) \sqrt{(r'(t))^2 + (s'(t))^2} \right] \Big|_{t=0}, \quad p = 0, 1, \dots, M-1,$$

and all the transmission coefficients $T^{u+}, T^\pm, T^{g_0^\Gamma}, T^{g_1^\Gamma}$ are uniquely determined by $r^{(k)}(0), s^{(k)}(0)$ for $k = 0, \dots, M$ and $\{a_\pm^{(m,n)} : (m,n) \in \Lambda_{M-1}\}$. Moreover, let $T_{m',n',m,n}^{u+}$ be the transmission coefficient of $u_+^{(m,n)}$ in (4.25) with $(m,n) \in \Lambda_M^{V,1}$, $m+n = m'+n'$ and $(m',n') \in \Lambda_M^{V,1}$. Then $T_{m',n',m,n}^{u+}$ only depends on $r^{(k)}(0), s^{(k)}(0)$ for $k = 0, \dots, M$ of (1.5) and $a_\pm^{(0,0)}$. Particularly,

$$T_{0,0,0,0}^{u+} = 1 \quad \text{and} \quad T_{m',n',0,0}^{u+} = 0 \quad \text{if} \quad (m',n') \neq (0,0). \quad (4.26)$$

Next, we provide the 13-point finite difference scheme for interior irregular points.

Theorem 4.8. Let $(u_h)_{i,j}$ be the numerical approximation to the solution of (4.1) at an interior irregular point (x_i, y_j) . Pick a base point (x_i^*, y_j^*) as in (4.23). Then the following 13-point scheme centered at the interior irregular point (x_i, y_j) :

$$\begin{aligned} & +C_{0,-2}(u_h)_{i,j-2} \\ & +C_{-1,-1}(u_h)_{i-1,j-1} \quad +C_{0,-1}(u_h)_{i,j-1} \quad +C_{1,-1}(u_h)_{i+1,j-1} \\ \mathcal{L}_h^\Gamma u_h := & \frac{1}{h} \left(C_{-2,0}(u_h)_{i-2,j} \quad +C_{-1,0}(u_h)_{i-1,j} \quad +C_{0,0}(u_h)_{i,j} \quad +C_{1,0}(u_h)_{i+1,j} \quad +C_{2,0}(u_h)_{i+2,j} \right) \\ & +C_{-1,1}(u_h)_{i-1,j+1} \quad +C_{0,1}(u_h)_{i,j+1} \quad +C_{1,1}(u_h)_{i+1,j+1} \\ & +C_{0,2}(u_h)_{i,j+2} \end{aligned} \quad (4.27)$$

$$= \sum_{(m,n) \in \Lambda_3} f_+^{(m,n)} h J_{m,n}^+ + \sum_{(m,n) \in \Lambda_3} f_-^{(m,n)} h J_{m,n}^- + \sum_{p=0}^5 g_{0,p}^\Gamma h^{-1} J_p^{g_0^\Gamma} + \sum_{p=0}^4 g_{1,p}^\Gamma h^{-1} J_p^{g_1^\Gamma},$$

achieves fifth order accuracy, where all $\{C_{k,\ell}\}$ in (4.27) are calculated by (4.28)-(4.39) with $M = 5$, $J_{m,n}^\pm := J_{m,n}^{\pm,0} + J_{m,n}^{\pm,T}$ for all $(m,n) \in \Lambda_3$,

$$J_{m,n}^{\pm,0} := \sum_{(k,\ell) \in d_{i,j}^\pm \cup e_{i,j}^\pm} C_{k,\ell} h^{-2} Q_{5,m,n}^{\pm,V}((v_0+k)h, (w_0+\ell)h), \quad \forall (m,n) \in \Lambda_3,$$

$$J_{m,n}^{\pm,T} := \sum_{(m',n') \in \Lambda_5^{V,1}} I_{m',n'}^\pm h^{-2} T_{m',n',m,n}^\pm, \quad \forall (m,n) \in \Lambda_3,$$

$$I_{m,n}^- := \sum_{(k,\ell) \in d_{i,j}^- \cup e_{i,j}^-} C_{k,\ell} G_{5,m,n}^{-,V}((v_0+k)h, (w_0+\ell)h), \quad \forall (m,n) \in \Lambda_5^{V,1},$$

$$J_p^{g_0^\Gamma} := \sum_{(m',n') \in \Lambda_5^{V,1}} I_{m',n'}^- T_{m',n',p}^{g_0^\Gamma}, \quad \forall p = 0, \dots, 5, \quad J_p^{g_1^\Gamma} := \sum_{(m',n') \in \Lambda_5^{V,1}} I_{m',n'}^- T_{m',n',p}^{g_1^\Gamma}, \quad \forall p = 0, \dots, 4.$$

The maximum accuracy order of a 13-point finite difference scheme using Taylor expansion

sion and our sort of technique for (4.1) at an interior irregular point (x_i, y_j) is five. For the 13-point scheme in Theorem 4.8, if only one point in the set $\{(x_i - h, y_j - h), (x_i - h, y_j + h), (x_i + h, y_j - h), (x_i + h, y_j + h)\}$ belongs to Ω_- and the other 12 points all belong to Ω_+ , we can set $C_{k,\ell} = 0$ for $(x_i + kh, y_j + \ell h) \in \Omega_-$, $x_i^* = x_i$, $y_i^* = y_i$ to achieve sixth order accuracy in (x_i, y_j) .

Finally, we provide a way of achieving an efficient implementation for the 13-point scheme in irregular points in Theorem 4.8.

Efficient implementation details:

By Theorem 4.7, a simpler $J_{m,n}^{u+,T}$ in (3.25) can be written as:

$$J_{m,n}^{u+,T} := \sum_{\substack{(m',n') \in \Lambda_M^{V,1} \\ m'+n' \geq m+n}} I_{m',n'}^- T_{m',n',m,n}^{u+}. \quad (4.28)$$

Replacing Λ_M^1 by $\Lambda_M^{V,1}$ for (3.27) and (3.28), we have

$$I_{m,n}^+ + J_{m,n}^{u+,T} = \mathcal{O}(h^{M+1}), \quad h \rightarrow 0, \quad \text{for all } (m,n) \in \Lambda_M^{V,1}. \quad (4.29)$$

Replacing $G_{m,n}^\pm$, $Q_{m,n}^\pm$ and $d_{i,j}^\pm$ by $G_{M,m,n}^{\pm,V}$, $Q_{M,m,n}^{\pm,V}$ and $d_{i,j}^\pm \cup e_{i,j}^\pm$ for (3.24), we obtain

$$\sum_{(k,\ell) \in d_{i,j}^+ \cup e_{i,j}^+} C_{k,\ell} G_{M,m,n}^{+,V}(v_0 h + kh, w_0 h + \ell h) + \sum_{\substack{(m',n') \in \Lambda_M^{V,1} \\ m'+n' \geq m+n}} I_{m',n'}^- T_{m',n',m,n}^{u+} = \mathcal{O}(h^{M+1}),$$

and

$$\begin{aligned} & \sum_{(k,\ell) \in d_{i,j}^+ \cup e_{i,j}^+} C_{k,\ell} G_{M,m,n}^{+,V}(v_0 h + kh, w_0 h + \ell h) \\ & + \sum_{\substack{(m',n') \in \Lambda_M^{V,1} \\ m'+n' \geq m+n}} \sum_{(k,\ell) \in d_{i,j}^- \cup e_{i,j}^-} C_{k,\ell} G_{M,m',n'}^{-,V}(v_0 h + kh, w_0 h + \ell h) T_{m',n',m,n}^{u+} = \mathcal{O}(h^{M+1}). \end{aligned}$$

So, (4.29) is equivalent to

$$\begin{aligned} & \sum_{(k,\ell) \in d_{i,j}^- \cup e_{i,j}^-} C_{k,\ell} \sum_{\substack{(m',n') \in \Lambda_M^{V,1} \\ m'+n' \geq m+n}} G_{M,m',n'}^{-,V}(v_0 h + kh, w_0 h + \ell h) T_{m',n',m,n}^{u+} \\ & + \sum_{(k,\ell) \in d_{i,j}^+ \cup e_{i,j}^+} C_{k,\ell} G_{M,m,n}^{+,V}(v_0 h + kh, w_0 h + \ell h) = \mathcal{O}(h^{M+1}), \quad \text{for all } (m,n) \in \Lambda_M^{V,1}. \end{aligned} \quad (4.30)$$

Let

$$C_{k,\ell} := \sum_{i=0}^M c_{k,\ell,i} h^i, \quad X_{k,\ell} := (c_{k,\ell,0}, c_{k,\ell,1}, \dots, c_{k,\ell,M})^T. \quad (4.31)$$

Since $G_{M,m,n}^{\pm,V}((k+v_0)h, (\ell+w_0)h)$ is the polynomial of h and the degree of h of every term in $G_{M,m,n}^{\pm,V}((k+v_0)h, (\ell+w_0)h)$ is non-negative, we deduce that

$$C_{k,\ell} G_{M,m,n}^{+,V}((k+v_0)h, (\ell+w_0)h) = DA_{k,\ell}^{+,m,n} X_{k,\ell} + \mathcal{O}(h^{M+1}), \quad (4.32)$$

$$C_{k,\ell} \sum_{\substack{(m',n') \in \Lambda_M^{V,1} \\ m'+n' \geq m+n}} G_{M,m',n'}^{-,V}((k+v_0)h, (\ell+w_0)h) T_{m',n',m,n}^{u+} = DA_{k,\ell}^{-,m,n} X_{k,\ell} + \mathcal{O}(h^{M+1}), \quad (4.33)$$

where

$$D = (h^0, h^1, \dots, h^M),$$

and $A_{k,\ell}^{\pm,m,n}$ is independent for h for all $(m, n) \in \Lambda_M^{V,1}$. So (4.30) is equivalent to

$$\sum_{(k,\ell) \in d_{i,j}^+ \cup e_{i,j}^+} DA_{k,\ell}^{+,m,n} X_{k,\ell} + \sum_{(k,\ell) \in d_{i,j}^- \cup e_{i,j}^-} DA_{k,\ell}^{-,m,n} X_{k,\ell} = \mathcal{O}(h^{M+1}), \quad \text{for all } (m, n) \in \Lambda_M^{V,1}. \quad (4.34)$$

Define

$$A_{k,\ell}^{m,n} := \begin{cases} A_{k,\ell}^{+,m,n}, & \text{if } (k, \ell) \in d_{i,j}^+ \cup e_{i,j}^+, \\ A_{k,\ell}^{-,m,n}, & \text{if } (k, \ell) \in d_{i,j}^- \cup e_{i,j}^-. \end{cases} \quad (4.35)$$

Then (4.34) is equivalent to

$$A^{m,n} X = 0, \quad \text{for all } (m, n) \in \Lambda_M^{V,1},$$

where

$$A^{m,n} = (A_{-1,-1}^{m,n}, A_{-1,0}^{m,n}, A_{-1,1}^{m,n}, A_{0,-1}^{m,n}, A_{0,0}^{m,n}, A_{0,1}^{m,n}, A_{1,-1}^{m,n}, A_{1,0}^{m,n}, A_{1,1}^{m,n}, A_{-2,0}^{m,n}, A_{2,0}^{m,n}, A_{0,-2}^{m,n}, A_{0,2}^{m,n}), \quad (4.36)$$

and

$$X = (X_{-1,-1}^T, X_{-1,0}^T, X_{-1,1}^T, X_{0,-1}^T, X_{0,0}^T, X_{0,1}^T, X_{1,-1}^T, X_{1,0}^T, X_{1,1}^T, X_{-2,0}^T, X_{2,0}^T, X_{0,-2}^T, X_{0,2}^T)^T. \quad (4.37)$$

Let

$$A = ((A^{0,0})^T, (A^{0,1})^T, \dots, (A^{0,M})^T, (A^{1,0})^T, (A^{1,1})^T, \dots, (A^{1,M-1})^T)^T. \quad (4.38)$$

Finally, (4.30) is equivalent to

$$AX = 0. \quad (4.39)$$

Since we use 13-point scheme for the irregular points, we have 13 components in (4.36) and (4.37). If we use 9-point compact scheme for the irregular points, we only need to delete the last four components in (4.36) and (4.37). For the 25-point or 36-point schemes for the irregular points, the only change is to add more $A_{k,\ell}^{m,n}$ and $X_{k,\ell}$ in (4.36) and (4.37). Even there are many different cases for the 13-point schemes for the irregular points depending on how the interface curve Γ partitions the 13 points in it, we can repeatedly use $A_{k,\ell}^{\pm,m,n}$ in (4.32), (4.33) and (4.35) to cover all the cases which significantly reduce the computation cost and make the implementation very effective and flexible. Furthermore, if we want to obtain the lower or higher finite schemes for irregular points, we only need to delete or add some $A^{0,n}$ and $A^{1,n-1}$ in (4.38).

After the above simplification, we find that the A in (4.39) is a 36 by 78 matrix for the 13-point scheme with fifth order accuracy while A is a 16 by 36 matrix and the 9-point scheme with third order accuracy. Observing the following identity (whose proof is given in Section 4.5)

$$c_{0,-2,i} + c_{-2,0,i} + c_{2,0,i} + c_{0,2,i} + \sum_{k=-1}^1 \sum_{\ell=-1}^1 c_{k,\ell,i} = 0, \quad \text{for } i = 0, 1, \dots, M, \quad (4.40)$$

we can further reduce the size of the matrix A in (4.39) to 30 by 72 for the 13-point scheme.

4.3 Numerical experiments

4.3.1 Numerical examples with known u

In this subsection, we provide five numerical examples with a known solution u of (4.1). Using Taylor expansion and our sort of technique, the maximum accuracy order for the compact 9-point finite difference scheme in irregular and regular points, for elliptic interface problems with discontinuous coefficients, is three and six, respectively. So, in Examples 4.1 and 4.2 we compare the proposed hybrid scheme with the compact 9-point scheme of a sixth order of accuracy at regular points and third order of accuracy at irregular points. That is, both uses the same compact 9-point stencils with accuracy order six at all regular points, and they only differ at irregular points such that the proposed hybrid scheme uses 13-point stencils having fifth order accuracy, while the compact 9-point scheme uses 9-point stencils having third order accuracy. Their computational costs are comparable, because the

percentage of the number of irregular points over all the grid points decays exponentially to 0 at the rate $\mathcal{O}(2^{-J})$, e.g., this percentage is less than or around 1% at the level $J = 9$ for all our numerical examples.

The five numerical examples can be characterized as follows:

- Examples [4.1](#) and [4.2](#) compare the proposed hybrid scheme and the 9-point compact scheme.
- In all examples, either a_+/a_- or a_-/a_+ is very large on Γ for high contrast coefficients a .
- 4-side Dirichlet boundary conditions are demonstrated in Examples [4.1](#), [4.2](#) and [4.5](#).
- 1-side Dirichlet, 1-side Neumann and 2-side Robin boundary conditions are considered in Examples [4.3](#) and [4.4](#).
- Results for smooth interface curves Γ are presented in Examples [4.1](#) and [4.3](#) to [4.5](#).
- Results for a sharp-edged interface curve Γ are demonstrated in Example [4.2](#).
- Results for two constant jump functions g_0^Γ and g_1^Γ are shown in Examples [4.1](#) and [4.3](#) to [4.5](#).
- Results for two non-constant jump functions g_0^Γ and g_1^Γ are presented in Example [4.2](#).

Example 4.1. Let $\Omega = (-1.5, 1.5)^2$ and the interface curve be given by $\Gamma := \{(x, y) \in \Omega : \psi(x, y) = 0\}$ with $\psi(x, y) = y^2 + \frac{2x^2}{x^2+1} - 1$. The functions in [\(4.1\)](#) are given by

$$\begin{aligned}
 a_+ &= 10^3(2 + \sin(x)\sin(y)), & a_- &= 10^{-3}(2 + \sin(x)\sin(y)), & g_0^\Gamma &= -200, & g_1^\Gamma &= 0, \\
 u_+ &= 10^{-3} \sin(4x) \sin(4y)(y^2(x^2 + 1) + x^2 - 1), \\
 u_- &= 10^3 \sin(4x) \sin(4y)(y^2(x^2 + 1) + x^2 - 1) + 200, \\
 u(-1.5, y) &= g_1, & u(1.5, y) &= g_2, & \text{for } y &\in (-1.5, 1.5), \\
 u(x, -1.5) &= g_3, & u(x, 1.5) &= g_4, & \text{for } x &\in (-1.5, 1.5),
 \end{aligned}$$

the other functions f^\pm, g_1, \dots, g_4 in [\(4.1\)](#) can be obtained by plugging the above functions into [\(4.1\)](#). Note the high contrast $a_+/a_- = 10^6$ on Γ . The numerical results are presented in Table [4.1](#) and Fig. [4.3](#).

Table 4.1: Performance in Example 4.1 of our proposed hybrid finite difference scheme and compact 9-point scheme on uniform Cartesian meshes with $h = 2^{-J} \times 3$. κ is the condition number of the coefficient matrix.

J	Our proposed hybrid scheme					Compact 9-point scheme				
	$\frac{\ u_h - u\ _2}{\ u\ _2}$	order	$\ u_h - u\ _\infty$	order	κ	$\frac{\ u_h - u\ _2}{\ u\ _2}$	order	$\ u_h - u\ _\infty$	order	κ
4	1.493E-01	0	1.362E+02	0	2.136E+02	5.465E-01	0	4.515E+02	0	8.685E+01
5	3.124E-03	5.6	3.872E+00	5.1	4.262E+02	4.751E-02	3.5	4.453E+01	3.3	4.896E+02
6	6.081E-05	5.7	7.168E-02	5.8	6.261E+03	2.464E-03	4.3	2.890E+00	3.9	2.069E+03
7	1.238E-06	5.6	1.490E-03	5.6	1.701E+04	2.745E-04	3.2	3.318E-01	3.1	9.171E+03
8	1.803E-08	6.1	3.305E-05	5.5	1.169E+05	1.557E-05	4.1	1.894E-02	4.1	4.054E+04
9						9.053E-07	4.1	1.185E-03	4.0	1.648E+05

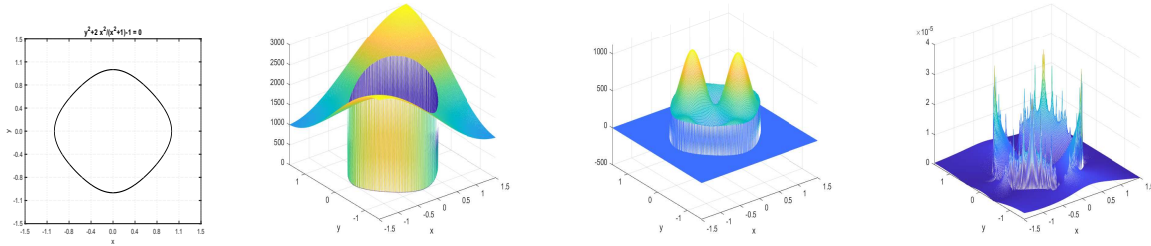


Figure 4.3: Example 4.1: the interface curve Γ (first panel), the coefficient $a(x, y)$ (second panel), the numerical solution u_h (third panel), and the error $|u_h - u|$ (fourth panel) with $h = 2^{-8} \times 3$, where u_h is computed by our proposed hybrid finite difference scheme.

Example 4.2. Let $\Omega = (-4.5, 4.5)^2$ and the interface curve be given by $\Gamma := \{(x, y) \in \Omega : \psi(x, y) = 0\}$ which is shown in Fig. 4.4. Precisely, the sharp-edged interface is a square with 4 corner points $(-2, 0)$, $(0, 2)$, $(2, 0)$ and $(0, -2)$. The functions in (4.1) are given by

$$\begin{aligned}
 a_+ &= 10^{-3}, & a_- &= 10^3, & u_+ &= 10^3 \sin(x - y), & u_- &= 10^{-3} \cos(x) \cos(y) + 1000, \\
 u(-4.5, y) &= g_1, & u(4.5, y) &= g_2, & \text{for } y &\in (-4.5, 4.5), \\
 u(x, -4.5) &= g_3, & u(x, 4.5) &= g_4, & \text{for } x &\in (-4.5, 4.5),
 \end{aligned}$$

the other functions f^\pm , g_0^Γ , g_1^Γ , g_1, \dots, g_4 in (4.1) can be obtained by plugging the above functions into (4.1). Clearly, g_0^Γ and g_1^Γ are not constants. Note the high contrast $a_-/a_+ = 10^6$ on Γ . The numerical results are presented in Table 4.2 and Fig. 4.4.

Example 4.3. Let $\Omega = (-2.5, 2.5)^2$ and the interface curve be given by $\Gamma := \{(x, y) \in \Omega : \psi(x, y) = 0\}$ with $\psi(x, y) = x^4 + 2y^4 - 2$. The functions in (4.1) are given by

$$\begin{aligned}
 a_+ &= 10^{-3}(2 + \sin(x) \sin(y)), & a_- &= 10^3(2 + \sin(x) \sin(y)), & g_0^\Gamma &= -10^5, & g_1^\Gamma &= 0, \\
 u_+ &= 10^3 \sin(4\pi x) \sin(4\pi y)(x^4 + 2y^4 - 2),
 \end{aligned}$$

Table 4.2: Performance in Example 4.2 of our proposed hybrid finite difference scheme and compact 9-point scheme on uniform Cartesian meshes with $h = 2^{-J} \times 9$. κ is the condition number of the coefficient matrix.

J	Our proposed hybrid scheme					Compact 9-point scheme				
	$\frac{\ u_h - u\ _2}{\ u\ _2}$	order	$\ u_h - u\ _\infty$	order	κ	$\frac{\ u_h - u\ _2}{\ u\ _2}$	order	$\ u_h - u\ _\infty$	order	κ
4	7.431E-03	0	2.062E+01	0	1.337E+03	6.254E-02	0	1.574E+02	0	1.238E+03
5	4.505E-04	4.0	1.322E+00	4.0	1.020E+04	1.110E-02	2.5	2.837E+01	2.5	6.529E+03
6	5.701E-06	6.3	1.778E-02	6.2	6.394E+04	6.953E-04	4.0	1.929E+00	3.9	4.152E+04
7	4.937E-08	6.9	1.869E-04	6.6	3.920E+05	2.993E-05	4.5	1.059E-01	4.2	3.286E+05
8	6.087E-10	6.3	2.942E-06	6.0	2.132E+07	1.155E-06	4.7	4.177E-03	4.7	1.474E+06
9						8.390E-08	3.8	3.391E-04	3.6	1.006E+07

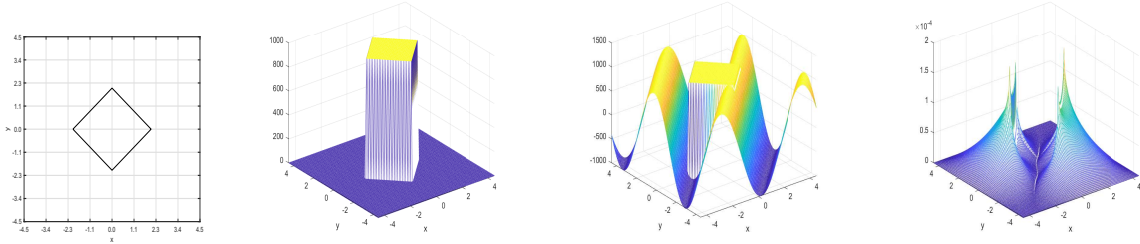


Figure 4.4: Example 4.2: the interface curve Γ (first panel), the coefficient $a(x, y)$ (second panel), the numerical solution u_h (third panel), and the error $|u_h - u|$ (fourth panel) with $h = 2^{-7} \times 9$, where u_h is computed by our proposed hybrid finite difference scheme.

$$\begin{aligned}
 u_- &= 10^{-3} \sin(4\pi x) \sin(4\pi y)(x^4 + 2y^4 - 2) + 10^5, \\
 -u_x(-2.5, y) + \alpha u(-2.5, y) &= g_1, \quad u(2.5, y) = g_2, \quad \alpha = \sin(y), \quad \text{for } y \in (-2.5, 2.5), \\
 -u_y(x, -2.5) = g_3, \quad u_y(x, 2.5) + \beta u(x, 2.5) &= g_4, \quad \beta = \cos(x), \quad \text{for } x \in (-2.5, 2.5),
 \end{aligned}$$

the other functions f^\pm, g_1, \dots, g_4 in (4.1) can be obtained by plugging the above functions into (4.1). Note the high contrast $a_-/a_+ = 10^6$ on Γ . The numerical results are presented in Table 4.3 and Fig. 4.5.

Table 4.3: Performance in Example 4.3 of our proposed hybrid finite difference scheme on uniform Cartesian meshes with $h = 2^{-J} \times 5$.

J	$\frac{\ u_h - u\ _2}{\ u\ _2}$	order	$\ u_h - u\ _\infty$	order	$\ u_h - u_{h/2}\ _2$	order	$\ u_h - u_{h/2}\ _\infty$	order
5	8.167E-01	0	1.758E+05	0	1.811E+05	0	1.734E+05	0
6	1.123E-02	6.2	2.488E+03	6.1	2.471E+03	6.2	2.441E+03	6.2
7	2.059E-04	5.8	4.711E+01	5.7	4.550E+01	5.8	4.640E+01	5.7
8	3.035E-06	6.1	7.028E-01	6.1	6.701E-01	6.1	6.919E-01	6.1
9	4.632E-08	6.0	1.087E-02	6.0	9.946E-03	6.1	1.037E-02	6.1

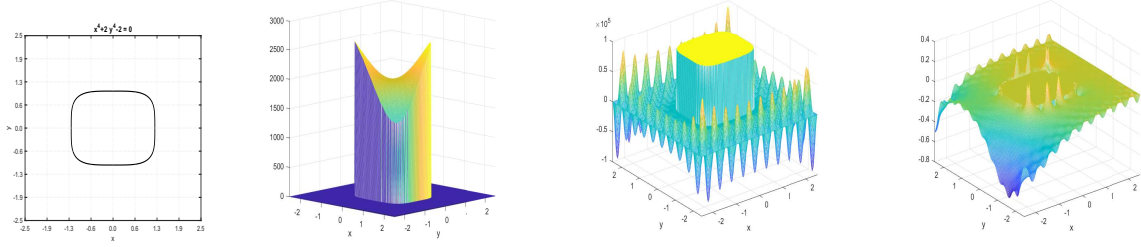


Figure 4.5: Example 4.3: the interface curve Γ (first panel), the coefficient $a(x, y)$ (second panel), the numerical solution u_h (third panel), and the error $u - u_h$ (fourth panel) with $h = 2^{-8} \times 5$, where u_h is computed by our proposed hybrid finite difference scheme.

Example 4.4. Let $\Omega = (-2, 2)^2$ and the interface curve be given by $\Gamma := \{(x, y) \in \Omega : \psi(x, y) = 0\}$ with $\psi(x, y) = x^2 + y^2 - 2$. The functions in (4.1) are given by

$$\begin{aligned}
a_+ &= 10^3(2 + \sin(x + y)), & a_- &= 10^{-3}(2 + \sin(x + y)), & g_0^\Gamma &= -10^3, & g_1^\Gamma &= 0, \\
u_+ &= 10^{-3} \cos(4(x - y))(x^2 + y^2 - 2), & u_- &= 10^3 \cos(4(x - y))(x^2 + y^2 - 2) + 10^3, \\
-u_x(-2, y) + \alpha u(-2, y) &= g_1, & u(2, y) &= g_2, & \alpha &= \sin(y), & \text{for } y &\in (-2, 2), \\
-u_y(x, -2) &= g_3, & u_y(x, 2) + \beta u(x, 2) &= g_4, & \beta &= \cos(x), & \text{for } x &\in (-2, 2),
\end{aligned}$$

the other functions f^\pm, g_1, \dots, g_4 in (4.1) can be obtained by plugging the above functions into (4.1). Note the high contrast $a_+/a_- = 10^6$ on Γ . The numerical results are presented in Table 4.4 and Fig. 4.6.

Table 4.4: Performance in Example 4.4 of our proposed hybrid finite difference scheme on uniform Cartesian meshes with $h = 2^{-J} \times 4$.

J	$\frac{\ u_h - u\ _2}{\ u\ _2}$	order	$\ u_h - u\ _\infty$	order	$\ u_h - u_{h/2}\ _2$	order	$\ u_h - u_{h/2}\ _\infty$	order
4	8.087E-01	0	4.191E+03	0	2.568E+03	0	4.141E+03	0
5	1.443E-02	5.8	1.061E+02	5.3	4.623E+01	5.8	1.048E+02	5.3
6	2.679E-04	5.8	2.154E+00	5.6	8.629E-01	5.7	2.132E+00	5.6
7	3.432E-06	6.3	3.518E-02	5.9	1.100E-02	6.3	3.477E-02	5.9
8	6.625E-08	5.7	6.192E-04	5.8	2.120E-04	5.7	6.118E-04	5.8

Example 4.5. Let $\Omega = (-2.5, 2.5)^2$ and the interface curve be given by $\Gamma := \{(x, y) \in \Omega : \psi(x, y) = 0\}$ with $\psi(x, y) = y^2 - 2x^2 + x^4 - \frac{1}{4}$. The functions in (4.1) are given by

$$\begin{aligned}
a_+ &= 10^{-3}(2 + \sin(x - y)), & a_- &= 10^3(2 + \sin(x - y)), & g_0^\Gamma &= -1.5 \times 10^4, & g_1^\Gamma &= 0, \\
u_+ &= 10^3 \sin(16(x + y))(y^2 - 2x^2 + x^4 - 1/4), \\
u_- &= 10^{-3} \sin(16(x + y))(y^2 - 2x^2 + x^4 - 1/4) + 1.5 \times 10^4,
\end{aligned}$$

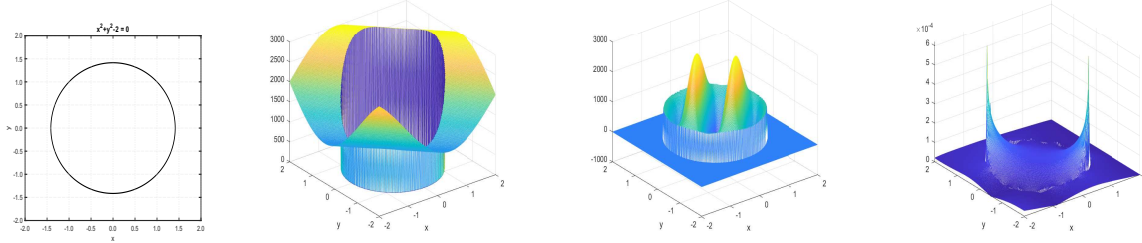


Figure 4.6: Example 4.4: the interface curve Γ (first panel), the coefficient $a(x, y)$ (second panel), the numerical solution u_h (third panel), and the error $|u_h - u|$ (fourth panel) with $h = 2^{-8} \times 4$, where u_h is computed by our proposed hybrid finite difference scheme.

$$\begin{aligned}
 u(-2.5, y) &= g_1, & u(2.5, y) &= g_2, & \text{for } y &\in (-2.5, 2.5), \\
 u(x, -2.5) &= g_3, & u(x, 2.5) &= g_4, & \text{for } x &\in (-2.5, 2.5),
 \end{aligned}$$

the other functions f^\pm, g_1, \dots, g_4 in (4.1) can be obtained by plugging the above functions into (4.1). Note the high contrast $a_-/a_+ = 10^6$ on Γ . The numerical results are presented in Table 4.5 and Fig. 4.7.

Table 4.5: Performance in Example 4.5 of our proposed hybrid finite difference scheme on uniform Cartesian meshes with $h = 2^{-J} \times 5$.

J	$\frac{\ u_h - u\ _2}{\ u\ _2}$	order	$\ u_h - u\ _\infty$	order	$\ u_h - u_{h/2}\ _2$	order	$\ u_h - u_{h/2}\ _\infty$	order
5	8.627E-01	0	9.480E+04	0	4.284E+04	0	9.338E+04	0
6	2.854E-02	4.9	2.758E+03	5.1	1.360E+03	5.0	2.736E+03	5.1
7	4.543E-04	6.0	5.673E+01	5.6	2.128E+01	6.0	5.658E+01	5.6
8	6.195E-06	6.2	1.184E+00	5.6	2.856E-01	6.2	1.177E+00	5.6
9	8.902E-08	6.1	1.738E-02	6.1	4.441E-03	6.0	1.788E-02	6.0

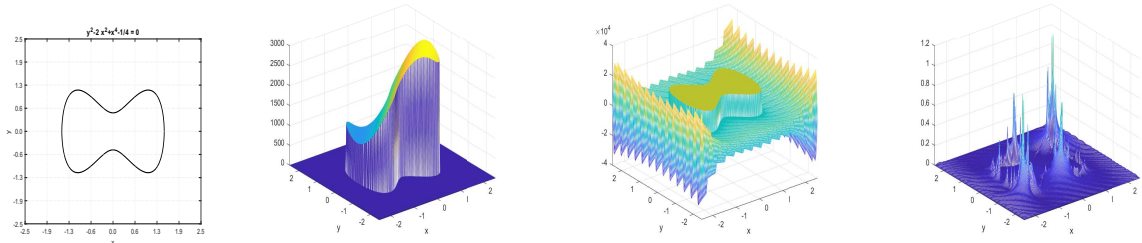


Figure 4.7: Example 4.5: the interface curve Γ (first panel), the coefficient $a(x, y)$ (second panel), the numerical solution u_h (third panel), and the error $|u_h - u|$ (fourth panel) with $h = 2^{-8} \times 5$, where u_h is computed by our proposed hybrid finite difference scheme.

4.3.2 Numerical examples with unknown u

In this subsection, we provide five numerical examples with unknown u of (4.1). They can be characterized as follows.

- In all examples, either a_+/a_- or a_-/a_+ is very large on Γ for high-contrast coefficients a .
- 4-side Dirichlet boundary conditions are demonstrated in Examples 4.6 and 4.9.
- 3-side Dirichlet and 1-side Robin boundary conditions in Examples 4.7 and 4.8.
- 1-side Dirichlet, 1-side Neumann and 2-side Robin boundary conditions in Example 4.10.
- All the interface curves Γ are smooth and all the jump functions g_0^Γ and g_1^Γ are non-constant.

Example 4.6. Let $\Omega = (-2.5, 2.5)^2$ and the interface curve be given by $\Gamma := \{(x, y) \in \Omega : \psi(x, y) = 0\}$ with $\psi(x, y) = x^4 + 2y^4 - 2$. The functions in (4.1) are given by

$$\begin{aligned} a_+ &= 2 + \cos(x) \cos(y), & a_- &= 10^3(2 + \sin(x) \sin(y)), & g_0^\Gamma &= \sin(x) \sin(y) - 1, \\ f_+ &= \sin(4\pi x) \sin(4\pi y), & f_- &= \cos(4\pi x) \cos(4\pi y), & g_1^\Gamma &= \cos(x) \cos(y), \\ u(-2.5, y) &= 0, & u(2.5, y) &= 0, & \text{for } y &\in (-2.5, 2.5), \\ u(x, -2.5) &= 0, & u(x, 2.5) &= 0, & \text{for } x &\in (-2.5, 2.5). \end{aligned}$$

Note the high contrast $a_-/a_+ \approx 10^3$ on Γ . The numerical results are presented in Table 4.6 and Fig. 4.8.

Table 4.6: Performance in Example 4.6 of our proposed hybrid finite difference scheme on uniform Cartesian meshes with $h = 2^{-J} \times 5$.

J	$\ u_h - u_{h/2}\ _2$	order	$\ u_h - u_{h/2}\ _\infty$	order
4	9.83385E+02	0	3.29078E+02	0
5	1.93678E+01	5.7	6.50631E+00	5.7
6	3.13024E-01	6.0	1.04785E-01	6.0
8	9.47776E-05	5.8	3.20754E-05	5.8

Example 4.7. Let $\Omega = (-\pi, \pi)^2$ and the interface curve be given by $\Gamma := \{(x, y) \in \Omega : \psi(x, y) = 0\}$ with $\psi(x, y) = x^2 + y^2 - 2$. The functions in (4.1) are given by

$$a_+ = 2 + \cos(x - y), \quad a_- = 10^3(2 + \cos(x - y)), \quad g_0^\Gamma = \sin(x - y) - 2,$$

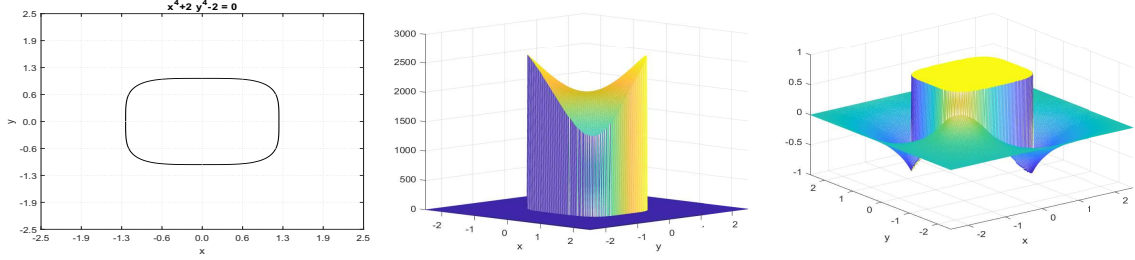


Figure 4.8: Example 4.6: the interface curve Γ (left), the coefficient $a(x, y)$ (middle) and the numerical solution u_h (right) with $h = 2^{-8} \times 5$, where u_h is computed by our proposed hybrid finite difference scheme. In order to show the graph of $a(x, y)$ clearly, we rotate the graph of $a(x, y)$ by $\pi/2$ in this figure.

$$\begin{aligned}
 f_+ &= \sin(8x) \sin(8y), & f_- &= \cos(8x) \cos(8y), & g_1^\Gamma &= \cos(x + y), \\
 -u_x(-\pi, y) + \cos(y)u(-\pi, y) &= \cos(y) + 1, & u(\pi, y) &= 0, & \text{for } y &\in (-\pi, \pi), \\
 u(x, -\pi) &= 0, & u(x, \pi) &= 0, & \text{for } x &\in (-\pi, \pi).
 \end{aligned}$$

Note the high contrast $a_-/a_+ = 10^3$ on Γ . The numerical results are presented in Table 4.7 and Fig. 4.9.

Table 4.7: Performance in Example 4.7 of our proposed hybrid finite difference scheme on uniform Cartesian meshes with $h = 2^{-J} \times 2\pi$.

J	$\ u_h - u_{h/2}\ _2$	order	$\ u_h - u_{h/2}\ _\infty$	order
4	7.02037E+02	0	1.84708E+02	0
5	9.69424E+00	6.2	2.54978E+00	6.2
6	2.26556E-01	5.4	5.97145E-02	5.4
7	2.57284E-03	6.5	6.79725E-04	6.5
8	5.07886E-05	5.7	1.34801E-05	5.7

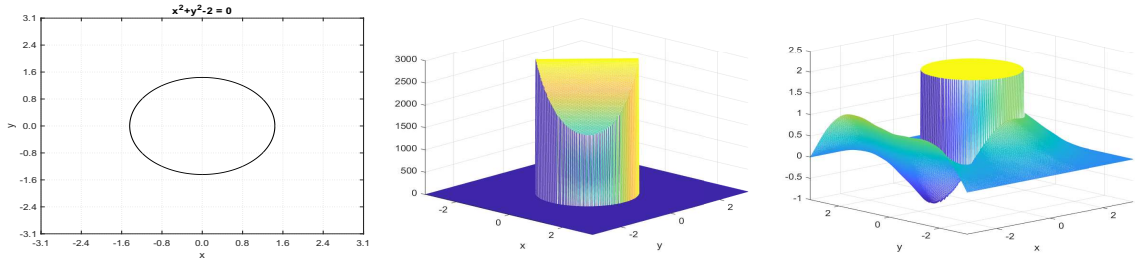


Figure 4.9: Example 4.7: the interface curve Γ (left), the coefficient $a(x, y)$ (middle) and the numerical solution u_h (right) with $h = 2^{-8} \times 2\pi$, where u_h is computed by our proposed hybrid finite difference scheme. In order to show the graph of $a(x, y)$ clearly, we rotate the graph of $a(x, y)$ by $\pi/2$ in this figure.

Example 4.8. Let $\Omega = (-\frac{\pi}{2}, \frac{\pi}{2})^2$ and the interface curve be given by $\Gamma := \{(x, y) \in \Omega : \psi(x, y) = 0\}$ with $\psi(x, y) = y^2 + \frac{2x^2}{x^2+1} - 1$. The functions in (4.1) are given by

$$\begin{aligned} a_+ &= 10^3(2 + \sin(x + y)), & a_- &= 10^{-3}(2 + \cos(x - y)), & g_0^\Gamma &= \sin(x) \cos(y) - 2, \\ f_+ &= \sin(6x) \sin(6y), & f_- &= \cos(6x) \cos(6y), & g_1^\Gamma &= \cos(x + y), \\ -u_x(-\frac{\pi}{2}, y) + \cos(y)u(-\frac{\pi}{2}, y) &= \sin(y + \frac{\pi}{2})(y - \frac{\pi}{2}), & u(\frac{\pi}{2}, y) &= 0, & \text{for } y &\in (-\frac{\pi}{2}, \frac{\pi}{2}), \\ u(x, -\frac{\pi}{2}) &= 0, & u(x, \frac{\pi}{2}) &= 0, & \text{for } x &\in (-\frac{\pi}{2}, \frac{\pi}{2}). \end{aligned}$$

The high contrast $a_+/a_- \approx 10^6$ on Γ . The numerical results are presented in Table 4.8 and Fig. 4.10.

Table 4.8: Performance in Example 4.8 of our proposed hybrid finite difference scheme on uniform Cartesian meshes with $h = 2^{-J} \times \pi$.

J	$\ u_h - u_{h/2}\ _2$	order	$\ u_h - u_{h/2}\ _\infty$	order
5	1.17512E-01	0	1.95534E-01	0
6	1.34603E-03	6.4	5.01334E-03	5.3
7	2.97345E-05	5.5	9.62920E-05	5.7
8	3.63705E-07	6.4	1.11523E-06	6.4

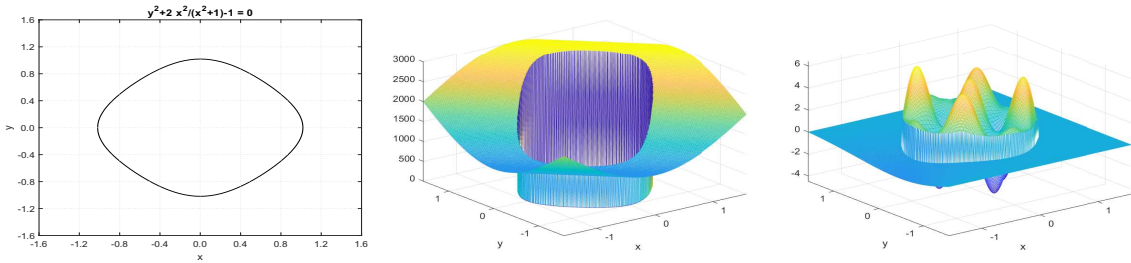


Figure 4.10: Example 4.8: the interface curve Γ (left), the coefficient $a(x, y)$ (middle) and the numerical solution u_h (right) with $h = 2^{-8} \times \pi$, where u_h is computed by our proposed hybrid finite difference scheme.

Example 4.9. Let $\Omega = (-2.5, 2.5)^2$ and the interface curve be given by $\Gamma := \{(x, y) \in \Omega : \psi(x, y) = 0\}$ with $\psi(x, y) = y^2 - 2x^2 + x^4 - \frac{1}{4}$. The functions in (4.1) are given by

$$\begin{aligned} a_+ &= 10^3(10 + \cos(x) \cos(y)), & a_- &= 10^{-3}(10 + \sin(x) \sin(y)), & g_0^\Gamma &= \sin(x) - 2, \\ f_+ &= \sin(4\pi x) \sin(4\pi y), & f_- &= \cos(4\pi x) \cos(4\pi y), & g_1^\Gamma &= \cos(y), \\ u(-2.5, y) &= 0, & u(2.5, y) &= 0, & \text{for } y &\in (-2.5, 2.5), \\ u(x, -2.5) &= 0, & u(x, 2.5) &= 0, & \text{for } x &\in (-2.5, 2.5). \end{aligned}$$

The high contrast $a_+/a_- \approx 10^6$ on Γ . The numerical results are presented in Table 4.9 and Fig. 4.11.

Table 4.9: Performance in Example 4.9 of our proposed hybrid finite difference scheme on uniform Cartesian meshes with $h = 2^{-J} \times 5$.

J	$\ u_h - u_{h/2}\ _2$	order	$\ u_h - u_{h/2}\ _\infty$	order
5	6.18678E+00	0	9.88338E+00	0
6	9.69535E-02	6.0	2.17089E-01	5.5
7	1.67043E-03	5.9	3.52407E-03	5.9
8	2.43148E-05	6.1	5.22530E-05	6.1

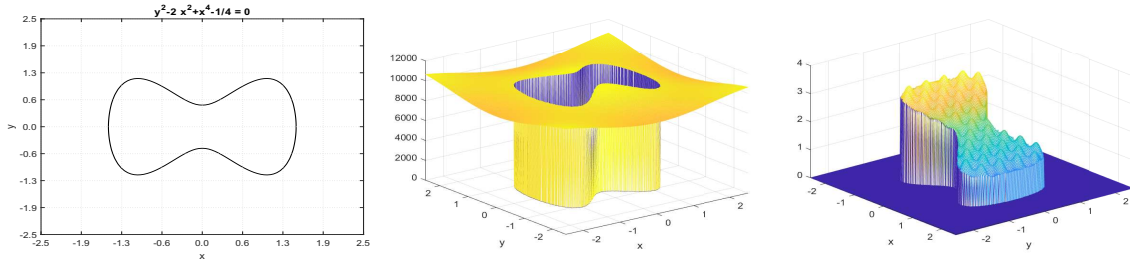


Figure 4.11: Example 4.9: the interface curve Γ (left), the coefficient $a(x, y)$ (middle) and the numerical solution u_h (right) with $h = 2^{-8} \times 5$. In order to show the graph of u_h clearly, we rotate the graph of u_h by $\pi/2$ in this figure.

Example 4.10. Let $\Omega = (-\pi, \pi)^2$ and the interface curve be given by $\Gamma := \{(x, y) \in \Omega : \psi(x, y) = 0\}$ with $\psi(x, y) = x^2 + y^2 - 4$. The functions in (4.1) are given by

$$\begin{aligned}
 a_+ &= 10(2 + \cos(x - y)), & a_- &= 10^{-6}(2 + \sin(x) \sin(y)), & g_0^\Gamma &= \sin(y) - 10, \\
 f_+ &= \sin(6x) \sin(6y), & f_- &= \cos(6x) \cos(6y), & g_1^\Gamma &= \cos(x), \\
 -u_x(-\pi, y) + \sin(y)u(-\pi, y) &= \cos(y), & u(\pi, y) &= 0, & \text{for } y &\in (-\pi, \pi), \\
 -u_y(x, -\pi) = \sin(x - \pi), & u_y(x, \pi) + \cos(x)u(x, \pi) &= \cos(x) + 1, & \text{for } x &\in (-\pi, \pi).
 \end{aligned}$$

The high contrast $a_+/a_- \approx 10^7$ on Γ . The numerical results are presented in Table 4.10 and Fig. 4.12.

4.4 Conclusion

To our best knowledge, so far there were no 13-point finite difference schemes for irregular points available in the literature, that can achieve fifth or sixth order for elliptic interface problems with discontinuous coefficients. Our contributions of this chapter are as follows:

Table 4.10: Performance in Example [4.10](#) of our proposed hybrid finite difference scheme on uniform Cartesian meshes with $h = 2^{-J} \times 2\pi$.

J	$\ u_h - u_{h/2}\ _2$	order	$\ u_h - u_{h/2}\ _\infty$	order
5	1.60217E+04	0	1.39059E+04	0
6	2.94197E+02	5.8	2.79828E+02	5.6
7	4.54676E+00	6.0	6.36193E+00	5.5
8	5.82759E-02	6.3	1.02577E-01	6.0

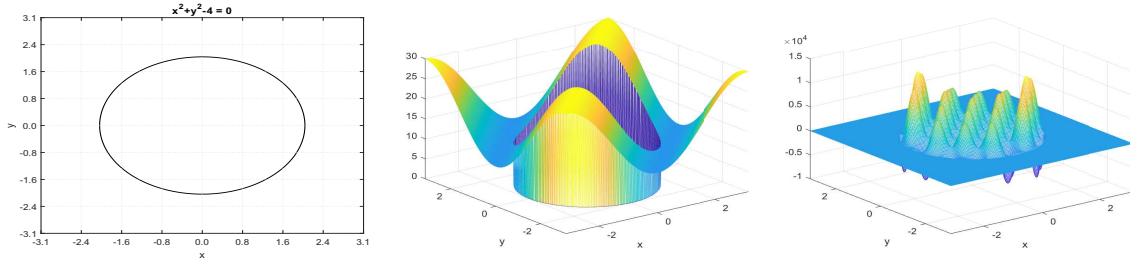


Figure 4.12: Example [4.10](#): the interface curve Γ (left), the coefficient $a(x, y)$ (middle) and the numerical solution u_h (right) with $h = 2^{-8} \times 2\pi$, where u_h is computed by our proposed hybrid finite difference scheme.

- We propose a hybrid (13-point for irregular points and 9-point for interior regular points) finite difference scheme, which demonstrates six order accuracy in all our numerical experiments, for elliptic interface problems with discontinuous, variable and high-contrast coefficients, discontinuous source terms and two non-homogeneous jump conditions.
- The proposed hybrid scheme demonstrates a robust high-order convergence for the challenging cases of high-contrast ratios of the coefficients a_{\pm} : $\sup(a_+)/\inf(a_-) = 10^{-3}, 10^{-6}, 10^6, 10^7$.
- Due to the flexibility and efficiency of the implementation, it is very simple to achieve the implementation for 25-point or 36-point schemes for irregular points of elliptic interface problems and Helmholtz interface equations with discontinuous wave numbers.
- From the results in Tables [4.1](#) and [4.2](#), we find that if we only replace the 13-point scheme for irregular points by a 9-point scheme, then the numerical errors increase significantly, while the condition number only slightly decreases. Thus, the proposed hybrid scheme could significantly improve the numerical performance with a slight increase in the complexity of the corresponding linear system.
- We also derive a 6-point/4-point schemes with a sixth order accuracy at the side/corner points for the case of smooth coefficients α and β in the Robin boundary conditions

$$\frac{\partial u}{\partial \bar{n}} + \alpha u = g_1 \text{ and } \frac{\partial u}{\partial \bar{n}} + \beta u = g_4.$$

- The presented numerical experiments confirm the sixth order of accuracy in the l_2 and l_∞ norms of our proposed hybrid scheme.

4.5 Proofs of Theorems 4.1 to 4.8

In this subsection, we provide the proofs to all the technical results stated in Section 4.2.

Proof of Theorem 4.1. Choose $M = 6$ and replace $G_{m,n}$, $Q_{m,n}$ and Λ_{M+1}^1 in Theorem 3.2 by $G_{M,m,n}^V$ given in (4.8), $Q_{M,m,n}^V$ in (4.9), and $\Lambda_{M+1}^{V,1}$ in (4.6). \square

Proof of Theorem 4.2. Since $-u_x + \alpha u = g_1$ on $\partial\Omega|_1$, we have $u^{(1,n)} = \sum_{i=0}^n \binom{n}{i} \alpha^{(n-i)} u^{(0,i)} - g_1^{(n)}$ for all $n = 0, \dots, M-1$. By (4.12) with M being replaced by $M-1$,

$$\begin{aligned} & u(x + x_i^*, y + y_j^*) \\ &= \sum_{(m,n) \in \Lambda_M^{V,1}} u^{(m,n)} G_{M,m,n}^V(x, y) + \sum_{(m,n) \in \Lambda_{M-2}} f^{(m,n)} Q_{M,m,n}^V(x, y) + \mathcal{O}(h^{M+1}) \\ &= \sum_{n=0}^M u^{(0,n)} G_{M,0,n}^V(x, y) + \sum_{n=0}^{M-1} u^{(1,n)} G_{M,1,n}^V(x, y) + \sum_{(m,n) \in \Lambda_{M-2}} f^{(m,n)} Q_{M,m,n}^V(x, y) + \mathcal{O}(h^{M+1}) \\ &= \sum_{n=0}^M u^{(0,n)} G_{M,0,n}^V(x, y) + \sum_{n=0}^{M-1} \left(\sum_{i=0}^n \binom{n}{i} \alpha^{(n-i)} u^{(0,i)} - g_1^{(n)} \right) G_{M,1,n}^V(x, y) \\ &\quad + \sum_{(m,n) \in \Lambda_{M-2}} f^{(m,n)} Q_{M,m,n}^V(x, y) + \mathcal{O}(h^{M+1}) \\ &= \sum_{n=0}^M u^{(0,n)} G_{M,0,n}^V(x, y) + \sum_{n=0}^{M-1} \sum_{i=0}^n \binom{n}{i} \alpha^{(n-i)} u^{(0,i)} G_{M,1,n}^V(x, y) - \sum_{n=0}^{M-1} g_1^{(n)} G_{M,1,n}^V(x, y) \\ &\quad + \sum_{(m,n) \in \Lambda_{M-2}} f^{(m,n)} Q_{M,m,n}^V(x, y) + \mathcal{O}(h^{M+1}) \\ &= \sum_{n=0}^M u^{(0,n)} G_{M,0,n}^V(x, y) + \sum_{i=0}^{M-1} \sum_{n=i}^{M-1} \binom{n}{i} \alpha^{(n-i)} u^{(0,i)} G_{M,1,n}^V(x, y) - \sum_{n=0}^{M-1} g_1^{(n)} G_{M,1,n}^V(x, y) \\ &\quad + \sum_{(m,n) \in \Lambda_{M-2}} f^{(m,n)} Q_{M,m,n}^V(x, y) + \mathcal{O}(h^{M+1}) \\ &= u^{(0,M)} G_{M,0,M}^V(x, y) + \sum_{n=0}^{M-1} u^{(0,n)} G_{M,0,n}^V(x, y) + \sum_{n=0}^{M-1} \sum_{i=n}^{M-1} \binom{i}{n} \alpha^{(i-n)} u^{(0,n)} G_{M,1,i}^V(x, y) \\ &\quad - \sum_{n=0}^{M-1} g_1^{(n)} G_{M,1,n}^V(x, y) + \sum_{(m,n) \in \Lambda_{M-2}} f^{(m,n)} Q_{M,m,n}^V(x, y) + \mathcal{O}(h^{M+1}), \quad \text{for } x, y \in (-2h, 2h). \end{aligned}$$

So, $x_i^* = x_i$ and $y_j^* = y_j$ lead to

$$\begin{aligned}\mathcal{L}_h^{\mathcal{B}_1} u &:= \frac{1}{h} \sum_{k=0}^1 \sum_{\ell=-1}^1 C_{k,\ell}^{\mathcal{B}_1} u(x_i + kh, y_j + \ell h) \\ &= \sum_{n=0}^M u^{(0,n)} h^{-1} I_n^{\mathcal{B}_1} + \sum_{(m,n) \in \Lambda_{M-2}} f^{(m,n)} h J_{m,n}^{\mathcal{B}_1} + \sum_{n=0}^{M-1} g_1^{(n)} h^{-1} J_{g_1,n}^{\mathcal{B}_1} = \mathcal{O}(h^M),\end{aligned}$$

as $h \rightarrow 0$, where

$$\begin{aligned}I_n^{\mathcal{B}_1} &:= \sum_{k=0}^1 \sum_{\ell=-1}^1 C_{k,\ell}^{\mathcal{B}_1} \left(G_{M,0,n}^V(kh, \ell h) + \sum_{i=n}^{M-1} \binom{i}{n} \alpha^{(i-n)} G_{M,1,i}^V(kh, \ell h) (1 - \delta_{n,M}) \right), \\ J_{m,n}^{\mathcal{B}_1} &:= \sum_{k=0}^1 \sum_{\ell=-1}^1 C_{k,\ell}^{\mathcal{B}_1} h^{-2} Q_{M,m,n}^V(kh, \ell h), \quad J_{g_1,n}^{\mathcal{B}_1} := - \sum_{k=0}^1 \sum_{\ell=-1}^1 C_{k,\ell}^{\mathcal{B}_1} G_{M,1,n}^V(kh, \ell h),\end{aligned}\tag{4.41}$$

$\delta_{a,a} = 1$, and $\delta_{a,b} = 0$ for $a \neq b$. Let

$$\mathcal{L}_h^{\mathcal{B}_1} u_h := \frac{1}{h} \sum_{k=0}^1 \sum_{\ell=-1}^1 C_{k,\ell}^{\mathcal{B}_1} (u_h)_{i+k,j+\ell} = \sum_{(m,n) \in \Lambda_{M-2}} f^{(m,n)} h J_{m,n}^{\mathcal{B}_1} + \sum_{n=0}^{M-1} g_1^{(n)} h^{-1} J_{g_1,n}^{\mathcal{B}_1}.\tag{4.42}$$

We have

$$\mathcal{L}_h^{\mathcal{B}_1} (u - u_h) = \mathcal{O}(h^M),$$

if $I_n^{\mathcal{B}_1} = \mathcal{O}(h^{M+1})$ in (4.41) for all $n = 0, \dots, M$. So (4.42) with $M = 6$ results in (4.14). □

Proof of Theorem 4.3. The proof is almost identical to the proof of Theorem 4.2. □

Proof of Theorem 4.4. The proof is almost identical to the proof of Theorem 4.2. □

Proof of Theorem 4.5. The proof is similar to the proof of Theorem 5.4. Precisely, replace $\mathcal{B}_1 u = \frac{\partial u}{\partial \bar{n}} - iku = g_1$ by $\mathcal{B}_1 u = \frac{\partial u}{\partial \bar{n}} + \alpha u = g_1$ in the proof of Theorem 5.4 with $M = M_f = M_{g_1} = M_{g_3} = 6$, and replace $G_{M,m,n}^V$, $Q_{M,m,n}^V$, $G_{M,m,n}^H$ and $Q_{M,m,n}^H$ in Theorem 5.4 by (4.8), (4.9), (4.10) and (4.11). □

Proof of Theorem 4.6. The proof is similar to the proof of Theorem 5.5. Precisely, replace $\mathcal{B}_1 u = \frac{\partial u}{\partial \bar{n}} - iku = g_1$ and $\mathcal{B}_4 u = \frac{\partial u}{\partial \bar{n}} - iku = g_4$ by $\mathcal{B}_1 u = \frac{\partial u}{\partial \bar{n}} + \alpha u = g_1$ and $\mathcal{B}_4 u = \frac{\partial u}{\partial \bar{n}} + \beta u = g_4$ respectively in the proof of Theorem 5.5 with $M = M_f = M_{g_1} = M_{g_4} = 6$ and replace $G_{M,m,n}^V$, $Q_{M,m,n}^V$, $G_{M,m,n}^H$ and $Q_{M,m,n}^H$ in Theorem 5.5 by (4.8), (4.9), (4.10) and (4.11). □

Proof of Theorem 4.7. (4.26) can be obtained by $u_-^{(0,0)} = u_+^{(0,0)} - g_{0,0}^\Gamma$ and (3.58). The rest of the proof is straightforward and follows from (3.48), (3.50), (3.56), and (3.58). \square

Proof of Theorem 4.8. Choose $M = 5$, replace $\Lambda_M^1, G_{m,n}^\pm, Q_{m,n}^\pm, d_{i,j}^\pm$ in (3.23)–(3.28) by $\Lambda_M^{V,1}, G_{M,m,n}^{\pm,V}, Q_{M,m,n}^{\pm,V}, d_{i,j}^\pm \cup e_{i,j}^\pm$ in this chapter. \square

Proof of (4.40). Replace $\Lambda_M^1, G_{m,n}^\pm, Q_{m,n}^\pm, d_{i,j}^\pm$ in Chapter 3 by $\Lambda_M^{V,1}, G_{M,m,n}^{\pm,V}, Q_{M,m,n}^{\pm,V}, d_{i,j}^\pm \cup e_{i,j}^\pm$ in this chapter. Consider $I_{0,0}(h) = \mathcal{O}(h^{M+1})$ in (3.28). According to (3.27) and (4.28), $I_{0,0}(h) = \mathcal{O}(h^{M+1})$ implies

$$\sum_{(k,\ell) \in d_{i,j}^+ \cup e_{i,j}^+} C_{k,\ell}(h) G_{M,0,0}^{+,V}(v_0h + kh, w_0h + \ell h) + \sum_{\substack{(m',n') \in \Lambda_M^{V,1} \\ m'+n' \geq 0}} I_{m',n'}^-(h) T_{m',n',0,0}^{u+} = \mathcal{O}(h^{M+1}). \quad (4.43)$$

By (4.26), (4.43) is equivalent to

$$\sum_{(k,\ell) \in d_{i,j}^+ \cup e_{i,j}^+} C_{k,\ell}(h) G_{M,0,0}^{+,V}(v_0h + kh, w_0h + \ell h) + I_{0,0}^-(h) = \mathcal{O}(h^{M+1}),$$

i.e.,

$$\sum_{(k,\ell) \in d_{i,j}^+ \cup e_{i,j}^+} C_{k,\ell}(h) G_{M,0,0}^{+,V}(v_0h + kh, w_0h + \ell h) + \sum_{(k,\ell) \in d_{i,j}^- \cup e_{i,j}^-} C_{k,\ell}(h) G_{M,0,0}^{-,V}(v_0h + kh, w_0h + \ell h) = \mathcal{O}(h^{M+1}). \quad (4.44)$$

According to the proof of Lemmas 2.2 and 3.1 and (4.8),

$$G_{M,0,0}^{\pm,V}(x, y) := 1. \quad (4.45)$$

Consider the coefficients of h^i for $i = 0, 1, \dots, M$ in (4.44), then (4.45) implies

$$\sum_{(k,\ell) \in d_{i,j}^+ \cup e_{i,j}^+} c_{k,\ell,i} + \sum_{(k,\ell) \in d_{i,j}^- \cup e_{i,j}^-} c_{k,\ell,i} = 0, \quad \text{for } i = 0, 1, \dots, M.$$

This proves (4.40). \square

Chapter 5

Sixth Order Compact Finite Difference Methods for 2D Helmholtz Equations with Singular Sources and Reduced Pollution Effect

5.1 Introduction and problem formulation

The Helmholtz equation is challenging to solve numerically due to several reasons. The first is due to its highly oscillatory solution, which necessitates the use of a very small mesh size h in many discretization methods. Taking a mesh size h proportional to the reciprocal of the wavenumber k is not enough to guarantee that a reasonable solution is obtained or a convergent behavior is observed. The mesh size h employed in a standard discretization method often has to be much smaller than the reciprocal of the wavenumber k . In the literature, this phenomenon is referred to as the pollution effect, which has close ties to the numerical dispersion (or a phase lag). The situation is further exacerbated by the fact that the discretization of the Helmholtz equation typically yields an ill-conditioned coefficient matrix. Taken together, one typically faces an enormous ill-conditioned linear system when dealing with the Helmholtz equation, where standard iterative schemes fail to work [28].

Let $\Omega = (l_1, l_2) \times (l_3, l_4)$ and ψ be a smooth two-dimensional function. The model problem

is explicitly defined as follows:

$$\begin{cases} \Delta u + k^2 u = f & \text{in } \Omega \setminus \Gamma, \\ [u] = g_0^\Gamma, \quad [\nabla u \cdot \vec{n}] = g_1^\Gamma & \text{on } \Gamma, \\ \mathcal{B}_1 u = g_1 \text{ on } \partial\Omega|_1 := \{l_1\} \times (l_3, l_4), \quad \mathcal{B}_2 u = g_2 \text{ on } \partial\Omega|_2 := \{l_2\} \times (l_3, l_4), \\ \mathcal{B}_3 u = g_3 \text{ on } \partial\Omega|_3 := (l_1, l_2) \times \{l_3\}, \quad \mathcal{B}_4 u = g_4 \text{ on } \partial\Omega|_4 := (l_1, l_2) \times \{l_4\}, \end{cases} \quad (5.1)$$

where k is the wavenumber, f is the source term, and for any point $(x_0, y_0) \in \Gamma$,

$$\begin{aligned} [u](x_0, y_0) &:= \lim_{(x,y) \in \Omega_+, (x,y) \rightarrow (x_0, y_0)} u(x, y) - \lim_{(x,y) \in \Omega_-, (x,y) \rightarrow (x_0, y_0)} u(x, y), \\ [\nabla u \cdot \vec{n}](x_0, y_0) &:= \lim_{(x,y) \in \Omega_+, (x,y) \rightarrow (x_0, y_0)} \nabla u(x, y) \cdot \vec{n} - \lim_{(x,y) \in \Omega_-, (x,y) \rightarrow (x_0, y_0)} \nabla u(x, y) \cdot \vec{n}, \end{aligned}$$

where \vec{n} is the unit normal vector of Γ pointing towards Ω_+ . In (5.1), the boundary operators $\mathcal{B}_1, \dots, \mathcal{B}_4 \in \{\mathbf{I}_d, \frac{\partial}{\partial \vec{n}}, \frac{\partial}{\partial \vec{n}} - ik\mathbf{I}_d\}$, where \mathbf{I}_d corresponds to the Dirichlet boundary condition (sound soft boundary condition for the identical zero boundary datum), $\frac{\partial}{\partial \vec{n}}$ corresponds to the Neumann boundary condition (sound hard boundary condition for the identical zero boundary datum), and $\frac{\partial}{\partial \vec{n}} - ik\mathbf{I}_d$ (with i being the imaginary unit) corresponds to the impedance boundary condition. Moreover, the Helmholtz equation of (5.1) with $g_0^\Gamma = 0$ is equivalent to finding the weak solution $u \in H^1(\Omega)$ of $\Delta u + k^2 u = f + g_1^\Gamma \delta_\Gamma$ in Ω , where δ_Γ is the Dirac distribution along the interface curve Γ . From the theoretical standpoint, as long as an impedance boundary condition appears on one of the boundary sides, the solution to Helmholtz equations exists and is unique as studied in [44]. When an impedance boundary condition is absent, we shall avoid wavenumbers that lead to nonuniqueness. The rigorous stability analysis of the problem of Helmholtz equations with $g_0^\Gamma = g_1^\Gamma = 0$ was also done in [50, 54]. For the situation where $g_0^\Gamma, g_1^\Gamma \neq 0$, the well-posedness, regularity, and stability were rigorously studied in [85].

We shall use the following assumptions in the derivation of our finite difference scheme (Note that the main results in this chapter have been written in [31]):

- (A1) The solution u and the source term f have uniformly continuous partial derivatives of (total) orders up to seven and six respectively in each of the subregions Ω_+ and Ω_- . However, both u and f may be discontinuous across the interface Γ .
- (A2) The interface curve Γ is smooth in the sense that for each $(x^*, y^*) \in \Gamma$, there exists a local parametric equation: $\gamma : (-\epsilon, \epsilon) \rightarrow \Gamma$ with $\epsilon > 0$ such that $\gamma(0) = (x^*, y^*)$ and $\|\gamma'(0)\|_2 \neq 0$. Furthermore, $x(t)$ and $y(t)$ in (1.5) should both have uniformly continuous derivatives of (total) order up to eight for the variable $t = 0$.

(A3) The one-dimensional functions $g_0^\Gamma \circ \gamma$ and $g_1^\Gamma \circ \gamma$ have uniformly continuous derivatives of (total) orders up to eight and seven respectively on the interface Γ , where γ is given in (A2).

(A4) Each of the functions g_1, \dots, g_4 has uniformly continuous derivatives of (total) order up to seven on the boundary $\partial\Omega|_j$.

The organization of this chapter is as follows.

In Section 5.2, we explain how our proposed sixth order compact finite difference scheme with reduced pollution effect is developed. We start our discussion by constructing the interior finite difference stencil with reduced pollution. Second, we construct the sixth order boundary and corner finite difference stencils with reduced pollution. Third, we construct the interface finite difference stencil. In Section 5.3, we present several numerical experiments to demonstrate the performance of our proposed sixth order compact finite difference scheme with reduced pollution effect. In Section 5.4, we summarize the main contributions of this chapter. In Section 5.5, we present the proofs of several theorems stated in Section 5.2.

5.2 Sixth order compact finite difference schemes with reduced pollution effect using uniform cartesian grids

Our focus of this section is to develop sixth order compact finite difference schemes with reduced pollution effect on uniform Cartesian grids. Recall that

$$x_i = l_1 + ih, \quad i = 0, \dots, N_1, \quad \text{and} \quad y_j = l_3 + jh, \quad j = 0, \dots, N_2, \quad (5.2)$$

$$x_i^* = x_i - v_0h \quad \text{and} \quad y_j^* = y_j - w_0h \quad \text{with} \quad -1 < v_0, w_0 < 1. \quad (5.3)$$

Similar as Lemma 2.2 and Lemma 3.1, since the function u is a solution to the partial differential equation in (5.1), all quantities $u^{(m,n)}$, $(m,n) \in \Lambda_{M+1}$ are not independent of each other. The next lemma describes this dependence.

Lemma 5.1. *Let u be a smooth function satisfying $\Delta u + k^2 u = f$ in $\Omega \setminus \Gamma$. If a point $(x_i^*, y_j^*) \in \Omega \setminus \Gamma$, then*

$$u^{(m,n)} = (-1)^{\lfloor \frac{m}{2} \rfloor} \sum_{i=0}^{\lfloor \frac{m}{2} \rfloor} \binom{\lfloor \frac{m}{2} \rfloor}{i} k^{2i} u^{(\text{odd}(m), 2\lfloor \frac{m}{2} \rfloor + n - 2i)} + \sum_{i=1}^{\lfloor \frac{m}{2} \rfloor} \sum_{j=0}^{i-1} (-1)^{i-1} \binom{i-1}{j} k^{2(i-j-1)} f^{(m-2i, n+2j)} \quad (5.4)$$

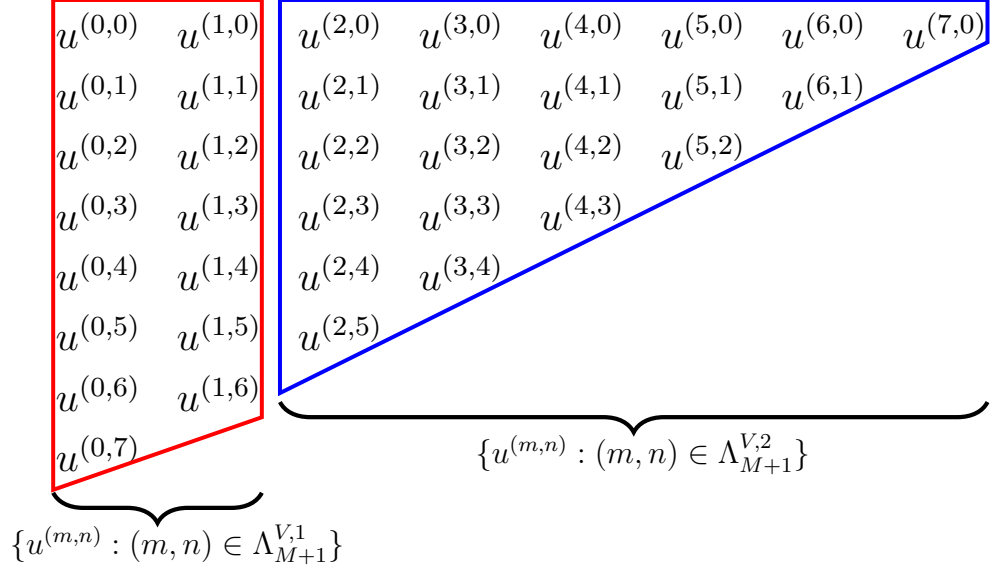


Figure 5.1: Red trapezoid: $\{u^{(m,n)} : (m,n) \in \Lambda_{M+1}^{V,1}\}$ with $M = 6$. Blue trapezoid: $\{u^{(m,n)} : (m,n) \in \Lambda_{M+1}^{V,2}\}$ with $M = 6$. Note that $\Lambda_{M+1} = \Lambda_{M+1}^{V,1} \cup \Lambda_{M+1}^{V,2}$.

for all $(m,n) \in \Lambda_{M+1}^{V,2}$, where

$$\Lambda_{M+1}^{V,2} := \Lambda_{M+1} \setminus \Lambda_{M+1}^{V,1} \quad \text{with} \quad \Lambda_{M+1}^{V,1} := \{(\ell, k - \ell) : k = \ell, \dots, M + 1 - \ell \text{ and } \ell = 0, 1\}. \quad (5.5)$$

Define

$$\Lambda_{M+1}^{H,j} := \{(n, m) : (m, n) \in \Lambda_{M+1}^{V,j}, j = 1, 2\}.$$

If a point $(x_i^*, y_j^*) \in \Omega \setminus \Gamma$, then

$$u^{(m,n)} = (-1)^{\lfloor \frac{n}{2} \rfloor} \sum_{i=0}^{\lfloor \frac{n}{2} \rfloor} \binom{\lfloor \frac{n}{2} \rfloor}{i} k^{2i} u^{(2\lfloor \frac{n}{2} \rfloor + m - 2i, \text{odd}(n))} + \sum_{i=1}^{\lfloor \frac{n}{2} \rfloor} \sum_{j=0}^{i-1} (-1)^{i-1} \binom{i-1}{j} k^{2(i-j-1)} f^{(m+2j, n-2i)} \quad (5.6)$$

for all $(m,n) \in \Lambda_{M+1}^{H,2}$.

Proof. The proof is similar to the proof of Lemma 2.2 and Lemma 3.1 □

See Figs. 5.1 and 5.2 and for illustrations of how each $u^{(m,n)}$ with $(m,n) \in \Lambda_7$ is catego-

$$\begin{aligned}
& \{u^{(m,n)} : (m,n) \in \Lambda_{M+1}^{H,1}\} \left\{ \begin{array}{cccccccc} u^{(0,0)} & u^{(1,0)} & u^{(2,0)} & u^{(3,0)} & u^{(4,0)} & u^{(5,0)} & u^{(6,0)} & u^{(7,0)} \\ u^{(0,1)} & u^{(1,1)} & u^{(2,1)} & u^{(3,1)} & u^{(4,1)} & u^{(5,1)} & u^{(6,1)} & \end{array} \right. \\
& \{u^{(m,n)} : (m,n) \in \Lambda_{M+1}^{H,2}\} \left\{ \begin{array}{cccccc} u^{(0,2)} & u^{(1,2)} & u^{(2,2)} & u^{(3,2)} & u^{(4,2)} & u^{(5,2)} \\ u^{(0,3)} & u^{(1,3)} & u^{(2,3)} & u^{(3,3)} & u^{(4,3)} & \\ u^{(0,4)} & u^{(1,4)} & u^{(2,4)} & u^{(3,4)} & & \\ u^{(0,5)} & u^{(1,5)} & u^{(2,5)} & & & \\ u^{(0,6)} & u^{(1,6)} & & & & \\ u^{(0,7)} & & & & & \end{array} \right.
\end{aligned}$$

Figure 5.2: Red rectangle: $\{u^{(m,n)} : (m,n) \in \Lambda_{M+1}^{H,1}\}$ with $M = 6$. Blue triangle: $\{u^{(m,n)} : (m,n) \in \Lambda_{M+1}^{H,2}\}$ with $M = 6$. Note that $\Lambda_{M+1} = \Lambda_{M+1}^{H,1} \cup \Lambda_{M+1}^{H,2}$.

rized based on $\Lambda_7^{V,j}$ and $\Lambda_7^{H,j}$ with $j \in \{1, 2\}$. From (5.4), we have

$$\begin{aligned}
\sum_{(m,n) \in \Lambda_{M+1}^{V,2}} \frac{x^m y^n}{m! n!} u^{(m,n)} &= \overbrace{\sum_{(m,n) \in \Lambda_{M+1}^{V,2}} \frac{x^m y^n}{m! n!} \left\{ (-1)^{\lfloor \frac{m}{2} \rfloor} \sum_{i=0}^{\lfloor \frac{m}{2} \rfloor} \binom{\lfloor \frac{m}{2} \rfloor}{i} \mathbf{k}^{2i} u^{(\text{odd}(m), 2\lfloor \frac{m}{2} \rfloor + n - 2i)} \right\}}^{=: I_1} \\
&+ \underbrace{\sum_{(m,n) \in \Lambda_{M+1}^{V,2}} \frac{x^m y^n}{m! n!} \left\{ \sum_{i=1}^{\lfloor \frac{m}{2} \rfloor} \sum_{j=0}^{i-1} (-1)^{i-1} \binom{i-1}{j} \mathbf{k}^{2i-2j-2} f^{(m-2i, n+2j)} \right\}}_{=: I_2},
\end{aligned} \tag{5.7}$$

where the first summation I_1 above can be expressed as

$$\begin{aligned}
I_1 &= \sum_{\substack{(m,n) \in \Lambda_{M+1}^{V,2} \\ \ell = \frac{m}{2}, \text{ even } m}} \frac{(-1)^\ell x^{2\ell} y^n}{(2\ell)! n!} \sum_{i=0}^{\ell} \binom{\ell}{i} \mathbf{k}^{2i} u^{(0, 2\ell + n - 2i)} \\
&+ \sum_{\substack{(m,n) \in \Lambda_{M+1}^{V,2} \\ \ell = \frac{m-1}{2}, \text{ odd } m}} \frac{(-1)^\ell x^{2\ell+1} y^n}{(2\ell+1)! n!} \sum_{i=0}^{\ell} \binom{\ell}{i} \mathbf{k}^{2i} u^{(1, 2\ell + n - 2i)} \\
&= \sum_{n=2}^{M+1} \sum_{\ell=1}^{\lfloor \frac{n}{2} \rfloor} \frac{(-1)^\ell x^{2\ell} y^{n-2\ell}}{(2\ell)! (n-2\ell)!} \sum_{i=0}^{\ell} \binom{\ell}{i} \mathbf{k}^{2i} u^{(0, n-2i)} + \sum_{n=2}^M \sum_{\ell=1}^{\lfloor \frac{n}{2} \rfloor} \frac{(-1)^\ell x^{2\ell+1} y^{n-2\ell}}{(2\ell+1)! (n-2\ell)!} \sum_{i=0}^{\ell} \binom{\ell}{i} \mathbf{k}^{2i} u^{(1, n-2i)} \\
&= \sum_{\substack{(m,n) \in \Lambda_{M+1}^{V,1} \\ n \geq 2}} \sum_{\ell=1}^{\lfloor \frac{n}{2} \rfloor} \frac{(-1)^\ell x^{m+2\ell} y^{n-2\ell}}{(m+2\ell)! (n-2\ell)!} \sum_{i=0}^{\ell} \binom{\ell}{i} \mathbf{k}^{2i} u^{(m, n-2i)},
\end{aligned}$$

and the second summation I_2 above can be expressed as

$$\begin{aligned}
I_2 &= \sum_{(m,n) \in \Lambda_{M-1}} \sum_{\ell=1}^{1+\lfloor \frac{n}{2} \rfloor} \sum_{p=0}^{\ell-1} (-1)^{\ell-1} \binom{\ell-1}{p} \mathbf{k}^{2(\ell-p-1)} f^{(m,n+2(p+1-\ell))} \frac{x^{m+2\ell} y^{n-2\ell+2}}{(m+2\ell)!(n-2\ell+2)!} \\
&= \sum_{(m,n) \in \Lambda_{M-1}} \sum_{\substack{j \in \{n+2p \mid p \in \mathbb{N}_0, \\ n+2p \leq M-1-m\}}} \sum_{\ell=1+\lfloor \frac{j-n}{2} \rfloor}^{1+\lfloor \frac{j}{2} \rfloor} (-1)^{\ell-1} \binom{\ell-1}{\frac{j-n}{2}} \mathbf{k}^{j-n} \frac{x^{m+2\ell} y^{j-2\ell+2}}{(m+2\ell)!(j-2\ell+2)!} f^{(m,n)} \\
&= \sum_{(m,n) \in \Lambda_{M-1}} \underbrace{\sum_{p=0}^{\lfloor \frac{M-1-m-n}{2} \rfloor} \sum_{\ell=1+p}^{1+\lfloor \frac{n}{2} \rfloor} (-1)^{\ell-1} \binom{\ell-1}{p} \mathbf{k}^{2p} \frac{x^{m+2\ell} y^{2p+n+2-2\ell}}{(m+2\ell)!(2p+n+2-2\ell)!} f^{(m,n)}}_{=: Q_{M+1,m,n}^V(x,y)}.
\end{aligned} \tag{5.8}$$

Hence, using the right-hand side of (1.9) and the definitions of $\Lambda_{M+1}^{V,1}$, $\Lambda_{M+1}^{V,2}$ in (5.5), we have

$$\begin{aligned}
I_1 + \sum_{(m,n) \in \Lambda_{M+1}^{V,1}} \frac{x^m y^n}{m!n!} u^{(m,n)} &= \sum_{(m,n) \in \Lambda_{M+1}^{V,1}} \sum_{i=0}^{\lfloor \frac{n}{2} \rfloor} \sum_{\ell=i}^{\lfloor \frac{n}{2} \rfloor} \frac{(-1)^\ell x^{m+2\ell} y^{n-2\ell}}{(m+2\ell)!(n-2\ell)!} \binom{\ell}{i} \mathbf{k}^{2i} u^{(m,n-2i)} \\
&= \sum_{(m,n) \in \Lambda_{M+1}^{V,1}} \sum_{\substack{i \in \{n+2p \mid p \in \mathbb{N}_0, \\ n+2p \leq M+1-m\}}} \sum_{\ell=\frac{i-n}{2}}^{\lfloor \frac{i}{2} \rfloor} \frac{(-1)^\ell x^{m+2\ell} y^{i-2\ell}}{(m+2\ell)!(i-2\ell)!} \binom{\ell}{\frac{i-n}{2}} \mathbf{k}^{i-n} u^{(m,n)} \\
&= \sum_{(m,n) \in \Lambda_{M+1}^{V,1}} \underbrace{\sum_{p=0}^{\lfloor \frac{M+1-m-n}{2} \rfloor} \sum_{\ell=p}^{p+\lfloor \frac{n}{2} \rfloor} \frac{(-1)^\ell x^{m+2\ell} y^{n+2p-2\ell}}{(m+2\ell)!(n+2p-2\ell)!} \binom{\ell}{p} \mathbf{k}^{2p} u^{(m,n)}}_{=: G_{M+1,m,n}^V(x,y)}.
\end{aligned} \tag{5.9}$$

Suppose $x, y \in (-2h, 2h)$. The lowest degree of h for each polynomial $G_{M+1,m,n}^V(x, y)$ with $(m, n) \in \Lambda_{M+1}^{V,1}$ in (5.9) is $m+n$. The lowest degree of h for each polynomial $Q_{M+1,m,n}^V(x, y)$ with $(m, n) \in \Lambda_{M-1}^V$ in (5.8) is $m+n+2$. Therefore, by (5.7)-(5.8), we can rewrite the approximation of $u(x+x_i^*, y+y_j^*)$ with $(x, y) \in (-2h, 2h)$ in (1.9) as follows:

$$u(x+x_i^*, y+y_j^*) = \sum_{(m,n) \in \Lambda_{M+1}^{V,1}} u^{(m,n)} G_{M+1,m,n}^V(x, y) + \sum_{(m,n) \in \Lambda_{M_f-1}^V} f^{(m,n)} Q_{M_f+1,m,n}^V(x, y) + \mathcal{O}(h^{M+2}), \tag{5.10}$$

where $M, M_f \in \mathbb{N}_0$ and $M_f \geq M$. By a similar calculation, for $(x, y) \in (-2h, 2h)$, we also have

$$u(x+x_i^*, y+y_j^*) = \sum_{(m,n) \in \Lambda_{M+1}^{H,1}} u^{(m,n)} G_{M+1,m,n}^H(x, y) + \sum_{(m,n) \in \Lambda_{M_f-1}^H} f^{(m,n)} Q_{M_f+1,m,n}^H(x, y) + \mathcal{O}(h^{M+2}), \tag{5.11}$$

where $M, M_f \in \mathbb{N}_0$, $M_f \geq M$ and

$$\begin{aligned} G_{M+1,m,n}^H(x,y) &:= G_{M+1,n,m}^V(y,x), \quad \text{for all } n \in \{0,1\}, m \in \mathbb{N}_0, \text{ and } m+n \leq M+1 \\ Q_{M_f+1,m,n}^H(x,y) &:= Q_{M_f+1,n,m}^V(y,x), \quad \text{for all } m,n \in \mathbb{N}_0, \text{ and } m+n \leq M_f-1. \end{aligned} \quad (5.12)$$

Identities (5.10)-(5.11) are critical in finding compact stencils achieving a desired accuracy order.

In the following subsections, we shall explicitly present our stencils having at least accuracy order 6 with reduced pollution effect for interior, boundary and corner points. As we shall explain in details in Section 5.5, we construct such stencils by first finding a general expression for all possible discretization stencils achieving the maximum order based on Taylor expansion and our sort of technique. Then we minimize the average truncation error of plane waves to determine the remaining free parameters in each stencil to reduce pollution effect. For simplicity, we cancel the (h) in $I_{m,n}(h)$, $J_{m,n}(h)$, $C_{k,\ell}(h)$ and other related notations.

5.2.1 Stencils for regular points (interior)

In this subsection, we state one of our main results on a sixth order compact 9-point finite difference scheme (with reduced pollution effect) centered at a regular point (x_i, y_j) and $(x_i, y_j) \notin \partial\Omega$. We let (x_i, y_j) be the base point (x_i^*, y_j^*) by setting $v_0 = w_0 = 0$ in (5.3). The proof of the following theorem is deferred to Section 5.5.

Theorem 5.2. *Let a grid point (x_i, y_j) be a regular point, i.e., either $d_{i,j}^+ = \emptyset$ or $d_{i,j}^- = \emptyset$ and $(x_i, y_j) \notin \partial\Omega$. Let $(u_h)_{i,j}$ be the numerically approximated solution of the exact solution u of the Helmholtz equation (5.1) at an interior regular point (x_i, y_j) . Then the following discretization stencil centered at (x_i, y_j)*

$$\begin{aligned} \mathcal{L}_h u_h := & \frac{1}{h^2} \left(\begin{array}{ccc} C_{1,1}(u_h)_{i-1,j-1} & +C_{1,0}(u_h)_{i,j-1} & +C_{1,1}(u_h)_{i+1,j-1} \\ +C_{1,0}(u_h)_{i-1,j} & +C_{0,0}(u_h)_{i,j} & +C_{1,0}(u_h)_{i+1,j} \\ +C_{1,1}(u_h)_{i-1,j+1} & +C_{1,0}(u_h)_{i,j+1} & +C_{1,1}(u_h)_{i+1,j+1} \end{array} \right) = \sum_{(m,n) \in \Lambda_6} f^{(m,n)} J_{m,n}, \end{aligned} \quad (5.13)$$

achieves the sixth order accuracy for $\Delta u + k^2 u = f$ at the point (x_i, y_j) with reduced pollution effect, where $J_{m,n} := \sum_{k=-1}^1 \sum_{\ell=-1}^1 C_{k,\ell} h^{-2} Q_{8,m,n}^V(kh, \ell h)$ for all $(m,n) \in \Lambda_6$, $Q_{8,m,n}^V(x,y)$ is

defined in (5.8), and

$$\begin{aligned}
C_{-1,-1} &= C_{-1,1} = C_{1,-1} = C_{1,1}, & C_{-1,0} &= C_{0,-1} = C_{0,1} = C_{1,0}, \\
C_{1,1} &= 1 - \frac{357462387}{25 \times 10^{10}} kh + \frac{1001065991}{2 \times 10^{10}} (kh)^2 - \frac{196477327}{2 \times 10^{12}} (kh)^3 + \frac{1155977087}{10^{12}} (kh)^4 \\
&\quad - \frac{116352513}{4 \times 10^{13}} (kh)^5 + \frac{1255955641}{10^{14}} (kh)^6, \\
C_{1,0} &= 4 - \frac{357462387}{625 \times 10^8} kh + \frac{532995477}{25 \times 10^{11}} (kh)^2 - \frac{267461861}{25 \times 10^{11}} (kh)^3 - \frac{288674231}{10^{11}} (kh)^4 \\
&\quad + \frac{2179972749}{5 \times 10^{14}} (kh)^5 - \frac{3473210401}{5 \times 10^{13}} (kh)^6, \\
C_{0,0} &= -20 + \frac{357462387}{125 \times 10^8} kh + \frac{5798934009}{10^9} (kh)^2 - \frac{969775457}{125 \times 10^9} (kh)^3 - \frac{1963785709}{5 \times 10^9} (kh)^4 \\
&\quad + \frac{4056581719}{10^{13}} (kh)^5 + \frac{795951403}{10^{11}} (kh)^6.
\end{aligned} \tag{5.14}$$

The maximum accuracy order of a compact 9-point finite difference scheme using Taylor expansion and our sort of technique for $\Delta u + k^2 u = f$ at the point (x_i, y_j) is six.

5.2.2 Stencils for boundary and corner points

In this subsection, we discuss how to find compact (6-point, 4-point) finite difference schemes centered at $(x_i, y_j) \in \partial\Omega$.

5.2.2.1 Boundary points

We first discuss in detail how the left boundary (i.e., $(x_i, y_j) \in \partial\Omega|_1 = \{l_1\} \times (l_3, l_4)$) stencil is constructed. The stencils for the other three boundaries can afterwards be obtained by symmetry. If $\mathcal{B}_1 u = u = g_1$ on $\partial\Omega|_1$, then the left boundary stencil can be directly obtained from (5.13)-(5.14) in Theorem 5.2 by replacing $(u_h)_{0,j-1}$, $(u_h)_{0,j}$, and $(u_h)_{0,j+1}$ with $g_1(y_{j-1})$, $g_1(y_j)$, and $g_1(y_{j+1})$ respectively, where $y_j \in (l_3, l_4)$, and moving terms involving these known boundary values to the right-hand side of (5.13). The other three boundary sides are dealt in a similar straightforward fashion if a Dirichlet boundary condition is present. On the other hand, the stencils for the other two boundary conditions are not trivial at all. The following theorem provides the explicit 6-point stencil of accuracy order at least six with reduced pollution effect for the left boundary operator $\mathcal{B}_1 \in \{\frac{\partial}{\partial \bar{n}} - ik\mathbf{I}_d, \frac{\partial}{\partial \bar{n}}\}$. The proof of the following result is deferred to Section 5.5.

Theorem 5.3. *Assume $\Omega = (l_1, l_2) \times (l_3, l_4)$. Let $(u_h)_{i,j}$ be the numerically approximated solution of the exact solution u of the Helmholtz equation (5.1) at the point (x_i, y_j) . Consider the following discretization stencil centered at $(x_0, y_j) \in \partial\Omega|_1$ for $\mathcal{B}_1 u = g_1$ on $\partial\Omega|_1$ with*

$\mathcal{B}_1 \in \left\{ \frac{\partial}{\partial \bar{n}} - ik\mathbf{I}_d, \frac{\partial}{\partial \bar{n}} \right\}$:

$$\begin{aligned} \mathcal{L}_h^{\mathcal{B}_1} u_h := & \frac{1}{h} \left(C_{0,1}^{\mathcal{B}_1}(u_h)_{0,j-1} + C_{1,1}^{\mathcal{B}_1}(u_h)_{1,j-1} \right. \\ & + C_{0,0}^{\mathcal{B}_1}(u_h)_{0,j} + C_{1,0}^{\mathcal{B}_1}(u_h)_{1,j} \\ & \left. + C_{0,1}^{\mathcal{B}_1}(u_h)_{0,j+1} + C_{1,1}^{\mathcal{B}_1}(u_h)_{1,j+1} \right) = \sum_{(m,n) \in \Lambda_6} f^{(m,n)} h J_{m,n}^{\mathcal{B}_1} + \sum_{n=0}^7 g_1^{(n)} h^{-1} J_{g_1,n}^{\mathcal{B}_1}, \end{aligned} \quad (5.15)$$

where $\{C_{k,\ell}^{\mathcal{B}_1}\}_{k \in \{0,1\}, \ell \in \{-1,0,1\}}$ are polynomials of kh , $J_{m,n}^{\mathcal{B}_1} = \sum_{k=0}^1 \sum_{\ell=-1}^1 C_{k,\ell}^{\mathcal{B}_1} h^{-2} Q_{8,m,n}^V(kh, \ell h)$ for all $(m,n) \in \Lambda_6$, $Q_{8,m,n}^V$ is defined in (5.8), $g_1^{(n)} := \frac{d^n g_1}{dy^n}(y_j)$, $J_{g_1,n}^{\mathcal{B}_1} = - \sum_{k=0}^1 \sum_{\ell=-1}^1 C_{k,\ell}^{\mathcal{B}_1} G_{8,1,n}^V(kh, \ell h)$ for all $n = 0, \dots, 7$, $G_{8,1,n}^V$ is defined in (5.9), $C_{0,-1}^{\mathcal{B}_1} = C_{0,1}^{\mathcal{B}_1}$, and $C_{1,-1}^{\mathcal{B}_1} = C_{1,1}^{\mathcal{B}_1}$.

(1) For $\mathcal{B}_1 = \frac{\partial}{\partial \bar{n}} - ik\mathbf{I}_d$, the coefficients for defining $\mathcal{L}_h^{\mathcal{B}_1} u_h$ in (5.15) are given by

$$\begin{aligned} C_{1,1}^{\mathcal{B}_1} &= 1 - \frac{218737123}{10^9} kh + \frac{6698622893i}{10^{10}} kh - \frac{1620223367}{10^{10}} (kh)^2 - \frac{1202725989i}{10^{10}} (kh)^2 \\ &\quad + \frac{3105005559}{10^{11}} (kh)^3 - \frac{1252107029i}{10^{11}} (kh)^3 - \frac{3412232989}{10^{12}} (kh)^4 - \frac{1505046263i}{10^{12}} (kh)^4, \\ C_{0,1}^{\mathcal{B}_1} &= 2 - \frac{218737123}{5 \times 10^8} kh + \frac{1139724579i}{10^9} kh - \frac{3034055489}{10^{10}} (kh)^2 - \frac{1967977733i}{10^{10}} (kh)^2 \\ &\quad + \frac{1090897501}{25 \times 10^9} (kh)^3 - \frac{7785677273i}{10^{11}} (kh)^3 + \frac{98544681}{4 \times 10^9} (kh)^4 + \frac{1218033221i}{5 \times 10^{10}} (kh)^4, \\ C_{1,0}^{\mathcal{B}_1} &= 4 - \frac{8749484921}{10^{10}} kh + \frac{2279449157i}{10^9} kh - \frac{946955529}{2 \times 10^9} (kh)^2 - \frac{1967977733i}{5 \times 10^9} (kh)^2 \\ &\quad + \frac{2905342517}{5 \times 10^{10}} (kh)^3 - \frac{1542150899i}{5 \times 10^{10}} (kh)^3 + \frac{2645544603}{10^{12}} (kh)^4 + \frac{302693249i}{25 \times 10^9} (kh)^4, \\ C_{0,0}^{\mathcal{B}_1} &= -10 + \frac{218737123}{10^8} kh + \frac{202754213i}{2 \times 10^9} kh + \frac{7851597997}{10^{10}} (kh)^2 - \frac{2846864471i}{10^{10}} (kh)^2 \\ &\quad - \frac{1147746931}{5 \times 10^9} (kh)^3 + \frac{2236631341i}{10^{10}} (kh)^3 - \frac{1738692843}{5 \times 10^{10}} (kh)^4 - \frac{898631349i}{25 \times 10^9} (kh)^4. \end{aligned} \quad (5.16)$$

Then the finite difference scheme in (5.15) achieves sixth order accuracy for $\mathcal{B}_1 u = \frac{\partial u}{\partial \bar{n}} - iku = g_1$ at the point $(x_0, y_j) \in \partial\Omega|_1$ with reduced pollution effect.

(2) For $\mathcal{B}_1 = \frac{\partial}{\partial \bar{n}}$, the coefficients for defining $\mathcal{L}_h^{\mathcal{B}_1} u_h$ in (5.15) are given by

$$\begin{aligned} C_{1,1}^{\mathcal{B}_1} &= 1 + \frac{1915061419}{25 \times 10^9} (kh)^2 + \frac{3019639439}{10^{12}} (kh)^4, \\ C_{0,1}^{\mathcal{B}_1} &= 2 + \frac{665061419}{125 \times 10^8} (kh)^2 - \frac{1071383831}{2 \times 10^{12}} (kh)^4, \\ C_{1,0}^{\mathcal{B}_1} &= 4 + \frac{106409827}{10^9} (kh)^2 - \frac{1071383831}{10^{12}} (kh)^4, \\ C_{0,0}^{\mathcal{B}_1} &= -10 + \frac{1316987716}{5 \times 10^8} (kh)^2 - \frac{1240891409}{10^{10}} (kh)^4. \end{aligned} \quad (5.17)$$

Then the finite difference scheme in (5.15) achieves seventh order accuracy for $\mathcal{B}_1 u = \frac{\partial u}{\partial \bar{n}} = g_1$ at the point $(x_0, y_j) \in \partial\Omega|_1$ with reduced pollution effect.

Using Taylor expansion and our sort of technique, the maximum accuracy order of a

6-point finite difference scheme for $\mathcal{B}_1 u = \frac{\partial u}{\partial \bar{n}} - \mathbf{i}k u = g_1$ at the point $(x_0, y_j) \in \partial\Omega|_1$ is six, and the maximum accuracy order of a 6-point finite difference scheme for $\mathcal{B}_1 u = \frac{\partial u}{\partial \bar{n}} = g_1$ at the point $(x_0, y_j) \in \partial\Omega|_1$ is seven.

By symmetry, we can immediately state the stencils for the other three boundary sides. Same accuracy order results as in Theorem 5.3 hold. First, consider the following discretization stencil for $\mathcal{B}_2 u = g_2$ on $\partial\Omega|_2$ with $\mathcal{B}_2 \in \{\frac{\partial}{\partial \bar{n}} - \mathbf{i}k \mathbf{I}_d, \frac{\partial}{\partial \bar{n}}\}$ centered at $(x_{N_1}, y_j) \in \partial\Omega|_2$:

$$\mathcal{L}_h^{\mathcal{B}_2} u_h := \frac{1}{h} \sum_{k=-1}^0 \sum_{\ell=-1}^1 C_{k,\ell}^{\mathcal{B}_2}(u_h)_{N_1+k,j+\ell} = \sum_{(m,n) \in \Lambda_6} f^{(m,n)} h J_{m,n}^{\mathcal{B}_2} + \sum_{n=0}^7 g_2^{(n)} h^{-1} J_{g_2,n}^{\mathcal{B}_2},$$

where $C_{-k,\ell}^{\mathcal{B}_2} = C_{k,\ell}^{\mathcal{B}_1}$ for all $k \in \{0, 1\}$, $\ell \in \{-1, 0, 1\}$, $J_{m,n}^{\mathcal{B}_2} = \sum_{k=-1}^0 \sum_{\ell=-1}^1 C_{k,\ell}^{\mathcal{B}_2} h^{-2} Q_{8,m,n}^V(kh, \ell h)$

for all $(m, n) \in \Lambda_6$, $g_2^{(n)} := \frac{d^n g_2}{dy^n}(y_j)$, $J_{g_2,n}^{\mathcal{B}_2} = \sum_{k=-1}^0 \sum_{\ell=-1}^1 C_{k,\ell}^{\mathcal{B}_2} G_{8,1,n}^V(kh, \ell h)$ for all $n = 0, \dots, 7$.

Second, the stencil for $\mathcal{B}_3 u = g_3$ on $\partial\Omega|_3$ with $\mathcal{B}_3 \in \{\frac{\partial}{\partial \bar{n}} - \mathbf{i}k \mathbf{I}_d, \frac{\partial}{\partial \bar{n}}\}$ centered at $(x_i, y_0) \in \partial\Omega|_3$ is

$$\mathcal{L}_h^{\mathcal{B}_3} u_h := \frac{1}{h} \sum_{k=-1}^1 \sum_{\ell=0}^1 C_{k,\ell}^{\mathcal{B}_3}(u_h)_{i+k,\ell} = \sum_{(m,n) \in \Lambda_6} f^{(m,n)} h J_{m,n}^{\mathcal{B}_3} + \sum_{n=0}^7 g_3^{(n)} h^{-1} J_{g_3,n}^{\mathcal{B}_3},$$

where $C_{\ell,k}^{\mathcal{B}_3} = C_{k,\ell}^{\mathcal{B}_1}$ for all $k \in \{0, 1\}$, $\ell \in \{-1, 0, 1\}$, $J_{m,n}^{\mathcal{B}_3} = \sum_{k=-1}^1 \sum_{\ell=0}^1 C_{k,\ell}^{\mathcal{B}_3} h^{-2} Q_{8,m,n}^H(kh, \ell h)$ for

all $(m, n) \in \Lambda_6$, $Q_{8,m,n}^H$ is defined in (5.12), $g_3^{(n)} := \frac{d^n g_3}{dx^n}(x_i)$, $J_{g_3,n}^{\mathcal{B}_3} = - \sum_{k=-1}^1 \sum_{\ell=0}^1 C_{k,\ell}^{\mathcal{B}_3} G_{8,n,1}^H(kh, \ell h)$ for all $n = 0, \dots, 7$, and $G_{8,n,1}^H$ is defined in (5.12).

Third, the stencil for $\mathcal{B}_4 u = g_4$ on $\partial\Omega|_4$ with $\mathcal{B}_4 \in \{\frac{\partial}{\partial \bar{n}} - \mathbf{i}k \mathbf{I}_d, \frac{\partial}{\partial \bar{n}}\}$ centered at $(x_i, y_{N_2}) \in \partial\Omega|_4$ is

$$\mathcal{L}_h^{\mathcal{B}_4} u_h := \frac{1}{h} \sum_{k=-1}^1 \sum_{\ell=-1}^0 C_{k,\ell}^{\mathcal{B}_4}(u_h)_{i+k,N_2+\ell} = \sum_{(m,n) \in \Lambda_6} f^{(m,n)} h J_{m,n}^{\mathcal{B}_4} + \sum_{n=0}^7 g_4^{(n)} h^{-1} J_{g_4,n}^{\mathcal{B}_4},$$

where $C_{\ell,-k}^{\mathcal{B}_4} = C_{k,\ell}^{\mathcal{B}_1}$ for all $k \in \{0, 1\}$, $\ell \in \{-1, 0, 1\}$, $J_{m,n}^{\mathcal{B}_4} = \sum_{k=-1}^1 \sum_{\ell=-1}^0 C_{k,\ell}^{\mathcal{B}_4} h^{-2} Q_{8,m,n}^H(kh, \ell h)$ for

all $(m, n) \in \Lambda_6$, $g_4^{(n)} := \frac{d^n g_4}{dx^n}(x_i)$, and $J_{g_4,n}^{\mathcal{B}_4} = \sum_{k=-1}^1 \sum_{\ell=-1}^0 C_{k,\ell}^{\mathcal{B}_4} G_{8,n,1}^H(kh, \ell h)$ for all $n = 0, \dots, 7$.

5.2.2.2 Corner points

For clarity of presentation, let us consider the following boundary configuration

$$\begin{aligned} \mathcal{B}_1 u &= \frac{\partial u}{\partial \bar{n}} - iku = g_1 \text{ on } \partial\Omega|_1, & \mathcal{B}_2 u &= u = g_2 \text{ on } \partial\Omega|_2, \\ \mathcal{B}_3 u &= \frac{\partial u}{\partial \bar{n}} = g_3 \text{ on } \partial\Omega|_3, & \mathcal{B}_4 u &= \frac{\partial u}{\partial \bar{n}} - iku = g_4 \text{ on } \partial\Omega|_4. \end{aligned} \quad (5.18)$$

See Fig. 5.3 for an illustration.

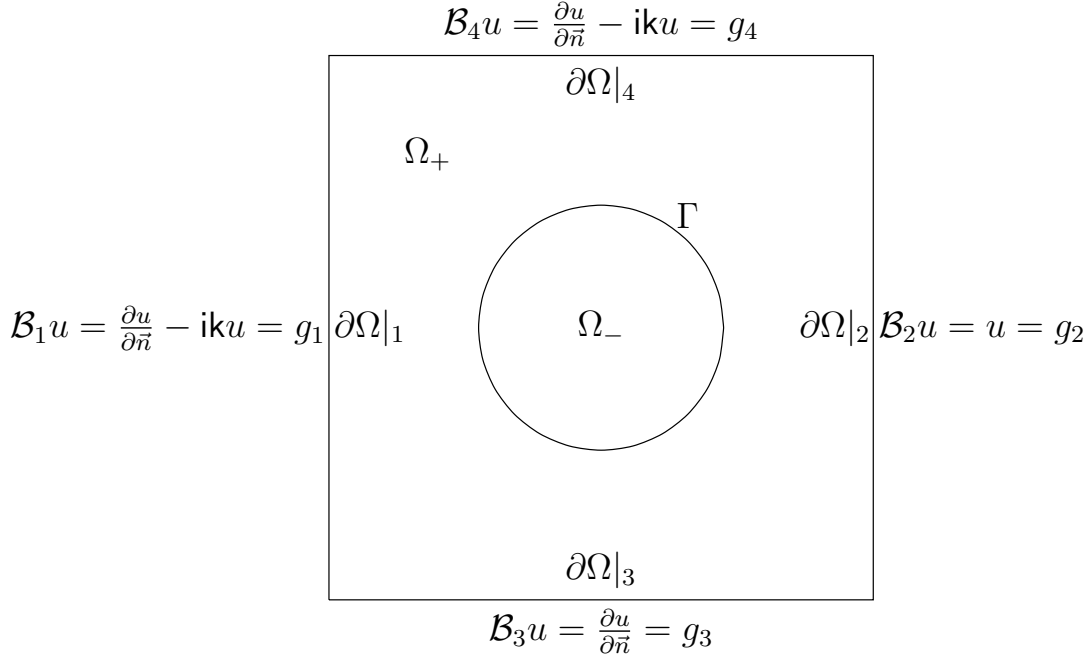


Figure 5.3: An illustration for the boundary configuration in (5.18), where $\psi(x, y) = x^2 + y^2 - 2$.

The corners coming from other boundary configurations can be handled in a similar way. When a corner involves at least one Dirichlet boundary condition, we can use Theorem 5.3 and subsequent remarks to handle it. We denote the bottom left corner (the intersection of $\partial\Omega|_1$ and $\partial\Omega|_3$) by \mathcal{R}_1 , and the top left corner (the intersection of $\partial\Omega|_1$ and $\partial\Omega|_4$) by \mathcal{R}_2 . In what follows, we discuss in detail how the bottom and top left stencils are constructed. The following two theorems provide the 4-point stencils of accuracy order at least six with reduced pollution effect for the left corners. Their proofs are deferred to Section 5.5.

Theorem 5.4. *Assume $\Omega = (l_1, l_2) \times (l_3, l_4)$. Let $(u_h)_{i,j}$ be the numerically approximated solution of the exact solution u of the Helmholtz equation (5.1) at the point (x_i, y_j) . Then*

the following discretization stencil centered at the corner point (x_0, y_0) :

$$\begin{aligned} \mathcal{L}_h^{\mathcal{R}_1} u_h := & \frac{1}{h} \begin{pmatrix} C_{0,0}^{\mathcal{R}_1}(u_h)_{0,0} & +C_{1,0}^{\mathcal{R}_1}(u_h)_{1,0} \\ +C_{0,1}^{\mathcal{R}_1}(u_h)_{0,1} & +C_{1,1}^{\mathcal{R}_1}(u_h)_{1,1} \end{pmatrix} = \sum_{(m,n) \in \Lambda_6} f^{(m,n)} h J_{m,n}^{\mathcal{R}_1} + \sum_{n=0}^7 g_1^{(n)} h^{-1} J_{g_1,n}^{\mathcal{R}_1} + \sum_{n=0}^7 g_3^{(n)} h^{-1} J_{g_3,n}^{\mathcal{R}_1}, \end{aligned} \quad (5.19)$$

where

$$\begin{aligned} C_{1,1}^{\mathcal{R}_1} &= 1 - \frac{2041589737}{10^{10}} kh + \frac{6666011379i}{10^{10}} kh - \frac{1213438849}{10^{10}} (kh)^2 - \frac{254718888i}{25 \times 10^8} (kh)^2 \\ &\quad + \frac{2199377569}{10^{11}} (kh)^3 + \frac{4307308979i}{5 \times 10^{11}} (kh)^3 - \frac{5536966589}{10^{12}} (kh)^4 - \frac{1556373503i}{10^{12}} (kh)^4, \\ C_{1,0}^{\mathcal{R}_1} &= 2 - \frac{2041589737}{5 \times 10^9} kh + \frac{566601138i}{5 \times 10^8} kh - \frac{156034209}{10^9} (kh)^2 - \frac{1629433157i}{10^{10}} (kh)^2 \\ &\quad + \frac{1855012159}{10^{11}} (kh)^3 + \frac{453336943i}{2 \times 10^{10}} (kh)^3 - \frac{3170819689}{5 \times 10^{11}} (kh)^4 + \frac{25677723i}{8 \times 10^9} (kh)^4, \\ C_{0,1}^{\mathcal{R}_1} &= 2 - \frac{2041589737}{5 \times 10^9} kh + \frac{566601138i}{5 \times 10^8} kh - \frac{556752189}{25 \times 10^8} (kh)^2 - \frac{1629433157i}{10^{10}} (kh)^2 \\ &\quad + \frac{3216071983}{10^{11}} (kh)^3 - \frac{3955100649i}{10^{11}} (kh)^3 + \frac{1546871341}{10^{11}} (kh)^4 + \frac{231176972i}{125 \times 10^8} (kh)^4, \\ C_{0,0}^{\mathcal{R}_1} &= -5 + \frac{510397434}{5 \times 10^8} kh + \frac{6699431033i}{10^{11}} kh + \frac{2002755557}{10^{10}} (kh)^2 - \frac{369405469i}{2 \times 10^9} (kh)^2 \\ &\quad - \frac{285280517}{25 \times 10^8} (kh)^3 + \frac{326982886i}{25 \times 10^8} (kh)^3 + \frac{35165403}{25 \times 10^9} (kh)^4 - \frac{9939550949i}{10^{12}} (kh)^4, \end{aligned} \quad (5.20)$$

$g_1^{(n)} := \frac{d^n g_1}{dy^n}(y_0)$, $g_3^{(n)} := \frac{d^n g_3}{dx^n}(x_0)$ for all $n = 0, \dots, 7$, and $\{J_{m,n}^{\mathcal{R}_1}\}_{(m,n) \in \Lambda_6}$, $\{J_{g_1,n}^{\mathcal{R}_1}\}_{n=0}^7$, $\{J_{g_3,n}^{\mathcal{R}_1}\}_{n=0}^7$ are well-defined stencil coefficients that uniquely depend on $\{C_{k,\ell}^{\mathcal{R}_1}\}_{k,\ell \in \{0,1\}}$, achieves sixth order for $\mathcal{B}_1 u = \frac{\partial u}{\partial \bar{n}} - iku = g_1$ and $\mathcal{B}_3 u = \frac{\partial u}{\partial \bar{n}} = g_3$ at the point (x_0, y_0) with reduced pollution effect.

The maximum accuracy order of a 4-point finite difference scheme using Taylor expansion and our sort of technique for $\mathcal{B}_1 u = \frac{\partial u}{\partial \bar{n}} - iku = g_1$ and $\mathcal{B}_3 u = \frac{\partial u}{\partial \bar{n}} = g_3$ at the point (x_0, y_0) is six.

Theorem 5.5. Assume $\Omega = (l_1, l_2) \times (l_3, l_4)$. Let $(u_h)_{i,j}$ be the numerically approximated solution of the exact solution u of the Helmholtz equation (5.1) at the point (x_i, y_j) . Then the following discretization stencil centered at the corner point (x_0, y_{N_2}) :

$$\begin{aligned} \mathcal{L}_h^{\mathcal{R}_2} u_h := & \frac{1}{h} \begin{pmatrix} C_{1,0}^{\mathcal{R}_2}(u_h)_{0,N_2-1} & +C_{1,-1}^{\mathcal{R}_2}(u_h)_{1,N_2-1} \\ +C_{0,0}^{\mathcal{R}_2}(u_h)_{0,N_2} & +C_{1,0}^{\mathcal{R}_2}(u_h)_{1,N_2} \end{pmatrix} \\ = & \sum_{(m,n) \in \Lambda_6} f^{(m,n)} h J_{m,n}^{\mathcal{R}_2} + \sum_{n=0}^7 g_1^{(n)} h^{-1} J_{g_1,n}^{\mathcal{R}_2} + \sum_{n=0}^7 g_4^{(n)} h^{-1} J_{g_4,n}^{\mathcal{R}_2}, \end{aligned} \quad (5.21)$$

where

$$\begin{aligned}
C_{1,-1}^{\mathcal{R}_2} &= 1 - \frac{535927359}{5 \times 10^9} kh + \frac{131913924i}{10^8} kh - \frac{4650641357}{10^{10}} (kh)^2 - \frac{3255802571i}{10^{11}} (kh)^2 \\
&\quad - \frac{1802358661}{10^{13}} (kh)^3 - \frac{137039551i}{25 \times 10^8} (kh)^3 - \frac{116115549}{625 \times 10^8} (kh)^4 - \frac{390383949i}{2 \times 10^{11}} (kh)^4, \\
C_{1,0}^{\mathcal{R}_2} &= 2 - \frac{428741887}{2 \times 10^9} kh + \frac{2238278479i}{10^9} kh - \frac{5558059089}{10^{10}} (kh)^2 - \frac{278023284i}{125 \times 10^8} (kh)^2 \\
&\quad + \frac{1525711827}{5 \times 10^{11}} (kh)^3 - \frac{57317954i}{5 \times 10^8} (kh)^3 + \frac{2099795921}{10^{11}} (kh)^4 + \frac{1100929919i}{2 \times 10^{11}} (kh)^4, \\
C_{0,0}^{\mathcal{R}_2} &= -5 + \frac{1339818397}{25 \times 10^8} kh + \frac{2043038021i}{10^{10}} kh - \frac{1519079742}{5 \times 10^8} (kh)^2 - \frac{2830355397i}{5 \times 10^9} (kh)^2 \\
&\quad - \frac{82143257}{5 \times 10^8} (kh)^3 + \frac{3401956461i}{10^{10}} (kh)^3, + \frac{1420360677}{5 \times 10^9} (kh)^4 + \frac{4391249797i}{10^{11}} (kh)^4,
\end{aligned} \tag{5.22}$$

$g_1^{(n)} := \frac{d^n g_1}{dy^n}(y_{N_2})$, $g_4^{(n)} := \frac{d^n g_4}{dx^n}(x_0)$ for all $n = 0, \dots, 7$, and $\{J_{m,n}^{\mathcal{R}_2}\}_{(m,n) \in \Lambda_6}$, $\{J_{g_1,n}^{\mathcal{R}_2}\}_{n=0}^7$, $\{J_{g_4,n}^{\mathcal{R}_2}\}_{n=0}^7$ are well-defined stencil coefficients that uniquely depend on $\{C_{k,\ell}^{\mathcal{R}_2}\}_{k \in \{0,1\}, \ell \in \{-1,0\}}$ with $C_{0,-1}^{\mathcal{R}_2} = C_{1,0}^{\mathcal{R}_2}$, achieves seventh order accuracy for $\mathcal{B}_1 u = \frac{\partial u}{\partial \bar{n}} - iku = g_1$ and $\mathcal{B}_4 u = \frac{\partial u}{\partial \bar{n}} - iku = g_4$ at the point (x_0, y_{N_2}) with reduced pollution effect.

The maximum accuracy order of a 4-point finite difference scheme using Taylor expansion and our sort of technique for $\mathcal{B}_1 u = \frac{\partial u}{\partial \bar{n}} - iku = g_1$ and $\mathcal{B}_4 u = \frac{\partial u}{\partial \bar{n}} - iku = g_4$ at the point (x_0, y_{N_2}) is seven. Note that the right-hand sides of (5.19) and (5.21) can be explicitly recovered. See the proofs of Theorems 5.4 and 5.5 in Section 5.5 for details.

5.2.3 Stencils for irregular points

Let (x_i, y_j) be an irregular point (i.e., both $d_{i,j}^+$ and $d_{i,j}^-$ are nonempty) and let us take a base point $(x_i^*, y_j^*) \in \Gamma \cap (x_i - h, x_i + h) \times (y_j - h, y_j + h)$ on the interface Γ and inside $(x_i - h, x_i + h) \times (y_j - h, y_j + h)$. By (5.3), we have

$$x_i^* = x_i - v_0 h \quad \text{and} \quad y_j^* = y_j - w_0 h \quad \text{with} \quad -1 < v_0, w_0 < 1 \quad \text{and} \quad (x_i^*, y_j^*) \in \Gamma. \tag{5.23}$$

Recall that u_{\pm} and f_{\pm} represent the solution u and source term f in Ω_+ or Ω_- , respectively, and

$$u_{\pm}^{(m,n)} := \frac{\partial^{m+n} u_{\pm}}{\partial m x \partial n y}(x_i^*, y_j^*), \quad f_{\pm}^{(m,n)} := \frac{\partial^{m+n} f_{\pm}}{\partial m x \partial n y}(x_i^*, y_j^*).$$

Identity similar to (5.10) still holds:

$$u_{\pm}(x + x_i^*, y + y_j^*) = \sum_{(m,n) \in \Lambda_{M+1}^{V,1}} u_{\pm}^{(m,n)} G_{M+1,m,n}^V(x, y) + \sum_{(m,n) \in \Lambda_{M_f-1}} f_{\pm}^{(m,n)} Q_{M_f+1,m,n}^V(x, y) + \mathcal{O}(h^{M+2}),$$

for $x, y \in (-2h, 2h)$, where $\Lambda_{M+1}^{V,1}$ is defined in (5.5), Λ_{M_f-1} is defined in (1.8), $G_{M+1,m,n}^V(x, y)$ is defined in (5.9), $Q_{M_f+1,m,n}^V(x, y)$ is defined in (5.8).

Theorem 5.6. Let u be the solution to the Helmholtz interface problem in (5.1) and the base point $(x_i^*, y_j^*) \in \Gamma$ be parameterized near (x_i^*, y_j^*) by (1.5). Then

$$\begin{aligned} u_-^{(m',n')} &= u_+^{(m',n')} + \sum_{(m,n) \in \Lambda_{M-2}} \left(T_{m',n',m,n}^+ f_+^{(m,n)} + T_{m',n',m,n}^- f_-^{(m,n)} \right) \\ &\quad + \sum_{p=0}^M T_{m',n',p}^{g_0^\Gamma} g_{0,p}^\Gamma + \sum_{p=0}^{M-1} T_{m',n',p}^{g_1^\Gamma} g_{1,p}^\Gamma, \quad \forall (m', n') \in \Lambda_M^{V,1}, \end{aligned}$$

where all the transmission coefficients $T^\pm, T^{g_0^\Gamma}, T^{g_1^\Gamma}$ are uniquely determined by $r^{(k)}(0), s^{(k)}(0)$, and k for $k = 0, \dots, M$.

Proof. The proof closely follows from the proof of Theorem 2.4. \square

Next, we state the compact 9-point finite difference stencil for interior irregular points.

Theorem 5.7. Let $(u_h)_{i,j}$ be the numerical solution of (5.1) at an interior irregular point (x_i, y_j) . Pick a base point (x_i^*, y_j^*) as in (5.23). Then the following compact 9-point scheme centered at the interior irregular point (x_i, y_j)

$$\begin{aligned} \mathcal{L}_h^\Gamma u_h &:= \frac{1}{h} \left(C_{1,1}(u_h)_{i-1,j-1} + C_{1,0}(u_h)_{i,j-1} + C_{1,1}(u_h)_{i+1,j-1} \right. \\ &\quad + C_{1,0}(u_h)_{i-1,j} + C_{0,0}(u_h)_{i,j} + C_{1,0}(u_h)_{i+1,j} \\ &\quad \left. + C_{1,1}(u_h)_{i-1,j+1} + C_{1,0}(u_h)_{i,j+1} + C_{1,1}(u_h)_{i+1,j+1} \right) \\ &= \sum_{(m,n) \in \Lambda_6} f_+^{(m,n)} h J_{m,n}^+ + \sum_{(m,n) \in \Lambda_6} f_-^{(m,n)} h J_{m,n}^- + \sum_{p=0}^8 g_{0,p}^\Gamma h^{-1} J_p^{g_0^\Gamma} + \sum_{p=0}^7 g_{1,p}^\Gamma h^{-1} J_p^{g_1^\Gamma}, \end{aligned}$$

achieves seventh order accuracy, where $\{C_{k,\ell}\}_{k,\ell \in \{-1,0,1\}}$ are defined in (5.14), $J_{m,n}^\pm := J_{m,n}^{\pm,0} + J_{m,n}^{\pm,T}$ for all $(m, n) \in \Lambda_6$,

$$\begin{aligned} J_{m,n}^{\pm,0} &:= \sum_{(k,\ell) \in d_{i,j}^\pm} C_{k,\ell} h^{-2} Q_{8,m,n}^V((v_0 + k)h, (w_0 + \ell)h), \quad \forall (m, n) \in \Lambda_6, \\ J_{m,n}^{\pm,T} &:= \sum_{(m',n') \in \Lambda_8^{V,1}} I_{m',n'}^\pm h^{-2} T_{m',n',m,n}^\pm, \quad \forall (m, n) \in \Lambda_6, \\ J_p^{g_0^\Gamma} &:= \sum_{(m',n') \in \Lambda_8^{V,1}} I_{m',n'}^- T_{m',n',p}^{g_0^\Gamma}, \quad \forall p = 0, \dots, 8, \quad J_p^{g_1^\Gamma} := \sum_{(m',n') \in \Lambda_8^{V,1}} I_{m',n'}^- T_{m',n',p}^{g_1^\Gamma}, \quad \forall p = 0, \dots, 7, \\ I_{m,n}^- &:= \sum_{(k,\ell) \in d_{i,j}^-} C_{k,\ell} G_{8,m,n}^V((v_0 + k)h, (w_0 + \ell)h), \quad \forall (m, n) \in \Lambda_8^{V,1}. \end{aligned}$$

The maximum accuracy order of a compact 9-point finite difference stencil using Taylor expansion and our sort of technique for (5.1) at an interior irregular point (x_i, y_j) is seven.

Proof. The proof closely follows from the proof of Theorem [2.5](#). □

5.3 Numerical experiments

In the following numerical experiments, ‘[20](#)’, ‘[104](#)’ and ‘[111](#)’ correspond to the sixth order compact finite difference methods proposed in [20](#), [104](#) and [111](#) respectively. ‘Proposed’ corresponds to the sixth order compact finite difference method with reduced pollution effect in Section [5.2](#) of this chapter. Recall that $\frac{2\pi}{kh}$ corresponds to the number of points per wavelength.

5.3.1 Numerical examples with no interfaces

We provide four numerical experiments here.

Example 5.1. Consider the problem [\(5.1\)](#) in $\Omega = (0, 1)^2$ with $f = 0$ and all Dirichlet boundary conditions such that the boundary data g_1, \dots, g_4 are picked such that the exact solution $u(x, y, \theta) = \exp(ik(\cos(\theta)x + \sin(\theta)y))$ is the plane wave with the angle θ . We define the following average error for plane wave solutions along all different angles θ by

$$\frac{\|u_h - u\|_{2,w}}{\|u\|_{2,w}} := \frac{1}{N_3} \sum_{k=0}^{N_3-1} \sqrt{\frac{\sum_{i=0}^{N_1} \sum_{j=0}^{N_1} ((u_h)_{i,j,k} - u(x_i, y_j, \theta_k))^2}{\sum_{i=0}^{N_1} \sum_{j=0}^{N_1} (u(x_i, y_j, \theta_k))^2}},$$

where $N_1 = 2^J$, $\theta_k = kh_\theta$, $h_\theta = 2\pi/N_3$ for $J, N_3 \in \mathbb{N}_0$, and $(u_h)_{i,j,k}$ is the value of the numerical solution u_h at the grid point (x_i, y_j) with a plane wave angle θ_k . See Table [5.1](#) for numerical results.

Example 5.2. Consider the problem [\(5.1\)](#) in $\Omega = (0, 1)^2$ with the boundary conditions

$$\begin{aligned} u(0, y) &= g_1, & \text{and} & & u(1, y) &= g_2 & \text{for } y \in (0, 1), \\ u(x, 0) &= g_3, & \text{and} & & u_y(x, 1) - iku(x, 1) &= 0 & \text{for } x \in (0, 1), \end{aligned}$$

where g_1, \dots, g_4 and f are chosen such that the exact solution $u = (y-1) \cos(\alpha x) \sin(\beta(y-1))$ with $\alpha, \beta \in \mathbb{R}$. See Table [5.2](#) for numerical results for various choices of α and β .

Example 5.3. Consider the problem [\(5.1\)](#) in $\Omega = (0, 1)^2$ with boundary conditions in [\(5.18\)](#). I.e., $\mathcal{B}_1 u = \frac{\partial u}{\partial \bar{n}} - iku = g_1$ on $\partial\Omega|_1$, $\mathcal{B}_2 u = u = g_2$ on $\partial\Omega|_2$, $\mathcal{B}_3 u = \frac{\partial u}{\partial \bar{n}} = g_3$ on $\partial\Omega|_3$ and $\mathcal{B}_4 u = \frac{\partial u}{\partial \bar{n}} - iku = g_4$ on $\partial\Omega|_4$, where g_1, \dots, g_4 and f are chosen such that the exact solution

Table 5.1: Numerical results for Example 5.1 with $h = 1/2^J$. The ratio r is equal to $\frac{\|u_h - u\|_{2,w}}{\|u\|_{2,w}}$ of [20] divided by $\frac{\|u_h - u\|_{2,w}}{\|u\|_{2,w}}$ of our proposed method. In other words, for the same mesh size h with $h = 2^{-J}$, the error of [20] is r times larger than that of our proposed method.

J	$k = 50, N_3 = 50$					$k = 150, N_3 = 30$					$k = 450, N_3 = 30$							
	[20]	Proposed		order	$\frac{2\pi}{kh}$	r	[20]	Proposed		order	$\frac{2\pi}{kh}$	r	[20]	Proposed		order	$\frac{2\pi}{kh}$	r
$\frac{\ u_h - u\ _{2,w}}{\ u\ _{2,w}}$				$\frac{\ u_h - u\ _{2,w}}{\ u\ _{2,w}}$	$\frac{\ u_h - u\ _{2,w}}{\ u\ _{2,w}}$	$\frac{\ u_h - u\ _{2,w}}{\ u\ _{2,w}}$				$\frac{\ u_h - u\ _{2,w}}{\ u\ _{2,w}}$	$\frac{\ u_h - u\ _{2,w}}{\ u\ _{2,w}}$	$\frac{\ u_h - u\ _{2,w}}{\ u\ _{2,w}}$						
4	9.83E+0	4.87E-01		2.0	20.2													
5	1.57E-02	1.01E-03	8.9	4.0	15.5													
6	5.01E-05	1.20E-05	6.4	8.0	4.19	3.67E+0	6.25E-02		2.7	58.7								
7	2.35E-07	1.77E-07	6.1	16.1	1.33	6.04E-03	6.82E-04	6.5	5.4	8.85								
8	2.78E-09	2.72E-09	6.0	32.2	1.02	2.56E-05	9.25E-06	6.2	10.7	2.77	1.26E+0	5.43E-02				3.6	23.1	
9						1.78E-07	1.40E-07	6.0	21.4	1.27	4.72E-03	7.83E-04	6.1	7.1	6.03			
10											2.25E-05	1.13E-05	6.1	14.3	1.99			
11											1.85E-07	1.75E-07	6.0	28.6	1.06			

Table 5.2: Numerical results of Example 5.2 with $h = 1/2^J$ and $k = 300$. The ratio r_1 is equal to $\frac{\|u_h - u\|_2}{\|u\|_2}$ of [104] divided by $\frac{\|u_h - u\|_2}{\|u\|_2}$ of our proposed method and the ratio r_2 is equal to $\frac{\|u_h - u\|_2}{\|u\|_2}$ of [111] divided by $\frac{\|u_h - u\|_2}{\|u\|_2}$ of our proposed method. In other words, for the same grid size h with $h = 2^{-J}$, the errors of [104] and [111] are r_1 and r_2 times larger than those of our proposed method, respectively.

J	$\frac{2\pi}{kh}$	$\alpha = 50, \beta = 290$					$\alpha = 100, \beta = 275$					$\alpha = 150, \beta = 255$				
		[104]	[111]	Proposed	r_1	r_2	[104]	[111]	Proposed	r_1	r_2	[104]	[111]	Proposed	r_1	r_2
$\frac{\ u_h - u\ _2}{\ u\ _2}$			$\frac{\ u_h - u\ _2}{\ u\ _2}$	$\frac{\ u_h - u\ _2}{\ u\ _2}$	$\frac{\ u_h - u\ _2}{\ u\ _2}$			$\frac{\ u_h - u\ _2}{\ u\ _2}$	$\frac{\ u_h - u\ _2}{\ u\ _2}$	$\frac{\ u_h - u\ _2}{\ u\ _2}$						
7	2.7	1.1E+0	9.8E-02	3.8E-02	29	2.6	2.4E+0	2.1E-01	4.4E-02	54	4.6	4.4E+0	1.2E-01	5.8E-02	77	2.1
8	5.4	8.6E-03	6.1E-04	1.3E-04	65	4.6	1.2E-02	1.3E-03	3.1E-04	40	4.4	1.7E-02	8.3E-04	1.3E-04	134	6.5
9	10.7	1.2E-04	8.4E-06	2.8E-06	43	3.0	1.7E-04	1.8E-05	5.7E-06	30	3.2	2.4E-04	1.1E-05	2.0E-06	121	5.7
10	21.4	1.8E-06	1.2E-07	4.6E-08	39	2.6	2.6E-06	2.7E-07	9.2E-08	28	2.9	3.7E-06	1.7E-07	3.3E-08	114	5.1
J	$\frac{2\pi}{kh}$	$\alpha = 200, \beta = 200$					$\alpha = 250, \beta = 160$					$\alpha = 290, \beta = 50$				
		[104]	[111]	Proposed	r_1	r_2	[104]	[111]	Proposed	r_1	r_2	[104]	[111]	Proposed	r_1	r_2
$\frac{\ u_h - u\ _2}{\ u\ _2}$			$\frac{\ u_h - u\ _2}{\ u\ _2}$	$\frac{\ u_h - u\ _2}{\ u\ _2}$	$\frac{\ u_h - u\ _2}{\ u\ _2}$			$\frac{\ u_h - u\ _2}{\ u\ _2}$	$\frac{\ u_h - u\ _2}{\ u\ _2}$	$\frac{\ u_h - u\ _2}{\ u\ _2}$						
7	2.7	1.1E+0	1.3E-01	1.4E-01	8	0.9	6.0E+0	1.8E-01	4.8E-02	125	3.7	8.9E+0	1.3E-01	5.5E-02	162	2.4
8	5.4	7.5E-03	9.7E-04	3.8E-04	20	2.6	4.0E-02	1.1E-03	8.1E-05	492	14.1	9.8E-03	7.4E-04	1.5E-04	66	4.9
9	10.7	1.1E-04	1.3E-05	3.4E-06	33	3.9	5.6E-04	1.6E-05	2.1E-06	264	7.6	1.5E-04	1.0E-05	1.6E-06	92	6.2
10	21.4	1.7E-06	2.0E-07	4.5E-08	38	4.4	8.6E-06	2.3E-07	3.7E-08	234	6.3	2.3E-06	1.5E-07	2.3E-08	101	6.4

$u = \sin(\alpha x + \beta y)$ with $\alpha, \beta \in \mathbb{R}$. See Table 5.3 for numerical results for various choices of α and β .

Table 5.3: Numerical results of Example 5.3 with $h = 1/2^J$ using our proposed method.

J	$k = 450, \alpha = 400, \beta = 200$					$k = 600, \alpha = 300, \beta = 500$				
	$\frac{2\pi}{kh}$	$\frac{\ u_h - u\ _2}{\ u\ _2}$	order	$\ u_h - u_{h/2}\ _2$	order	$\frac{2\pi}{kh}$	$\frac{\ u_h - u\ _2}{\ u\ _2}$	order	$\ u_h - u_{h/2}\ _2$	order
7	1.79	1.3753E+01		9.8073E+00		1.34	9.0200E+01		6.4272E+01	
8	3.57	1.7358E-02	9.630	1.2212E-02	9.649	2.68	9.4259E-02	9.902	6.6801E-02	9.910
9	7.15	1.6528E-04	6.715	1.1540E-04	6.725	5.36	2.7428E-04	8.425	1.9430E-04	8.425
10	14.30	2.4370E-06	6.084	1.6971E-06	6.087	10.72	1.7971E-06	7.254	1.2453E-06	7.286
11	28.60	3.9410E-08	5.950			21.45	4.5869E-08	5.292		

Example 5.4. Consider the problem (5.1) in $\Omega = (0, 1)^2$ with boundary conditions in (5.18), where $f(x, y) = k^2 \sin(8x) \cos(6y)$, $g_1 = \sin(5y)$, $g_2 = 0$, $g_3 = (x - 1) \sin(4x)$, and $g_4 = \cos(5x)$. Note that the exact solution u is unknown in this example. See Table 5.4 and Fig. 5.4 for numerical results.

Table 5.4: Numerical results of Example 5.4 with $h = 1/2^J$ using our proposed method.

J	$k = 200$				$k = 400$				$k = 800$			
	$\frac{2\pi}{kh}$	$\ u_h - u_{h/2}\ _2$	order	$\ u_h\ _2$	$\frac{2\pi}{kh}$	$\ u_h - u_{h/2}\ _2$	order	$\ u_h\ _2$	$\frac{2\pi}{kh}$	$\ u_h - u_{h/2}\ _2$	order	$\ u_h\ _2$
6	2.01	8.776E-01		5.81E-01								
7	4.02	3.716E-03	7.88	9.84E-01	2.01	7.936E-01		5.28E-01				
8	8.04	4.430E-05	6.39	9.81E-01	4.02	7.410E-03	6.74	9.76E-01	2.01	8.453E-01		5.08E-01
9	16.08			9.80E-01	8.04	8.579E-05	6.43	9.75E-01	4.02	1.486E-02	5.83	9.70E-01
10					16.08			9.74E-01	8.04	1.715E-04	6.44	9.70E-01
11									16.08			9.69E-01

5.3.2 Numerical examples with interfaces

We provide three numerical experiments here.

Example 5.5. Consider the problem (5.1) in $\Omega = (-3/2, 3/2)^2$ with boundary conditions in (5.18), where $k = 100$, $\Gamma := \{(x, y) \in \Omega : \psi(x, y) = 0\}$ with $\psi(x, y) = y^2/2 + x^2/(1+x^2) - 1/2$ (see Fig. 5.5 (left)), $g_0^\Gamma = -1$, and $g_1^\Gamma = 0$. The boundary data g_1, \dots, g_4 and f_\pm are chosen such that the exact solution u is given by $u_+ = u\chi_{\Omega_+} = \cos(50x) \cos(80y)$ and $u_- = u\chi_{\Omega_-} = \cos(50x) \cos(80y) + 1$. See Table 5.5 for numerical results.

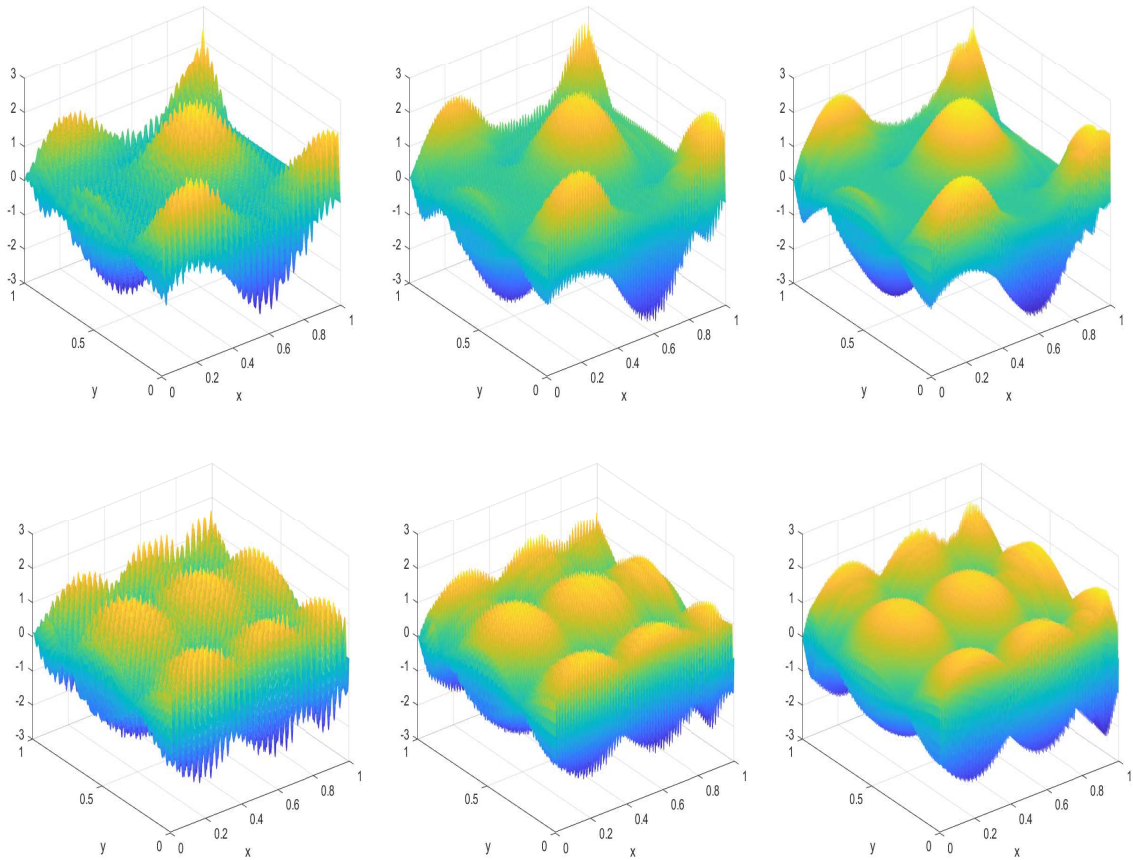


Figure 5.4: First row: the real part of u_h in Example 5.4, where $k = 200$ and $h = 1/2^9$ (left), $k = 400$ and $h = 1/2^{10}$ (middle), $k = 800$ and $h = 1/2^{11}$ (right). Second row: the imaginary part of u_h in Example 5.4, where $k = 200$ and $h = 1/2^9$ (left), $k = 400$ and $h = 1/2^{10}$ (middle), $k = 800$ and $h = 1/2^{11}$ (right).

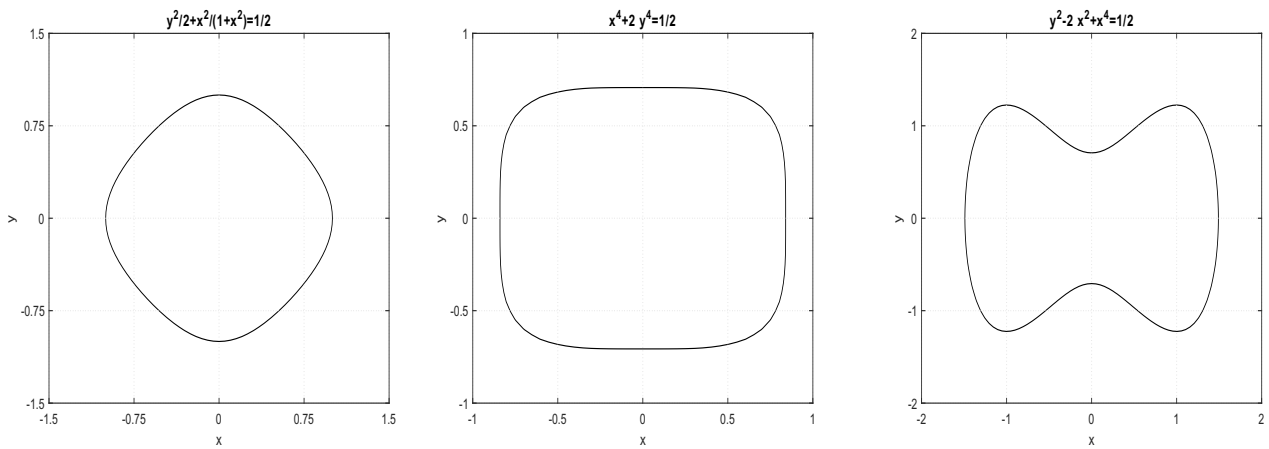


Figure 5.5: $y^2/2 + x^2/(1+x^2) = 1/2$ (left), $x^4 + 2y^4 = 1/2$ (middle), and $y^2 - 2x^2 + x^4 = 1/2$ (right).

Example 5.6. Consider the problem (5.1) in $\Omega = (-1, 1)^2$ with boundary conditions in (5.18), where $k = 300$, $\Gamma := \{(x, y) \in \Omega : \psi(x, y) = 0\}$ with $\psi(x, y) = x^4 + 2y^4 - 1/2$ (see Fig. 5.5 (middle)), $f_+ = 75^2 \sin(3(x+y))$, $f_- = 75^2 \cos(4x) \cos(3y)$, $g_0^\Gamma = \sin(2\pi x) \sin(2\pi y) + 3$, and $g_1^\Gamma = \cos(2\pi x) \cos(2\pi y)$. The following boundary data are given by $g_1 = e^y + e^{-y}$, $g_2 = 0$, $g_3 = (x-1)e^x$, and $g_4 = \sin(2x)$. Note that the exact solution u is unknown in this example. See Table 5.5 for numerical results.

Example 5.7. Consider the problem (5.1) in $\Omega = (-2, 2)^2$ with boundary conditions in (5.18), where $k = 150$, $\Gamma := \{(x, y) \in \Omega : \psi(x, y) = 0\}$ with $\psi(x, y) = y^2 - 2x^2 + x^4 - 1/2$ (see Fig. 5.5 (right)), $f_+ = \sin(5(x-y))$, $f_- = 10^4 \sin(5x) \sin(5y)$, $g_0^\Gamma = \sin(2\pi(x-y))$, and $g_1^\Gamma = \cos(2\pi(x+y))$. The following boundary data are given by $g_1 = \cos(y) \sin(y)$, $g_2 = 0$, $g_3 = \sin(2x-4)$, and $g_4 = e^x \sin(x)$. Note that the exact solution u is unknown in this example. See Table 5.5 for numerical results.

Table 5.5: Numerical results of Examples 5.5 to 5.7 with $h = (l_2 - l_1)/2^J$ using our proposed method.

J	Example 5.5 with $h = \frac{3}{2^J}$				Example 5.6 with $h = \frac{2}{2^J}$				Example 5.7 with $h = \frac{4}{2^J}$				
	$\frac{2\pi}{hk}$	$\frac{\ u_h - u\ _2}{\ u\ _2}$	order	$\ u_h - u_{h/2}\ _2$	order	$\frac{2\pi}{hk}$	$\ u_h - u_{h/2}\ _2$	order	$\ u_{h/2}\ _2$	$\frac{2\pi}{hk}$	$\ u_h - u_{h/2}\ _2$	order	$\ u_{h/2}\ _2$
7	2.7	1.28E+00		2.90E+00		2.7	1.06E+01		7.039	2.7	8.19E+00		3.467
8	5.4	2.44E-03	9.0	5.51E-03	9.0	5.4	1.49E-02	9.5	7.037	5.4	7.96E-03	10.0	3.469
9	10.7	5.82E-06	8.7	1.31E-05	8.7	10.7	1.69E-04	6.5	7.035	10.7	7.66E-05	6.7	3.468

5.4 Conclusion

Our contributions of this chapter are as follows:

- (1) Our proposed compact finite difference scheme attains at least sixth accuracy order and reduced pollution effect everywhere on the domain for the problem (5.1).
- (2) Our method that reduces the pollution effect differs from existing dispersion minimization methods in the literature in several ways. First, our method does not require us to compute the numerical wavenumber. Second, we use our pollution minimization procedure in the construction of all interior, boundary, and corner stencils.
- (3) We provide a comprehensive treatment of mixed inhomogeneous boundary conditions. In particular, our approach is capable of handling all possible combinations of Dirichlet, Neumann, and impedance boundary conditions for the 2D Helmholtz equation defined on a rectangular domain.

- (4) Our proposed compact finite difference scheme with reduced pollution effect outperforms several state-of-the-art finite difference schemes in the literature, particularly in the pre-asymptotic critical region where kh is near 1. When a large wavenumber k is present, this means that our proposed finite difference scheme is more accurate than others at a computationally feasible grid size.
- (5) For the irregular points, we derive a seventh order compact finite difference scheme to handle nonzero jump functions at the interface. For a fixed wavenumber k and for any given interface and boundary data, the coefficient matrix of our linear system does not change; only the vector on the right-hand side of the linear system changes.
- (6) In the numerical experiments, we compare our proposed scheme with the latest compact schemes. The numerical results show that our proposed scheme could produce smaller errors even the coefficients of our scheme are simpler.

5.5 Proofs of Theorems 5.2 to 5.5

In this section, we prove the main results stated in Section 5.2. The idea of proofs is to first construct all possible compact stencils with the maximum accuracy order based on Taylor expansion and our sort of technique, and then to minimize the average truncation error of plane waves over the free parameters of stencils to reduce pollution effect.

Proof of Theorem 5.2. Let us consider the following discretization operator at a regular point (x_i, y_j) :

$$\mathcal{L}_h u := h^{-2} \sum_{k=-1}^1 \sum_{\ell=-1}^1 C_{k,\ell}(h) u(x_i + kh, y_j + \ell h) \quad \text{with} \quad C_{k,\ell}(h) = \sum_{p=0}^{M+1} c_{k,\ell,p} (kh)^p,$$

where $c_{k,\ell,p} \in \mathbb{R}$ for all $k, \ell \in \{-1, 0, 1\}$. Furthermore, we let $C_{-1,-1} = C_{-1,1} = C_{1,-1} = C_{1,1}$ and $C_{-1,0} = C_{0,-1} = C_{0,1} = C_{1,0}$ for symmetry. Approximating $u(x_i + kh, y_j + \ell h)$ as in (5.10) with $x_i^* = x_i$ and $y_j^* = y_j$, we have

$$\mathcal{L}_h u = \sum_{(m,n) \in \Lambda_{M+1}^{V_1}} u^{(m,n)} h^{-2} I_{m,n} + \sum_{(m,n) \in \Lambda_{M_f-1}} f^{(m,n)} J_{m,n} = \mathcal{O}(h^M), \quad h \rightarrow 0,$$

where

$$I_{m,n} := \sum_{k=-1}^1 \sum_{\ell=-1}^1 C_{k,\ell} G_{M+1,m,n}^V(kh, \ell h), \quad \text{and} \quad J_{m,n} := \sum_{k=-1}^1 \sum_{\ell=-1}^1 C_{k,\ell} h^{-2} Q_{M_f+1,m,n}^V(kh, \ell h). \quad (5.24)$$

Let

$$\mathcal{L}_h u_h := h^{-2} \sum_{k=-1}^1 \sum_{\ell=-1}^1 C_{k,\ell} (u_h)_{i+k,j+\ell} = \sum_{(m,n) \in \Lambda_{M_f-1}} f^{(m,n)} J_{m,n}. \quad (5.25)$$

Then

$$\mathcal{L}_h(u - u_h) = \mathcal{L}_h u - \sum_{(m,n) \in \Lambda_{M_f-1}} f^{(m,n)} J_{m,n} = \mathcal{O}(h^M), \quad h \rightarrow 0,$$

if $I_{m,n}$ in (5.24) satisfies

$$I_{m,n} = \mathcal{O}(h^{M+2}), \quad h \rightarrow 0, \quad \text{for all } (m,n) \in \Lambda_{M+1}^{V,1}. \quad (5.26)$$

By calculation, we find that $M = 6$ is the maximum positive integer such that the linear system (5.26) has a non-trivial solution. All such non-trivial solutions for $M = 6$ can be uniquely written (up to a constant multiple) as

$$\begin{aligned} C_{1,1} &= c_9(kh)^7 + c_3(kh)^6 + c_2(kh)^5 + c_1(kh)^4 + (-12c_2 + c_4 - 6c_6 + 24c_{10} + 6c_{11} + 24c_9)(kh)^3 + (1/15 \\ &\quad + 4c_1 + 2c_5 - 8c_7 - 2c_8 - 8c_3)(kh)^2 + (-240c_2 + 15c_4 - 120c_6 + 480c_{10} + 120c_{11} + 480c_9)(kh) + 1 \\ C_{1,0} &= c_{10}(kh)^7 + c_7(kh)^6 + c_6(kh)^5 + c_5(kh)^4 + c_4(kh)^3 + (1/15 + 16c_1 + 8c_5 - 32c_7 - 8c_8 - 32c_3)(kh)^2 \\ &\quad + (-960c_2 + 60c_4 - 480c_6 + 1920c_{10} + 480c_{11} + 1920c_9)(kh) + 4 \\ C_{0,0} &= c_{11}(kh)^7 + c_8(kh)^6 + (92c_2 - (9/2)c_4 + 44c_6 - 192c_{10} - 48c_{11} - 192c_9)(kh)^5 + (-3/10 + 20c_1 + 8c_5 \\ &\quad - 48c_7 - 12c_8 - 48c_3)(kh)^4 + (-1392c_2 + 82c_4 - 696c_6 + 2784c_{10} + 696c_{11} + 2784c_9)(kh)^3 \\ &\quad + (82/15 - 80c_1 - 40c_5 + 160c_7 + 40c_8 + 160c_3)(kh)^2 + (4800c_2 - 300c_4 + 2400c_6 - 9600c_{10} \\ &\quad - 2400c_{11} - 9600c_9)(kh) - 20, \end{aligned} \quad (5.27)$$

where $c_i \in \mathbb{R}$ for $i = 1, \dots, 11$ are free parameters. Note that any interior symmetric compact 9-point stencil has accuracy order 6 if and only if the 7th-degree Taylor polynomials of the stencil coefficients are given by (5.27). Choosing $M_f = 7$ in (5.24) and (5.25) yields the right-hand side of (5.13).

Next, consider a general compact 9-point stencil $\{C_{k,\ell}^w\}_{k,\ell \in \{-1,0,1\}}$ parameterized by $C_{1,1}^w, C_{1,0}^w \in \mathbb{R}$ satisfying

$$C_{-1,-1}^w = C_{-1,1}^w = C_{1,-1}^w = C_{1,1}^w, \quad C_{-1,0}^w = C_{0,-1}^w = C_{0,1}^w = C_{1,0}^w, \quad \text{and} \quad C_{0,0}^w = -20,$$

where we normalized the stencil by $C_{0,0}^w = -20$. Take a plane wave solution $u(x, y, \theta) := \exp(ik(\cos(\theta)x + \sin(\theta)y))$ for any $\theta \in [0, 2\pi)$. Clearly, we have $\Delta u + k^2 u = 0$. Hence, the truncation error associated with the general compact 9-point stencil coefficients $\{C_{k,\ell}^w\}_{k,\ell \in \{-1,0,1\}}$ at the grid point $(x_i, y_j) \notin \partial\Omega$ is $\frac{1}{h^2}(T(\theta|kh))_{x_i, y_j}$, where

$$(T(\theta|kh))_{x_i, y_j} := \sum_{k=-1}^1 \sum_{\ell=-1}^1 C_{k,\ell}^w \exp(ik(\cos(\theta)(x_i + kh) + \sin(\theta)(y_j + \ell h))).$$

Recall that $\frac{2\pi}{kh}$ is the number of points per wavelength. Hence, it is reasonable to choose $kh \in [1/4, 1]$. Without loss of generality, we let $(x_i, y_j) = (0, 0)$. Define $S := \{\frac{1}{4} + \frac{3s}{4000} : s = 0, \dots, 1000\}$ and let

$$(\tilde{C}_{1,1}^w(kh), \tilde{C}_{1,0}^w(kh)) := \arg \min_{C_{1,1}^w, C_{1,0}^w \in \mathbb{R}} \int_0^{2\pi} |(T(\theta|kh))_{0,0}|^2 d\theta, \quad kh \in S. \quad (5.28)$$

We use the Simpson's 3/8 rule with 900 uniform sampling points to calculate $\int_0^{2\pi} |(T(\theta|kh))_{0,0}|^2 d\theta$. Now, we link $C_{0,0}, C_{1,0}, C_{1,1}$ in (5.27) with $C_{0,0}^w, \tilde{C}_{1,0}^w(kh), \tilde{C}_{1,1}^w(kh)$ in (5.28) for $kh \in S$. To further simplify the presentation of our stencil coefficients, we set $c_9 = c_{10} = c_{11} = 0$ in (5.27) so that the coefficients of the polynomials in (5.27) for degree 7 are zero. Because $C_{0,0}^w = -20$ is our normalization, we determine the free parameters c_i for $i = 1, \dots, 8$ in (5.27) by considering the following least-square problem:

$$(\tilde{c}_1, \tilde{c}_2, \dots, \tilde{c}_8) := \arg \min_{c_1, c_2, \dots, c_8 \in \mathbb{R}} \sum_{kh \in S} |C_{1,1}(kh) - \tilde{C}_{1,1}^w(kh)C_{0,0}(kh)/(-20)|^2 + |C_{1,0}(kh) - \tilde{C}_{1,0}^w(kh)C_{0,0}(kh)/(-20)|^2.$$

For simplicity of presentation, we replace each above calculated coefficient \tilde{c}_i with its approximated fractional form $[10^8 \tilde{c}_i]/10^8$, where $[\cdot]$ is a rounding operation to the nearest integer. Plugging these approximated fractional forms into coefficients c_i for $i = 1, \dots, 8$ in (5.27), we obtain (5.14). \square

Proof of Theorem 5.3. We only prove item (1). The proof of item (2) is very similar. Since $-u_x - iku = g_1$ on $\partial\Omega|_1$, we have $u^{(1,n)} = -iku^{(0,n)} - g_1^{(n)}$ for all $n = 0, \dots, M_{g_1} - 1$. By (5.10) with M, M_f being replaced by $M - 1, M_f - 1$ and choosing $M_{g_1} \geq M$, we have

$$\begin{aligned} & u(x + x_i^*, y + y_j^*) \\ &= \sum_{(m,n) \in \Lambda_M^{V,1}} u^{(m,n)} G_{M,m,n}^V(x, y) + \sum_{(m,n) \in \Lambda_{M_f-2}} f^{(m,n)} Q_{M_f,m,n}^V(x, y) + \mathcal{O}(h^{M+1}), \\ &= \sum_{n=0}^M u^{(0,n)} G_{M,0,n}^V(x, y) + \sum_{n=0}^{M-1} u^{(1,n)} G_{M,1,n}^V(x, y) + \sum_{(m,n) \in \Lambda_{M_f-2}} f^{(m,n)} Q_{M_f,m,n}^V(x, y) + \mathcal{O}(h^{M+1}) \end{aligned}$$

$$\begin{aligned}
&= \sum_{n=0}^M u^{(0,n)} G_{M,0,n}^V(x, y) + \sum_{n=0}^{M_{g_1}-1} u^{(1,n)} G_{M_{g_1},1,n}^V(x, y) + \sum_{(m,n) \in \Lambda_{M_f-2}} f^{(m,n)} Q_{M_f,m,n}^V(x, y) + \mathcal{O}(h^{M+1}) \\
&= \sum_{n=0}^M u^{(0,n)} G_{M,0,n}^V(x, y) - \sum_{n=0}^{M_{g_1}-1} (iku^{(0,n)} + g_1^{(n)}) G_{M_{g_1},1,n}^V(x, y) + \sum_{(m,n) \in \Lambda_{M_f-2}} f^{(m,n)} Q_{M_f,m,n}^V(x, y) \\
&\quad + \mathcal{O}(h^{M+1}) \\
&= u^{(0,M)} G_{M,0,M}^V(x, y) + \sum_{n=0}^{M-1} u^{(0,n)} \left(G_{M,0,n}^V(x, y) - ik G_{M,1,n}^V(x, y) \right) - \sum_{n=0}^{M_{g_1}-1} g_1^{(n)} G_{M_{g_1},1,n}^V(x, y) \\
&\quad + \sum_{(m,n) \in \Lambda_{M_f-2}} f^{(m,n)} Q_{M_f,m,n}^V(x, y) + \mathcal{O}(h^{M+1}), \quad \text{for } x, y \in (-2h, 2h).
\end{aligned}$$

We set $C_{k,\ell}^{\mathcal{B}_1} := \sum_{p=0}^M (c_{k,\ell,p} + id_{k,\ell,p})(kh)^p$, where $c_{k,\ell,p}, d_{k,\ell,p} \in \mathbb{R}$ for all $k \in \{0, 1\}$ and $\ell \in \{-1, 0, 1\}$. Furthermore, we let $C_{0,-1}^{\mathcal{B}_1} = C_{0,1}^{\mathcal{B}_1}$ and $C_{1,-1}^{\mathcal{B}_1} = C_{1,1}^{\mathcal{B}_1}$ for symmetry. So, $x_i^* = x_i$ and $y_j^* = y_j$ lead to

$$\begin{aligned}
\mathcal{L}_h^{\mathcal{B}_1} u &:= \frac{1}{h} \sum_{k=0}^1 \sum_{\ell=-1}^1 C_{k,\ell}^{\mathcal{B}_1} u(x_i + kh, y_j + \ell h) \\
&= \sum_{n=0}^M u^{(0,n)} h^{-1} I_n^{\mathcal{B}_1} + \sum_{(m,n) \in \Lambda_{M_f-2}} f^{(m,n)} h J_{m,n}^{\mathcal{B}_1} + \sum_{n=0}^{M_{g_1}-1} g_1^{(n)} h^{-1} J_{g_1,n}^{\mathcal{B}_1} = \mathcal{O}(h^M),
\end{aligned}$$

as $h \rightarrow 0$, where

$$\begin{aligned}
I_n^{\mathcal{B}_1} &:= \sum_{k=0}^1 \sum_{\ell=-1}^1 C_{k,\ell}^{\mathcal{B}_1} \left(G_{M,0,n}^V(kh, \ell h) - ik G_{M,1,n}^V(kh, \ell h) (1 - \delta_{n,M}) \right), \\
J_{m,n}^{\mathcal{B}_1} &:= \sum_{k=0}^1 \sum_{\ell=-1}^1 C_{k,\ell}^{\mathcal{B}_1} h^{-2} Q_{M_f,m,n}^V(kh, \ell h), \quad J_{g_1,n}^{\mathcal{B}_1} := - \sum_{k=0}^1 \sum_{\ell=-1}^1 C_{k,\ell}^{\mathcal{B}_1} G_{M_{g_1},1,n}^V(kh, \ell h),
\end{aligned} \tag{5.29}$$

$\delta_{a,a} = 1$, and $\delta_{a,b} = 0$ for $a \neq b$. Let

$$\mathcal{L}_h^{\mathcal{B}_1} u_h := \frac{1}{h} \sum_{k=0}^1 \sum_{\ell=-1}^1 C_{k,\ell}^{\mathcal{B}_1} (u_h)_{i+k,j+\ell} = \sum_{(m,n) \in \Lambda_{M_f-2}} f^{(m,n)} h J_{m,n}^{\mathcal{B}_1} + \sum_{n=0}^{M_{g_1}-1} g_1^{(n)} h^{-1} J_{g_1,n}^{\mathcal{B}_1}. \tag{5.30}$$

We have

$$\mathcal{L}_h^{\mathcal{B}_1} (u - u_h) = \mathcal{O}(h^M),$$

if $I_n^{\mathcal{B}_1}$ in [\(5.29\)](#) satisfies

$$I_n^{\mathcal{B}_1} = \mathcal{O}(h^{M+1}), \quad \text{for all } n = 0, \dots, M. \tag{5.31}$$

By calculation, we find that $M = 6$ is the maximum positive integer such that the linear system of (5.31) has a non-trivial solution. To further simplify such a solution, we set coefficients associated with kh of degrees higher than 4 to zero; i.e., we now have polynomials of kh , whose highest degree is now 4. All such non-trivial solutions for $M = 6$ can be uniquely written (up to a constant multiple) as

$$\begin{aligned}
C_{1,1}^{B_1} &= (c_3 + ic_7)(kh)^4 + (c_2 + ic_6)(kh)^3 + 12(ic_8 - (7i/3)c_2 + (7i/3)c_5 + (13i/3)c_7 + (7/3)c_1 + (13/3)c_3 + c_4 \\
&\quad + (7/3)c_6 - 4/135)(kh)^2 - 60(ic_1 + 2ic_3 + (i/2)c_4 + ic_6 - 4i/225 - (1/2)c_8 + c_2 - c_5 - 2c_7)kh + 1 \\
C_{0,1}^{B_1} &= (c_1 + ic_5)(kh)^4 + 13(ic_1 + (20i/13)c_3 + (7i/26)c_4 + (12i/13)c_6 - 17i/1170 - (7/26)c_8 + (12/13)c_2 - c_5 \\
&\quad - (20/13)c_7)(kh)^3 + 18(ic_8 - (22i/9)c_2 + (22i/9)c_5 + (40i/9)c_7 + (22/9)c_1 + (40/9)c_3 + c_4 + (22/9)c_6 \\
&\quad - 11/324)(kh)^2 - 120(ic_1 + (2i)c_3 + (i/2)c_4 + ic_6 - 29i/1800 - (1/2)c_8 + c_2 - c_5 - 2c_7)kh + 2 \\
C_{1,0}^{B_1} &= (c_4 + ic_8)(kh)^4 + 18(ic_1 + (4i/3)c_3 + (i/6)c_4 + (8i/9)c_6 - i/90 - (1/6)c_8 + (8/9)c_2 - c_5 \\
&\quad - (4/3)c_7)(kh)^3 + 36(ic_8 - (22i/9)c_2 + (22i/9)c_5 + (40i/9)c_7 + (22/9)c_1 + (40/9)c_3 + c_4 + (22/9)c_6 \\
&\quad - 49/1620)(kh)^2 - 240(ic_1 + (2i)c_3 + (i/2)c_4 + ic_6 - 29i/1800 - (1/2)c_8 + c_2 - c_5 - 2c_7)kh + 4 \\
C_{0,0}^{B_1} &= -4(ic_8 - (3i/2)c_2 + (2i)c_5 + (7i/2)c_7 + 2c_1 + (7/2)c_3 + c_4 + (3/2)c_6 - 1/80)(kh)^4 - 80(ic_1 + (2i)c_3 \\
&\quad + (i/2)c_4 + (39i/40)c_6 - 7i/720 - (1/2)c_8 + (39/40)c_2 - c_5 - 2c_7)(kh)^3 + 84(ic_8 - (32i/21)c_2 \\
&\quad + (32i/21)c_5 + (74i/21)c_7 + (32/21)c_1 + (74/21)c_3 + c_4 + (32/21)c_6 + 1/3780)(kh)^2 + 600(ic_1 + (2i)c_3 \\
&\quad + (i/2)c_4 + ic_6 - 29i/4500 - (1/2)c_8 + c_2 - c_5 - 2c_7)kh - 10,
\end{aligned}$$

where each $c_i \in \mathbb{R}$ for $i = 1, \dots, 8$ are free parameters. Choosing $M_f = M_{g_1} = 8$ in (5.29) and (5.30) yields the right-hand side of (5.15).

Next, consider a compact 6-point stencil $\{C_{k,\ell}^w\}_{k \in \{0,1\}, \ell \in \{-1,0,1\}}$ parameterized by $C_{1,1}^w, C_{0,1}^w, C_{1,0}^w \in \mathbb{C}$ with

$$C_{1,-1}^w = C_{1,1}^w, \quad C_{0,-1}^w = C_{0,1}^w, \quad \text{and} \quad C_{0,0}^w = -10,$$

where we normalized the general stencil by $C_{0,0}^w = -10$. Take a plane wave solution $u(x, y, \theta) := \exp(ik(\cos(\theta)x + \sin(\theta)y))$ for any $\theta \in [0, 2\pi)$. Clearly, we have $\Delta u + \mathbf{k}^2 u = 0$ and $-u_x - iku = g_1 \neq 0$ on $\partial\Omega|_1$, where g_1 and its derivatives are explicitly known by plugging the plane wave solution $u(x, y, \theta)$ into the boundary condition. Hence, the truncation error associated with the compact 6-point general stencil coefficients $\{C_{k,\ell}^w\}_{k \in \{0,1\}, \ell \in \{-1,0,1\}}$ at the grid point $(x_0, y_j) \in \partial\Omega|_1$ is $\frac{1}{h}(T(\theta|kh))_{x_0, y_j}$, where

$$\begin{aligned}
(T(\theta|kh))_{x_0, y_j} &:= \sum_{k=0}^1 \sum_{\ell=-1}^1 C_{k,\ell}^w \exp(ik(\cos(\theta)(x_0 + kh) + \sin(\theta)(y_j + \ell h))) \\
&\quad + \sum_{n=0}^8 g_1^{(n)} \sum_{k=0}^1 \sum_{\ell=-1}^1 C_{k,\ell}^w G_{8,1,n}^V(kh, \ell h).
\end{aligned}$$

Without loss of generality, we let $(x_0, y_j) = (0, 0)$. Afterwards, we follow a similar minimization procedure as in the proof of Theorem 5.2 to obtain the concrete stencils in Theorem 5.3. \square

Proof of Theorem 5.4. Clearly, we have

$$u^{(1,n)} = -iku^{(0,n)} - g_1^{(n)} \quad \text{and} \quad u^{(m,1)} = -g_3^{(m)}, \quad \text{for all } m, n \in \mathbb{N}_0. \quad (5.32)$$

Let $C_{k,\ell}^{\mathcal{R}_1} := C_{k,\ell}^{\mathcal{R}_1,V} + C_{k,\ell}^{\mathcal{R}_1,H}$ for $k, \ell \in \{0, 1\}$, where $C_{k,\ell}^{\mathcal{R}_1,V}$ and $C_{k,\ell}^{\mathcal{R}_1,H}$ are to be determined polynomials of kh . Note that $x_i^* = x_i$ and $y_j^* = y_j$. Approximating $u(x_0 + kh, y_0 + \ell h)$ by (5.10), (5.11) with M, M_f being replaced by $M - 1, M_f - 1$, choosing $M_{g_1} \geq M, M_{g_3} \geq M$, and using (5.32), we have

$$\begin{aligned} \mathcal{L}_h^{\mathcal{R}_1} u &:= \frac{1}{h} \sum_{k=0}^1 \sum_{\ell=0}^1 (C_{k,\ell}^{\mathcal{R}_1,V} + C_{k,\ell}^{\mathcal{R}_1,H}) u(x_0 + kh, y_0 + \ell h) \\ &= \sum_{n=0}^M u^{(0,n)} h^{-1} I_n^{\mathcal{R}_1,V} + \sum_{m=0}^M u^{(m,0)} h^{-1} I_m^{\mathcal{R}_1,H} + \sum_{(m,n) \in \Lambda_{M_f-2}} f^{(m,n)} h S_{m,n}^{\mathcal{R}_1} \\ &\quad + \sum_{n=0}^{M_{g_1}-1} g_1^{(n)} h^{-1} K_n^{\mathcal{R}_1,V} + \sum_{m=0}^{M_{g_3}-1} g_3^{(m)} h^{-1} K_m^{\mathcal{R}_1,H} + \mathcal{O}(h^M), \end{aligned} \quad (5.33)$$

where

$$\begin{aligned} I_m^{\mathcal{R}_1,H} &:= \sum_{k=0}^1 \sum_{\ell=0}^1 C_{k,\ell}^{\mathcal{R}_1,H} G_{M,m,0}^H(kh, \ell h), \\ I_n^{\mathcal{R}_1,V} &:= \sum_{k=0}^1 \sum_{\ell=0}^1 C_{k,\ell}^{\mathcal{R}_1,V} (G_{M,0,n}^V(kh, \ell h) - ik G_{M,1,n}^V(kh, \ell h)(1 - \delta_{n,M})), \\ S_{m,n}^{\mathcal{R}_1} &:= \sum_{k=0}^1 \sum_{\ell=0}^1 h^{-2} (C_{k,\ell}^{\mathcal{R}_1,V} Q_{M_f,m,n}^V(kh, \ell h) + C_{k,\ell}^{\mathcal{R}_1,H} Q_{M_f,m,n}^H(kh, \ell h)), \\ K_n^{\mathcal{R}_1,V} &:= - \sum_{k=0}^1 \sum_{\ell=0}^1 C_{k,\ell}^{\mathcal{R}_1,V} G_{M_{g_1},1,n}^V(kh, \ell h), \quad \text{and} \quad K_m^{\mathcal{R}_1,H} := - \sum_{k=0}^1 \sum_{\ell=0}^1 C_{k,\ell}^{\mathcal{R}_1,H} G_{M_{g_3},m,1}^H(kh, \ell h). \end{aligned}$$

By replacing $u^{(m,0)}$ for $m = 2, \dots, M$ with (5.4), using (5.32), and rearranging some terms, (5.33) implies

$$\begin{aligned} h \mathcal{L}_h^{\mathcal{R}_1} u &= u^{(0,0)} \left(I_0^{\mathcal{R}_1,V} + I_0^{\mathcal{R}_1,H} - ik I_1^{\mathcal{R}_1,H} + \sum_{p=1}^{\lfloor \frac{M}{2} \rfloor} (-1)^p k^{2p} I_{2p}^{\mathcal{R}_1,H} + i \sum_{p=1}^{\lfloor \frac{M-1}{2} \rfloor} (-1)^{p+1} k^{2p+1} I_{2p+1}^{\mathcal{R}_1,H} \right) \\ &\quad + \sum_{\ell=0}^{\lfloor \frac{M-1}{2} \rfloor} u^{(0,2\ell+1)} I_{2\ell+1}^{\mathcal{R}_1,V} \end{aligned}$$

$$\begin{aligned}
& + \sum_{\ell=1}^{\lfloor \frac{M-1}{2} \rfloor} u^{(0,2\ell)} \left(\sum_{p=\max\{\ell,1\}}^{\lfloor \frac{M}{2} \rfloor} (-1)^p \binom{p}{\ell} k^{2(p-\ell)} I_{2p}^{\mathcal{R}_1, H} + i \sum_{p=\max\{\ell,1\}}^{\lfloor \frac{M-1}{2} \rfloor} (-1)^{p+1} \binom{p}{\ell} k^{2(p-\ell)+1} I_{2p+1}^{\mathcal{R}_1, H} + I_{2\ell}^{\mathcal{R}_1, V} \right) \\
& + u^{(0,2\lfloor \frac{M}{2} \rfloor)} \left((-1)^{\lfloor \frac{M}{2} \rfloor} I_{2\lfloor \frac{M}{2} \rfloor}^{\mathcal{R}_1, H} + I_{2\lfloor \frac{M}{2} \rfloor}^{\mathcal{R}_1, V} \right) \left(1 - \delta_{\lfloor \frac{M}{2} \rfloor, \lfloor \frac{M-1}{2} \rfloor} \right) + \sum_{\ell=0}^{\lfloor \frac{M_{g_1}-2}{2} \rfloor} g_1^{(2\ell+1)} K_{2\ell+1}^{\mathcal{R}_1, V} \\
& + \sum_{\ell=0}^{\lfloor \frac{M_{g_1}-1}{2} \rfloor} g_1^{(2\ell)} \left(K_{2\ell}^{\mathcal{R}_1, V} + \sum_{p=\max\{\ell,1\}}^{\lfloor \frac{M_{g_1}-1}{2} \rfloor} (-1)^{p+1} \binom{p}{\ell} k^{2(p-\ell)} I_{2p+1}^{\mathcal{R}_1, H} - I_1^{\mathcal{R}_1, H} \delta_{\ell,0} \right) \\
& + \sum_{\ell=0}^{M_{g_3}-1} g_3^{(\ell)} K_{\ell}^{\mathcal{R}_1, H} + \sum_{j=0}^{\lfloor \frac{M_f-1}{2} \rfloor} \sum_{\ell=0}^{M_f-2j-3} f^{(\ell,2j+1)} h^2 S_{\ell,2j+1}^{\mathcal{R}_1} + \sum_{\gamma \in \{0,1\}} \sum_{\ell=0}^{\lfloor \frac{M_f-\gamma}{2} \rfloor - 1} \sum_{j=0}^{\lfloor \frac{M_f-\gamma}{2} \rfloor - \ell - 1} f^{(2\ell+\gamma,2j)} \\
& \left(\sum_{p=\max\{j+\ell+1,1\}}^{\lfloor \frac{M_f-\gamma}{2} \rfloor} (-1)^{p-\ell-1} \binom{p-\ell-1}{j} k^{2(p-\ell-j-1)} I_{2p+\gamma}^{\mathcal{R}_1, H} + h^2 S_{2\ell+\gamma,2j}^{\mathcal{R}_1} \right) + \mathcal{O}(h^{M+1}), \quad h \rightarrow 0.
\end{aligned}$$

We set $C_{k,\ell}^{\mathcal{R}_1, V} = \sum_{p=0}^M (a_{k,\ell,p} + ib_{k,\ell,p})(kh)^p$ and $C_{k,\ell}^{\mathcal{R}_1, H} = \sum_{p=0}^M (c_{k,\ell,p} + id_{k,\ell,p})(kh)^p$, where $a_{k,\ell,p}, b_{k,\ell,p}, c_{k,\ell,p}, d_{k,\ell,p} \in \mathbb{R}$ for all $k \in \{0, 1\}$ and $\ell \in \{-1, 0, 1\}$. By calculation, $M = 6$ is the maximum positive integer such that the linear system, obtained by setting each coefficient of $u^{(0,n)}$ for $n = 0, \dots, 6$ to be $\mathcal{O}(h^7)$ as $h \rightarrow 0$, has a non-trivial solution. Afterwards, to further simplify such a solution, we can set remaining coefficients associated with $(kh)^5$ or $(kh)^6$ to zero.

By using the minimization procedure described in the proofs of Theorems [5.2](#) and [5.3](#), we can verify that $C_{0,1}^{\mathcal{R}_1, V} = C_{1,1}^{\mathcal{R}_1, V} = C_{0,0}^{\mathcal{R}_1, H} = C_{1,0}^{\mathcal{R}_1, H} = 0$, $C_{0,0}^{\mathcal{R}_1, V} = C_{0,0}^{\mathcal{R}_1}$, $C_{1,0}^{\mathcal{R}_1, V} = C_{1,0}^{\mathcal{R}_1}$, $C_{0,1}^{\mathcal{R}_1, H} = C_{0,1}^{\mathcal{R}_1}$, and $C_{1,1}^{\mathcal{R}_1, H} = C_{1,1}^{\mathcal{R}_1}$, where $\{C_{k,\ell}^{\mathcal{R}_1}\}_{k,\ell \in \{0,1\}}$ are defined in [5.20](#). Given these $\{C_{k,\ell}^{\mathcal{R}_1, V}\}_{k,\ell \in \{0,1\}}$ and $\{C_{k,\ell}^{\mathcal{R}_1, H}\}_{k,\ell \in \{0,1\}}$, we set $M_f = M_{g_1} = M_{g_3} = 8$ and plug them into the following relations

$$\begin{aligned}
J_{g_1,2\ell}^{\mathcal{R}_1} &= K_{2\ell}^{\mathcal{R}_1, V} + \sum_{p=\max\{\ell,1\}}^{\lfloor \frac{M_{g_1}-1}{2} \rfloor} (-1)^{p+1} \binom{p}{\ell} k^{2(p-\ell)} I_{2p+1}^{\mathcal{R}_1, H} - I_1^{\mathcal{R}_1, H} \delta_{\ell,0}, \quad \ell = 0, \dots, \lfloor \frac{M_{g_1}-1}{2} \rfloor, \\
J_{g_1,2\ell+1}^{\mathcal{R}_1} &= K_{2\ell+1}^{\mathcal{R}_1, V}, \quad \ell = 0, \dots, \lfloor \frac{M_{g_1}-2}{2} \rfloor, \quad J_{g_3,\ell}^{\mathcal{R}_1} = K_{\ell}^{\mathcal{R}_1, H}, \quad \ell = 0, \dots, M_{g_3} - 1, \\
J_{\ell,2j+1}^{\mathcal{R}_1} &= h^2 S_{\ell,2j+1}^{\mathcal{R}_1}, \quad \ell = 0, \dots, M_f - 2j - 3, j = 0, \dots, \lfloor \frac{M_f-1}{2} \rfloor - 1, \quad \text{and} \\
J_{2\ell+\gamma,2j}^{\mathcal{R}_1} &= \sum_{p=\max\{j+\ell+1,1\}}^{\lfloor \frac{M_f-\gamma}{2} \rfloor} (-1)^{p-\ell-1} \binom{p-\ell-1}{j} k^{2(p-\ell-j-1)} I_{2p+\gamma}^{\mathcal{R}_1, H} + h^2 S_{2\ell+\gamma,2j}^{\mathcal{R}_1},
\end{aligned} \tag{5.34}$$

where $\gamma \in \{0, 1\}$, $j = 0, \dots, \lfloor \frac{M_f-\gamma}{2} \rfloor - \ell - 1$, and $\ell = 0, \dots, \lfloor \frac{M_f-\gamma}{2} \rfloor - 1$. This completes the proof of Theorem [5.4](#). \square

Proof of Theorem 5.5. The proof is almost identical to the proof of Theorem 5.4. Note that we need to replace $u^{(m,1)} = -g_3^{(m)}$ with $u^{(m,1)} = iku^{(m,0)} + g_4^{(m)}$ for all $m \in \mathbb{N}_0$ in (5.32). \square

Chapter 6

Sixth Order Compact 9-Point Finite Difference Schemes for Elliptic Interface Problems with Particular Intersecting Interfaces

6.1 Introduction and problem formulation

In Chapters [3](#) and [4](#), we derive high order finite difference schemes for the elliptic interface problems with smooth interfaces and discontinuous coefficients. In this chapter, we consider the elliptic interface problems with intersecting interfaces. Let $\Omega = (l_1, l_2) \times (l_1, l_2)$, $\Omega_1 = (l_1, \frac{l_1+l_2}{2}) \times (\frac{l_1+l_2}{2}, l_2)$, $\Omega_2 = (\frac{l_1+l_2}{2}, l_2) \times (\frac{l_1+l_2}{2}, l_2)$, $\Omega_3 = (\frac{l_1+l_2}{2}, l_2) \times (l_1, \frac{l_1+l_2}{2})$, $\Omega_4 = (l_1, \frac{l_1+l_2}{2}) \times (l_1, \frac{l_1+l_2}{2})$, $\Gamma_1 = \{(\frac{l_1+l_2}{2}, y) : \frac{l_1+l_2}{2} < y < l_2\}$, $\Gamma_2 = \{(\frac{l_1+l_2}{2}, y) : l_1 < y < \frac{l_1+l_2}{2}\}$, $\Gamma_3 = \{(x, \frac{l_1+l_2}{2}) : \frac{l_1+l_2}{2} < x < l_2\}$, $\Gamma_4 = \{(x, \frac{l_1+l_2}{2}) : l_1 < x < \frac{l_1+l_2}{2}\}$. We define $a_i := a\chi_{\Omega_i}$, $f_i := f\chi_{\Omega_i}$ and $u_i := u\chi_{\Omega_i}$ for $i = 1, 2, 3, 4$. Then we consider the following elliptic interface problem with intersecting interfaces as following:

$$\begin{cases} -\nabla \cdot (a\nabla u) = f, & \text{in } \Omega \setminus \bar{\Gamma}, \\ [u] = 0, & \text{on } \Gamma, \\ [a\nabla u \cdot \vec{n}] = \psi_i, & \text{on } \Gamma_i, \\ u = g, & \text{on } \partial\Omega, \end{cases} \quad (6.1)$$

where $\Gamma = \Gamma_1 \cup \Gamma_2 \cup \Gamma_3 \cup \Gamma_4$, for $(\xi, y) \in \Gamma_p$ with $p = 1, 2$ and $\xi = (l_1 + l_2)/2$ (i.e., on the vertical line of the cross-interface),

$$[u](\xi, y) := \lim_{x \rightarrow \xi^+} u(x, y) - \lim_{x \rightarrow \xi^-} u(x, y), \quad [a \nabla u \cdot \vec{n}](\xi, y) := \lim_{x \rightarrow \xi^+} a(x, y) \frac{\partial u}{\partial x}(x, y) - \lim_{x \rightarrow \xi^-} a(x, y) \frac{\partial u}{\partial x}(x, y);$$

while for $(x, \xi) \in \Gamma_p$ with $p = 3, 4$ and $\xi = (l_1 + l_2)/2$ (i.e., on the horizontal line of the cross-interface),

$$[u](x, \xi) := \lim_{y \rightarrow \xi^+} u(x, y) - \lim_{y \rightarrow \xi^-} u(x, y), \quad [a \nabla u \cdot \vec{n}](x, \xi) := \lim_{y \rightarrow \xi^+} a(x, y) \frac{\partial u}{\partial y}(x, y) - \lim_{y \rightarrow \xi^-} a(x, y) \frac{\partial u}{\partial y}(x, y).$$

The direction of \vec{n} is shown in Fig. 6.1. See Fig. 6.1 for an illustration of (6.1). In this chapter, we derive a sixth order compact 9-point finite difference scheme to solve (6.1) given the following assumptions:

- (A1) The coefficient $a \chi_{\Omega_i}$ is a positive constant for $i = 1, 2, 3, 4$, and coefficient a is discontinuous across the interface Γ_i for $i = 1, 2, 3, 4$.
- (A2) The solution u and the source term f have uniformly continuous partial derivatives of (total) orders up to seven and five respectively in each Ω_i for $i = 1, 2, 3, 4$. f can be continuous or discontinuous across the interface Γ_i for $i = 1, 2, 3, 4$.
- (A3) The 1D function ψ_i in (6.1) has uniformly continuous derivatives of (total) orders up to six on the interface Γ_i for $i = 1, 2, 3, 4$.

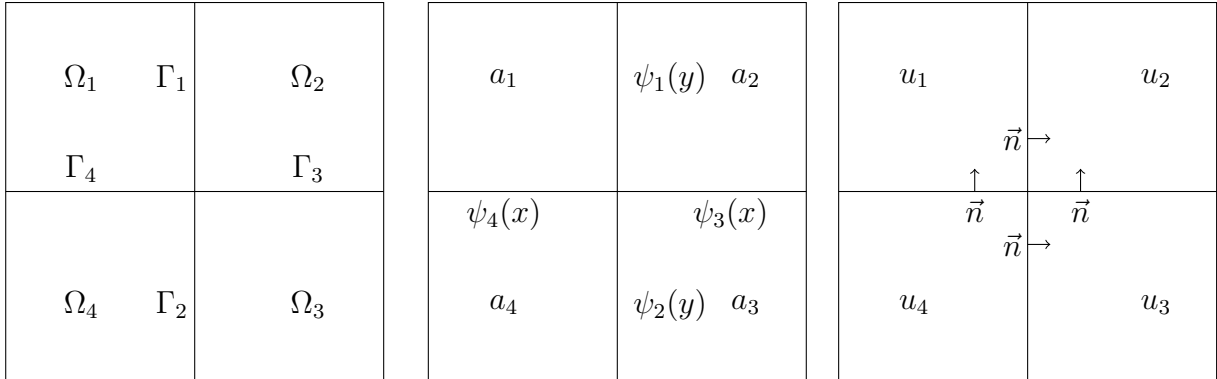


Figure 6.1: An illustration for (6.1)

This chapter is organized as follows.

In Section 6.2.1, we construct the sixth order compact 9-point finite difference scheme for regular points. The explicit formula of the scheme at regular points is shown in Theorem 6.1.

In Section 6.2.2, we derive the seventh order compact 9-point finite difference scheme for interface points. The explicit formula of the scheme at interface points is shown in Theorems 6.2 to 6.5.

In Section [6.2.3](#), we derive the seventh order compact 9-point finite difference scheme for the intersection point. The explicit formula of the scheme at the intersection point is shown in Theorem [6.6](#).

In Section [6.2.4](#), we prove the sixth order convergence rate of our proposed compact 9-point finite difference scheme by the discrete maximum principle in Theorem [6.7](#).

In Section [6.3](#), we provide numerical results to verify the convergence rate measured in the l_2 and l_∞ norms for our proposed compact 9-point scheme.

In Section [6.4](#), we summarize the main contributions of this chapter. Finally, in Section [6.5](#), we present the proofs of Theorems [6.2](#) to [6.6](#).

6.2 Sixth order compact 9-point finite difference schemes using uniform Cartesian grids

Since $\Omega = (l_1, l_2) \times (l_1, l_2)$ in this chapter, we define that

$$x_i = l_1 + ih, \quad i = 0, \dots, N_1, \quad \text{and} \quad y_j = l_1 + jh, \quad j = 0, \dots, N_1, \quad h = \frac{l_2 - l_1}{N_1},$$

where N_1 is an even integer. By the setting of [\(6.1\)](#), we can say that the centered points of compact 9-point schemes of all the irregular points in this chapter lie on the closure of the interface curve (see Figs. [6.4](#) and [6.5](#) for illustrations). Furthermore, by the definitions of Ω_p and Γ_p for $p = 1, 2, 3, 4$ in [\(6.1\)](#), we should choose $(x_i^*, y_j^*) = (x_i, y_j)$ in this chapter. Recall that

$$\Lambda_{M+1} := \{(m, n - m) : n = 0, \dots, M + 1 \text{ and } m = 0, \dots, n\}, \quad M + 1 \in \mathbb{N}_0, \quad (6.2)$$

$$\Lambda_{M+1}^{V,2} := \Lambda_{M+1} \setminus \Lambda_{M+1}^{V,1} \quad \text{with} \quad \Lambda_{M+1}^{V,1} := \{(\ell, k - \ell) : k = \ell, \dots, M + 1 - \ell \text{ and } \ell = 0, 1\}, \quad (6.3)$$

$$\Lambda_{M+1}^{H,j} := \{(n, m) : (m, n) \in \Lambda_{M+1}^{V,j}, j = 1, 2\}. \quad (6.4)$$

The illustrations for $\Lambda_7^{V,1}$, $\Lambda_7^{V,2}$, $\Lambda_7^{H,1}$, $\Lambda_7^{H,2}$ are shown in Figs. [6.2](#) and [6.3](#).

By [\(2.9\)](#), [\(4.12\)](#), $a_p := a\chi_{\Omega_p}$ is a positive constant, $f_p := f\chi_{\Omega_p}$, $u_p := u\chi_{\Omega_p}$ for $p = 1, 2, 3, 4$, and choose $(x_i^*, y_j^*) = (x_i, y_j)$, we have

$$\begin{aligned} u_p(x + x_i, y + y_j) &= \sum_{(m,n) \in \Lambda_{M+1}^{V,1}} u_p^{(m,n)} G_{M+1,m,n}^V(x, y) \\ &+ \sum_{(m,n) \in \Lambda_{M-1}} f_p^{(m,n)} Q_{M+1,m,n}^V(x, y) + \mathcal{O}(h^{M+2}), \quad \text{for } x, y \in [-h, h], \end{aligned} \quad (6.5)$$

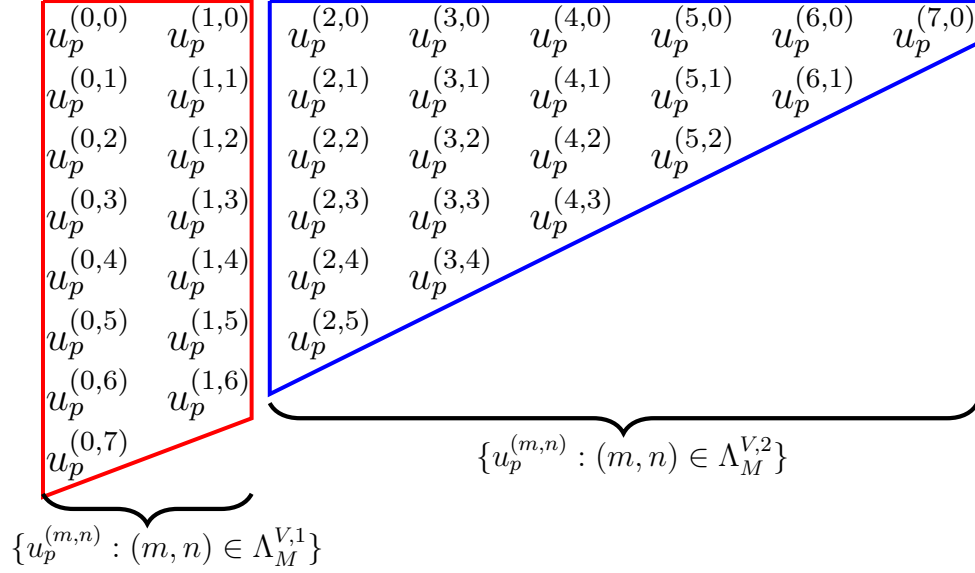


Figure 6.2: Red trapezoid: $\{u_p^{(m,n)} : (m,n) \in \Lambda_M^{V,1}\}$ with $M = 7$ and $p = 1, 2, 3, 4$. Blue trapezoid: $\{u_p^{(m,n)} : (m,n) \in \Lambda_M^{V,2}\}$ with $M = 7$ and $p = 1, 2, 3, 4$. Note that $\Lambda_M = \Lambda_M^{V,1} \cup \Lambda_M^{V,2}$.

$$\begin{aligned}
u_p(x + x_i, y + y_j) &= \sum_{(m,n) \in \Lambda_{M+1}^{H,1}} u_p^{(m,n)} G_{M+1,m,n}^H(x, y) \\
&+ \sum_{(m,n) \in \Lambda_{M-1}} f_p^{(m,n)} Q_{M+1,m,n}^H(x, y) + \mathcal{O}(h^{M+2}), \quad \text{for } x, y \in [-h, h],
\end{aligned} \tag{6.6}$$

where $p = 1, 2, 3, 4$,

$$G_{M+1,m,n}^V(x, y) := \sum_{\ell=0}^{\lfloor \frac{n}{2} \rfloor} (-1)^\ell \frac{x^{m+2\ell} y^{n-2\ell}}{(m+2\ell)!(n-2\ell)!}, \quad (m, n) \in \Lambda_{M+1}^{V,1} \tag{6.7}$$

$$Q_{M+1,m,n}^V(x, y) := \sum_{\ell=1}^{1+\lfloor \frac{n}{2} \rfloor} \frac{(-1)^\ell x^{m+2\ell} y^{n-2\ell+2}}{(m+2\ell)!(n-2\ell+2)!} \frac{1}{a(x_i, y_j)}, \quad (m, n) \in \Lambda_{M-1}. \tag{6.8}$$

$$G_{M+1,m,n}^H(x, y) := \sum_{\ell=0}^{\lfloor \frac{m}{2} \rfloor} \frac{(-1)^\ell y^{n+2\ell} x^{m-2\ell}}{(n+2\ell)!(m-2\ell)!}, \quad (m, n) \in \Lambda_{M+1}^{H,1}, \tag{6.9}$$

$$Q_{M+1,m,n}^H(x, y) := \sum_{\ell=1}^{1+\lfloor \frac{m}{2} \rfloor} \frac{(-1)^\ell y^{n+2\ell} x^{m-2\ell+2}}{(n+2\ell)!(m-2\ell+2)!} \frac{1}{a(x_i, y_j)}, \quad (m, n) \in \Lambda_{M-1}, \tag{6.10}$$

$$u_p^{(m,n)} := \frac{\partial^{m+n} u_p}{\partial^m x \partial^n y}(x_i, y_j) \quad \text{and} \quad f_p^{(m,n)} := \frac{\partial^{m+n} f_p}{\partial^m x \partial^n y}(x_i, y_j), \quad p = 1, 2, 3, 4, \tag{6.11}$$

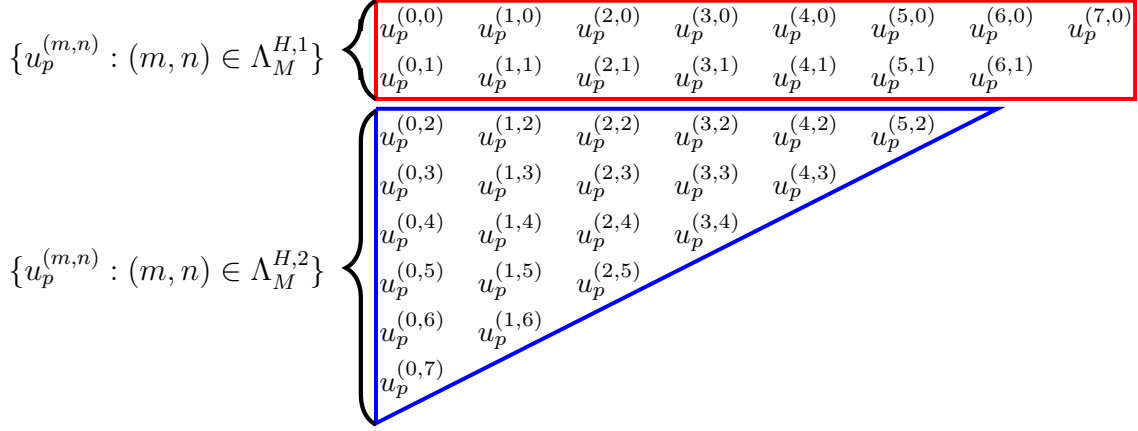


Figure 6.3: Red rectangle: $\{u_p^{(m,n)} : (m, n) \in \Lambda_M^{H,1}\}$ with $M = 7$ and $p = 1, 2, 3, 4$. Blue triangle: $\{u_p^{(m,n)} : (m, n) \in \Lambda_M^{H,2}\}$ with $M = 7$ and $p = 1, 2, 3, 4$. Note that $\Lambda_M = \Lambda_M^{H,1} \cup \Lambda_M^{H,2}$.

$$\psi_1^{(n)} := \frac{d^n \psi_1}{d^n y}(y_j), \quad \psi_2^{(n)} := \frac{d^n \psi_2}{d^n y}(y_j), \quad \psi_3^{(m)} := \frac{d^m \psi_3}{d^m x}(x_i), \quad \psi_4^{(m)} := \frac{d^m \psi_4}{d^m x}(x_i). \quad (6.12)$$

6.2.1 Stencils for regular points

The following sixth order compact 9-point finite difference scheme for (6.1) at the regular points is straightforward by Theorem 2.3.

Theorem 6.1. *Let a grid point (x_i, y_j) be a regular point, i.e., either $d_{i,j}^+ = \emptyset$ or $d_{i,j}^- = \emptyset$. Let $(u_h)_{i,j}$ be the numerically approximated solution of the exact solution u of the partial differential equation (6.1) at a regular point (x_i, y_j) . Then the compact 9-point scheme:*

$$\begin{aligned} \mathcal{L}_h u_h &:= \frac{a_r}{h^2} \left((u_h)_{i-1,j-1} + 4(u_h)_{i,j-1} + (u_h)_{i+1,j-1} \right. \\ &\quad + 4(u_h)_{i-1,j} - 20(u_h)_{i,j} + 4(u_h)_{i+1,j} \\ &\quad \left. + (u_h)_{i-1,j+1} + 4(u_h)_{i,j+1} + (u_h)_{i+1,j+1} \right) \\ &= -6f^{(0,0)} - \frac{1}{2}h^2(f^{(0,2)} + f^{(2,0)}) - \frac{1}{60}h^4(f^{(0,4)} + f^{(4,0)}) - \frac{1}{15}h^4 f^{(2,2)}, \end{aligned} \quad (6.13)$$

achieves sixth order accuracy for $-\nabla \cdot (a \nabla u) = f$ at the regular point (x_i, y_j) , where $f^{(m,n)} := \frac{\partial^{m+n} f}{\partial x^m \partial y^n}(x_i, y_j)$ and $a_r = a(x_i, y_j)$.

6.2.2 Stencils for interface points

In this subsection, we discuss how to find a seventh order compact 9-point finite difference scheme centered at $(x_i, y_j) \in \Gamma_p$ for $p = 1, 2, 3, 4$ and $(x_i, y_j) \notin \overline{\Gamma_1 \cup \Gamma_2} \cap \overline{\Gamma_3 \cup \Gamma_4}$ (see Fig. 6.4)

for an illustration).

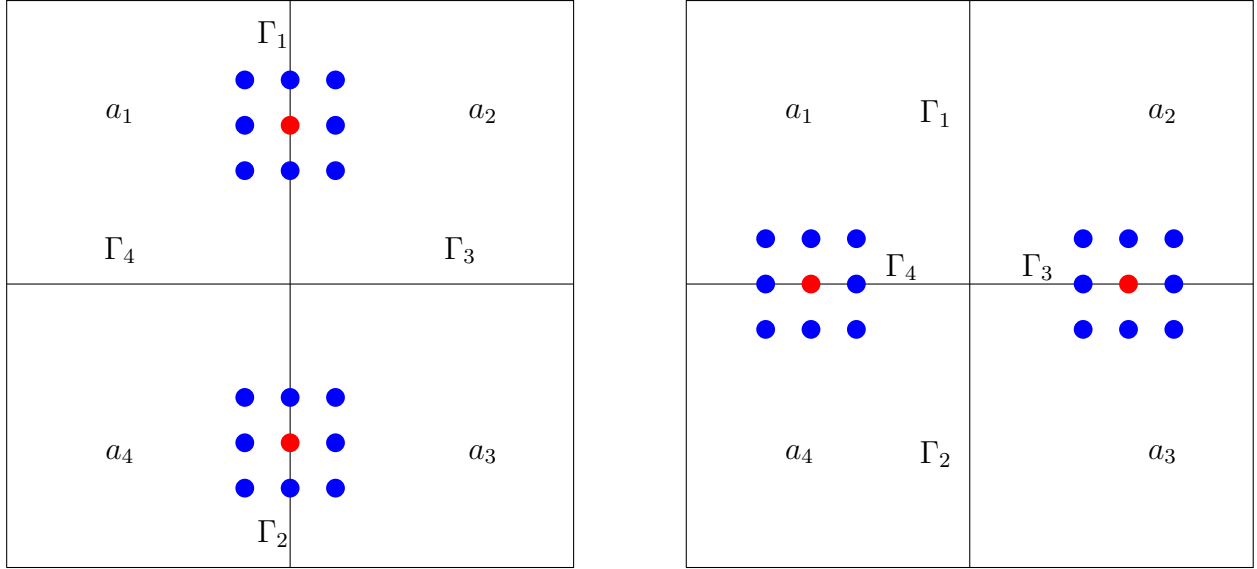


Figure 6.4: Compact 9-point schemes for irregular points of (6.1) (the center red point is not the intersection point)

Theorem 6.2. *Let a grid point (x_i, y_j) be an irregular point such that $(x_i, y_j) \in \Gamma_1$ and $(x_i, y_j) \notin \overline{\Gamma_1 \cup \Gamma_2} \cap \overline{\Gamma_3 \cup \Gamma_4}$ (see Fig. 6.4 for an illustration). Let $(u_h)_{i,j}$ be the numerically approximated solution of the exact solution u of the partial differential equation (6.1) at the irregular point (x_i, y_j) . Then the compact 9-point scheme:*

$$\begin{aligned}
\mathcal{L}_h^{\Gamma_1} u_h &:= \frac{1}{h} \left(C_{-1,-1}(u_h)_{i-1,j-1} + C_{0,-1}(u_h)_{i,j-1} + C_{1,-1}(u_h)_{i+1,j-1} \right. \\
&\quad + C_{-1,0}(u_h)_{i-1,j} + C_{0,0}(u_h)_{i,j} + C_{1,0}(u_h)_{i+1,j} \\
&\quad \left. + C_{-1,1}(u_h)_{i-1,j+1} + C_{0,1}(u_h)_{i,j+1} + C_{1,1}(u_h)_{i+1,j+1} \right) \\
&= \sum_{(m,n) \in \Lambda_5} f_1^{(m,n)} h J_{m,n}^{f_1} + \sum_{(m,n) \in \Lambda_5} f_2^{(m,n)} h J_{m,n}^{f_2} + \sum_{n=0}^6 \psi_1^{(n)} h^{-1} J_{\psi_1, n},
\end{aligned} \tag{6.14}$$

achieves seventh order accuracy at the irregular point $(x_i, y_j) \in \Gamma_1$, where

$$\begin{aligned}
C_{-1,-1} &= \frac{a_1}{a_2}, & C_{0,-1} &= \frac{2(a_1 + a_2)}{a_2}, & C_{1,-1} &= 1, \\
C_{-1,0} &= \frac{4a_1}{a_2}, & C_{0,0} &= \frac{-10(a_1 + a_2)}{a_2}, & C_{1,0} &= 4, \\
C_{-1,1} &= \frac{a_1}{a_2}, & C_{0,1} &= \frac{2(a_1 + a_2)}{a_2}, & C_{1,1} &= 1,
\end{aligned} \tag{6.15}$$

$$\begin{aligned}
J_{m,n}^{f_1} &:= \sum_{\ell=-1}^1 C_{-1,\ell} h^{-2} Q_{7,m,n}^V(-h, \ell h), & J_{m,n}^{f_2} &:= \sum_{k=0}^1 \sum_{\ell=-1}^1 C_{k,\ell} h^{-2} Q_{7,m,n}^V(kh, \ell h), \\
J_{\psi_1,n} &:= - \sum_{\ell=-1}^1 C_{-1,\ell} \frac{1}{a_1} G_{7,1,n}^V(-h, \ell h).
\end{aligned} \tag{6.16}$$

Theorem 6.3. *Let a grid point (x_i, y_j) be an irregular point such that $(x_i, y_j) \in \Gamma_2$ and $(x_i, y_j) \notin \overline{\Gamma_1 \cup \Gamma_2} \cap \overline{\Gamma_3 \cup \Gamma_4}$ (see Fig. 6.4 for an illustration). Let $(u_h)_{i,j}$ be the numerically approximated solution of the exact solution u of the partial differential equation (6.1) at the irregular point (x_i, y_j) . Then the compact 9-point scheme:*

$$\begin{aligned}
\mathcal{L}_h^{\Gamma_2} u_h &:= \frac{1}{h} \left(C_{-1,-1}(u_h)_{i-1,j-1} + C_{0,-1}(u_h)_{i,j-1} + C_{1,-1}(u_h)_{i+1,j-1} \right. \\
&\quad + C_{-1,0}(u_h)_{i-1,j} + C_{0,0}(u_h)_{i,j} + C_{1,0}(u_h)_{i+1,j} \\
&\quad \left. + C_{-1,1}(u_h)_{i-1,j+1} + C_{0,1}(u_h)_{i,j+1} + C_{1,1}(u_h)_{i+1,j+1} \right) \\
&= \sum_{(m,n) \in \Lambda_5} f_4^{(m,n)} h J_{m,n}^{f_4} + \sum_{(m,n) \in \Lambda_5} f_3^{(m,n)} h J_{m,n}^{f_3} + \sum_{n=0}^6 \psi_2^{(n)} h^{-1} J_{\psi_2,n},
\end{aligned}$$

achieves seventh order accuracy at the irregular point $(x_i, y_j) \in \Gamma_2$, where

$$\begin{aligned}
C_{-1,-1} &= \frac{a_4}{a_3}, & C_{0,-1} &= \frac{2(a_4 + a_3)}{a_3}, & C_{1,-1} &= 1, \\
C_{-1,0} &= \frac{4a_4}{a_3}, & C_{0,0} &= \frac{-10(a_4 + a_3)}{a_3}, & C_{1,0} &= 4, \\
C_{-1,1} &= \frac{a_4}{a_3}, & C_{0,1} &= \frac{2(a_4 + a_3)}{a_3}, & C_{1,1} &= 1,
\end{aligned}$$

$$\begin{aligned}
J_{m,n}^{f_4} &:= \sum_{\ell=-1}^1 C_{-1,\ell} h^{-2} Q_{7,m,n}^V(-h, \ell h), & J_{m,n}^{f_3} &:= \sum_{k=0}^1 \sum_{\ell=-1}^1 C_{k,\ell} h^{-2} Q_{7,m,n}^V(kh, \ell h), \\
J_{\psi_2,n} &:= - \sum_{\ell=-1}^1 C_{-1,\ell} \frac{1}{a_4} G_{7,1,n}^V(-h, \ell h).
\end{aligned}$$

Theorem 6.4. *Let a grid point (x_i, y_j) be an irregular point such that $(x_i, y_j) \in \Gamma_3$ and $(x_i, y_j) \notin \overline{\Gamma_1 \cup \Gamma_2} \cap \overline{\Gamma_3 \cup \Gamma_4}$ (see Fig. 6.4 for an illustration). Let $(u_h)_{i,j}$ be the numerically approximated solution of the exact solution u of the partial differential equation (6.1) at the*

irregular point (x_i, y_j) . Then the compact 9-point scheme:

$$\begin{aligned} \mathcal{L}_h^{\Gamma_3} u_h &:= \frac{1}{h} \left(C_{-1,-1}(u_h)_{i-1,j-1} + C_{0,-1}(u_h)_{i,j-1} + C_{1,-1}(u_h)_{i+1,j-1} \right. \\ &\quad + C_{-1,0}(u_h)_{i-1,j} + C_{0,0}(u_h)_{i,j} + C_{1,0}(u_h)_{i+1,j} \\ &\quad \left. + C_{-1,1}(u_h)_{i-1,j+1} + C_{0,1}(u_h)_{i,j+1} + C_{1,1}(u_h)_{i+1,j+1} \right) \\ &= \sum_{(m,n) \in \Lambda_5} f_3^{(m,n)} h J_{m,n}^{f_3} + \sum_{(m,n) \in \Lambda_5} f_2^{(m,n)} h J_{m,n}^{f_2} + \sum_{m=0}^6 \psi_3^{(m)} h^{-1} J_{\psi_3,m}, \end{aligned}$$

achieves seventh order accuracy at the irregular point $(x_i, y_j) \in \Gamma_3$, where

$$\begin{aligned} C_{-1,-1} &= \frac{a_3}{a_2}, & C_{0,-1} &= \frac{4a_3}{a_2}, & C_{1,-1} &= \frac{a_3}{a_2}, \\ C_{-1,0} &= \frac{2(a_3 + a_2)}{a_2}, & C_{0,0} &= \frac{-10(a_3 + a_2)}{a_2}, & C_{1,0} &= \frac{2(a_3 + a_2)}{a_2}, \\ C_{-1,1} &= 1, & C_{0,1} &= 4, & C_{1,1} &= 1, \end{aligned}$$

$$\begin{aligned} J_{m,n}^{f_3} &:= \sum_{k=-1}^1 C_{k,-1} h^{-2} Q_{7,m,n}^H(kh, -h), & J_{m,n}^{f_2} &:= \sum_{k=-1}^1 \sum_{\ell=0}^1 C_{k,\ell} h^{-2} Q_{7,m,n}^H(kh, \ell h), \\ J_{\psi_3,m} &:= - \sum_{k=-1}^1 C_{k,-1} \frac{1}{a_3} G_{7,m,1}^H(kh, -h). \end{aligned}$$

Theorem 6.5. Let a grid point (x_i, y_j) be an irregular point such that $(x_i, y_j) \in \Gamma_4$ and $(x_i, y_j) \notin \overline{\Gamma_1} \cup \overline{\Gamma_2} \cap \overline{\Gamma_3} \cup \overline{\Gamma_4}$ (see Fig. 6.4 for an illustration). Let $(u_h)_{i,j}$ be the numerically approximated solution of the exact solution u of the partial differential equation (6.1) at the irregular point (x_i, y_j) . Then the compact 9-point scheme:

$$\begin{aligned} \mathcal{L}_h^{\Gamma_4} u_h &:= \frac{1}{h} \left(C_{-1,-1}(u_h)_{i-1,j-1} + C_{0,-1}(u_h)_{i,j-1} + C_{1,-1}(u_h)_{i+1,j-1} \right. \\ &\quad + C_{-1,0}(u_h)_{i-1,j} + C_{0,0}(u_h)_{i,j} + C_{1,0}(u_h)_{i+1,j} \\ &\quad \left. + C_{-1,1}(u_h)_{i-1,j+1} + C_{0,1}(u_h)_{i,j+1} + C_{1,1}(u_h)_{i+1,j+1} \right) \\ &= \sum_{(m,n) \in \Lambda_5} f_4^{(m,n)} h J_{m,n}^{f_4} + \sum_{(m,n) \in \Lambda_5} f_1^{(m,n)} h J_{m,n}^{f_1} + \sum_{m=0}^6 \psi_4^{(m)} h^{-1} J_{\psi_4,m}, \end{aligned}$$

achieves seventh order accuracy at the irregular point $(x_i, y_j) \in \Gamma_4$, where

$$\begin{aligned}
C_{-1,-1} &= \frac{a_4}{a_1}, & C_{0,-1} &= \frac{4a_4}{a_1}, & C_{1,-1} &= \frac{a_4}{a_1}, \\
C_{-1,0} &= \frac{2(a_4 + a_1)}{a_1}, & C_{0,0} &= \frac{-10(a_4 + a_1)}{a_1}, & C_{1,0} &= \frac{2(a_4 + a_1)}{a_1}, \\
C_{-1,1} &= 1, & C_{0,1} &= 4, & C_{1,1} &= 1, \\
J_{m,n}^{f_4} &:= \sum_{k=-1}^1 C_{k,-1} h^{-2} Q_{7,m,n}^H(kh, -h), & J_{m,n}^{f_1} &:= \sum_{k=-1}^1 \sum_{\ell=0}^1 C_{k,\ell} h^{-2} Q_{7,m,n}^H(kh, \ell h), \\
J_{\psi_4,m} &:= - \sum_{k=-1}^1 C_{k,-1} \frac{1}{a_4} G_{7,m,1}^H(kh, -h).
\end{aligned}$$

6.2.3 Stencils for the intersection point

In this subsection, we discuss how to find a seventh order compact 9-point finite difference scheme centered at $(x_i, y_j) = \overline{\Gamma_1 \cup \Gamma_2} \cap \overline{\Gamma_3 \cup \Gamma_4}$ (see Fig. 6.5 for an illustration).

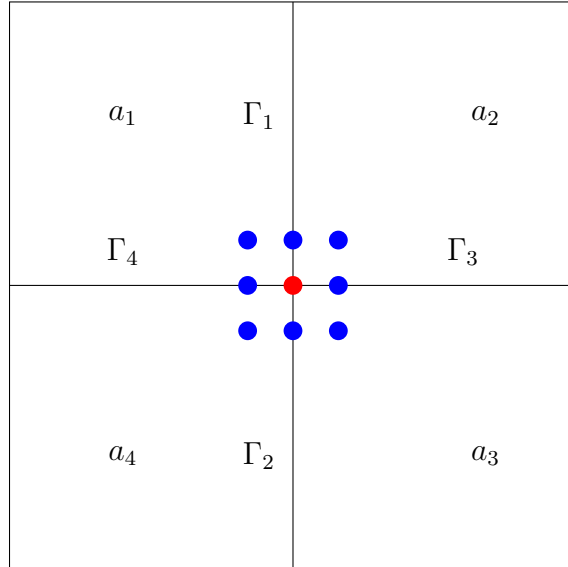


Figure 6.5: An illustration for the compact 9-point scheme for the intersection point of (6.1)

Theorem 6.6. Let a grid point (x_i, y_j) be an irregular point such that $(x_i, y_j) = \overline{\Gamma_1 \cup \Gamma_2} \cap \overline{\Gamma_3 \cup \Gamma_4}$ (see Fig. 6.5 for an illustration). Let $(u_h)_{i,j}$ be the numerically approximated solution of the exact solution u of the partial differential equation (6.1) at the irregular point (x_i, y_j) .

Then the compact 9-point scheme:

$$\begin{aligned}
\mathcal{L}_h^S u_h &:= \frac{1}{h} \left(C_{-1,-1}(u_h)_{i-1,j-1} + C_{0,-1}(u_h)_{i,j-1} + C_{1,-1}(u_h)_{i+1,j-1} \right. \\
&\quad + C_{-1,0}(u_h)_{i-1,j} + C_{0,0}(u_h)_{i,j} + C_{1,0}(u_h)_{i+1,j} \\
&\quad \left. + C_{-1,1}(u_h)_{i-1,j+1} + C_{0,1}(u_h)_{i,j+1} + C_{1,1}(u_h)_{i+1,j+1} \right) \\
&= \sum_{(m,n) \in \Lambda_7^{H,1}} h F_{7,m,n}^{H,1} + \sum_{(m,n) \in \Lambda_5} h F_{7,m,n} + \sum_{(m,n) \in \Lambda_7^{H,1}} h^{-1} \Psi_{7,m,n}^{H,1} + \sum_{m=0}^6 h^{-1} \Psi_{7,m},
\end{aligned} \tag{6.17}$$

achieves seventh order accuracy at the irregular point (x_i, y_j) , where

$$\begin{aligned}
C_{-1,-1} &= \frac{a_1 a_4 (a_2 + a_3)}{a_2^2 (a_1 + a_4)}, & C_{0,-1} &= \frac{2a_4 (a_2 + a_3) (a_1 + a_2)}{a_2^2 (a_1 + a_4)}, & C_{1,-1} &= \frac{a_3}{a_2}, \\
C_{-1,0} &= \frac{2a_1 (a_2 + a_3)}{a_2^2}, & C_{0,0} &= \frac{-5(a_2 + a_3) (a_1 + a_2)}{a_2^2}, & C_{1,0} &= \frac{2(a_2 + a_3)}{a_2}, \\
C_{-1,1} &= \frac{a_1^2 (a_2 + a_3)}{a_2^2 (a_1 + a_4)}, & C_{0,1} &= \frac{2a_1 (a_2 + a_3) (a_1 + a_2)}{a_2^2 (a_1 + a_4)}, & C_{1,1} &= 1,
\end{aligned} \tag{6.18}$$

and $F_{7,m,n}^{H,1}$, $F_{7,m,n}$, $\Psi_{7,m,n}^{H,1}$, $\Psi_{7,m}$ are defined in (6.51), (6.52), (6.53), (6.54), $\{C_{k,\ell}^- : k = -1, 0, \ell = -1, 0, 1\}$ and $\{C_{k,\ell}^+ : k = 0, 1, \ell = -1, 0, 1\}$ are defined in (6.58).

6.2.4 Convergence analysis

We now prove the following convergence result for the sixth or seventh order compact 9-point finite difference schemes developed in Theorems 6.1 to 6.6.

Theorem 6.7. *Under the assumptions (A1)–(A3) in Section 6.1, we consider the compact 9-point finite difference scheme in Theorems 6.1 to 6.6. Then the compact 9-point scheme for the elliptic interface problem in (6.1) has the convergence rate of order 6, that is, there exists a positive constant C independent of h such that*

$$\|u - u_h\|_\infty \leq Ch^6, \tag{6.19}$$

where u and u_h are the exact solution and the numerical solution of (6.1), respectively.

Proof. Clearly, all the $\{C_{k,\ell}\}_{k,\ell=-1,0,1}$ in Theorems 6.1 to 6.6 satisfy the following sign condition,

$$\begin{cases} C_{k,\ell} < 0, & \text{if } (k, \ell) = (0, 0), \\ C_{k,\ell} > 0, & \text{if } (k, \ell) \neq (0, 0), \end{cases}$$

and the summation condition,

$$\sum_{k=-1}^1 \sum_{\ell=-1}^1 C_{k,\ell} = 0.$$

So by the proof of Theorem 3.6, we could obtain (6.19). □

6.3 Numerical experiments

Example 6.1. Let $\Omega = (0, 1)^2$. The functions in (6.1) are given by

$$\begin{aligned} a_1 &= a\chi_{\Omega_1} = 10^{-5}, & a_2 &= a\chi_{\Omega_2} = 10^5, & a_3 &= a\chi_{\Omega_3} = 10^{-5}, & a_4 &= a\chi_{\Omega_4} = 10^5, \\ u_1 &= u\chi_{\Omega_1} = -\sin(2\pi x) \exp(-y) - \sin(2\pi(-y+1)) \exp(-y), \\ u_2 &= u\chi_{\Omega_2} = -\sin(2\pi(-x+1)) \exp(-y) - \sin(2\pi(-y+1)) \exp(-y), \\ u_3 &= u\chi_{\Omega_3} = -\sin(2\pi(-x+1)) \exp(-y) - \sin(2\pi y) \exp(-y), \\ u_4 &= u\chi_{\Omega_4} = -\sin(2\pi x) \exp(-y) - \sin(2\pi y) \exp(-y), \end{aligned}$$

the other functions f_p, ψ_p for $p = 1, 2, 3, 4$ in (6.1) can be obtained by plugging the above functions into (6.1). The numerical results are presented in Table 6.1 and Fig. 6.6.

Table 6.1: Performance in Example 6.1 of our proposed sixth order compact 9-point finite difference scheme on uniform Cartesian meshes with $h = 2^{-J} \times 1$.

J	$\frac{\ u_h - u\ _2}{\ u\ _2}$	order	$\ u_h - u\ _\infty$	order
2	8.2852E-04	0	1.1208E-03	0
3	1.1540E-05	6.16588	1.8687E-05	5.90641
4	1.7254E-07	6.06356	2.9743E-07	5.97331
5	2.6489E-09	6.02534	4.7148E-09	5.97921
6	4.1095E-11	6.01031	7.4568E-11	5.98251
7	7.5388E-13	5.76847	1.3224E-12	5.81727

Example 6.2. Let $\Omega = (0, 1)^2$. The functions in (6.1) are given by

$$\begin{aligned} a_1 &= a\chi_{\Omega_1} = 10^7, & a_2 &= a\chi_{\Omega_2} = 10^{-3}, & a_3 &= a\chi_{\Omega_3} = 10^4, & a_4 &= a\chi_{\Omega_4} = 10^{-6}, \\ u_1 &= u\chi_{\Omega_1} = (x^3 + (1-y)^3) \exp(-x+y), \\ u_2 &= u\chi_{\Omega_2} = ((1-x)^3 + (1-y)^3) \exp(-x+y), \\ u_3 &= u\chi_{\Omega_3} = ((1-x)^3 + y^3) \exp(-x+y), \\ u_4 &= u\chi_{\Omega_4} = (x^3 + y^3) \exp(-x+y), \end{aligned}$$

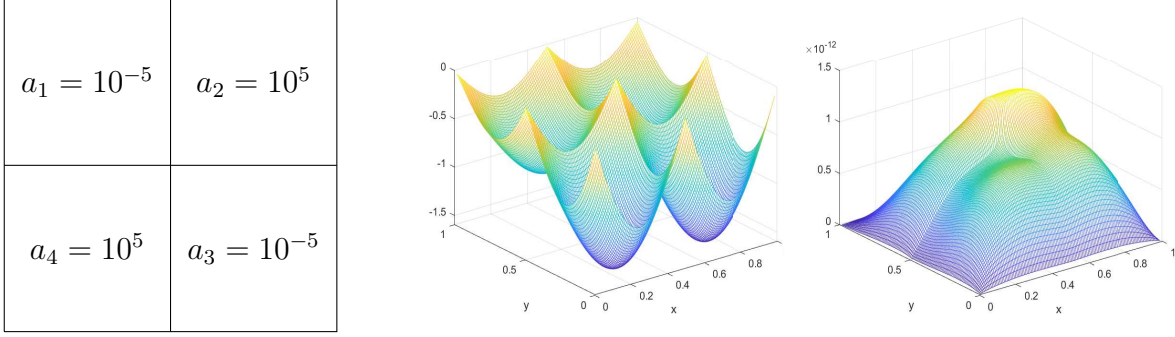


Figure 6.6: Example [6.1](#): the coefficient $a(x, y)$ (left), the numerical solution u_h (middle) and the error $|u_h - u|$ (right) with $h = 2^{-7} \times 1$, where u_h is computed by our proposed sixth order compact 9-point finite difference scheme.

the other functions f_p, ψ_p for $p = 1, 2, 3, 4$ in [\(6.1\)](#) can be obtained by plugging the above functions into [\(6.1\)](#). The numerical results are presented in Table [6.2](#) and Fig. [6.7](#).

Table 6.2: Performance in Example [6.2](#) of our proposed sixth order compact 9-point finite difference scheme on uniform Cartesian meshes with $h = 2^{-J} \times 1$.

J	$\frac{\ u_h - u\ _2}{\ u\ _2}$	order	$\ u_h - u\ _\infty$	order
2	1.6488E-05	0	4.0342E-06	0
3	2.5239E-07	6.02960	5.8604E-08	6.10514
4	3.9327E-09	6.00398	8.9118E-10	6.03913
5	6.1615E-11	5.99611	1.3797E-11	6.01326
6	9.5329E-13	6.01421	2.0797E-13	6.05185

Example 6.3. Let $\Omega = (0, 1)^2$. The functions in [\(6.1\)](#) are given by

$$\begin{aligned}
 a_1 &= a\chi_{\Omega_1} = 10^{-4}, & a_2 &= a\chi_{\Omega_2} = 10^5, & a_3 &= a\chi_{\Omega_3} = 10^{-4}, & a_4 &= a\chi_{\Omega_4} = 10^6, \\
 u_1 &= u\chi_{\Omega_1} = \sin(\pi x) \sin(\pi y) 2x(2 - 2y), \\
 u_2 &= u\chi_{\Omega_2} = \sin(\pi x) \sin(\pi y) (2 - 2x)(2 - 2y), \\
 u_3 &= u\chi_{\Omega_3} = \sin(\pi x) \sin(\pi y) (2 - 2x) 2y, \\
 u_4 &= u\chi_{\Omega_4} = \sin(\pi x) \sin(\pi y) 2x 2y,
 \end{aligned}$$

the other functions f_p, ψ_p for $p = 1, 2, 3, 4$ in [\(6.1\)](#) can be obtained by plugging the above functions into [\(6.1\)](#). The numerical results are presented in Table [6.3](#) and Fig. [6.8](#).

$a_1 = 10^7$	$a_2 = 10^{-3}$
$a_4 = 10^{-6}$	$a_3 = 10^4$

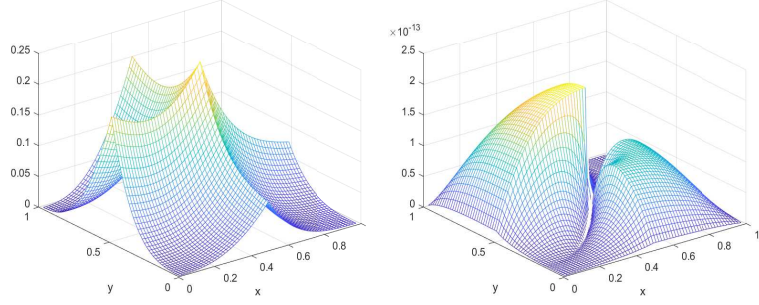


Figure 6.7: Example [6.2](#): the coefficient $a(x, y)$ (left), the numerical solution u_h (middle) and the error $|u_h - u|$ (right) with $h = 2^{-6} \times 1$, where u_h is computed by our proposed sixth order compact 9-point finite difference scheme.

Table 6.3: Performance in Example [6.3](#) of our proposed sixth order compact 9-point finite difference scheme on uniform Cartesian meshes with $h = 2^{-J} \times 1$.

J	$\frac{\ u_h - u\ _2}{\ u\ _2}$	order	$\ u_h - u\ _\infty$	order
2	6.2929E-04	0	6.6139E-04	0
3	4.1295E-06	7.25162	2.5461E-06	8.02110
4	7.1880E-08	5.84423	4.1784E-08	5.92915
5	1.1898E-09	5.91684	6.6635E-10	5.97054
6	1.8897E-11	5.97638	1.0523E-11	5.98470
7	3.9230E-13	5.59003	1.8095E-13	5.86181

$a_1 = 10^{-4}$	$a_2 = 10^5$
$a_4 = 10^6$	$a_3 = 10^{-4}$

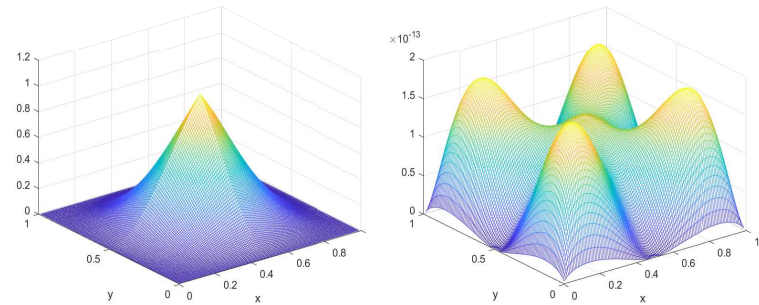


Figure 6.8: Example [6.3](#): the coefficient $a(x, y)$ (left), the numerical solution u_h (middle) and the error $|u_h - u|$ (right) with $h = 2^{-7} \times 1$, where u_h is computed by our proposed sixth order compact 9-point finite difference scheme.

6.4 Conclusion

To our best knowledge, so far there were no compact 9-point finite difference schemes available in the literature, that can achieve fifth or sixth order for elliptic interface problems with intersecting interfaces (6.1). Our contributions of this chapter are as follows:

- (1) We construct the sixth order compact 9-point finite difference scheme on uniform meshes for (6.1) with 4 discontinuous constant coefficients.
- (2) The formulas of the proposed sixth order compact 9-point finite difference scheme are constructed explicitly for all grid points (regular points, interface points, and the intersection point).
- (3) We prove the sixth order convergence rate of our proposed compact 9-point finite difference scheme by the discrete maximum principle.
- (4) Our numerical experiments confirm the flexibility and the sixth order accuracy in l_2 and l_∞ norms of our proposed compact 9-point scheme.

6.5 Proofs of Theorems 6.2 to 6.6

Proof of Theorem 6.2. Since $[u] = 0$ and $[a\nabla u \cdot \vec{n}] = \psi_1$ on Γ_1 , $u_1^{(0,0)} - u_2^{(0,0)} = 0$ and $a_1 u_1^{(1,0)} - a_2 u_2^{(1,0)} = -\psi_1^{(0)}$. Then we have $u_1^{(0,n)} = u_2^{(0,n)}$ and $u_1^{(1,n)} = \frac{a_2}{a_1} u_2^{(1,n)} - \frac{1}{a_1} \psi_1^{(n)}$ for all $n = 0, \dots, M$. By (6.5) with M being replaced by $M - 1$, for $x, y \in [-h, h]$, we have

$$\begin{aligned}
& u_1(x + x_i, y + y_j) + \mathcal{O}(h^{M+1}) \\
&= \sum_{(m,n) \in \Lambda_M^{V,1}} u_1^{(m,n)} G_{M,m,n}^V(x, y) + \sum_{(m,n) \in \Lambda_{M-2}} f_1^{(m,n)} Q_{M,m,n}^V(x, y), \\
&= \sum_{n=0}^M u_1^{(0,n)} G_{M,0,n}^V(x, y) + \sum_{n=0}^{M-1} u_1^{(1,n)} G_{M,1,n}^V(x, y) + \sum_{(m,n) \in \Lambda_{M-2}} f_1^{(m,n)} Q_{M,m,n}^V(x, y), \\
&= \sum_{n=0}^M u_2^{(0,n)} G_{M,0,n}^V(x, y) + \sum_{n=0}^{M-1} \left(\frac{a_2}{a_1} u_2^{(1,n)} - \frac{\psi_1^{(n)}}{a_1} \right) G_{M,1,n}^V(x, y) + \sum_{(m,n) \in \Lambda_{M-2}} f_1^{(m,n)} Q_{M,m,n}^V(x, y), \quad (6.20) \\
&= \sum_{n=0}^M u_2^{(0,n)} G_{M,0,n}^V(x, y) + \sum_{n=0}^{M-1} \frac{a_2}{a_1} u_2^{(1,n)} G_{M,1,n}^V(x, y) - \sum_{n=0}^{M-1} \frac{1}{a_1} \psi_1^{(n)} G_{M,1,n}^V(x, y) \\
&\quad + \sum_{(m,n) \in \Lambda_{M-2}} f_1^{(m,n)} Q_{M,m,n}^V(x, y), \\
&= \sum_{(m,n) \in \Lambda_M^{V,1}} u_2^{(m,n)} \left(\frac{a_2}{a_1} \right)^m G_{M,m,n}^V(x, y) - \sum_{n=0}^{M-1} \frac{\psi_1^{(n)}}{a_1} G_{M,1,n}^V(x, y) + \sum_{(m,n) \in \Lambda_{M-2}} f_1^{(m,n)} Q_{M,m,n}^V(x, y),
\end{aligned}$$

and

$$u_2(x + x_i, y + y_j) = \sum_{(m,n) \in \Lambda_M^{V,1}} u_2^{(m,n)} G_{M,m,n}^V(x, y) + \sum_{(m,n) \in \Lambda_{M-2}} f_2^{(m,n)} Q_{M,m,n}^V(x, y) + \mathcal{O}(h^{M+1}). \quad (6.21)$$

From (6.7) and (6.8), we observe that

$$\begin{aligned} & u_1(x_i, y + y_j) + \mathcal{O}(h^{M+1}) \\ &= \sum_{(m,n) \in \Lambda_M^{V,1}} u_2^{(m,n)} \left(\frac{a_2}{a_1} \right)^m G_{M,m,n}^V(0, y) - \sum_{n=0}^{M-1} \frac{\psi_1^{(n)}}{a_1} G_{M,1,n}^V(0, y) + \sum_{(m,n) \in \Lambda_{M-2}} f_1^{(m,n)} Q_{M,m,n}^V(0, y), \\ &= \sum_{n=0}^M u_2^{(0,n)} G_{M,0,n}^V(0, y) = u_2(x_i, y + y_j) + \mathcal{O}(h^{M+1}), \end{aligned}$$

i.e.,

$$u_1(x_i, y + y_j) = u_2(x_i, y + y_j) + \mathcal{O}(h^{M+1}), \quad y \in [-h, h]. \quad (6.22)$$

By (6.20), (6.21) and (6.22), we could define that

$$\begin{aligned} \mathcal{L}_h^{\Gamma_1} u &:= \frac{1}{h} \left(C_{-1,-1} u_1(x_i - h, y_j - h) + C_{0,-1} u_2(x_i, y_j - h) + C_{1,-1} u_2(x_i + h, y_j - h) \right. \\ &\quad + C_{-1,0} u_1(x_i - h, y_j) + C_{0,0} u_2(x_i, y_j) + C_{1,0} u_2(x_i + h, y_j) \\ &\quad \left. + C_{-1,1} u_1(x_i - h, y_j + h) + C_{0,1} u_2(x_i, y_j + h) + C_{1,1} u_2(x_i + h, y_j + h) \right) \\ &= \sum_{(m,n) \in \Lambda_M^{V,1}} u_2^{(m,n)} h^{-1} I_{m,n} + \sum_{(m,n) \in \Lambda_{M-2}} f_1^{(m,n)} h J_{m,n}^{f_1} \\ &\quad + \sum_{(m,n) \in \Lambda_{M-2}} f_2^{(m,n)} h J_{m,n}^{f_2} + \sum_{n=0}^{M-1} \psi_1^{(n)} h^{-1} J_{\psi_1,n} = \mathcal{O}(h^M), \quad \text{as } h \rightarrow 0 \end{aligned}$$

where

$$\begin{aligned} C_{k,\ell} &:= \sum_{p=0}^M c_{k,\ell,p} h^p \quad \text{with } c_{k,\ell,p} \in \mathbb{R}, \\ I_{m,n} &:= \sum_{\ell=-1}^1 C_{-1,\ell} \left(\frac{a_2}{a_1} \right)^m G_{M,m,n}^V(-h, \ell h) + \sum_{k=0}^1 \sum_{\ell=-1}^1 C_{k,\ell} G_{M,m,n}^V(kh, \ell h), \\ J_{m,n}^{f_1} &:= \sum_{\ell=-1}^1 C_{-1,\ell} h^{-2} Q_{M,m,n}^V(-h, \ell h), \quad J_{m,n}^{f_2} := \sum_{k=0}^1 \sum_{\ell=-1}^1 C_{k,\ell} h^{-2} Q_{M,m,n}^V(kh, \ell h), \\ J_{\psi_1,n} &:= - \sum_{\ell=-1}^1 C_{-1,\ell} \frac{1}{a_1} G_{M,1,n}^V(-h, \ell h). \end{aligned} \quad (6.23)$$

Let

$$\begin{aligned}
\mathcal{L}_h^{\Gamma_1} u_h &:= \frac{1}{h} \sum_{k=-1}^1 \sum_{\ell=-1}^1 C_{k,\ell}(u_h)_{i+k,j+\ell} \\
&= \sum_{(m,n) \in \Lambda_{M-2}} f_1^{(m,n)} h J_{m,n}^{f_1} + \sum_{(m,n) \in \Lambda_{M-2}} f_2^{(m,n)} h J_{m,n}^{f_2} + \sum_{n=0}^{M-1} \psi_1^{(n)} h^{-1} J_{\psi_1, n}.
\end{aligned} \tag{6.24}$$

Then

$$\mathcal{L}_h^{\Gamma_1}(u - u_h) = \mathcal{O}(h^M),$$

if $I_{m,n}$ in (6.23) satisfies

$$I_{m,n} = \mathcal{O}(h^{M+1}), \quad \text{for all } n = 0, \dots, M. \tag{6.25}$$

By calculation, the maximum integer M for the linear system in (6.25) to have a nontrivial solution $\{C_{k,\ell}(0)\}_{k,\ell=-1,0,1}$ is $M = 7$. In particular, one nontrivial solution of (6.25) with $M = 7$ is given in (6.15). So (6.24) and (6.25) with $M = 7$ result in (6.14), (6.15) and (6.16). \square

Proofs of Theorems 6.3 to 6.5. The proofs are similar to the proof of Theorem 6.2. \square

Proof of Theorem 6.6. Since $[u] = 0$ and $[a \nabla u \cdot \vec{n}] = \psi_3$ on Γ_3 , $u_3^{(0,0)} - u_2^{(0,0)} = 0$ and $a_3 u_3^{(0,1)} - a_2 u_2^{(0,1)} = -\psi_3^{(0)}$. Then we have $u_3^{(m,0)} = u_2^{(m,0)}$ and $u_3^{(m,1)} = \frac{a_2}{a_3} u_2^{(m,1)} - \frac{1}{a_3} \psi_3^{(m)}$ for all $m = 0, \dots, M$. By (6.6) with M being replaced by $M - 1$, for $x, y \in [-h, h]$, we have

$$\begin{aligned}
&u_3(x + x_i, y + y_j) + \mathcal{O}(h^{M+1}) \\
&= \sum_{(m,n) \in \Lambda_M^{H,1}} u_3^{(m,n)} G_{M,m,n}^H(x, y) + \sum_{(m,n) \in \Lambda_{M-2}} f_3^{(m,n)} Q_{M,m,n}^H(x, y), \\
&= \sum_{m=0}^M u_3^{(m,0)} G_{M,m,0}^H(x, y) + \sum_{m=0}^{M-1} u_3^{(m,1)} G_{M,m,1}^H(x, y) + \sum_{(m,n) \in \Lambda_{M-2}} f_3^{(m,n)} Q_{M,m,n}^H(x, y), \\
&= \sum_{m=0}^M u_2^{(m,0)} G_{M,m,0}^H(x, y) + \sum_{m=0}^{M-1} \left(\frac{a_2}{a_3} u_2^{(m,1)} - \frac{\psi_3^{(m)}}{a_3} \right) G_{M,m,1}^H(x, y) + \sum_{(m,n) \in \Lambda_{M-2}} f_3^{(m,n)} Q_{M,m,n}^H(x, y), \\
&= \sum_{m=0}^M u_2^{(m,0)} G_{M,m,0}^H(x, y) + \sum_{m=0}^{M-1} \frac{a_2}{a_3} u_2^{(m,1)} G_{M,m,1}^H(x, y) - \sum_{m=0}^{M-1} \frac{1}{a_3} \psi_3^{(m)} G_{M,m,1}^H(x, y) \\
&\quad + \sum_{(m,n) \in \Lambda_{M-2}} f_3^{(m,n)} Q_{M,m,n}^H(x, y), \\
&= \sum_{(m,n) \in \Lambda_M^{H,1}} u_2^{(m,n)} \left(\frac{a_2}{a_3} \right)^n G_{M,m,n}^H(x, y) - \sum_{m=0}^{M-1} \frac{\psi_3^{(m)}}{a_3} G_{M,m,1}^H(x, y) + \sum_{(m,n) \in \Lambda_{M-2}} f_3^{(m,n)} Q_{M,m,n}^H(x, y),
\end{aligned}$$

i.e.,

$$\begin{aligned}
u_3(x + x_i, y + y_j) &= \sum_{(m,n) \in \Lambda_M^{H,1}} u_2^{(m,n)} \left(\frac{a_2}{a_3} \right)^n G_{M,m,n}^H(x, y) - \sum_{m=0}^{M-1} \frac{1}{a_3} \psi_3^{(m)} G_{M,m,1}^H(x, y) \\
&+ \sum_{(m,n) \in \Lambda_{M-2}} f_3^{(m,n)} Q_{M,m,n}^H(x, y) + \mathcal{O}(h^{M+1}), \quad x, y \in [-h, h],
\end{aligned} \tag{6.26}$$

Similarly, we have

$$\begin{aligned}
u_4(x + x_i, y + y_j) &= \sum_{(m,n) \in \Lambda_M^{H,1}} u_1^{(m,n)} \left(\frac{a_1}{a_4} \right)^n G_{M,m,n}^H(x, y) - \sum_{m=0}^{M-1} \frac{1}{a_4} \psi_4^{(m)} G_{M,m,1}^H(x, y) \\
&+ \sum_{(m,n) \in \Lambda_{M-2}} f_4^{(m,n)} Q_{M,m,n}^H(x, y) + \mathcal{O}(h^{M+1}), \quad x, y \in [-h, h],
\end{aligned} \tag{6.27}$$

$$\begin{aligned}
u_1(x + x_i, y + y_j) &= \sum_{(m,n) \in \Lambda_M^{H,1}} u_1^{(m,n)} G_{M,m,n}^H(x, y) \\
&+ \sum_{(m,n) \in \Lambda_{M-2}} f_1^{(m,n)} Q_{M,m,n}^H(x, y) + \mathcal{O}(h^{M+1}), \quad x, y \in [-h, h],
\end{aligned} \tag{6.28}$$

$$\begin{aligned}
u_2(x + x_i, y + y_j) &= \sum_{(m,n) \in \Lambda_M^{H,1}} u_2^{(m,n)} G_{M,m,n}^H(x, y) \\
&+ \sum_{(m,n) \in \Lambda_{M-2}} f_2^{(m,n)} Q_{M,m,n}^H(x, y) + \mathcal{O}(h^{M+1}), \quad x, y \in [-h, h].
\end{aligned} \tag{6.29}$$

On the other hand, we have

$$u_1^{(0,n)} = u_2^{(0,n)}, \quad u_1^{(1,n)} = \frac{a_2}{a_1} u_2^{(1,n)} - \frac{1}{a_1} \psi_1^{(n)}, \quad \text{for } n = 0, \dots, M, \tag{6.30}$$

$$\text{odd}(m) := \begin{cases} 0, & \text{if } m \text{ is even,} \\ 1, & \text{if } m \text{ is odd,} \end{cases} \tag{6.31}$$

So (6.30) and (6.31) lead to

$$u_1^{(\text{odd}(m), n+m-\text{odd}(m))} = \begin{cases} u_2^{(0, n+m)}, & \text{if } m \text{ is even,} \\ \frac{a_2}{a_1} u_2^{(1, m+n-1)} - \frac{1}{a_1} \psi_1^{(m+n-1)}, & \text{if } m \text{ is odd,} \end{cases} \quad \text{for all } (m, n) \in \Lambda_M^{V,2},$$

i.e.,

$$u_1^{(\text{odd}(m), n+m-\text{odd}(m))} = \left(\frac{a_2}{a_1}\right)^{\text{odd}(m)} u_2^{(\text{odd}(m), m+n-\text{odd}(m))} - \frac{\text{odd}(m)}{a_1} \psi_1^{(m+n-\text{odd}(m))}, \quad \text{for all } (m, n) \in \Lambda_M^{V,2}. \quad (6.32)$$

(2.4) implies

$$u_i^{(m,n)} = (-1)^{\lfloor \frac{m}{2} \rfloor} u_i^{(\text{odd}(m), n+m-\text{odd}(m))} + \sum_{\ell=1}^{\lfloor m/2 \rfloor} \frac{(-1)^\ell}{a_i} f_i^{(m-2\ell, n+2\ell-2)}, \quad \forall (m, n) \in \Lambda_M^{V,2}, \text{ and } i = 1, 2. \quad (6.33)$$

From (6.32) and (6.33), we observe that

$$\begin{aligned} u_1^{(m,n)} &= (-1)^{\lfloor \frac{m}{2} \rfloor} u_1^{(\text{odd}(m), n+m-\text{odd}(m))} + \sum_{\ell=1}^{\lfloor m/2 \rfloor} \frac{(-1)^\ell}{a_1} f_1^{(m-2\ell, n+2\ell-2)}, \\ &= (-1)^{\lfloor \frac{m}{2} \rfloor} \left(\frac{a_2}{a_1}\right)^{\text{odd}(m)} u_2^{(\text{odd}(m), m+n-\text{odd}(m))} - (-1)^{\lfloor \frac{m}{2} \rfloor} \frac{\text{odd}(m)}{a_1} \psi_1^{(m+n-\text{odd}(m))} \\ &\quad + \sum_{\ell=1}^{\lfloor m/2 \rfloor} \frac{(-1)^\ell}{a_1} f_1^{(m-2\ell, n+2\ell-2)}, \quad \text{for all } (m, n) \in \Lambda_M^{V,2}, \end{aligned} \quad (6.34)$$

and

$$u_2^{(m,n)} = (-1)^{\lfloor \frac{m}{2} \rfloor} u_2^{(\text{odd}(m), n+m-\text{odd}(m))} + \sum_{\ell=1}^{\lfloor m/2 \rfloor} \frac{(-1)^\ell}{a_2} f_2^{(m-2\ell, n+2\ell-2)}, \quad \text{for all } (m, n) \in \Lambda_M^{V,2}. \quad (6.35)$$

Note that for $m = 0, 1$, the summation $\sum_{\ell=1}^{\lfloor m/2 \rfloor}$ in (6.34) and (6.35) is empty. From Figs. 6.2 and 6.3, we have $\Lambda_M^{H,1} \setminus \Lambda_M^{V,2} = \{(0, 0), (0, 1), (1, 0), (1, 1)\}$. So (6.35) implies

$$u_2^{(m,n)} = (-1)^{\lfloor \frac{m}{2} \rfloor} u_2^{(\text{odd}(m), n+m-\text{odd}(m))} + \sum_{\ell=1}^{\lfloor m/2 \rfloor} \frac{(-1)^\ell}{a_2} f_2^{(m-2\ell, n+2\ell-2)}, \quad \forall (m, n) \in \Lambda_M^{H,1}. \quad (6.36)$$

From (6.30),

$$\begin{aligned} u_1^{(0,0)} &= u_2^{(0,0)}, & u_1^{(0,1)} &= u_2^{(0,1)}, \\ u_1^{(1,0)} &= \frac{a_2}{a_1} u_2^{(1,0)} - \frac{1}{a_1} \psi_1^{(0)}, & u_1^{(1,1)} &= \frac{a_2}{a_1} u_2^{(1,1)} - \frac{1}{a_1} \psi_1^{(1)}. \end{aligned} \quad (6.37)$$

So $\Lambda_M^{H,1} \setminus \Lambda_M^{V,2} = \{(0,0), (0,1), (1,0), (1,1)\}$, (6.34) and (6.37) result in

$$\begin{aligned} u_1^{(m,n)} &= (-1)^{\lfloor \frac{m}{2} \rfloor} \left(\frac{a_2}{a_1} \right)^{\text{odd}(m)} u_2^{(\text{odd}(m), m+n-\text{odd}(m))} - (-1)^{\lfloor \frac{m}{2} \rfloor} \frac{\text{odd}(m)}{a_1} \psi_1^{(m+n-\text{odd}(m))} \\ &\quad + \sum_{\ell=1}^{\lfloor m/2 \rfloor} \frac{(-1)^\ell}{a_1} f_1^{(m-2\ell, n+2\ell-2)}, \quad \forall (m, n) \in \Lambda_M^{H,1}. \end{aligned} \quad (6.38)$$

By (6.28) and (6.38), we have

$$\begin{aligned} &u_1(x + x_i, y + y_j) + \mathcal{O}(h^{M+1}) \\ &= \sum_{(m,n) \in \Lambda_M^{H,1}} u_1^{(m,n)} G_{M,m,n}^H(x, y) + \sum_{(m,n) \in \Lambda_{M-2}} f_1^{(m,n)} Q_{M,m,n}^H(x, y), \\ &= \sum_{(m,n) \in \Lambda_M^{H,1}} \left((-1)^{\lfloor \frac{m}{2} \rfloor} \left(\frac{a_2}{a_1} \right)^{\text{odd}(m)} u_2^{(\text{odd}(m), m+n-\text{odd}(m))} - (-1)^{\lfloor \frac{m}{2} \rfloor} \frac{\text{odd}(m)}{a_1} \psi_1^{(m+n-\text{odd}(m))} \right. \\ &\quad \left. + \sum_{\ell=1}^{\lfloor m/2 \rfloor} \frac{(-1)^\ell}{a_1} f_1^{(m-2\ell, n+2\ell-2)} \right) G_{M,m,n}^H(x, y) + \sum_{(m,n) \in \Lambda_{M-2}} f_1^{(m,n)} Q_{M,m,n}^H(x, y) \\ &= \sum_{(m,n) \in \Lambda_M^{H,1}} (-1)^{\lfloor \frac{m}{2} \rfloor} \left(\frac{a_2}{a_1} \right)^{\text{odd}(m)} u_2^{(\text{odd}(m), m+n-\text{odd}(m))} G_{M,m,n}^H(x, y) \\ &\quad + \sum_{(m,n) \in \Lambda_M^{H,1}} \left(-\frac{\text{odd}(m)}{(-1)^{\lfloor \frac{m}{2} \rfloor} a_1} \psi_1^{(m+n-\text{odd}(m))} + \sum_{\ell=1}^{\lfloor m/2 \rfloor} \frac{(-1)^\ell}{a_1} f_1^{(m-2\ell, n+2\ell-2)} \right) G_{M,m,n}^H(x, y) \\ &\quad + \sum_{(m,n) \in \Lambda_{M-2}} f_1^{(m,n)} Q_{M,m,n}^H(x, y), \quad x, y \in [-h, h]. \end{aligned} \quad (6.39)$$

Similarly, (6.29) and (6.36) imply

$$\begin{aligned} &u_2(x + x_i, y + y_j) + \mathcal{O}(h^{M+1}) \\ &= \sum_{(m,n) \in \Lambda_M^{H,1}} (-1)^{\lfloor \frac{m}{2} \rfloor} u_2^{(\text{odd}(m), n+m-\text{odd}(m))} G_{M,m,n}^H(x, y) \\ &\quad + \sum_{(m,n) \in \Lambda_M^{H,1}} \sum_{\ell=1}^{\lfloor m/2 \rfloor} \frac{(-1)^\ell}{a_2} f_2^{(m-2\ell, n+2\ell-2)} G_{M,m,n}^H(x, y) \\ &\quad + \sum_{(m,n) \in \Lambda_{M-2}} f_2^{(m,n)} Q_{M,m,n}^H(x, y), \quad x, y \in [-h, h], \end{aligned} \quad (6.40)$$

(6.26) and (6.36) imply

$$\begin{aligned}
& u_3(x + x_i, y + y_j) + \mathcal{O}(h^{M+1}) \\
&= \sum_{(m,n) \in \Lambda_M^{H,1}} (-1)^{\lfloor \frac{m}{2} \rfloor} u_2^{(\text{odd}(m), n+m-\text{odd}(m))} \left(\frac{a_2}{a_3} \right)^n G_{M,m,n}^H(x, y) \\
&+ \sum_{(m,n) \in \Lambda_M^{H,1}} \sum_{\ell=1}^{\lfloor m/2 \rfloor} \frac{(-1)^\ell}{a_2} f_2^{(m-2\ell, n+2\ell-2)} \left(\frac{a_2}{a_3} \right)^n G_{M,m,n}^H(x, y) - \sum_{m=0}^{M-1} \frac{1}{a_3} \psi_3^{(m)} G_{M,m,1}^H(x, y) \\
&+ \sum_{(m,n) \in \Lambda_{M-2}} f_3^{(m,n)} Q_{M,m,n}^H(x, y), \quad x, y \in [-h, h].
\end{aligned} \tag{6.41}$$

(6.27) and (6.38) imply

$$\begin{aligned}
& u_4(x + x_i, y + y_j) + \mathcal{O}(h^{M+1}) \\
&= \sum_{(m,n) \in \Lambda_M^{H,1}} (-1)^{\lfloor \frac{m}{2} \rfloor} \left(\frac{a_2}{a_1} \right)^{\text{odd}(m)} u_2^{(\text{odd}(m), m+n-\text{odd}(m))} \left(\frac{a_1}{a_4} \right)^n G_{M,m,n}^H(x, y) \\
&- \sum_{(m,n) \in \Lambda_M^{H,1}} (-1)^{\lfloor \frac{m}{2} \rfloor} \frac{\text{odd}(m)}{a_1} \psi_1^{(m+n-\text{odd}(m))} \left(\frac{a_1}{a_4} \right)^n G_{M,m,n}^H(x, y) \\
&+ \sum_{(m,n) \in \Lambda_M^{H,1}} \sum_{\ell=1}^{\lfloor m/2 \rfloor} \frac{(-1)^\ell}{a_1} f_1^{(m-2\ell, n+2\ell-2)} \left(\frac{a_1}{a_4} \right)^n G_{M,m,n}^H(x, y) \\
&- \sum_{m=0}^{M-1} \frac{1}{a_4} \psi_4^{(m)} G_{M,m,1}^H(x, y) + \sum_{(m,n) \in \Lambda_{M-2}} f_4^{(m,n)} Q_{M,m,n}^H(x, y), \quad x, y \in [-h, h].
\end{aligned} \tag{6.42}$$

Note that

$$\begin{aligned}
& \sum_{(m,n) \in \Lambda_M^{H,1}} (-1)^{\lfloor \frac{m}{2} \rfloor} \left(\frac{a_2}{a_1} \right)^{\text{odd}(m)} u_2^{(\text{odd}(m), m+n-\text{odd}(m))} G_{M,m,n}^H(x, y) \\
&= \sum_{m=0}^M (-1)^{\lfloor \frac{m}{2} \rfloor} \left(\frac{a_2}{a_1} \right)^{\text{odd}(m)} u_2^{(\text{odd}(m), m-\text{odd}(m))} G_{M,m,0}^H(x, y) \\
&+ \sum_{m=0}^{M-1} (-1)^{\lfloor \frac{m}{2} \rfloor} \left(\frac{a_2}{a_1} \right)^{\text{odd}(m)} u_2^{(\text{odd}(m), m+1-\text{odd}(m))} G_{M,m,1}^H(x, y) \\
&= \sum_{w=0}^{\lfloor \frac{M}{2} \rfloor} (-1)^{\lfloor \frac{2w}{2} \rfloor} \left(\frac{a_2}{a_1} \right)^{\text{odd}(2w)} u_2^{(\text{odd}(2w), 2w-\text{odd}(2w))} G_{M,2w,0}^H(x, y) \\
&+ \sum_{w=0}^{\lfloor \frac{M+1}{2} \rfloor - 1} (-1)^{\lfloor \frac{2w+1}{2} \rfloor} \left(\frac{a_2}{a_1} \right)^{\text{odd}(2w+1)} u_2^{(\text{odd}(2w+1), 2w+1-\text{odd}(2w+1))} G_{M,2w+1,0}^H(x, y) \\
&+ \sum_{w=0}^{\lfloor \frac{M-1}{2} \rfloor} (-1)^{\lfloor \frac{2w}{2} \rfloor} \left(\frac{a_2}{a_1} \right)^{\text{odd}(2w)} u_2^{(\text{odd}(2w), 2w+1-\text{odd}(2w))} G_{M,2w,1}^H(x, y)
\end{aligned}$$

$$\begin{aligned}
& + \sum_{w=0}^{\lfloor \frac{M}{2} \rfloor - 1} (-1)^{\lfloor \frac{2w+1}{2} \rfloor} \left(\frac{a_2}{a_1} \right)^{\text{odd}(2w+1)} u_2^{(\text{odd}(2w+1), 2w+1+1-\text{odd}(2w+1))} G_{M,2w+1,1}^H(x, y) \\
& = \sum_{w=0}^{\lfloor \frac{M}{2} \rfloor} (-1)^w u_2^{(0,2w)} G_{M,2w,0}^H(x, y) + \sum_{w=0}^{\lfloor \frac{M+1}{2} \rfloor - 1} (-1)^w \frac{a_2}{a_1} u_2^{(1,2w)} G_{M,2w+1,0}^H(x, y) \\
& \quad + \sum_{w=0}^{\lfloor \frac{M-1}{2} \rfloor} (-1)^w u_2^{(0,2w+1)} G_{M,2w,1}^H(x, y) + \sum_{w=0}^{\lfloor \frac{M}{2} \rfloor - 1} (-1)^w \frac{a_2}{a_1} u_2^{(1,2w+1)} G_{M,2w+1,1}^H(x, y).
\end{aligned}$$

and

$$\begin{aligned}
& \sum_{w=0}^{\lfloor \frac{M}{2} \rfloor} (-1)^w u_2^{(0,2w)} G_{M,2w,0}^H(x, y) + \sum_{w=0}^{\lfloor \frac{M-1}{2} \rfloor} (-1)^w u_2^{(0,2w+1)} G_{M,2w,1}^H(x, y) \\
& \quad + \sum_{w=0}^{\lfloor \frac{M+1}{2} \rfloor - 1} (-1)^w \frac{a_2}{a_1} u_2^{(1,2w)} G_{M,2w+1,0}^H(x, y) + \sum_{w=0}^{\lfloor \frac{M}{2} \rfloor - 1} (-1)^w \frac{a_2}{a_1} u_2^{(1,2w+1)} G_{M,2w+1,1}^H(x, y) \\
& = \sum_{n=0}^M (-1)^{\lfloor \frac{n}{2} \rfloor} u_2^{(0,n)} G_{M,n-\text{odd}(n),\text{odd}(n)}^H(x, y) + \sum_{n=0}^{M-1} (-1)^{\lfloor \frac{n}{2} \rfloor} \frac{a_2}{a_1} u_2^{(1,n)} G_{M,n+1-\text{odd}(n),\text{odd}(n)}^H(x, y) \\
& = \sum_{(m,n) \in \Lambda_M^{V,1}} u_2^{(m,n)} (-1)^{\lfloor \frac{n}{2} \rfloor} \left(\frac{a_2}{a_1} \right)^m G_{M,n+m-\text{odd}(n),\text{odd}(n)}^H(x, y).
\end{aligned}$$

In summary,

$$\begin{aligned}
& \sum_{(m,n) \in \Lambda_M^{H,1}} (-1)^{\lfloor \frac{m}{2} \rfloor} \left(\frac{a_2}{a_1} \right)^{\text{odd}(m)} u_2^{(\text{odd}(m), m+n-\text{odd}(m))} G_{M,m,n}^H(x, y) \\
& = \sum_{(m,n) \in \Lambda_M^{V,1}} u_2^{(m,n)} (-1)^{\lfloor \frac{n}{2} \rfloor} \left(\frac{a_2}{a_1} \right)^m G_{M,n+m-\text{odd}(n),\text{odd}(n)}^H(x, y).
\end{aligned} \tag{6.43}$$

By (6.39) and (6.43),

$$\begin{aligned}
& u_1(x + x_i, y + y_j) \\
& = \sum_{(m,n) \in \Lambda_M^{V,1}} u_2^{(m,n)} (-1)^{\lfloor \frac{n}{2} \rfloor} \left(\frac{a_2}{a_1} \right)^m G_{M,n+m-\text{odd}(n),\text{odd}(n)}^H(x, y) \\
& \quad + \sum_{(m,n) \in \Lambda_M^{H,1}} \left(\frac{\text{odd}(m)}{-(-1)^{\lfloor \frac{m}{2} \rfloor} a_1} \psi_1^{(m+n-\text{odd}(m))} + \sum_{\ell=1}^{\lfloor m/2 \rfloor} \frac{(-1)^\ell}{a_1} f_1^{(m-2\ell, n+2\ell-2)} \right) G_{M,m,n}^H(x, y) \\
& \quad + \sum_{(m,n) \in \Lambda_{M-2}} f_1^{(m,n)} Q_{M,m,n}^H(x, y) + \mathcal{O}(h^{M+1}), \quad x, y \in [-h, h].
\end{aligned} \tag{6.44}$$

By (6.40) and (6.43),

$$\begin{aligned}
& u_2(x + x_i, y + y_j) \\
&= \sum_{(m,n) \in \Lambda_M^{V,1}} u_2^{(m,n)} (-1)^{\lfloor \frac{n}{2} \rfloor} G_{M,n+m-\text{odd}(n),\text{odd}(n)}^H(x, y) \\
&\quad + \sum_{(m,n) \in \Lambda_M^{H,1}} \sum_{\ell=1}^{\lfloor m/2 \rfloor} \frac{(-1)^\ell}{a_2} f_2^{(m-2\ell, n+2\ell-2)} G_{M,m,n}^H(x, y) \\
&\quad + \sum_{(m,n) \in \Lambda_{M-2}} f_2^{(m,n)} Q_{M,m,n}^H(x, y) + \mathcal{O}(h^{M+1}), \quad x, y \in [-h, h].
\end{aligned} \tag{6.45}$$

By (6.41) and (6.43),

$$\begin{aligned}
& u_3(x + x_i, y + y_j) \\
&= \sum_{(m,n) \in \Lambda_M^{V,1}} u_2^{(m,n)} (-1)^{\lfloor \frac{n}{2} \rfloor} \left(\frac{a_2}{a_3} \right)^{\text{odd}(n)} G_{M,n+m-\text{odd}(n),\text{odd}(n)}^H(x, y) \\
&\quad + \sum_{(m,n) \in \Lambda_M^{H,1}} \sum_{\ell=1}^{\lfloor m/2 \rfloor} \frac{(-1)^\ell}{a_2} f_2^{(m-2\ell, n+2\ell-2)} \left(\frac{a_2}{a_3} \right)^n G_{M,m,n}^H(x, y) \\
&\quad - \sum_{m=0}^{M-1} \frac{1}{a_3} \psi_3^{(m)} G_{M,m,1}^H(x, y) \\
&\quad + \sum_{(m,n) \in \Lambda_{M-2}} f_3^{(m,n)} Q_{M,m,n}^H(x, y) + \mathcal{O}(h^{M+1}), \quad x, y \in [-h, h].
\end{aligned} \tag{6.46}$$

By (6.42) and (6.43),

$$\begin{aligned}
& u_4(x + x_i, y + y_j) \\
&= \sum_{(m,n) \in \Lambda_M^{V,1}} u_2^{(m,n)} (-1)^{\lfloor \frac{n}{2} \rfloor} \left(\frac{a_2}{a_1} \right)^m \left(\frac{a_1}{a_4} \right)^{\text{odd}(n)} G_{M,n+m-\text{odd}(n),\text{odd}(n)}^H(x, y) \\
&\quad - \sum_{(m,n) \in \Lambda_M^{H,1}} (-1)^{\lfloor \frac{m}{2} \rfloor} \frac{\text{odd}(m)}{a_1} \psi_1^{(m+n-\text{odd}(m))} \left(\frac{a_1}{a_4} \right)^n G_{M,m,n}^H(x, y) \\
&\quad + \sum_{(m,n) \in \Lambda_M^{H,1}} \sum_{\ell=1}^{\lfloor m/2 \rfloor} \frac{(-1)^\ell}{a_1} f_1^{(m-2\ell, n+2\ell-2)} \left(\frac{a_1}{a_4} \right)^n G_{M,m,n}^H(x, y) - \sum_{m=0}^{M-1} \frac{1}{a_4} \psi_4^{(m)} G_{M,m,1}^H(x, y) \\
&\quad + \sum_{(m,n) \in \Lambda_{M-2}} f_4^{(m,n)} Q_{M,m,n}^H(x, y) + \mathcal{O}(h^{M+1}), \quad x, y \in [-h, h].
\end{aligned} \tag{6.47}$$

By (6.45), (6.46), (6.9), and (6.10), we have

$$\begin{aligned}
& u_2(x + x_i, y_j) + \mathcal{O}(h^{M+1}) \\
&= \sum_{(m,n) \in \Lambda_M^{V,1}} u_2^{(m,n)} (-1)^{\lfloor \frac{n}{2} \rfloor} G_{M,n+m-\text{odd}(n),\text{odd}(n)}^H(x, 0) \\
&+ \sum_{(m,n) \in \Lambda_M^{H,1}} \sum_{\ell=1}^{\lfloor m/2 \rfloor} \frac{(-1)^\ell}{a_2} f_2^{(m-2\ell, n+2\ell-2)} G_{M,m,n}^H(x, 0) + \sum_{(m,n) \in \Lambda_{M-2}} f_2^{(m,n)} Q_{M,m,n}^H(x, 0), \\
&= \sum_{\substack{(m,n) \in \Lambda_M^{V,1} \\ \text{odd}(n)=0}} u_2^{(m,n)} (-1)^{\lfloor \frac{n}{2} \rfloor} G_{M,n+m,0}^H(x, 0) + \sum_{m=0}^M \sum_{\ell=1}^{\lfloor m/2 \rfloor} \frac{(-1)^\ell}{a_2} f_2^{(m-2\ell, 2\ell-2)} G_{M,m,0}^H(x, 0),
\end{aligned}$$

$$\begin{aligned}
& u_3(x + x_i, y_j) + \mathcal{O}(h^{M+1}) \\
&= \sum_{(m,n) \in \Lambda_M^{V,1}} u_2^{(m,n)} (-1)^{\lfloor \frac{n}{2} \rfloor} \left(\frac{a_2}{a_3} \right)^{\text{odd}(n)} G_{M,n+m-\text{odd}(n),\text{odd}(n)}^H(x, 0) \\
&+ \sum_{(m,n) \in \Lambda_M^{H,1}} \sum_{\ell=1}^{\lfloor m/2 \rfloor} \frac{(-1)^\ell}{a_2} f_2^{(m-2\ell, n+2\ell-2)} \left(\frac{a_2}{a_3} \right)^n G_{M,m,n}^H(x, 0) - \sum_{m=0}^{M-1} \frac{1}{a_3} \psi_3^{(m)} G_{M,m,1}^H(x, 0) \\
&+ \sum_{(m,n) \in \Lambda_{M-2}} f_3^{(m,n)} Q_{M,m,n}^H(x, 0) \\
&= \sum_{\substack{(m,n) \in \Lambda_M^{V,1} \\ \text{odd}(n)=0}} u_2^{(m,n)} (-1)^{\lfloor \frac{n}{2} \rfloor} G_{M,n+m,0}^H(x, 0) + \sum_{m=0}^M \sum_{\ell=1}^{\lfloor m/2 \rfloor} \frac{(-1)^\ell}{a_2} f_2^{(m-2\ell, 2\ell-2)} G_{M,m,0}^H(x, 0),
\end{aligned}$$

i.e,

$$u_2(x + x_i, y_j) = u_3(x + x_i, y_j) + \mathcal{O}(h^{M+1}), \quad \text{for any } x \in [-h, h]. \quad (6.48)$$

Similarly, by (6.44), (6.47), (6.9), and (6.10), we have

$$\begin{aligned}
& u_1(x + x_i, y_j) + \mathcal{O}(h^{M+1}) \\
&= \sum_{(m,n) \in \Lambda_M^{V,1}} u_2^{(m,n)} (-1)^{\lfloor \frac{n}{2} \rfloor} \left(\frac{a_2}{a_1} \right)^m G_{M,n+m-\text{odd}(n),\text{odd}(n)}^H(x, 0) \\
&\quad + \sum_{(m,n) \in \Lambda_M^{H,1}} \left(\frac{\text{odd}(m)}{-(-1)^{\lfloor \frac{m}{2} \rfloor} a_1} \psi_1^{(m+n-\text{odd}(m))} + \sum_{\ell=1}^{\lfloor m/2 \rfloor} \frac{(-1)^\ell}{a_1} f_1^{(m-2\ell, n+2\ell-2)} \right) G_{M,m,n}^H(x, 0) \\
&\quad + \sum_{(m,n) \in \Lambda_{M-2}} f_1^{(m,n)} Q_{M,m,n}^H(x, 0) \\
&= \sum_{\substack{(m,n) \in \Lambda_M^{V,1} \\ \text{odd}(n)=0}} u_2^{(m,n)} (-1)^{\lfloor \frac{n}{2} \rfloor} \left(\frac{a_2}{a_1} \right)^m G_{M,n+m,0}^H(x, 0) \\
&\quad + \sum_{m=0}^M \left(\frac{\text{odd}(m)}{-(-1)^{\lfloor \frac{m}{2} \rfloor} a_1} \psi_1^{(m-\text{odd}(m))} + \sum_{\ell=1}^{\lfloor m/2 \rfloor} \frac{(-1)^\ell}{a_1} f_1^{(m-2\ell, 2\ell-2)} \right) G_{M,m,0}^H(x, 0)
\end{aligned}$$

$$\begin{aligned}
& u_4(x + x_i, y_j) + \mathcal{O}(h^{M+1}) \\
&= \sum_{(m,n) \in \Lambda_M^{V,1}} u_2^{(m,n)} (-1)^{\lfloor \frac{n}{2} \rfloor} \left(\frac{a_2}{a_1} \right)^m \left(\frac{a_1}{a_4} \right)^{\text{odd}(n)} G_{M,n+m-\text{odd}(n),\text{odd}(n)}^H(x, 0) \\
&\quad - \sum_{(m,n) \in \Lambda_M^{H,1}} (-1)^{\lfloor \frac{m}{2} \rfloor} \frac{\text{odd}(m)}{a_1} \psi_1^{(m+n-\text{odd}(m))} \left(\frac{a_1}{a_4} \right)^n G_{M,m,n}^H(x, 0) \\
&\quad + \sum_{(m,n) \in \Lambda_M^{H,1}} \sum_{\ell=1}^{\lfloor m/2 \rfloor} \frac{(-1)^\ell}{a_1} f_1^{(m-2\ell, n+2\ell-2)} \left(\frac{a_1}{a_4} \right)^n G_{M,m,n}^H(x, 0) - \sum_{m=0}^{M-1} \frac{1}{a_4} \psi_4^{(m)} G_{M,m,1}^H(x, 0) \\
&\quad + \sum_{(m,n) \in \Lambda_{M-2}} f_4^{(m,n)} Q_{M,m,n}^H(x, 0) \\
&= \sum_{\substack{(m,n) \in \Lambda_M^{V,1} \\ \text{odd}(n)=0}} u_2^{(m,n)} (-1)^{\lfloor \frac{n}{2} \rfloor} \left(\frac{a_2}{a_1} \right)^m G_{M,n+m,0}^H(x, 0) \\
&\quad - \sum_{m=0}^M (-1)^{\lfloor \frac{m}{2} \rfloor} \frac{\text{odd}(m)}{a_1} \psi_1^{(m-\text{odd}(m))} G_{M,m,0}^H(x, 0) + \sum_{m=0}^M \sum_{\ell=1}^{\lfloor m/2 \rfloor} \frac{(-1)^\ell}{a_1} f_1^{(m-2\ell, 2\ell-2)} G_{M,m,0}^H(x, 0),
\end{aligned}$$

i.e.,

$$u_1(x + x_i, y_j) = u_4(x + x_i, y_j) + \mathcal{O}(h^{M+1}), \quad \text{for any } x \in [-h, h]. \quad (6.49)$$

Now, by (6.44)–(6.49), we could define that

$$\begin{aligned}
\mathcal{L}_h^S u &:= \\
&\frac{1}{h} \left(C_{-1,-1}^- u_4(x_i - h, y_j - h) + C_{0,-1}^- u_4(x_i, y_j - h) + C_{0,-1}^+ u_3(x_i, y_j - h) + C_{1,-1}^+ u_3(x_i + h, y_j - h) \right. \\
&\quad + C_{-1,0}^- u_1(x_i - h, y_j) + C_{0,0}^- u_1(x_i, y_j) + C_{0,0}^+ u_2(x_i, y_j) + C_{1,0}^+ u_2(x_i + h, y_j) \\
&\quad \left. + C_{-1,1}^- u_1(x_i - h, y_j + h) + C_{0,1}^- u_1(x_i, y_j + h) + C_{0,1}^+ u_2(x_i, y_j + h) + C_{1,1}^+ u_2(x_i + h, y_j + h) \right) \\
&= \sum_{(m,n) \in \Lambda_M^{V,1}} u_2^{(m,n)} h^{-1} I_{m,n} + \sum_{(m,n) \in \Lambda_M^{H,1}} h F_{M,m,n}^{H,1} + \sum_{(m,n) \in \Lambda_{M-2}} h F_{M,m,n} + \sum_{(m,n) \in \Lambda_M^{H,1}} h^{-1} \Psi_{M,m,n}^{H,1} \\
&\quad + \sum_{m=0}^{M-1} h^{-1} \Psi_{M,m} = \mathcal{O}(h^M), \quad \text{as } h \rightarrow 0,
\end{aligned}$$

where

$$C_{k,\ell}^\pm := \sum_{p=0}^M c_{k,\ell,p}^\pm h^p \quad \text{with } c_{k,\ell,p}^\pm \in \mathbb{R},$$

$$\begin{aligned}
I_{m,n} &:= \sum_{k=-1}^0 \sum_{\ell=0}^1 C_{k,\ell}^- (-1)^{\lfloor \frac{n}{2} \rfloor} \left(\frac{a_2}{a_1} \right)^m G_{M,n+m-\text{odd}(n),\text{odd}(n)}^H(kh, \ell h) \\
&\quad + \sum_{k=0}^1 \sum_{\ell=0}^1 C_{k,\ell}^+ (-1)^{\lfloor \frac{n}{2} \rfloor} G_{M,n+m-\text{odd}(n),\text{odd}(n)}^H(kh, \ell h) \\
&\quad + \sum_{k=0}^1 C_{k,-1}^+ (-1)^{\lfloor \frac{n}{2} \rfloor} \left(\frac{a_2}{a_3} \right)^{\text{odd}(n)} G_{M,n+m-\text{odd}(n),\text{odd}(n)}^H(kh, -h) \\
&\quad + \sum_{k=-1}^0 C_{k,-1}^- (-1)^{\lfloor \frac{n}{2} \rfloor} \left(\frac{a_2}{a_1} \right)^m \left(\frac{a_1}{a_4} \right)^{\text{odd}(n)} G_{M,n+m-\text{odd}(n),\text{odd}(n)}^H(kh, -h),
\end{aligned} \tag{6.50}$$

$$\begin{aligned}
F_{M,m,n}^{H,1} &:= \sum_{k=-1}^0 \sum_{\ell=0}^1 C_{k,\ell}^- \sum_{s=1}^{\lfloor m/2 \rfloor} \frac{(-1)^s}{a_1 h^2} f_1^{(m-2s,n+2s-2)} G_{M,m,n}^H(kh, \ell h) \\
&\quad + \sum_{k=0}^1 \sum_{\ell=0}^1 C_{k,\ell}^+ \sum_{s=1}^{\lfloor m/2 \rfloor} \frac{(-1)^s}{a_2 h^2} f_2^{(m-2s,n+2s-2)} G_{M,m,n}^H(kh, \ell h) \\
&\quad + \sum_{k=0}^1 C_{k,-1}^+ \sum_{s=1}^{\lfloor m/2 \rfloor} \frac{(-1)^s}{a_2 h^2} \left(\frac{a_2}{a_3} \right)^n f_2^{(m-2s,n+2s-2)} G_{M,m,n}^H(kh, -h) \\
&\quad + \sum_{k=-1}^0 C_{k,-1}^- \sum_{s=1}^{\lfloor m/2 \rfloor} \frac{(-1)^s}{a_1 h^2} \left(\frac{a_1}{a_4} \right)^n f_1^{(m-2s,n+2s-2)} G_{M,m,n}^H(kh, -h),
\end{aligned} \tag{6.51}$$

$$\begin{aligned}
F_{M,m,n} := & \frac{f_1^{(m,n)}}{h^2} \sum_{k=-1}^0 \sum_{\ell=0}^1 C_{k,\ell}^- Q_{M,m,n}^H(kh, \ell h) + \frac{f_2^{(m,n)}}{h^2} \sum_{k=0}^1 \sum_{\ell=0}^1 C_{k,\ell}^+ Q_{M,m,n}^H(kh, \ell h) \\
& + \frac{f_3^{(m,n)}}{h^2} \sum_{k=0}^1 C_{k,-1}^+ Q_{M,m,n}^H(kh, -h) + \frac{f_4^{(m,n)}}{h^2} \sum_{k=-1}^0 C_{k,-1}^- Q_{M,m,n}^H(kh, -h),
\end{aligned} \tag{6.52}$$

$$\begin{aligned}
\Psi_{M,m,n}^{H,1} := & -\psi_1^{(m+n-\text{odd}(m))} \sum_{k=-1}^0 \sum_{\ell=0}^1 C_{k,\ell}^- \frac{\text{odd}(m)}{(-1)^{\lfloor \frac{m}{2} \rfloor} a_1} G_{M,m,n}^H(kh, \ell h) \\
& - \psi_1^{(m+n-\text{odd}(m))} \sum_{k=-1}^0 C_{k,-1}^- (-1)^{\lfloor \frac{m}{2} \rfloor} \frac{\text{odd}(m)}{a_1} \left(\frac{a_1}{a_4}\right)^n G_{M,m,n}^H(kh, -h),
\end{aligned} \tag{6.53}$$

$$\Psi_{M,m} := -\psi_3^{(m)} \sum_{k=0}^1 C_{k,-1}^+ \frac{1}{a_3} G_{M,m,1}^H(kh, -h) - \psi_4^{(m)} \sum_{k=-1}^0 C_{k,-1}^- \frac{1}{a_4} G_{M,m,1}^H(kh, -h). \tag{6.54}$$

Let

$$\begin{aligned}
\mathcal{L}_h^S u_h := & \frac{1}{h} \sum_{k=-1}^1 \sum_{\ell=-1}^1 C_{k,\ell}(u_h)_{i+k,j+\ell} = \sum_{(m,n) \in \Lambda_M^{H,1}} h F_{M,m,n}^{H,1} + \sum_{(m,n) \in \Lambda_{M-2}} h F_{M,m,n} \\
& + \sum_{(m,n) \in \Lambda_M^{H,1}} h^{-1} \Psi_{M,m,n}^{H,1} + \sum_{m=0}^{M-1} h^{-1} \Psi_{M,m},
\end{aligned} \tag{6.55}$$

where

$$\begin{aligned}
C_{-1,-1} &= C_{-1,-1}^-, & C_{0,-1} &= C_{0,-1}^- + C_{0,-1}^+, & C_{1,-1} &= C_{1,-1}^+, \\
C_{-1,0} &= C_{-1,0}^-, & C_{0,0} &= C_{0,0}^- + C_{0,0}^+, & C_{1,0} &= C_{1,0}^+, \\
C_{-1,1} &= C_{-1,1}^-, & C_{0,1} &= C_{0,1}^- + C_{0,1}^+, & C_{1,1} &= C_{1,1}^+.
\end{aligned} \tag{6.56}$$

Then

$$\mathcal{L}_h^S(u - u_h) = \mathcal{O}(h^M),$$

if $I_{m,n}$ in (6.50) satisfies

$$I_{m,n} = \mathcal{O}(h^{M+1}), \quad \text{for all } n = 0, \dots, M. \tag{6.57}$$

By calculation, the maximum integer M for the linear system in (6.57) to have a nontrivial solution $\{C_{k,\ell}(0)\}_{k,\ell=-1,0,1}$ is $M = 7$. In particular, one nontrivial solution of (6.57) with

$M = 7$ is

$$\begin{aligned}
C_{-1,-1}^- &= \frac{a_1 a_4 (a_2 + a_3)}{a_2^2 (a_1 + a_4)}, & C_{0,-1}^- &= \frac{2a_4 (a_2 + a_3) (a_1 + a_2)}{a_2^2 (a_1 + a_4)}, & C_{0,-1}^+ &= 0, & C_{1,-1}^+ &= \frac{a_3}{a_2}, \\
C_{-1,0}^- &= \frac{2a_1 (a_2 + a_3)}{a_2^2}, & C_{0,0}^- &= \frac{-5(a_2 + a_3) (a_1 + a_2)}{a_2^2}, & C_{0,0}^+ &= 0, & C_{1,0}^+ &= \frac{2(a_2 + a_3)}{a_2}, \\
C_{-1,1}^- &= \frac{a_1^2 (a_2 + a_3)}{a_2^2 (a_1 + a_4)}, & C_{0,1}^- &= \frac{2a_1 (a_2 + a_3) (a_1 + a_2)}{a_2^2 (a_1 + a_4)}, & C_{0,1}^+ &= 0, & C_{1,1}^+ &= 1.
\end{aligned} \tag{6.58}$$

So (6.55), (6.56) and (6.58) with $M = 7$ imply (6.17) and (6.18). \square

Chapter 7

Future Work

In Chapter 5, we have derived a compact finite difference scheme with reduced pollution effect for huge wave numbers k . In case of elliptic interface problems with discontinuous coefficients, high-contrast coefficients across the interface must also lead to pollution errors. So, motivated by the method in Chapter 5, we plan to construct a robust compact finite difference scheme with the higher order accuracy and reduced pollution effect for elliptic interface problems with high-contrast coefficients. By the efficient implementation in Chapter 4, it is very easy to achieve implementation for the higher order compact finite difference scheme for the Helmholtz interface problems with discontinuous wave numbers. Clearly, the high-contrast discontinuous wave numbers also result in pollution effects. So we also plan to extend the new pollution minimization strategy in Chapter 5 to the Helmholtz interface problems with discontinuous, high-contrast, and variable wave numbers. We can also construct a compact finite difference scheme with a reduced pollution effect for the Helmholtz equation with a perfectly matched layer (PML) boundary condition.

In Chapter 3, we numerically verify the sign conditions of our proposed compact finite difference scheme and prove the convergence rate by the discrete maximum principle. Motivated by the numerical verifications, we plan to construct a complete theoretical proof for sign conditions of the compact scheme in Chapter 3. Similarly, we also plan to derive the complete theoretical proof for the convergence analysis of the proposed hybrid scheme in Chapter 4. Furthermore, if we could not prove the sign conditions for 9-point scheme and 13-point scheme for irregular points. Then we would try to derive a sixth order 25-point finite difference scheme which theoretically satisfies the sign conditions for the irregular points for the elliptic interface problems with discontinuous coefficients. As the 25-point scheme will give us more free parameters, it is highly possible to achieve this goal. Since the irregular points only exist along the interface, compared with the whole domain Ω in 2D, irregular points can be considered as 1D data. Thus, the entire computation cost will not increase too

much, if we only modify the irregular points in the finite difference scheme. We also plan to construct the higher order compact finite difference scheme and derive the convergence analysis for the problem $-\nabla \cdot (A\nabla u) = f$ in $\Omega \setminus \Gamma$, $[u] = g_0^\Gamma$ and $[A\nabla u \cdot \vec{n}] = g_1^\Gamma$ on Γ , where $A = \begin{pmatrix} a & b \\ b & c \end{pmatrix}$ is a symmetric positive definite matrix.

Since we have done the compact finite difference schemes for the Poisson (Chapter 2), elliptic (Chapters 3, 4 and 6), and Helmholtz (Chapter 5) interface problems, it is natural to extend our methods to more complicated and popular problems: Maxwell interface problems [57], Stokes interface problems [1, 48, 99], elliptic equations with complex interfaces or boundaries [2, 19, 78], and other interface problems in [100]. It is straightforward to derive the higher order compact finite difference scheme for the singularly perturbed problems in [43, 84] by the method in Chapter 3. While the small ϵ in singularly perturbed problems would also cause the pollution errors, so we also plan to extend the method in Chapter 5 to the most general singularly perturbed problems to reduce the pollution effect. Furthermore, we can use wavelet bases in [49, 61, 62] to construct numerical schemes with bounded condition numbers which can reduce the relative errors for the numerical solutions in the elliptic interface problems with high-contrast coefficients. We also plan to derive a new efficient and highly parallelizable compact finite difference scheme for the Navier-Stokes equations in the spirit of the schemes described in [45, 46]. Finally, we can use parallel computation skills to achieve the implementation for 3D equations with high-frequency solutions.

Bibliography

- [1] S. Adjerid, N. Chaabane, and T. Lin, An immersed discontinuous finite element method for Stokes interface problems. *Comput. Methods Appl. Mech. Engrg.* **293** (2015), 170-190.
- [2] M. Ahmad, S. Islam, and E. Larsson, Local meshless methods for second order elliptic interface problems with sharp corners. *J. Comput. Phys.* **416** (2020), 109500.
- [3] M. Ainsworth, Discrete dispersion relation for hp -version finite element approximation at high wave number. *SIAM J. Numer. Anal.* **42** (2004), no. 2, 553-575.
- [4] I. T. Angelova and L. G. Vulkov, High-order finite difference schemes for elliptic problems with intersecting interfaces. *Appl. Math. Comput.* **187** (2007), 824-843.
- [5] I. Babuška, The finite element method for elliptic equations with discontinuous coefficients. *Computing.* **5** (1970), 207-213.
- [6] I. Babuška, B. Andersson, B. Guo, J. M. Melenk, and H. S. Oh, Finite element method for solving problems with singular solutions. *J. Comput. Appl. Math.* **74** (1996), no. 1-2, 51-70.
- [7] I. M. Babuška and S. A. Sauter, Is the pollution effect of the FEM avoidable for the Helmholtz equation considering high wave numbers? *SIAM Rev.* **42** (2000), no. 3, 451-484.
- [8] M. Blumenfeld, The regularity of interface-problems on corner-regions. *Lecture Notes in Math.* **1121** (1985), 38-54.
- [9] J. H. Bramble and J. T. King, A finite element method for interface problems in domains with smooth boundaries and interfaces. *Adv. Comput. Math.* **6** (1996), 109-138.
- [10] G. Brandstetter and S. Govindjee, A high-order immersed boundary discontinuous-Galerkin method for Poissons equation with discontinuous coefficients and singular sources. *Int. J. Numer. Meth. Engng.* **101** (2015), no. 11, 847-869.
- [11] S. Britt, S. Tsynkov, and E. Turkel, A compact fourth order scheme for the Helmholtz equation in polar coordinates. *J. Sci. Comput.* **45** (2010), 26-47.
- [12] S. Britt, S. Tsynkov, and E. Turkel, Numerical simulation of time-harmonic waves in inhomogeneous media using compact high order schemes. *Commun. Comput. Phys.* **9** (2011), no. 3, 520-541.

- [13] S. Britt, S. Tsynkov, and E. Turkel, A high order numerical method for the Helmholtz equation with nonstandard boundary conditions. *SIAM J. Sci. Comput.* **35** (2013), no. 5, A2255-A2292.
- [14] Z. Cai and S. Kim, A finite element method using singular functions for the Poisson equation: corner singularities. *SIAM J. Numer. Anal.* **39** (2001), no. 1, 286-299.
- [15] J. M. Chadam and H. M. Yin, A diffusion equation with localized chemical reactions. *Proc. Edinburgh Math. Soc.* **37** (1993), 101-118.
- [16] Z. Chen, D. Cheng, W. Feng, and T. Wu, An optimal 9-point finite difference scheme for the Helmholtz equation with PML. *Int. J. Numer. Anal. Mod.* **10** (2013), no. 2, 389-410.
- [17] X. Chen, X. Feng, and Z. Li, A direct method for accurate solution and gradient computations for elliptic interface problems. *Numer. Algorithms.* **80** (2019), 709-740.
- [18] Z. Chen, T. Wu, and H. Yang, An optimal 25-point finite difference scheme for the Helmholtz equation with PML. *J. Comput. Appl. Math.* **236** (2011), 1240-1258.
- [19] X. Cheng and A. W. Shaikh, Iterative methods for the Poisson equation in L-shape domain based on domain decomposition method. *Appl. Math. Comput.* **180** (2006), 393-400.
- [20] P.-H. Cocquet, M. J. Gander, and X. Xiang, Closed form dispersion corrections including a real shifted wavenumber for finite difference discretizations of 2D constant coefficient Helmholtz problems. *SIAM J. Sci. Comput.* **43** (2021), no. 1, A278-A308.
- [21] H. Dastour and W. Liao, A fourth-order optimal finite difference scheme for the Helmholtz equation with PML. *Comput. Math. Appl.* **78** (2019), no. 6, 2147-2165.
- [22] H. Dastour and W. Liao, An optimal 13-point finite difference scheme for a 2D Helmholtz equation with a perfectly matched layer boundary condition. *Numer. Algorithms.* **86** (2021), 1109-1141.
- [23] B. Dong, X. Feng, and Z. Li, An FE-FD method for anisotropic elliptic interface problems. *SIAM J. Sci. Comput.* **42** (2020), no. 4, B1041-B1066.
- [24] Y. Du and H. Wu, Preasymptotic error analysis of higher order FEM and CIP-FEM for Helmholtz equation with high wave number. *SIAM J. Numer. Anal.* **53** (2015), no. 2, 782-804.
- [25] V. Dwarka and C. Vuik, Pollution and accuracy of solutions of the Helmholtz equation: a novel perspective from the eigenvalues. *J. Comput. Appl. Math.* **395** (2021), 1-21.
- [26] R. Egan and F. Gibou, Geometric discretization of the multidimensional Dirac delta distribution-Application to the Poisson equation with singular source terms. *J. Comput. Phys.* **346** (2017), 71-90.
- [27] A. Ern and J.-L. Guermond, Theory and practice of finite elements. *Vol. 159. Springer Science & Business Media*, 2013.

- [28] O. G. Ernst and M. J. Gander, Why is it difficult to solve Helmholtz problems with classical iterative methods. Numerical analysis of multiscale problems, *Lecture Notes in Computational Science and Engineering* **83**, Springer, Berlin, Heidelberg, 2011, 325-363.
- [29] R. Ewing, O. Iliev, and R. Lazarov, A modified finite volume approximation of second-order elliptic equations with discontinuous coefficients. *SIAM J. Sci. Comput.* **23** (2001), no. 4, 1335-1351.
- [30] R. Ewing, Z. Li, T. Lin, and Y. Lin, The immersed finite volume element methods for the elliptic interface problems. *Math. Comput. Simul.* **50** (1999), 63-76.
- [31] Q.W. Feng, B. Han, and M. Michelle, Sixth order compact finite difference method for 2D Helmholtz equations with singular sources and reduced pollution effect, arXiv:2112.07154 (2021), 20 pp.
- [32] Q.W. Feng, B. Han, and P. Minev, Sixth order compact finite difference schemes for Poisson interface problems with singular sources. *Comp. Math. Appl.* **99** (2021), 2-25.
- [33] Q.W. Feng, B. Han, and P. Minev, A high order compact finite difference scheme for elliptic interface problems with discontinuous and high-contrast coefficients. *Appl. Math. Comput.* **431** (2022), 127314.
- [34] Q.W. Feng, B. Han, and P. Minev, Hybrid finite difference schemes for elliptic interface problems with discontinuous and high-contrast variable coefficients, arXiv:2205.01256 (2022), 23 pp.
- [35] X. Feng, Z. Li, and Z. Qiao, High order compact finite difference schemes for the Helmholtz equation with discontinuous coefficients. *J. Comput. Math.* **29** (2011), no. 3, 324-340.
- [36] X. Feng and H. Wu, Discontinuous Galerkin methods for the Helmholtz equation with large wave number. *SIAM J. Numer. Anal.* **47** (2009), no. 4, 2872-2896.
- [37] X. Feng and H. Wu, hp -discontinuous Galerkin methods for the Helmholtz equation with large wave number. *Math. Comp.* **80** (2011), no. 276, 1997-2024.
- [38] H. Feng and S. Zhao, FFT-based high order central difference schemes for three-dimensional Poissons equation with various types of boundary conditions. *J. Comput. Phys.* **410** (2020), 109391.
- [39] H. Feng and S. Zhao, A fourth order finite difference method for solving elliptic interface problems with the FFT acceleration. *J. Comput. Phys.* **419** (2020), 109677.
- [40] G. J. Fix, S. Gulati, and G. I. Wakoff, On the use of singular functions with finite element approximations. *J. Comput. Phys.* **13** (1973), 209-228.
- [41] M. J. Gander and H. Zhang, A class of iterative solvers for the Helmholtz equation: factorizations, sweeping preconditioners, source transfer, single layer potentials, polarized traces, and optimized Schwarz methods. *SIAM Rev.* **61** (2019), no. 1, 3-76.

- [42] Y. Gong, B. Li, and Z. Li, Immersed-interface finite-element methods for elliptic interface problems with nonhomogeneous jump conditions. *SIAM J. Numer. Anal.* **46** (2008), no. 1, 472-495.
- [43] J. L. Gracia and C. Clavero, A compact finite difference scheme for 2D reaction-diffusion singularly perturbed problems. *J. Comput. Appl. Math.* **192** (2006), 152-167.
- [44] I. G. Graham and S. A. Sauter, Stability and finite element error analysis for the Helmholtz equation with variable coefficients. *Math. Comp.* **89** (2020), no. 321, 105-138.
- [45] J. Guermond and P. Mineev, High-order time stepping for the incompressible Navier-Stokes equations. *SIAM J. Sci. Comput.* **37** (2015), A2656-A2681.
- [46] J. Guermond and P. Mineev, High-order time stepping for the Navier-Stokes equations with minimal computational complexity. *J. Comput. Appl. Math.* **310** (2017), 92-103.
- [47] B. Guo and H. S. Oh, The h-p version of the finite element method for problems with interfaces. *Int. J. Numer. Methods. Eng.* **37** (1994), no. 10, 1741-1762.
- [48] J. Guzmán, M. A. Sánchez, and M. Sarkis, Higher-order finite element methods for elliptic problems with interfaces. *ESAIM: Mathematical Modelling and Numerical Analysis* **50** (2016), 1561-1583.
- [49] B. Han and M. Michelle, Derivative-orthogonal Riesz wavelets in Sobolev spaces with applications to differential equations. *Appl. Comput. Harmon. Anal.* **47** (2019), 759-794.
- [50] B. Han and M. Michelle, Sharp wavenumber-explicit stability bounds for 2D Helmholtz equations. *SIAM J. Numer. Anal.* **60** (2022), no. 4, 1985-2013.
- [51] B. Han and M. Michelle, and Y. S. Wong, Dirac assisted tree method for 1D heterogeneous Helmholtz equations with arbitrary variable wave numbers. *Comput. Math. Appl.* **97** (2021), 416-438.
- [52] A. Hansbo and P. Hansbo, An unfitted finite element method, based on Nitsches method, for elliptic interface problems. *Comput. Methods Appl. Mech. Engrg.* **191** (2002), 5537-5552.
- [53] X. He, T. Lin, and Y. Lin, Immersed finite element methods for elliptic interface problems with non-homogeneous jump conditions. *Int. J. Numer. Anal. Model.* **8** (2011), no. 2, 284-301.
- [54] U. Hetmaniuk, Stability estimates for a class of Helmholtz problems. *Commun. Math. Sci.* **5** (2007), no. 3, 665-678.
- [55] R. Hiptmair, A. Moiola, and I. Perugia, A survey of Trefftz methods for the Helmholtz equation. Building bridges: connections and challenges in modern approaches to numerical partial differential equations, *Lecture Notes in Computational Science and Engineering* **114**, Springer, Cham, 2016, 237-279.

- [56] T. Y. Hou and X. Wu, A multiscale finite element method for elliptic problems in composite materials and porous media. *J. Comput. Phys.* **134** (1997), 169-189.
- [57] J. Huang and J. Zou, Uniform a priori estimates for elliptic and static Maxwell interface problems. *Discrete Continuous Dynamical Systems-B* **7** (2007), 145-170.
- [58] F. Ihlenburg and I. M. Babuška, Finite element solution of the Helmholtz equation with high wave number part II: the *hp* version of the FEM. *SIAM J. Numer. Anal.* **34** (2006), no. 1, 315-358.
- [59] K. Ito, Z. Li, and Y. Kyei, Higher-order, Cartesian grid based finite difference schemes for elliptic equations on irregular domains. *SIAM J. Sci. Comput.* **27** (2005), 346-367.
- [60] H. Ji, J. Chen, and Z. Li, A high-order source removal finite element method for a class of elliptic interface problems. *Appl. Numer. Math.* **130** (2018), 112-130.
- [61] R-Q. Jia and S-T. Liu, Wavelet bases of Hermite cubic splines on the interval. *Adv. Comput. Math.* **25** (2006), 23-39.
- [62] R-Q. Jia and W. Zhao, Riesz bases of wavelets and applications to numerical solutions of elliptic equations. *Math. Comput.* **80** (2011), 1525-1556.
- [63] J. D. Kandilarov and L. G. Vulkov, The immersed interface method for two-dimensional heat-diffusion equations with singular own sources. *Appl. Numer. Math.* **57** (2007), no. 5-7, 486-497.
- [64] R. B. Kellogg, Singularities in interface problems. *Numerical Solution of Partial Differential Equations-II* (1971), 351-400.
- [65] R. B. Kellogg, Higher order singularities for interface problems. *The Mathematical Foundations of the Finite Element Method with Applications to Partial Differential Equations* (1972), 589-602.
- [66] R. B. Kellogg, On the Poisson equation with intersecting interfaces. *Appl. Anal.* **4** (1975), no. 2, 101-129.
- [67] S. Kim, Z. Cai, J. Pyo, and S. Kong, A finite element method using singular functions: interface problems. *Hokkaido Math. J.* **36** (2007), no. 4, 815-836.
- [68] S. Kim and S. Kong, A finite element method dealing the singular points with a cut-off function. *J. Appl. Math. Comput.* **21** (2006), no. 1-2, 141-152.
- [69] R. J. Leveque and Z. Li, The Immersed interface method for elliptic equations with discontinuous coefficients and singular sources. *SIAM J. Numer. Anal.* **31** (1994), no. 4, 1019-1044.
- [70] R. J. Leveque and Z. Li, Immersed interface methods for stokes flow with elastic boundaries or surface tension. *SIAM J. Sci. Comput.* **18** (1997), no. 3, 709-735.

- [71] Z. Li, A note on immersed interface method for three-dimensional elliptic equations. *Comput. Math. with Appl.* **31** (1996), no. 3, 9-17.
- [72] Z. Li, A fast iterative algorithm for elliptic interface problems. *SIAM J. Numer. Anal.* **35** (1998), no. 1, 230-254.
- [73] J. Li, Y. Chen, and G. Liu, High-order compact ADI methods for parabolic equations. *Comput. Math. with Appl.* **52** (2006), 1343-1356.
- [74] Z. Li and K. Ito, Maximum principle preserving schemes for interface problems with discontinuous coefficients. *SIAM J. Sci. Comput.* **23** (2001), no. 1, 339-361.
- [75] Z. Li and K. Ito, The immersed interface method: numerical solutions of PDEs involving interfaces and irregular domains. *Society for Industrial and Applied Mathematics*. 2006.
- [76] Z. Li and K. Pan, Can 4th-order compact schemes exist for flux type BCs? arxiv:2109.05638 (2021), 22 pp.
- [77] T. Lin, Y. Lin, and X. Zhang, Partially penalized immersed finite element methods for elliptic interface problems. *SIAM J. Numer. Anal.* **53** (2015), no. 2, 1121-1144.
- [78] J. Lin, L. Qiu, and F. Wang, Localized singular boundary method for the simulation of large-scale problems of elliptic operators in complex geometries. *Comp. Math. Appl.* **105** (2022), 94-106.
- [79] T. Ma and Y. Ge, A higher-order blended compact difference (BCD) method for solving the general 2D linear second-order partial differential equation. *Advances in Difference Equations.* **98** (2019), 1-21.
- [80] T. Ma and Y. Ge, High-order blended compact difference schemes for the 3D elliptic partial differential equation with mixed derivatives and variable coefficients. *Advances in Difference Equations.* **525** (2020), 1-30.
- [81] A. C. Medina and R. Schmid, Solution of high order compact discretized 3D elliptic partial differential equations by an accelerated multigrid method. *J. Comput. Appl. Math.* **350** (2019), 343-352.
- [82] M. Medvinsky, S. Tsynkov, and E. Turkel, The method of difference potentials for the Helmholtz equation using compact high order schemes. *J.Sci. Comput.* **53** (2012), 150-193.
- [83] J. M. Melenk and S. Sauter, Wavenumber explicit convergence analysis for Galerkin discretizations of the Helmholtz equation. *SIAM J. Numer. Anal.* **49** (2011), no. 3, 1210-1243.
- [84] R. K. Mohanty, The smart-BLAGE algorithm for singularly perturbed 2D elliptic partial differential equations. *Appl. Math. Comput.* **190** (2007), 321-331.

- [85] A. Moiola and E. A. Spence, Acoustic transmission problems: wavenumber-explicit bounds and resonance-free regions. *Math. Models Methods Appl. Sci.* **29** (2019), no. 2, 317-354.
- [86] M. Nabavi, M. H. Kamran Siddiqui and J. Dargahi, A new 9-point sixth-order accurate compact finite-difference method for the Helmholtz equation. *J. Sound Vib.* **307** (2007), 972-982.
- [87] S. Nicaise, Polygonal interface problems: higher regularity results. *Commun. Partial. Differ. Equ.* **15** (1990), no. 10, 1475-1508.
- [88] S. Nicaise and A. M. Sandig, General interface problems-I. *Math. Methods Appl. Sci.* **17** (1994), 395-429.
- [89] K. Pan, D. He, and Z. Li, A high order compact FD framework for elliptic BVPs involving singular sources, interfaces, and irregular domains. *J. Sci. Comput.* **88** (2021), 1-25.
- [90] C. S. Peskin, The immersed boundary method. *Acta Numerica* (2002), 479-517.
- [91] D. Peterseim, Eliminating the pollution effect in Helmholtz problems by local subscale correction. *Math. Comp.* **86** (2017), no. 305, 1005-1036.
- [92] M. Petzoldt, Regularity results for Laplace interface problems in two dimensions. *J. Anal. Appl.* **20** (2001), no. 2, 431-455.
- [93] M. Petzoldt, A posteriori error estimators for elliptic equations with discontinuous coefficients. *Adv. Comput. Math.* **16** (2002), no. 1, 47-75.
- [94] D. A. D. Pietro and A. Ern, Mathematical aspects of discontinuous Galerkin methods. *Springer Science and Business Media*. 2011.
- [95] Y. Ren, H. Feng, and S. Zhao, A FFT accelerated high order finite difference method for elliptic boundary value problems over irregular domains. *J. Comput. Phys.* **448** (2022), 110762.
- [96] A. A. Samarskii, V. L. Makarov, and R. D. Lazarov, Difference schemes for differential equations with generalized solutions. Vysshaya Shkola, (Russian), Moscow (1987).
- [97] M. Sari and G. Gürarslan, A sixth-order compact finite difference scheme to the numerical solutions of Burgers' equation. *Appl. Math. Comput.* **208** (2009), 475-483.
- [98] S. O. Settle, C. C. Douglas, I. Kim, and D. Sheen, On the derivation of highest-order compact finite difference schemes for the one- and two-dimensional Poisson equation with Dirichlet boundary conditions. *SIAM J. Numer. Anal.* **51** (2013), no. 4, 2470-2490.
- [99] L. Song and H. Gao, Analysis of a Stokes interface problem in multi-subdomains. *Appl. Math. Lett.* **64** (2017), 131-136.

- [100] S. Srivastava, A. Verma, and M. Kumar, An elliptic interface problem: a review. *Appl. Math. Inf. Sci. Lett.* **7** (2019), 51-59.
- [101] C. C. Stolk, M. Ahmed, and S. K. Bhowmik, A multigrid method for the Helmholtz equation with optimized coarse grid corrections. *SIAM J. Sci. Comput.* **36** (2014), no. 6, A2819-A2841.
- [102] A. K. Tornberg and B. Engquist, Numerical approximations of singular source terms in differential equations. *J. Comput. Phys.* **200** (2004), no. 2, 462-488.
- [103] J. D. Towers, Finite difference methods for discretizing singular source terms in a Poisson interface problem. *Contemp. Math.* **526** (2010), 359-389.
- [104] E. Turkel, D. Gordon, R. Gordon, and S. Tsynkov, Compact 2D and 3D sixth order schemes for the Helmholtz equation with variable wave number. *J. Comp. Phys.* **232** (2013), no. 1, 272-287.
- [105] J. L. Vazquez, The Porous medium equation: mathematical theory. *Clarendon Press*. 2007. p19.
- [106] Y. M. Wang, B. Y. Guo, and W. J. Wu, Fourth-order compact finite difference methods and monotone iterative algorithms for semilinear elliptic boundary value problems. *Comput. Math. with Appl.* **68** (2014), 1671-1688.
- [107] K. Wang and Y. S. Wong, Pollution-free finite difference schemes for non-homogeneous Helmholtz equation. *Int. J. Numer. Anal. Mod.* **11** (2014), no. 4, 787-815.
- [108] K. Wang and Y. S. Wong, Is pollution effect of finite difference schemes avoidable for multi-dimensional Helmholtz equations with high wave numbers? *Commun. Comput. Phys.* **21** (2017), no. 2, 490-514.
- [109] Y. Wang and J. Zhang, Sixth order compact scheme combined with multigrid method and extrapolation technique for 2D Poisson equation. *J. Comput. Phys.* **228** (2009), no. 1, 137-146.
- [110] A. Wiegmann and K. P. Bube, The explicit-jump immersed interface method: finite difference methods for PDEs with piecewise smooth solutions. *SIAM J. Numer. Anal.* **37** (2000), no. 3, 827-862.
- [111] T. Wu and R. Xu, An optimal compact sixth-order finite difference scheme for the Helmholtz equation. *Comput. Math. Appl.* **75** (2018), no. 7, 2520-2537.
- [112] S. Yu and G. W. Wei, Three-dimensional matched interface and boundary (MIB) method for treating geometric singularities. *J. Comput. Phys.* **227** (2007), 602-632.
- [113] S. Yu, Y. Zhou, and G. W. Wei, Matched interface and boundary (MIB) method for elliptic problems with sharp-edged interfaces. *J. Comput. Phys.* **224** (2007), 729-756.

- [114] S. Zhai, X. Feng, and Y. He, A family of fourth-order and sixth-order compact difference schemes for the three-dimensional Poisson equation. *J. Sci. Comput.* **54** (2013), 97-120.
- [115] J. Zhang, An explicit fourth-order compact finite difference scheme for three-dimensional convection-diffusion equation. *Commun. Numer. Methods Eng.* **14** (1998), 209-218.
- [116] Y. Zhang, K. Wang, and R. Guo, Sixth-order finite difference scheme for the Helmholtz equation with inhomogeneous Robin boundary condition. *Adv. Differ. Equ.* **362** (2019), 1-15.
- [117] X. Zhong, A new high-order immersed interface method for solving elliptic equations with imbedded interface of discontinuity. *J. Comput. Phys.* **225** (2007), 1066-1099.
- [118] Y. C. Zhou and G. W. Wei, On the fictitious-domain and interpolation formulations of the matched interface and boundary (MIB) method. *J. Comput. Phys.* **219** (2006), 228-246.
- [119] Y. C. Zhou, S. Zhao, M. Feig, and G. W. Wei, High order matched interface and boundary method for elliptic equations with discontinuous coefficients and singular sources. *J. Comput. Phys.* **213** (2006), no. 1, 1-30.